

**Design, Synthesis and Biological Evaluation of Coumarin
Analogues as Potent Pancreatic Lipase Inhibitors for
Obesity Treatment**

THESIS

Submitted in partial fulfilment
of the requirements for the degree of
DOCTOR OF PHILOSOPHY

by

Nisha Yadav

ID. No. 2018PHXF0046P

Under the Supervision of
Prof. Paul Atish Tulshiram



BITS Pilani

Pilani | Dubai | Goa | Hyderabad | Mumbai

BIRLA INSTITUTE OF TECHNOLOGY & SCIENCE, PILANI

2024

Dedicated

To My parents,

Savita Devi and Hoshiar Singh,

and my brother,

Manoj Kumar

For your unwavering support, love, and encouragement.
Your belief in me has been the foundation of my journey.
Thank you for inspiring me to pursue my dreams.

DECLARATION

I hereby declare that the work carried out in this thesis titled “**Design, Synthesis and Biological Evaluation of Coumarin Analogues as Potent Pancreatic Lipase Inhibitors for Obesity Treatment**” is an original piece of research work carried out under the supervision of **Prof. Paul Atish Tulshiram** at Department of Pharmacy, Birla Institute of Technology and Science, Pilani (BITS-Pilani), Pilani Campus. This thesis has not been submitted by me for the award of any other degree of any other University/Institute.

Nisha Yadav

ID No 2018PHXF0446P

Research scholar

BITS-Pilani, Pilani Campus

Date:

BIRLA INSTITUTE OF TECHNOLOGY AND SCIENCE, PILANI

CERTIFICATE

This is to certify that the thesis titled “**Design, Synthesis and Biological Evaluation of Coumarin Analogues as Potent Pancreatic Lipase Inhibitors for Obesity Treatment**” submitted by **Nisha Yadav** ID No. **2018PHXF0446P** for the award of Ph.D of the institute embodies original work done by her under my supervision.

Signature of the Supervisor

Name in capital letters: Prof. PAUL ATISH TULSHIRAM

Designation: Associate Professor,

Department of Pharmacy,

Birla Institute of Technology and Science, Pilani (BITS Pilani)

Pilani campus, Rajasthan

Date:

ACKNOWLEDGEMENTS

I would like to express my sincere appreciation and gratitude to numerous individuals who have played a pivotal role in assisting me to reach this juncture in my life. I shall commence by addressing the Almighty, whose predestination has led me down this path of righteousness and ultimately enabled me to realize my full potential. I wish to extend my sincere appreciation and affection to my family for their unwavering encouragement and support throughout the duration of my thesis.

I would like to extend my heartfelt gratitude to **Prof. Paul Atish Tulshiram**, my research supervisor. I consider it an honour to complete my doctoral research under his guidance. I am profoundly grateful to him for his supervision, unwavering support and understanding throughout my most baffling times. His counsel has facilitated the formation of a prospective research milieu by encouraging independent thought. I express my gratitude to him for furnishing me with academic assistance, emotional counsel, and moral fortitude during the course of my doctoral studies. I am profoundly grateful to his family (**Dr. Monika Paul, Avni, and Anika**) for their unfailing love and support. Words cannot adequately convey the depth of my appreciation for their familial support.

I would like to thank **Dr. Kumar Mangalam Birla** (Chancellor, BITS Pilani, Pilani Campus), **Prof. V. Ramgopal Rao** (Vice Chancellor, BITS Pilani, Pilani Campus), **Prof. Souvik Bhattacharyya** (Ex-Vice Chancellor, BITS Pilani, Pilani Campus) **Prof. Sudhir Kumar Barai** (Director, BITS Pilani, Pilani Campus) and **Prof. A. K. Sarkar** (Ex-Director, BITS Pilani, Pilani Campus), for allowing me to pursue my doctoral thesis. I would like to express my gratitude to **Prof. V. Venkata Vamsi Krishna** (Dean, Academic - Graduate Studies and Research (AGSR), BITS Pilani, Hyderabad Campus) and **Prof. Shamik Chakraborty** (Associate Dean, AGSR, BITS Pilani, Pilani Campus) for their kind support.

My whole-hearted gratitude to **Prof. Hemant R. Jadhav**, **Prof. S Murugesan** (Doctoral Advisory Committee members, BITS Pilani, Pilani Campus), **Prof. Anil Gaikwad** (Former Head, Department of Pharmacy), **Prof. Rajeev Taliyan Gaikwad** (Head, Department of Pharmacy), and **Prof. Anil Jindal** (Convener, Departmental Research Committee (DRC), Department of Pharmacy), for their official support and encouragement. I would like to acknowledge the Department of Science and Technology - Innovation in Science Pursuit for Inspired Research (DST-INSPIRE), for providing the **Fellowship** during 2019-2024 (INSPIRE Fellowship: IF180833).

My sincere appreciation goes out to the following faculty members of the Pharmacy department: **Prof. R. Mahesh, Prof. Deepak Chitkara, Prof. Anupama Mittal, Prof. Gautam Singhvi, Prof. Aniruddha Roy, Prof. Murali Manohar Pandey** and **Prof. Sandeep Sundriyal** for their support and encouragement.

My special thanks to **Prof. Richa Shrivastava** (Assistant Professor, Department of Pharmacy, BITS Pilani, Pilani Campus) and **Prof. Priya C. Sande** (Convener - Academia Council, BITS Pilani, Pilani Campus) who were always available when I needed their advice despite their excessive academic engagement. Their suggestions and guidance have significantly contributed to the smoothing of this voyage.

I would like to acknowledge **Birla Institute of Technology and Science (BITS), Pilani**, Pilani Campus, Rajasthan, India for providing the necessary laboratory facilities.

Heartfelt gratitude to all the **seniors, colleagues and juniors** (Department of Pharmacy, BITS Pilani, Pilani Campus) who enriched my life at BITS Pilani. Sincere admiration to **Dr. SNC Sridhar, Dr. Ginson George, Dr. Pracheta Sengupta, Dr. Priyadeep Manchanda, Dr. Prashant, Dr. Ravali, Ms. BB Lavanya, Mr. Utkarsh, Mr. Samarth, Mr. Sanket, Ms. Falguni** (PhD scholars), **Mr. Saksham Palawat, Mr. Dileep P S, Mr. Arjun Jeswani, Ms. Sakshi, Ms. Shweta** and **Mr. Ganesh** (M. Pharm students) of our group for their extended support during the final phase of my thesis. I would like to thank the **Central Animal facility staff**, and **Dr. Sushil K Yadav**, (Senior Vet. In charge) and staff members, **Mr. Vishal, Mr. Shyam, Mr. Mukesh** and **Mr. Shiva Kumar** for their assistance and their friendly behaviour during my work. I wish to extend my appreciation for the administrative staff **Mr. Puran Singh, Mr. Laxman Saini, Mr. Abhishek, Mr. Sandeep, Mr. Mandeep, Mr. Ram Suthar, Mr. Naveen, Mr. Tarachand** and **Mr. Vikas** (Department of Pharmacy, BITS Pilani, Pilani Campus) for their support in conducting labs.

I have been privileged to have colleagues and friends who are so devoted and helpful **Dr. Moumita, Dr. Arihant, Dr. Prabhjeet, Mr. Shivanshu, Ms. Aarti, Mr. Yash** and **Mr. Prateek**. I will always cherish those good times spent with them. Their companionship and assistance rendered my doctoral studies a turning point in my life.

Friendship and family are invaluable assets. In a nutshell, I express my gratitude to my father, **Mr. Hoshiar Singh** mother, **Mrs. Savita Devi**, brother, **Mr. Manoj Kumar**, and spouse, **Mr. Gunjan Kumar Yadav**, for their unwavering support in encouraging me to undertake this doctoral pursuit and for all the love, support, and encouragement they have given me throughout my Ph.D. journey. I would like to extend my gratitude towards my grandparents (**Mr. Harphul Singh, Mrs. Shakuntala Devi, Mr. Sher Singh, Mrs. Mishri Devi, Mr.**

Sohan Lal Yadav and **Mrs Chander Kanta Devi**), my extended family, with a special mention to my aunts (**Mrs. Santosh** and **Mrs. Sarita Yadav**) and my in-laws (**Mr. Radhey Shyam Yadav**, **Mrs. Kamlesh Yadav**, **Mr. Ish Kumar Yadav**, and **Mrs. Shweta Yadav**), for their moral support, encouragement, and supplication to the divine, all of which have motivated me to strive for excellence. Additionally, I wish to extend my gratitude to them for their unwavering, ceaseless affection and assistance throughout my academic pursuits. I would like to express my appreciation to my close friends, **Mrs. Neelam Shukla**, **Ms. Rinki Kumari**, **Dr. Kavya**, and **Ms. Lavanya**, for their unwavering support and motivation throughout the challenges and obstacles that life presented me. Without their moral support, it was truly unimaginable that I could have survived through this difficult period. I appreciate their motivation, encouragement, and affection towards me.

The assistance received throughout this tenure is incalculable and cannot be detailed on these pages. Everyone who assisted me in any way, whether directly or indirectly, is thanked.

Ms. Nisha Yadav

ABSTRACT

World Health Organization (WHO) defines obesity as an atypical and excessive buildup of adipose tissue within the body as a result of unhealthy dietary practices, sedentary behaviour, inadequate healthcare, genetics and sedentary lifestyles, that gives rise to a multitude of health complications (e.g., type 2 diabetes, hypertension, ischemic heart disease, fatty liver disease etc.). As per a new study published in the Lancet report, the global prevalence of obesity has surpassed one billion individuals in 2022 with 43% of adults being overweight in 2022. Triglycerides, that make up nearly 90% of dietary fat, are hydrolyzed to monoacylglycerol and unbound fatty acids before being absorbed into the systemic circulation leading to obesity. In the management and prevention of obesity, inhibition of food digestion and absorption are regarded as key strategy. The category of fat-digesting enzymes known as lipases are responsible for the enzymatic digestion of phospholipids and triglycerides. Since the majority of triglyceride digestion occurs *via* pancreatic lipase (PL), inhibition of PL is regarded as a viable therapeutic target for obesity treatment. Orlistat, a potent PL inhibitor, is widely prescribed for the treatment of obesity over the long term. However, protracted exposure to this drug, has led to severe adverse effects such as hepatotoxicity and pancreatitis, emphasizing the need for the development of safer and effective anti-obesity drugs.

Natural products have historically been regarded as reliable resources for the treatment of a wide range of human ailments. Traditional knowledge reveals an abundance of information pertaining to the various pharmacological activities of natural products, which emphasizes their significance. Anti-obesity properties of a multitude of plants have been documented in ancient texts, which is quite intriguing. Motivated by these encouraging findings, a collection of medicinal plants indigenous to India were chosen, extracted, and evaluated for their potential as PL inhibitors. Out of the numerous extracts that were screened, the methanol extract of unripe fruit from *Aegle marmelos*, that was prepared using sonication, demonstrated a significantly higher PL inhibitory potential ($IC_{50} = 13.02 \mu\text{g/mL}$). Due to the fact that crude extract is a mixture of natural products, the bioactive constituents accountable for PL inhibition were identified *via* bioassay-guided fractionation. As a consequence of these investigations, alloimperatorin was identified as a prospective PL inhibitory lead ($IC_{50} = 27.75 \mu\text{M}$).

Though alloimperatorin exhibited a potential PL inhibition, its activity was lower than the Orlistat ($IC_{50} = 0.97 \mu\text{M}$). An *in-silico* analysis of alloimperatorin in the active site of Human

PL (PDB ID: 1LPB) highlighted unfavourable steric interactions. Moreover, furan ring of alloimperatorin that did not exhibit any important interactions with the amino acids present at the active site of PL. These might be the putative reasons attributed to the comparatively lower PL inhibition of alloimperatorin.

In literature, Coumarins has gained a privileged place in the design and development of new clinical drugs with high affinity and specificity for various molecular targets. This heterocycle is a one-of-a-kind pharmacophore in the field of medicinal chemistry due to the presence of several key characteristics, such as a planar aromatic ring fused with lactone functionality, a readily available group for hydrogen bonding as well as for protein-ligand interaction. Recognizing the existence of these characteristics inside the coumarin template, this scaffold has been widely investigated in search of structurally varied therapeutic development drugs/leads. Various coumarin analogues, such as osthole, pteryxin, esculetin and umbelliferone have also been discovered to exhibit anti-obesity action. Also, cleomiscosin A, C and B from *Fraxinus rhynchophylla* stem barks have been reported to inhibit pancreatic lipase activity. Nevertheless, coumarins have been least explored for the PL inhibition and those reported exhibit moderate PL inhibitory activity. On the contrary, structural modifications that include various substitutions on the coumarins have resulted in a significant enhancement in their PL inhibitory activity. These results suggest the utility of coumarin based analogues as potential PL inhibitors. However, no report exists regarding the systematic development of synthetic PL inhibitory analogues based on coumarin scaffold.

In light of the aforementioned findings, a lead optimization strategy based on molecular modeling was employed to design coumarin analogues, which were subsequently synthesized and assessed for their ability to inhibit PL. In addition, these analogues possessed various structural characteristics required for PL inhibition, as determined by our prior research.

In order to design PL inhibitors, an amide fragment was also employed to engage in an interaction with Ser 152 which is an important amino acid of the catalytic triad. Further substituted aromatic rings were appended to the amide fragment. The electron-rich coumarin scaffold facilitated interaction with amino acids present in the lid domain. Prototypes of this type were docked using 1LPB (PDB ID) that showed favourable results in terms of the docking score and interactions with amino acids. In accordance with the feasibility of the reaction, a **series I** of 17 analogues were synthesized using a suitable scheme. **5q** was the most potent analogue, exhibiting an IC_{50} value of 19.41 μ M. The analogue **5q** demonstrated a competitive mode of inhibition, as determined by an enzyme kinetics study, with a K_i value of

10.386 μM . Molecular dynamic studies indicated that **5q** analogue was stable in active site of PL in the dynamic environment.

Further the **series I** analogues were optimized by exploring the sixth position of coumarin scaffold with addition of a linker (2 or 3 carbon) between the amide and aromatic/heteroaromatic moieties. It was hypothesized that incorporating of various substituents on the sixth position with a linker would lead to better interactions with both catalytic triad and hydrophobic lid domain amino acid. Thus, **series II** of **36** analogues were synthesized and characterized using various spectroscopic techniques. Through the *in vitro* results the analogue possessing linker length of two carbon atoms were found to be efficient with analogue **5df** ($\text{IC}_{50} = 21.24 \mu\text{M}$) as compared to the analogue with linker length of three carbon atom **5di** ($\text{IC}_{50} = 24.11 \mu\text{M}$) and one carbon atom **5da** ($\text{IC}_{50} = 28.17 \mu\text{M}$). Amongst all the analogues **5dh** and **5de** were found to exhibit potential PL inhibitory activities with IC_{50} values of 9.20 and 11.40 μM , respectively. With K_i value of 4.504 μM , the analogue **5dh** inhibited PL in competitive mode. Furthermore, molecular dynamic simulation revealed that the protein-ligand complex of the most potent analogue **5dh** remained stable at the PL active site under physiological conditions (100 ns).

Finally in **series III** the seventh and eighth positions of the coumarin scaffold were sequentially investigated in order to gain a thorough understanding of the most effective position for PL inhibition. Thus, **series III** of **38** analogues were synthesized, with analogues **7b** and **7a** exhibiting the most potent PL inhibitory activity with IC_{50} values of 1.25 and 4.25 μM , respectively. On the basis of enzyme kinetics investigations, it was determined that analogue **7b** exhibited a competitive inhibition with a K_i value of 0.698 μM . A 100 ns molecular dynamics simulation was subsequently performed on the analogue **7b**. The stability of analogue **7b** was confirmed by an RMSD value between 3 and 7 \AA .

Further, top two analogues from all the three series were selected and subjected to the *in-silico* ADMET predictions by using tools such as SwissADME and ProTox-2. The studies highlighted that the **7a** and **7b** analogues were devoid of any toxic effects. Based on the ADMET profiles and *in-vitro* PL inhibitory profiles, **7b** was finally selected for the *in-vivo* pharmacological evaluation. Four different studies were performed in the *in-vivo* experiments namely (1) Oral Triglyceride Tolerance Test (OTTT); (2) Anti-obesity studies using high fat diet (HFD) model development in mice (3) Quantification of faecal triglycerides and (4) Histopathological studies were performed. OTTT of **7b** was performed at three doses (5, 10 and 20 mg/kg) and the study revealed that the 10 and 20 mg/kg dose of **7b** significantly inhibited the absorption of triglyceride content. Thus, these doses (10 and 20 mg/kg) were

selected for further *in-vivo* experiments. The model was developed by feeding HFD to male *Swiss albino* mice and the induction of obesity was monitored weekly using body weight measurements and biochemical parameters (serum triglycerides (TG), total cholesterol (TC), high-density lipids (HDL) and low-density lipids (LDL) levels). After the induction of obesity, a four-week treatment with **7b** (10 and 20 mg/kg) and Orlistat was initiated. After four-week treatment the body weight of treatment group (**7b** and Orlistat) were lower as compared to the disease control group. Also, the biochemical parameters (TG, TC and LDL) were lowered as compared to the disease control group. The investigation into faecal triglyceride profiles yielded insights into the PL inhibitory characteristics of **7b**, wherein it demonstrated an anti-obesity impact similar in nature to that of Orlistat. The findings from the faecal triglyceride study offered insights into the PL inhibitory profiles of **7b**, revealing that it exhibited a comparable anti-obesity effect to Orlistat. Moreover, the estimation of faecal triglyceride levels unequivocally demonstrated that this anti-obesity effect was attributable to PL inhibition. Histopathology analyses of liver and adipose tissue following treatment with **7b** demonstrated that it inhibited adipocyte hypertrophy. Additionally, it decreased collagen levels, neutrophil infiltration, and other hepatic damages caused by prolonged HFD exposure. Further, normal hepatic function was not disrupted, and there was no evidence of hepatotoxicity.

Thus, utilizing structural modification and molecular modelling approaches, the research discussed in the thesis ultimately paved the way for the investigation of potent PL inhibitors that draw inspiration from alloimperatorin. In general, these findings may serve as motivation for further investigation into natural products containing bioactive coumarin or its synthetic analogues, with the aim of discovering novel antiobesity drugs or drug candidates.

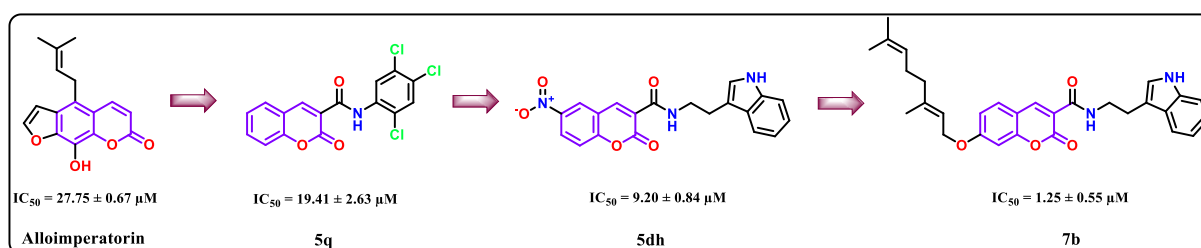


Table of Contents

Content	Title	Page No.
	<i>Declaration</i>	<i>i</i>
	<i>Certificate</i>	<i>ii</i>
	<i>Acknowledgements</i>	<i>iii</i>
	<i>Abstract</i>	<i>vi</i>
	<i>List of Tables</i>	<i>xi</i>
	<i>List of Figures</i>	<i>xiii</i>
	<i>List of Schemes and Formulae</i>	<i>xvi</i>
	<i>List of Abbreviations and Symbols</i>	<i>xvii</i>
Chapter 1	Introduction	1
Chapter 2	Literature Review, Aim and Objectives	28
Chapter 3	Materials and Methods	38
Chapter 4	Identification of NP Lead from <i>Aegle marmelos</i>	46
Chapter 5	Synthesis of Coumarin Analogues - Series I	67
Chapter 6	Synthesis of Coumarin Analogues - Series II	89
Chapter 7	Synthesis of Coumarin Analogues - Series III	118
Chapter 8	ADMET Prediction and <i>In vivo</i> experiments	149
Chapter 9	Conclusion, Future Perspectives and Limitations	164
	<i>Publications</i>	<i>A1</i>
	<i>Conferences</i>	<i>A2</i>
<i>Appendices</i>	<i>Brief Biography of the Supervisor</i>	<i>A4</i>
	<i>Brief Biography of the Candidate</i>	<i>A5</i>

List of Tables

#	Title	Page
Table 1.1	Summary of BMI based classification for overweight and obesity in different age groups	2
Table 1.2	Anti-obesity medications: approval, age group, mechanism of action, dose, adverse effects, and contraindications	4
Table 1.3	Clinical trials data for Orlistat and other drug combinations with Orlistat	11
Table 1.4	Protein Data Bank (PDB) of PL in the human species	17
Table 4.1	PL inhibition of selected plants using different extraction techniques with hexane and methanol	46
Table 4.2	Taxonomical classification of AM	48
Table 4.3	Summary of various coumarins and their pharmacological properties reported from AM	52
Table 4.4	Column dimensions and other parameters used in column chromatography	58
Table 4.5	Docking scores and interactions exhibited by isolated phytoconstituents from AM	62
Table 5.1	<i>In vitro</i> PL inhibitory activity of the synthesized analogues 5(a-q)	76
Table 5.2	K_m , V_{max} and K_i values of 5q and Orlistat retrieved from the PL enzyme kinetics	77
Table 5.3	Bimolecular quenching constant (k_q), binding constant (K_b) and the number of binding sites (n) at different temperatures for 5q	80
Table 5.4	MolDock score (kcal/mol) and interaction summary of 5(a-q) analogues at the active site of the PL	82
Table 6.1	<i>In vitro</i> PL inhibitory activity of the synthesized analogues (5a(a-i) , 5b(a-i) , 5c(a-i) and 5d(a-i))	102
Table 6.2	K_m , V_{max} and K_i values of 5dh and Orlistat retrieved from the PL enzyme kinetics	104
Table 6.3	Bimolecular quenching constant (k_q), binding constant (K_b) and the number of binding sites (n) at different temperatures for 5dh	106
Table 6.4	MolDock score (kcal/mol) and interaction summary of analogues (5a(a-i) , 5b(a-i) , 5c(a-i) and 5d(a-i)) at the active site of the PL	109

Table 7.1	<i>In vitro</i> PL inhibitory activity of the synthesized analogues (5e(a-i), 5f(a-i), 5g(a-i), 5h(a-i) and 7(a-b))	133
Table 7.2	K_m , V_{max} and K_i values of 7b and Orlistat retrieved from the PL enzyme kinetics	135
Table 7.3	Bimolecular quenching constant (k_q), binding constant (K_b) and the number of binding sites (n) at different temperatures for 7b	137
Table 7.4	MolDock score (kcal/mol) and interaction summary of analogues (5e(a-i), 5f(a-i), 5g(a-i), 5h(a-i) and 7(a-b)) at the active site of the PL	140
<hr/>		
Table 8.1	High Fat Diet Composition for development of obese mice	151
Table 8.2	Summary of ADMET parameters predicted for the potential analogues from each series along with alloimperatorin and Orlistat	154

List of Figures

#	Title	Page
Fig. 1.1	Lipid metabolic pathway of <i>Homo sapiens</i>	14
Fig. 1.2	Representation of open and closed lid forms of human PL (A) Hydrophobic surface representing the closed and open lid conformations (in brown); (B) Amino acid alignment in the active site	16
Fig. 1.3	Mechanism for hydrolysis of ester bond by PL	19
Fig. 1.4	(A) Orlistat (1), mechanism of action against PL (B) Metabolic degradation products (4-7)	21
Fig. 1.5	Plausible metabolite (9-12) for Cetilistat (8) using UPLC-QTOFMS/MS	22
Fig. 2.1	Examples of natural product leads and their corresponding synthetic products	29
Fig. 2.2	Biologically important oxygen heterocycles	30
Fig. 2.3	Examples of coumarin skeleton-based drugs	31
Fig. 2.4	Naturally occurring coumarin possessing <i>in vivo</i> anti-obesity activity	32
Fig. 2.5	Naturally occurring coumarin and isocoumarins with PL inhibitory activity	33
Fig. 2.6	Synthetic coumarin derivatives with PL inhibitory activity	34
Fig. 3.1	Secondary structure of the human PL-colipase complex co-crystallised with MUP at the active site (PDB Code: 1LPB)	39
Fig. 3.2	(A) Structure of MUP; (B) Superimposition of the re-docked pose of MUP (Yellow) with the co-crystallised pose (Red)	40
Fig. 3.3	The enzymatic hydrolysis of <i>p</i> -nitrophenyl butyrate (<i>p</i> -NPB) (A) in the absence of an inhibitor; (B) in the presence of an inhibitor	42
Fig. 4.1	<i>Aegle marmelos</i> , (A) The whole tree, (B) unripe fruit, (C) ripe fruit, (D) leaves and (E) trunk	47
Fig. 4.2	Alkaloids identified and isolated from the fruits of AM	49
Fig. 4.3	Coumarins identified and isolated from the fruits of AM	50
Fig. 4.4	Schematic flow of bioassay guided fractionation of methanolic extract of AM	58
Fig. 4.5	HPTLC of all the AM fractions (Mobile phase - Toluene: Ethyl acetate: Glacial acetic acid (7:3:0.1 % v/v/v))	60

Fig. 5.1	Rationale for selecting coumarin analogues as PL inhibitors	68
Fig. 5.2	2D poses of psoralen, xanthotoxol and alloimperatorin in the active site of PL	69
Fig. 5.3	Double reciprocal Lineweaver-Burk plots of 5q and Orlistat	77
Fig. 5.4	SAR study of coumarin analogues (Series I)	78
Fig. 5.5	(A) The fluorescence spectra of PL in the presence of 5q at various concentrations (pH 7.4, T = 298 K, a to h in increasing concentrations); (B) Stern-Volmer plot for the quenching of 5q on the PL	79
Fig. 5.6	2D and 3D interaction diagram of 5q and Orlistat in the active site of PL (1LPB)	81
Fig. 5.7	(A) RMSD plot of the protein-ligand (5q) complex (PDB ID: 1LPB); (B) Protein RMSF plot	85
Fig. 5.8	(A) Protein-ligand (5q) interaction bar charts stacked vertically (PDB ID: 1LPB); (B) Protein-ligand contact timeline (H-bonds, hydrophobic, ionic, water bridges)	86
Fig. 6.1	Rationale for designing series II coumarin analogues as PL inhibitors	89
Fig. 6.2	Double reciprocal Lineweaver-Burk plots of 5dh and Orlistat	103
Fig. 6.3	SAR study of coumarin analogues (Series II)	105
Fig. 6.4	(A) The fluorescence spectra of PL in the presence of 5dh at various concentrations (pH 7.4, T = 298 K, a to h in increasing concentrations); (B) Stern-Volmer plot for the quenching of 5dh on the PL	105
Fig. 6.5	2D and 3D interaction diagram of 5dh and Orlistat in the active site of PL (1LPB)	107
Fig. 6.6	(A) RMSD plot of the protein-ligand (5dh) complex (PDB ID: 1LPB); (B) Protein RMSF plot	113
Fig. 6.7	(A) Protein-ligand (5dh) interaction bar charts stacked vertically (PDB ID: 1LPB); (B) Protein-ligand contact timeline (H-bonds, hydrophobic, ionic, water bridges)	115
Fig. 7.1	Rationale for designing series III coumarin analogues as PL inhibitors	118
Fig. 7.2	Double reciprocal Lineweaver-Burk plots of 7b and Orlistat	134

Fig. 7.3	SAR study of coumarin analogues (Series III)	136
Fig. 7.4	(A) The fluorescence spectra of PL in the presence of 7b at various concentrations (pH 7.4, T = 298 K, a to h in increasing concentrations); (B) Stern-Volmer plot for the quenching of 7b on the PL	136
Fig. 7.5	2D and 3D interaction diagram of 7b and Orlistat in the active site of PL (1LPB)	138
Fig. 7.6	(A) RMSD plot of the protein-ligand (7b) complex (PDB ID: 1LPB); (B) Protein RMSF plot	145
Fig. 7.7	(A) Protein-ligand (7b) interaction bar charts stacked vertically (PDB ID: 1LPB); (B) Protein-ligand contact timeline (H-bonds, hydrophobic, ionic, water bridges)	146
<hr/>		
Fig. 8.1	The <i>in-vivo</i> experiments performed on <i>Swiss albino</i> mice	150
Fig. 8.2	Summary of various groups and treatment given for the <i>in-vivo</i> experiments	151
Fig. 8.3	Results of the OTTT summarising the serum triglyceride levels at various time points	155
Fig. 8.4	Body weights of animals after four week treatment	156
Fig. 8.5	Effect of 7b and Orlistat on various biochemical parameters determined after the treatment period	157
Fig. 8.6	Faecal triglyceride levels determined from various groups	158
Fig. 8.7	H&E Staining of liver	159
Fig. 8.8	PSR Staining of liver	159
Fig. 8.9	H&E Staining of Adipose tissue	160
<hr/>		

List of Schemes and Formulae

#	Title	Page
Scheme 5.1	Reagents and conditions: (a) K ₂ CO ₃ , H ₂ O, RT, 20 h; (b) DMF, 0 °C, EDC.HCl, HOBt, Ar-NH ₂ , DIPEA, 20-30 °C, 15-20 h	70
Scheme 6.1	Reagents and conditions: (a) K ₂ CO ₃ , H ₂ O, RT, 20 h; (b) DMF, 0 °C, EDC.HCl, HOBt, Ar-(CH ₂) _n -NH ₂ , DIPEA, 20-30°C, 15-20 h	90
Scheme 7.1	Reagents and conditions: (a) K ₂ CO ₃ , H ₂ O, RT, 20 h; (b) DMF, 0 °C, EDC.HCl, HOBt, Ar-(CH ₂) _n -NH ₂ , DIPEA, 20-30 °C, 15-20 h; (c) K ₂ CO ₃ , acetone, alkyl halides, reflux 60 °C	120
Formula 1.1	Calculation of BMI	1
Formula 3.1	Calculation for PL inhibition	42
Formula 3.2	Stern-Volmer equation	43
Formula 3.3	Modified Stern-Volmer equation	43
Formula 8.1	Calculation of LDL levels	152

List of Abbreviations and Symbols

%	Percentage
% CV	Percent coefficient of variation
% RSD	Percent relative standard deviation
% v/v	Percent volume by volume
% w/v	Percent weight by volume
Å	Angstrom
°C	Degree celsius
δ	Delta
μg	Microgram
μL	Microliter
μM	Micromolar
<i>p</i> -NPB	para-nitrophenyl butyrate
5-HT _{2C}	5-Hydroxytryptamine type 2C receptor
ADMET	Absorption, Distribution, Metabolism, Excretion and Toxicity
AM	<i>Aegle marmelos</i>
ANOVA	One-way analysis of variance
ATR	Attenuated total reflectance
BBB	Blood Brain Barrier
BMI	Body Mass Index
CB ₁	Cannabinoid type 1 receptor
CDCl ₃	Deuterated chloroform
CNS	Central Nervous System
Conc.	Concentration
CYP	Cytochrome P
Da	Dalton
DCM	Dichloromethane
DMF	Dimethyl formamide
DMSO	Dimethyl sulfoxide
DMSO- <i>d</i> ₆	Deuterated Dimethyl sulfoxide
e.g.	Example
ESI	Electrospray ionization
eV	Electron volt
FDA	Food and drug administration
Fig	Figure
g	gram
GABA	Gamma aminobutyric acid
GI	Gastro-Intestinal
GLP-1	Glucagon like peptide type 1 receptor
h	Hour
H & E	Hematoxylin and Eosin staining
HCl	Hydrochloric acid

HDL	High-density lipoproteins
HFD	High Fat Diet
HoBt	Hydroxybenzotriazole
HPLC	High Performance Liquid Chromatography
HPTLC	High Performance Thin Layer Chromatography
HRMS	High Resolution Mass Spectrometry
<i>i.e</i>	That is
IC ₅₀	Half maximal inhibitory concentration
ICH	International Conference on Harmonization
IEAC	Institutional animal ethics committee
K	Kelvin
kcal/mol	Kilocalorie per mole
kg	kilogram
KOH	Potassium hydroxide
LCMS	Liquid Chromatography Mass Spectrometry
LD ₅₀	Half maximal Lethal Dose
LDL	Low-density lipoproteins
m.p.	Melting point
MD	Molecular Dynamics
mg	Milligram
mins	Minutes
mL	Millilitre
mM	Millimolar
MQC	Mid quality control
MUP	Methoxyundecyl phosphinic acid
ng	Nanogram
NMR	Nuclear Magnetic Resonance
NP	Natural Product
NPD	Normal Pellet Diet
NPT	Number of particles, Pressure and Temperature
ns	not significant
NVT	No. of particles, Volume and Temperature
OTTT	Oral Triglyceride Tolerance Test
PDB	Protein Data Bank
Pgp	P-glycoprotein
PL	Pancreatic lipase
PRS	Picrosirius red staining
RMSD	Root Mean Square Deviation
rpm	Rotations per minute
RSD	Relative Standard Deviation
RT	Room Temperature
S.E.M	Standard error of mean
SD	Standard Deviation

STEPS	STEPwise Approach to Surveillance
TC	Total cholesterol
TCM	Traditional Chinese Medicine
TEA	Triethylamine
TG	Triglycerides
TLC	Thin Layer Chromatography
US	United States
UV	Ultraviolet
WHO	World Health Organization
WHR	Waist-Hip Ratio

Introduction

1. Introduction

1.1. Obesity

1.1.1. Definition, etymology and statistics

The epidemic of obesity has been called as a “silent public health crisis” due to its pervasiveness throughout the globe and its failure to garner enough attention [1]. Obesity is derived from the Latin word ‘*Obesitas*’, which means “fat, stout, or plump” (*Ob* - over; *Esus* - eating) [2]. Definition of obesity states it as an abnormal increase in body fat due to a persistent discrepancy between food intake and energy expenditure over time [3]. Amongst various metabolic illness, Type 2 diabetes [4], dyslipidemia [5], non-alcoholic fatty liver disease [6], and cancer are the chronic metabolic illnesses that are linked to obesity [7]. Obesity can be prevented and treated with a wide variety of pharmacological therapies, surgical procedures, and behavioural health programmes that emphasize lifestyle modification. However, achieving this aim might take a long time [8,9]. Thus, understanding pharmacological treatments is crucial as they are still an important choice of therapy.

According to recent report published by the World Obesity Federation (WOF), an investigation was conducted to examine and forecast the worldwide prevalence of obesity between 2010 and 2030. The findings of this study indicated that by the year 2030, the number of individuals classified as obese is projected to exceed 1 billion. Among this population, it is estimated that around 250 million will consist of children and adolescents [1]. Another report from the World Obesity Report states that, “Over the past two decades, obesity rates have risen in almost every age group across the globe. An estimated 268 million children and 2.7 billion adults will be overweight or obese by 2025.” [10]. Obesity, was previously classified as a metabolic disorder but recently has been reclassified as a chronic, relapsing progressive disease process by the WOF in 2017 [11].

1.1.2. Classification

The Body Mass Index (BMI), which is computed utilizing the given formula, is initially employed to categorize overweight and obesity.

$$\mathbf{BMI} = \frac{\text{weight of the individual (in kg)}}{\text{square of the height of the individual (in m}^2\text{)}} \text{-----} \boxed{\text{Formula 1.1}}$$

As indicated in **Table 1.1**, body mass index (BMI) classification for overweight is 25-29.9 kg/m², whereas for obesity is exceeding 30 kg/m². Likewise, the determination of overweight and obesity in children below the age of 5 or between 5-19 years is conducted utilizing the WHO Growth Reference Medians [12-14].

Table 1.1. Summary of BMI based classification for overweight and obesity in different age groups

	Adults (>19 years)	Children (5-19 years)	Children (< 5 years)
Overweight	25 - 29.9 kg/m ²	BMI-for-age > 1 standard deviation above WHO Growth Reference Median	BMI-for-age > 2 standard deviations above WHO Growth Reference Median
Obesity	30 - 34.9 kg/m ² (Class I) 35 - 39.9 kg/m ² (Class II) ≥ 40 kg/m ² (Class III)	BMI-for-age > 2 standard deviations above WHO Growth Reference Median	BMI-for-age > 3 standard deviations above WHO Growth Reference Median

Although consistent evidence suggests that BMI is a highly specific metric, its sensitivity in classifying individuals as overweight or obese has been reported to range from low to moderate. For example, existing literature indicates that approximately 50% of adults who have surplus body fat are classified as non-obese based on their BMI. An equivalent proportion (ranging from 25-50%), of children and adolescents who have surplus body fat are classified as having a healthy BMI for their age [15-17].

In contrast to BMI, the Waist-Hip Ratio (WHR) is an additional metric utilized to ascertain obesity and is regarded as a more precise indicator. The waist and hip circumferences are measured in accordance with the WHO STEPwise Approach to Surveillance (STEPS), which stipulates the following:

1. The waist circumference should be approximated at the midpoint between the upper margin of the final palpable rib and the apex of the iliac crest.
 2. Determining the hip circumference necessitates locating the broadest point of the buttocks.
- In addition, the subject's posture and the tape's tension must be maintained in accordance with the STEPS protocol. Individuals with a WHR exceeding 0.85 (for women) or 1.00 (for males) are categorized as obese [18].

1.1.3. Treatment

In order to attain substantial weight loss, the existing recommendations put forth by the American Heart Association/American College of Cardiology/The Obesity Society (AHA/ACC/TOS) stipulate a minimum daily caloric restriction of 500 kcal. To achieve this, individuals should engage in physical activity and modify their diet [19]. However, in cases where lifestyle modification fails to produce the desired results, additional approaches such as bariatric surgery or anti-obesity pharmacotherapy is required in order to attain substantial

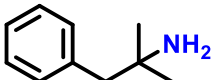
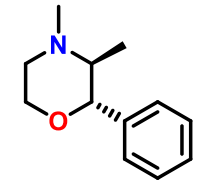
CHAPTER I

weight loss [20]. Bariatric surgery is exclusively advised for patients who meet the following criteria: $\text{BMI} \geq 40 \text{ kg/m}^2$ or $\text{BMI} \geq 35 \text{ kg/m}^2$ with comorbidities. In contrast, anti-obesity pharmacotherapy is recommended for the remaining categories of obese patients who do not meet the surgical eligibility criteria [21].

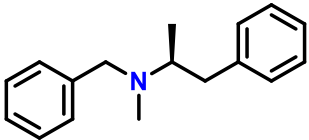
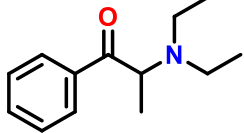
Numerous medications have been approved for the treatment of obesity since the 1930s; nevertheless, the majority of these drugs were withdrawn during post-marketing surveillance due to their severe adverse effects. At present, the FDA has granted approval to twelve primary anti-obesity medications. A concise summary of the FDA approved drugs used in the treatment of obesity is given in **Table 1.2**. [22-25].

CHAPTER I

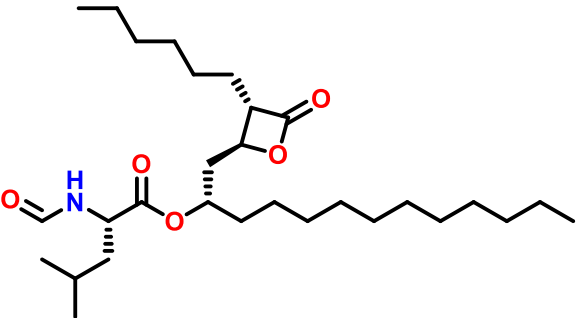
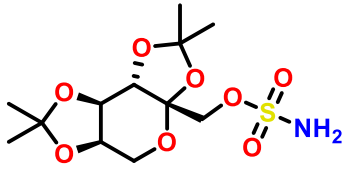
Table 1.2. Anti-obesity medications: approval, age group, mechanism of action, dose, adverse effects, and contraindications [26,27].

Drug (dosage)	Approval FDA/EMA (year)	Approved for age group	Mechanism of action	Dose/ Administration	Adverse effects ^a	Contraindications ^b in
<p>Phentermine</p> 	FDA 1959	Adults and children (17 years of age and older)	Appetite suppressors	15 mg or 37.5 mg orally once daily; 8 mg orally 2-3 times daily; can start with a quarter or a half of a 37.5 mg tablet once daily and titrate upwards to a maximum dosage of 37.5 mg	Increase in HR and/or BP, dizziness, dry mouth, constipation, insomnia and irritability	Patient of drug abuse, allergic to sympathomimetic amine drugs (monoamine oxidase inhibitor (MAOI)), cardiovascular disease, hyperthyroidism, or glaucoma, pregnancy, or breast-feeding
<p>Phendimetrazine</p> 	FDA 2010	Adults and teenagers (17 years of age and older)	Norepinephrine-dopamine releasing agent (NRDA), appetite suppressors	Immediate-release 35 mg tablets twice or thrice a day (before meals), 105 mg extended-release capsule for once a day before breakfast	Anxiety, chest pain or discomfort, difficult or painful urination, dizziness, dry mouth, headache, hyperventilation, nausea, vomiting,	Patient with MAOI therapy, alcohol consumption, pregnancy, or breast-feeding

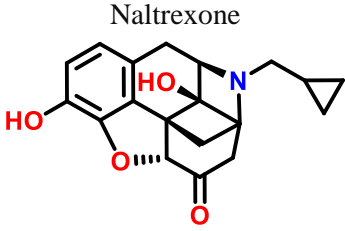
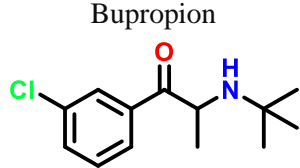
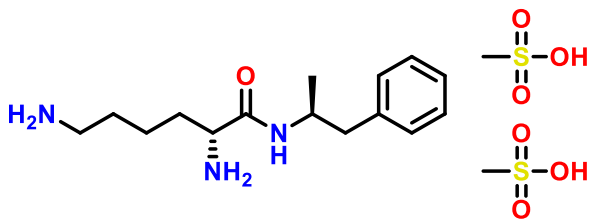
CHAPTER I

					weakness, insomnia and irritability	
<p>Benzphetamine</p> 	FDA 2010	Adults	Appetite suppressors	25 to 50 mg once a day	Agitation, anxiety, confusion, dizziness, fast, irregular, pounding, or racing heartbeat, itching, skin rash, numbness or tingling in the arms or legs, seizures, sweating, insomnia	Patient with MAOI therapy, pregnancy or breast-feeding
<p>Diethylpropion</p> 	FDA 2011	Adults	NRDA and appetite suppressors	ER tablets (75 mg once a day), immediate-release formulation (one 25 mg tablet three times daily)	Dry mouth, unpleasant taste, restlessness, anxiety, dizziness, depression, tremors, upset stomach, vomiting,	Patient with drug abuse, guanethidine, insulin, and MAOI therapy, anorectic agents, pregnancy, or breast-feeding

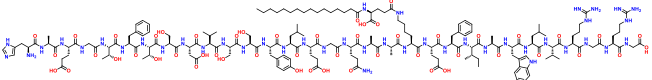
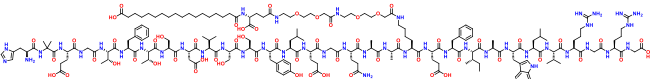
CHAPTER I

					increased urination	
<p>Orlistat</p>  <p>The chemical structure of Orlistat is a lipase inhibitor. It features a central chiral carbon atom bonded to a butyl group (wedge), a propyl group (dash), a 2-oxo-1,3-dioxolane ring (wedge), and a 1,3-bis(4-oxo-4-oxopentyl)propan-2-yl group (wedge). The propyl group is further substituted with an isopropyl group and a formamide group.</p>	<p>FDA 1999 EMA 1998</p>	<p>Adults and children (ages 12 years and older)</p>	<p>Pancreatic and gastric lipase inhibitor, inhibits dietary lipid digestion</p>	<p>60 mg OTC, 120 mg orally three times daily</p>	<p>Flatulence, bloating and diarrhea</p>	<ul style="list-style-type: none"> - Patients with chronic malabsorption syndrome or cholestasis, pregnancy - Rare cases of severe liver injury have been reported - Avoid taking with cyclosporine
<p>Phentermine/ topiramate ER</p>  <p>The chemical structure of Phentermine/topiramate ER is a combination of two drugs. It consists of a phentermine moiety (a phenethylamine derivative) and a topiramate moiety (a cyclohexane ring with two ester groups and a sulfonamide group). The phentermine moiety is attached to the topiramate ring via an ester linkage.</p>	<p>FDA 2012</p>	<p>Adults and children (ages 12 years and older)</p>	<p>Appetite suppressors, altered satiety perception</p>	<p>Start with 3.75/23 mg orally once daily for 14 days; increase to 7.5/46 mg once daily and monthly titration upwards to achieve weight loss; discontinue if < 3 % weight loss on 11.25/69 mg or < 5 % weight loss on a maximum dose of 15/92 mg after 12 weeks</p>	<p>Peripheral neuropathy (usually transient), dyspepsia, insomnia, constipation and dry mouth</p>	<p>Patient with glaucoma, hyperthyroidism, during or within 14 days following the administration of MAOI therapy, hypersensitivity to sympathomimetic amines, pregnancy, or breastfeeding</p>

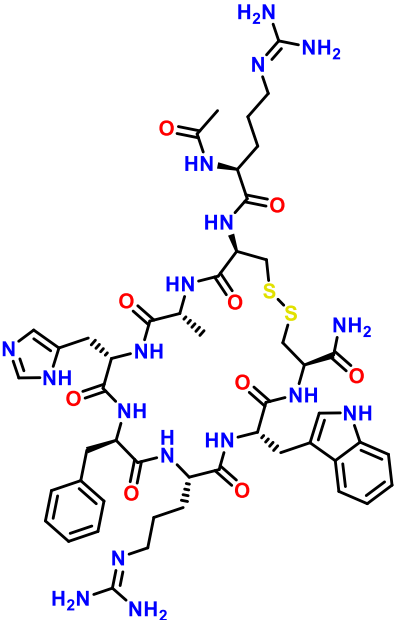
CHAPTER I

<p>Naltrexone</p>  <p>Bupropion</p> 	<p>FDA 2014 EMA 2015</p>	<p>Adults</p>	<p>Appetite suppressors, Opioid receptor antagonist/aminoketone antidepressant</p>	<p>Naltrexone SR (8 mg)/ Bupropion SR (90 mg), Upwards titration over 4 weeks to a maximum of two tablets twice daily</p>	<p>Nausea, constipation, headache, vomiting, dizziness, dry mouth and diarrhea</p>	<p>Patients with chronic opioid use, acute opioid withdrawal, uncontrolled hypertension, seizure disorder, bulimia or anorexia nervosa, abrupt discontinuation of alcohol, benzodiazepines, barbiturates, and antiseizure drugs; concomitant use of MAOIs therapy, patient receiving linezolid, pregnancy</p>
<p>Lisdexamfetamine dimesylate</p> 	<p>FDA 2007</p>	<p>Adults</p>	<p>CNS stimulant, helps manage symptoms of binge eating disorder by blocking dopamine and norepinephrine reuptake and increasing their levels in</p>	<p>50 mg to 70 mg per day</p>	<p>Sleepiness, dizziness, headache, dry mouth, constipation, diarrhea, nausea, weight loss</p>	<p>Patients with MAOI therapy, alcohol consumption, pregnancy, or breastfeeding</p>

CHAPTER I

			the extra neuronal space			
<p style="text-align: center;">Liraglutide</p> 	<p>FDA 2014 EMA 2015</p>	<p>Adults and children (ages 12 years and older)</p>	<p>Reduces appetite and slows digestion, glucagon-like peptide-1 (GLP-1) receptor agonist</p>	<p>Start with 0.6 mg subcutaneously once daily for 7 days; titrate upwards weekly to 1.2 mg, 2.4 mg, and then the maximum dosage of 3.0 mg once daily</p>	<p>Nausea, hypoglycemia, diarrhea, constipation, vomiting, headache, decreased appetite, dyspepsia, abdominal pain, fatigue, dizziness, increase in lipase levels and suicidal behavior or ideation</p>	<p>Patients with personal or family history of medullary thyroid carcinoma or multiple endocrine neoplasia syndrome type 2, pregnancy</p>
<p style="text-align: center;">Semaglutide</p> 	<p>FDA 2021 EMA 2021</p>	<p>Adults and children (ages 12 years and older)</p>	<p>Appetite suppressors, mimics a hormone called GLP-1 that targets areas of the brain that regulate appetite and food intake</p>	<p>Start with 0.25 mg (week 1-4), 0.5 mg (week 5-8), 1 mg (week 9-12), 1.7 mg (week 13-16), 1.7 mg or 2.4 mg (week 17 and onward)</p>	<p>Nausea, diarrhea, vomiting, constipation, abdominal pain, headache, fatigue</p>	<p>Patients with personal or family history of medullary thyroid carcinoma or in patients with multiple endocrine neoplasia syndrome type 2, pregnancy, use with other anti-obesity drugs</p>

CHAPTER I

<p style="text-align: center;">Setmelanotide</p> 	<p style="text-align: center;">FDA 2020 EMA 2021</p>	<p>People aged 6 years and older with obesity due to three specific rare genetic conditions only (proopiomelanocortin (POMC) deficiency, proprotein convertase subtilisin/kexin type 1 (PCSK1) deficiency & leptin receptor (LEPR) deficiency)</p>	<p style="text-align: center;">Melanocortin 4 Receptor Agonist</p>	<p>Starting dose: 2 mg Subcutaneous (SC) once for 2 weeks, then if tolerated increase the dose to 3 mg and if not then reduced to 1 mg</p>	<p>Injection site reactions, hyperpigmentation, nausea, headache, diarrhea, vomiting, abdominal pain</p>	<p style="text-align: center;">Patients with pregnancy or breastfeeding</p>
--	--	--	--	--	--	---

Abbreviations: EMA - European Medicines Agency; FDA - Food and Drug Administration; GI - gastrointestinal; GLP-1 - Glucagon-like peptide 1; MAOIs - Monoamine Oxidase Inhibitors; MC4R - Melanocortin-4 Receptor; NE - Norepinephrine. POMC - Proopiomelanocortin; PCSK1 - Proprotein Convertase Subtilisin/Kexin type 1; LEPR - Leptin Receptor. ^aAdverse events presented here are those that are present in more than 10% of the population, based on the FDA approval leaflet. ^bContraindications are based on the FDA approval leaflet.

Nevertheless, the majority of these drugs targets (except Orlistat) appetite suppression, which would impede overall nutrient consumption and therefore cannot be regarded as a legitimate strategy. Currently, Orlistat is the only clinically prescribed antiobesity drug which prevents the digestion and absorption of fat by inhibiting pancreatic lipase (PL). Thus, it is evident from the data that: (i) the majority of the targets being investigated for the treatment of obesity are centred around appetite suppression and are associated with severe adverse effects; and (ii) the food environment containing a higher percentage of dietary fats is responsible for the worldwide increase in obesity. Therefore, it can be concluded that inhibiting PL is a validated therapeutic target for obesity, as it prevents the digestion and absorption of dietary fat. Furthermore, the PL inhibition does not require any systemic absorption, which eliminates the possibility of unintended consequences. Further, the clinical investigation of other drug/phytoconstituents and Orlistat-based combination therapies are being conducted and these various clinical studies are summarised in the **Table 1.3** [28].

CHAPTER I

Table 1.3. Clinical trials data for Orlistat and other drug combinations with Orlistat.

NCT Number	Study Title	Interventions	Location	Ages Eligible for Study	Accepts Healthy Volunteers	Phases	Study Status
NCT03675191	Orlistat/Phentermine Versus Placebo/Phentermine	Drug: Orlistat 120 mg Cap, Drug: Phentermine Pill	Korea, Republic of	20 Years and older	No	NA	Completed
NCT03582722	Weight Loss Aid in an Exposed Population	Drug: Orlistat, Drug: Placebo capsule	United States	18 Years and older	No	IV	Completed
NCT05076474	Pharmacodynamic Equivalence Study of Orlistat Capsules 60 mg	Drug: Orlistat 60 mg Cap	China	18 Years and older	Yes	NA	Completed
NCT03799198	Real World Effectiveness of Combining an Employer-based Weight Management Program with Medication for Chronic Weight Management in Employees with Obesity	Other: Weight Management Program (WMP), Drug: Medication for chronic weight management (R _x)	United States	18 Years and older	No	IV	Completed
NCT02372526	The Effect of Different Macronutrients on Gastrointestinal Hormone Secretion After Gastric Bypass Operation	Other: mealtest: high protein 200 kcal/200 mL liquid meal consumed during 10 min, Other: mealtest: high fat 200 kcal/200 mL liquid meal consumed during 10 mins, Other: mealtest: high	Denmark	25 Years to 55 Years	Yes	NA	Unknown

CHAPTER I

		carbohydrate 200 kcal/200 mL liquid meal consumed during 10 mins, other: mealtest: high fat 200 kcal/200 mL liquid meal with PL inhibitor consumed during 10 mins					
NCT05069298	Effect of Silibinin(A) as a Potential Anti-obesity Agent	Dietary Supplement: Silibinin A	Spain	18 Years to 60 Years	Yes	NA	Active (Not Recruiting)
NCT05934110	Study Exploring the Supportive Effect of Acarbose in Weight Management	Drug: EMP16-120/40, Drug: MR Orlistat 120 mg, Drug: Conventional Orlistat 120 mg, Drug: EMP16-60/20, Drug: Placebo	Sweden	18 Years and older	No	II	Recruiting
NCT05579249	A Research Study Comparing Wegovy to Other Weight Management Drugs in People Living with Obesity in America	Drug: Semaglutide, Drug: Orlistat, Drug: Phentermine/Topiramate, Drug: Naltrexone/Bupropion, Drug: Liraglutide	United States	18 Years and older	No	IV	Recruiting

Abbreviations: Cap - Capsule; NA-Not applicable

1.2. Pancreatic lipase (PL)

1.2.1. Structure of PL

Triglyceride lipases (3.1.1.3) are lipolytic enzymes that hydrolyses triacylglycerol (TAG), ester bonds. Lipases are commonly found in animals, plants, and prokaryotes [29,30]. In higher vertebrates, at least three tissue-specific isozymes exist namely, gastric/lingual, hepatic and pancreatic lipase. Lipoprotein lipase (3.1.1.34), which hydrolyses chylomicron and very low density lipoprotein (VLDL), TAG, is closely linked to these lipases [29]. By hydrolysing dietary long chain TAG to free fatty acids (FA) and monoacylglycerols (MAG) in the intestinal lumen, PL plays a crucial role in dietary fat absorption [31,32]. PL exhibits the highest activity at alkaline pH within the range of 7.3-9.0. It is a mesophilic enzyme that exhibits maximum activity for hydrolysis of TAG at 35-40 °C [32-34]. The influence of biliary salts on PL is an additional important aspect of lipase activity in the duodenum. Low bile salt concentrations stimulate PL activity, whereas high concentrations inhibit it. Colipase is an additional protein that interacts with interfaces between bile salts, and PL [35].

1.2.2. Function of PL in the pathway

Lingual and gastric lipases are endogenous to humans and aid in the digestion of fats. For short and medium-chain triglycerides, gastric lipase preferentially cleaves at position *sn*-3 and hydrolyse 25-30 % of ingested TAG into diglycerides (DAG) and FA. Pancreatic acinar cells secrete PL, a crucial pancreatic enzyme responsible for the metabolism of dietary 50-70 % TAG in the proximal small intestine. PL hydrolyzes long-chain TAG preferentially at position *sn*-2, leading to the formation of FA and MAG (**Fig 1.1**) [36-44]. PL has a high degree of solubility in aqueous solutions and functions at the interface of oil droplets. The digestion of dietary lipids commences with the emulsification of stable emulsion particles, that serve as PL substrates. PL is required for fat absorption by intestinal enterocytes. The accessibility to the PL active site is regulated by the lid's aperture, that in its closed state, conceals the hydrophobic surface around the active site. The lid exhibits an opening response while encountering an oil-water interface, a phenomenon known as interfacial activation [36]. The functionality of the PL requires the presence of a protein cofactor, (namely colipase), in order to mitigate the inhibitory impact exerted by bile salts. Secreted procolipase in the duodenum is activated by trypsin to colipase that is then activated to complex with PL for dietary TAG digestion [36-38].

CHAPTER I

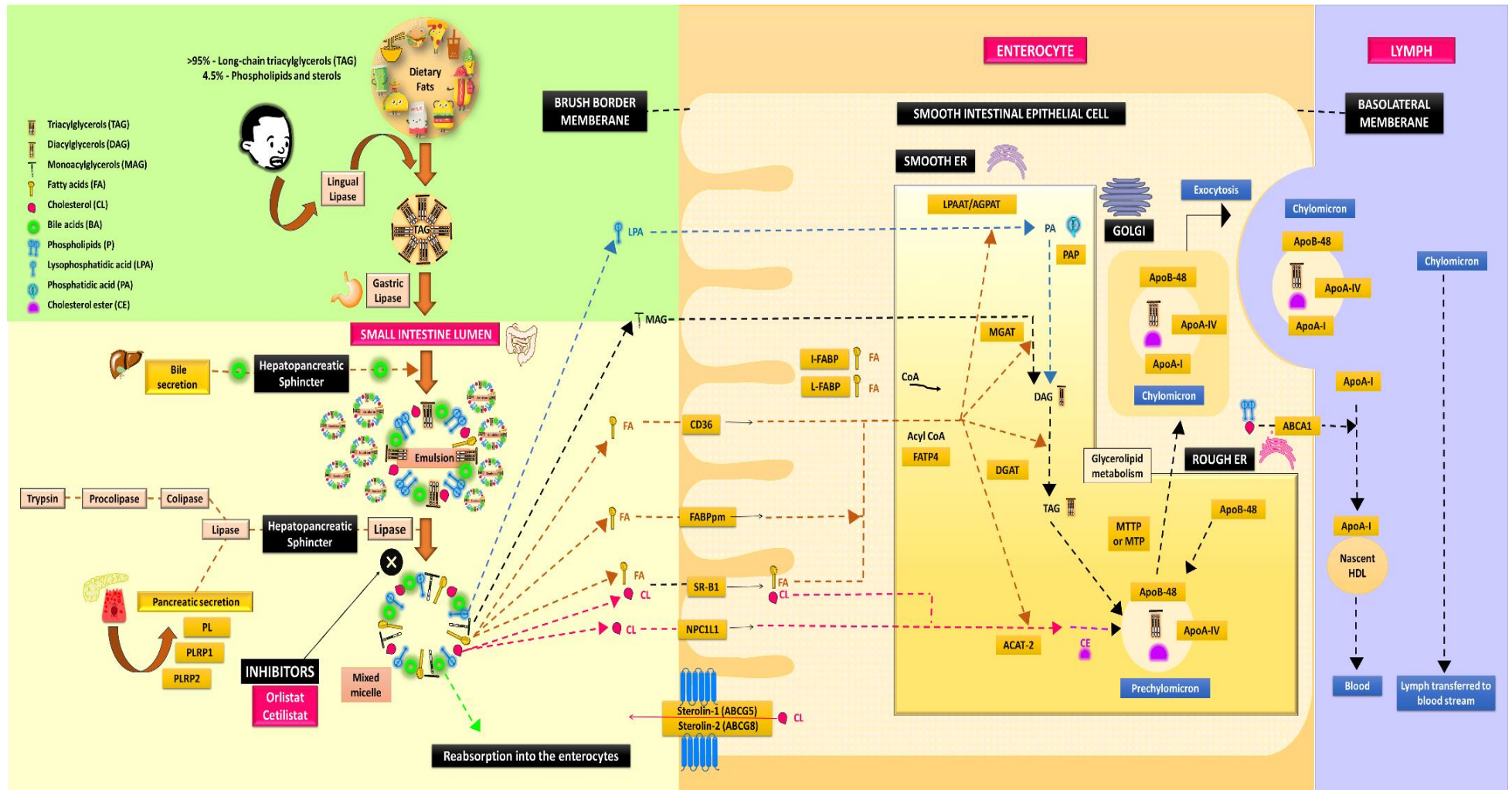


Figure 1.1. Lipid metabolic pathway of *Homo sapiens*.

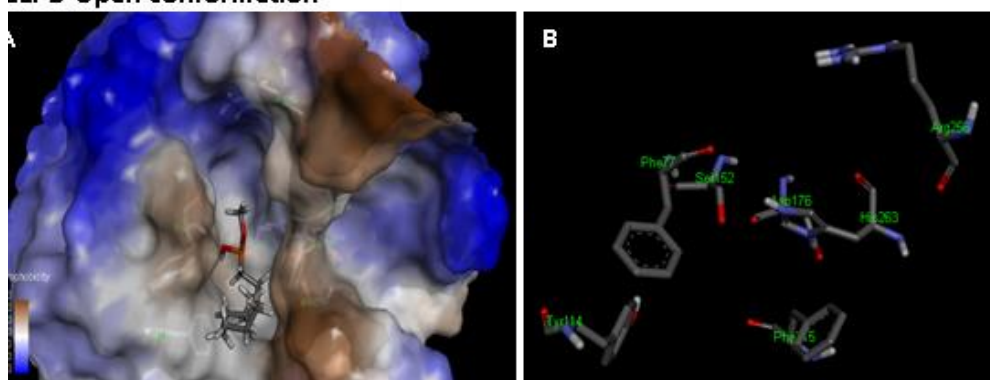
CHAPTER I

The **Fig 1.1** depicts the lipid metabolic pathway of *Homo sapiens*. The dietary fat is an essential source of energy. TAG comprise more than 95% of dietary fat, with phospholipids (4.5%) and sterols comprising the remainder. Bile and pancreatic enzymes reach the lumen of the small intestine *via* the hepatopancreatic sphincter in the upper duodenum. PL converts dietary TAG to FA and MAG in the lumen of the small intestine. The phospholipids (P) and bile acids (BA) present in bile then emulsify these substances to form micelles [37-39]. In order to be absorbed, MAG, lysophosphatidic acid (LPA), and cholesterol (CL) must first undergo reacylation after entering the enterocyte. Monoacylglycerol acyltransferase (MGAT) and diacylglycerol acyltransferase (DGAT) enzymes sequentially acylate MAG to form TAG. Lysophosphatidic acid acyltransferase (LPAAT) converts LPA to phosphatidic acid (PA), which is then dephosphorylated by phosphatidic acid phosphorylase (PAP) to yield DAG. Acyl-CoA: cholesterol acyltransferase (ACAT-2) converts dietary CL to cholesteryl esters (CE) [40]. FAT/CD36 (Fatty acid translocase/cluster determinant 36) appears to play an important role in the absorption of long-chain fatty acids in the small intestine [40]. The FA are subsequently obligated to either intestinal-type fatty acid-binding protein (I-FABP), liver-type fatty acid-binding protein (L-FABP) or FABPpm, plasma membrane fatty acid binding protein, while the MAG is bound to L-FABP. Alternatively, the FA can be acylated to CoA through the activity of fatty acid transport protein 4 (FATP4) within the endoplasmic reticulum (ER) and further converted to TAG [39-41]. Enterocyte brush border membrane (BBM) expresses SR-BI, an 82-kDa protein, near the top of intestinal villus and in the proximal gut, where cholesterol absorption occurs [42]. The protein known as Niemann-Pick C1-like 1 (NPC1L1) act as a transporter responsible for the inflow of sterols [43]. It is mostly found in the apical membrane of the enterocyte, where it plays a role in facilitating the active absorption of cholesterol. This is achieved by encouraging the passage of sterols through the brush border membrane of the enterocyte. Cholesterol is acylated to cholesterol esters (CE) after absorption [39,42]. ABCA1 (ATP-binding cassette (ABC) transporter) dominates intestinal cell basolateral expression and effluxes cholesterol on HDL particles [39]. Within the ER, TAG combines with CE and apolipoprotein B (apoB) with the aid of microsomal triglyceride transfer protein (MTP or MTTP) to produce chylomicrons, which are subsequently released into the lymphatic system [39]. The ABCG5 and ABCG8 transporters are responsible for facilitating the active removal of cholesterol and plant sterols from enterocytes, therefore promoting their export from the apical side of the cell into the intestinal lumen for subsequent excretion [40,44].

1.2.3. PL and its crystal structure

Till date 3 crystal structure of human PL have been reported (**Table 1.4**). X-ray crystallography of human PL has revealed that it as a single-chain glycoprotein of 449 amino acids. Structural evidence suggest that Ser 152 is the essential nucleophilic residue for catalysis [45]. This residue is located in the N-terminal domain at the C-terminal edge of a parallel β -sheet and is part of an Asp-His-Ser triad. Therefore, the putative hydrolytic site is inaccessible to solvent as it is covered by a surface loop. Interfacial activation is believed to involve a reorientation of this flap in PL [45,46]. This catalytic triad is protected by a hydrophobic lid domain, comprised of Gly 76 - Lys 80 and Leu 213 - Met 217 amino acids, which prevents solvents and substrates from entering the active sites. On the contrary, when the PL is activated, a conformational alteration occurs in the lid domain, which subsequently opens the active site (**Fig 1.2**). The conformational change is additionally facilitated by the formation of a salt bridge between Arg 256 - Asp 257 with Tyr 267 - Lys 268 [32]. X-ray diffraction has been used to determine the crystal structures of both conformations, which have been subsequently deposited in the PDB under the accession numbers 1LPB (open conformation) and 1N8S (closed conformation) [47].

1LPB-Open conformation



1N8S-Closed conformation

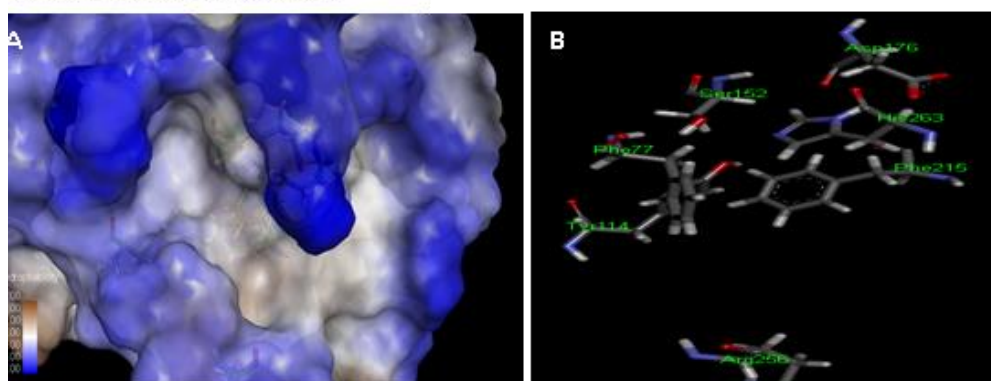


Figure 1.2. Representation of open and closed lid forms of human PL. (A) Hydrophobic surface representing the closed and open lid conformations (in brown); (B) Amino acid alignment in the active site.

Table 1.4. Protein Data Bank (PDB) of PL in the human species [47].

PDB ID	Title	Released	Method	Organisms	Macromolecule	Unique Ligands	Chains	Sequence Length
1LPA	Interfacial Activation of The Lipase-Procolipase Complex by Mixed Micelles Revealed by X-Ray Crystallography	1994-11-01	X-ray diffraction 3.04 Å	<i>Homo sapiens</i> (lipase), <i>Sus scrofa</i> (colipase)	Colipase (protein), PL (protein)	BNG, Ca, PLC	Colipase - Chain A, Lipase - Chain B	Colipase - 95, Lipase - 449
1LPB	The 2.46 Angstroms Resolution Structure of The Pancreatic Lipase Colipase Complex Inhibited By A C11 Alkyl Phosphonate	1994-11-01	X-ray diffraction 2.46 Å	<i>Homo sapiens</i> (lipase), <i>Sus scrofa</i> (colipase)	Colipase (protein), PL (protein)	BOG, Ca, MUP	Colipase - Chain A, Lipase - Chain B	Colipase - 95, Lipase - 449
1N8S	Structure of the pancreatic lipase-colipase complex	2002-12-18	X-ray diffraction 3.04 Å	<i>Homo sapiens</i> (lipase), <i>Sus scrofa</i> (colipase)	PL (protein), colipase II (protein)	-	Colipase II - Chain B, Lipase - Chain A	Colipase II - 95, Lipase - 449

BNG - nonyl β -D-glucopyranoside, Ca - Calcium ion, PLC - Diundecyl Phosphatidyl Choline, BOG - octyl β -D-glucopyranoside, MUP - Methoxyundecylphosphinic acid.

1.2.4. Activation of PL and digestion of lipids

The physiology of lipid digestion involves a series of events, as depicted in the **Fig 1.3**. The negative charge on Asp 176 changes the pKa of His 263, increasing its basicity. By deprotonating Ser 152, His 263 functions as a base that prepares Ser 152 for a nucleophilic attack on the carbonyl carbon of the ester bond [48]. This results in the formation of a negatively charged tetrahedral intermediate, which is stabilised by the oxyanion cavity created by the main chain amides of Phe 77 and Leu 153 [49,50]. As the carbonyl is reformed, the ester bond is severed, and His 263 protonates the leaving group. His 263 then once more acts as base, deprotonating a water molecule to activate it for nucleophilic attack on the substrate carbonyl. A second negatively-charged tetrahedral intermediate is formed, which is again stabilised by the oxyanion hole. As the carbonyl is reformed, the bond between the substrate and Ser 152 is severed, and Ser 152 is re-protonated by His 263 [50-53].

CHAPTER I

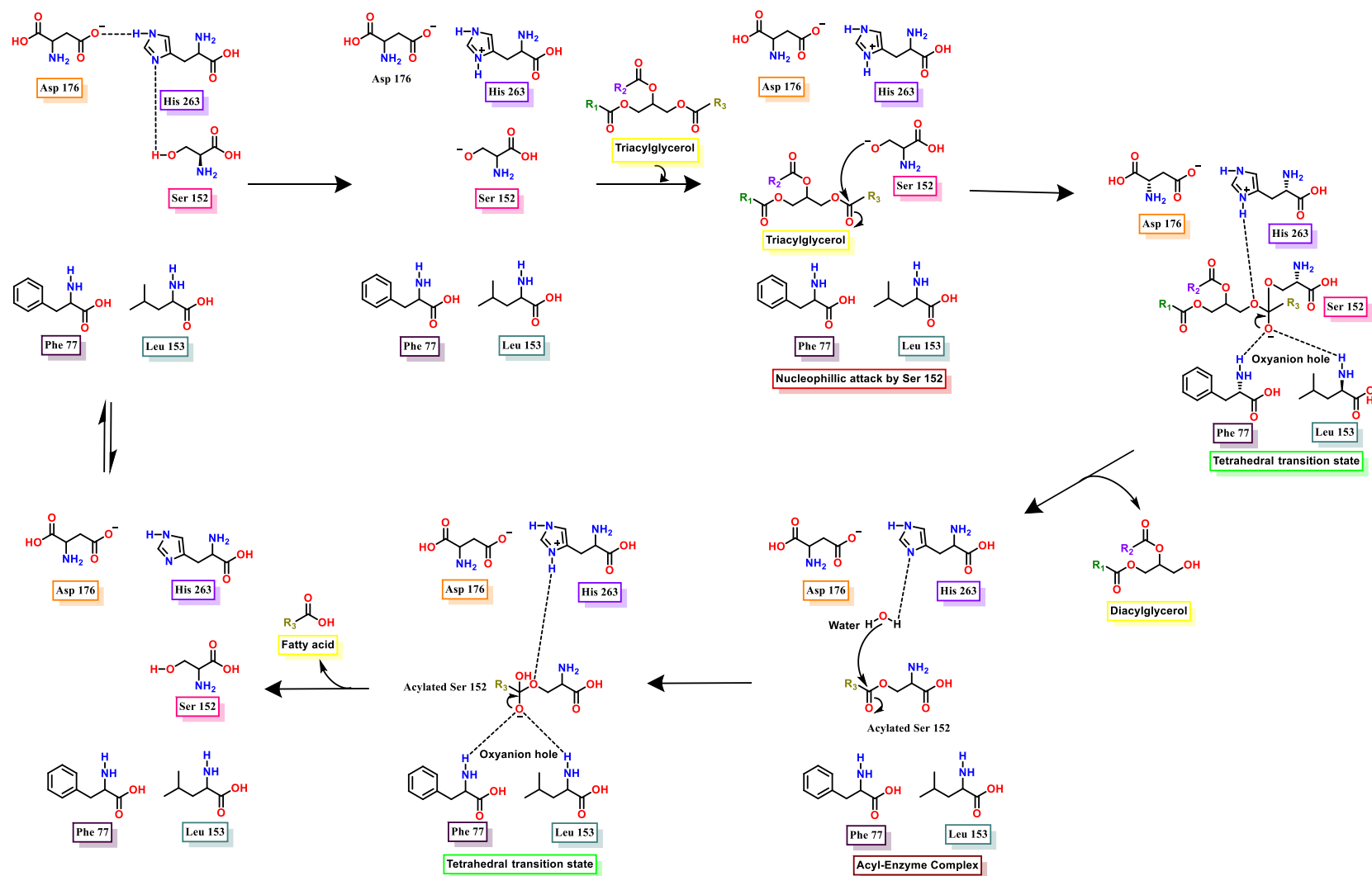


Figure 1.3. Mechanism for hydrolysis of ester bond by PL. The catalytic triad consists of Ser 152, His 263, and Asp 176; Phe 77 and Leu 153 are the residues in the oxyanion hole and substrate is TAG. The diagram presented above illustrates (a) the nucleophilic attack of the serine hydroxyl on the carbonyl carbon of the TAG ester bond, (b) the tetrahedral transition state, and (c) the acyl-enzyme complex.

1.2.5. Pharmacological targeting of PL

1.2.5.1. *In-vivo* mechanism of action and metabolism of Orlistat

PL has been widely studied for development of inhibitors that have been reviewed [54]. Lipstatin, (isolated from *Streptomyces toxitricini*) and its derivative tetrahydrolipstatin are the first selective irreversible lipase inhibitors [55,56]. Orlistat, a hydrogenated derivative of lipstatin, inhibits gastric and PL and reduces dietary fat absorption. Orlistat exerts its effects by covalently binding to the Ser152 at the active site of gastric and PL. Orlistat partially inhibits the hydrolysis of TAG when administered with fat-containing diets, thereby reducing the absorption of MAG and free FA. Orlistat's inhibitory efficacy is firmly linked to its amphiphilic structure. Loose stools, steatorrhea, stomach cramps, deficiency in fat-soluble vitamins, faecal urgency, incontinence, and flatulence are all undesirable side effects of Orlistat administration. The drug's effectiveness is hindered by the above unpleasant gastrointestinal side effects, that reduce patient compliance [56,57]. In early studies, it has been shown that Orlistat's inhibition on human carboxylester lipase (HCEL) was reversible [49,50].

The **Fig 1.4** depicts a schematic nucleophilic attack on the β -lactone ring of Orlistat (**1**) by the Ser 152 present in the PL active site, that results in the formation of the long-lived acyl-enzyme complex **2**. This covalent adduct is hydrolysed to liberate the active enzyme and yield β -hydroxy carboxylic acid (**3**) as the primary product. Further **3** is isomerized either to secondary product **4** by migration of the *N*-formyl-*L*-leucine (NFL) group of Orlistat, or to dihydroxy acid (**5**) by hydrolysis of NFL. Hydrolysis of NFL from **4** will also give to **5**, while cyclization of **4** to δ -lactone will give **6**. Subsequently **7** is formed from **5** (*via*. ring closure to forms **4**-hydroxy- δ -lactone) and **6** (hydrolysis of NFL) [49-57].

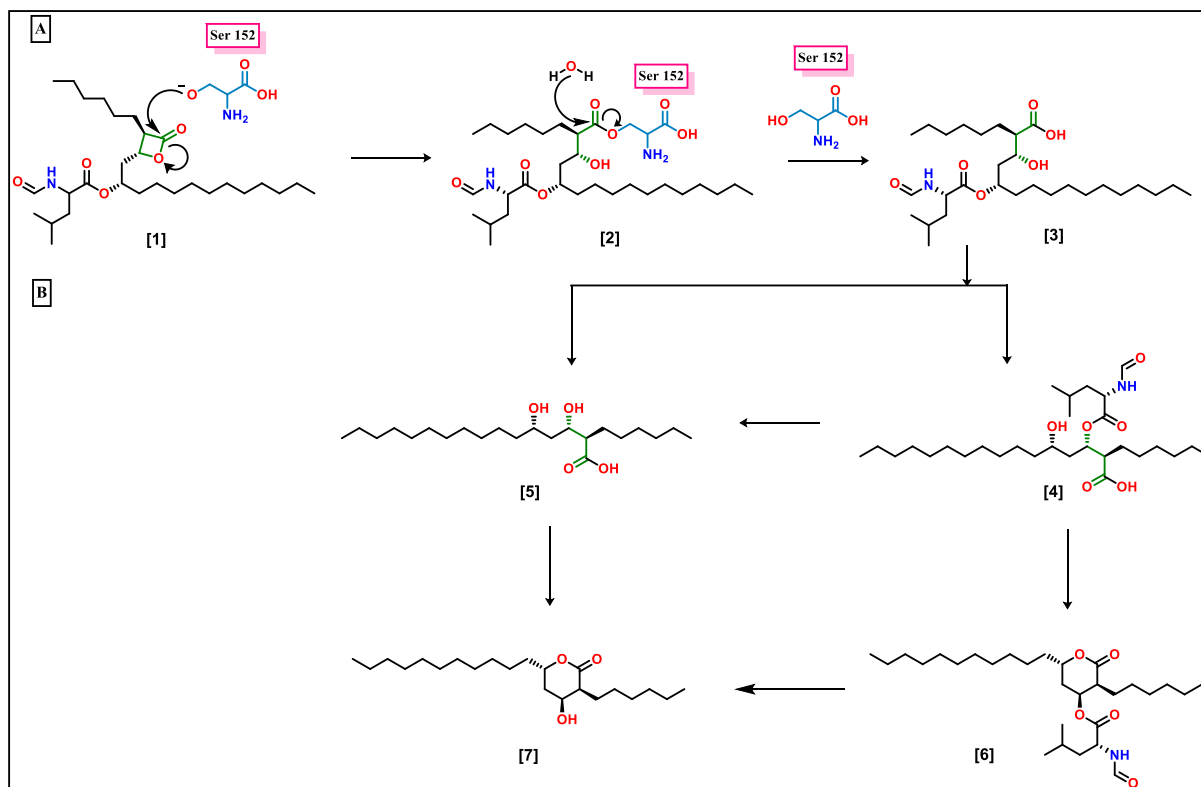


Figure 1.4. (A) Orlistat (1), mechanism of action against PL. (B) Metabolic degradation products (4-7).

1.2.5.2. *In-vivo* metabolic pathway of Cetilistat

In September of 2013, the Pharmaceuticals Medical Devices Agency of Japan (PMDA) approved Cetilistat for the treatment of obesity. In Japan, Takeda marketed it under the brand name Oblean®. The recommended dosage is 120 mg three times daily, immediately after each meal. The adverse effects include defecation that are oily and loose, faecal incontinence, frequent bowel movements, and diarrhoea [58].

A comprehensive review of the literature reveals the absence of detailed reports on its biotransformation. Only one study reports the identification and characterization of Cetilistat metabolites in rodents using UPLC-MS/MS. The reported study involved the administration of a drug suspension to pseudo-germ-free male *Sprague-Dawley* rats and normal untreated rats, followed by the collection of urine, faeces, and blood at regular intervals. Four Cetilistat metabolites namely 9, 10, 11 and 12 were detected *in vivo* matrices, as depicted in **Fig 1.5** [59].

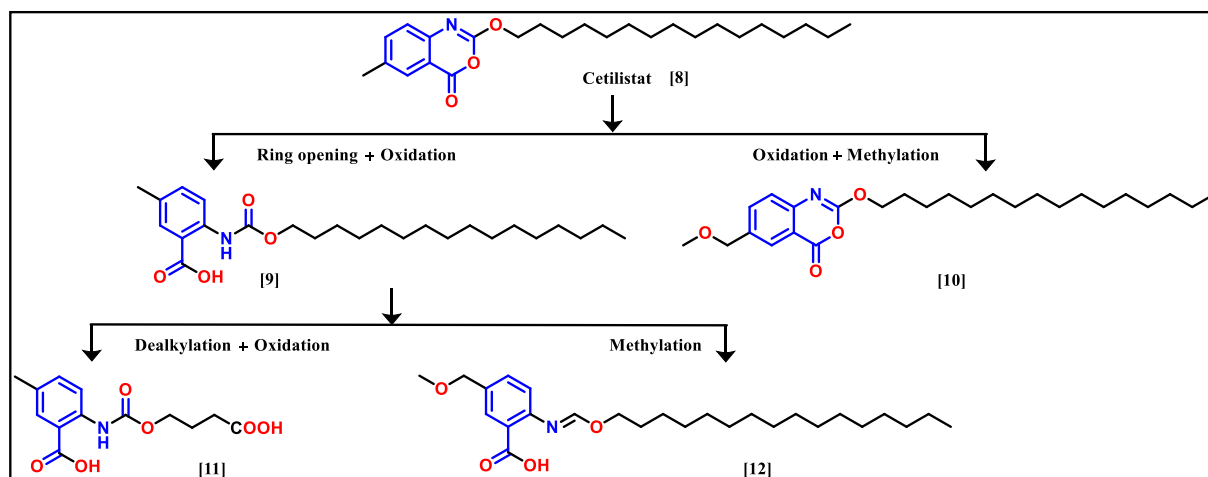


Figure 1.5. Plausible metabolite (9-12) for Cetilistat (8) using UPLC-QTOFMS/MS.

1.3. Problem Statement

Obesity is a disease with epidemic proportions and a worrisome upward trend. Unfortunately, there are only a limited number of safe and effective interventions and remedies available for the management of obesity. One intriguing strategy for the development of safer and more effective anti-obesity medications involves the inhibition of fat accumulation *via* PL inhibition, which is among the numerous putative targets utilized in the management of obesity. As the activity of PL is confined to the intestinal tract, inhibiting it does not result in any major discernible systemic consequences. This further provides the benefit of reducing adverse effects and complications. Therefore, PL inhibition presents a relatively less risky pharmaceutical approach for the treatment of obesity. The aforementioned information suggests that obesity treatment is severely constrained by the scarcity of approved medications, the inadequate efficacy of those that are available, and the serious adverse effects associated with them. In conclusion, it is crucial to develop novel and safe drug candidates for the pharmacological treatment of obesity, given the current scarcity of viable options in this field.

References

1. Kapoor, N., Furler, J., Paul, T. V., Thomas, N., & Oldenburg, B. (2019). Normal weight obesity: An underrecognized problem in individuals of South Asian descent. *Clinical Therapeutics*, *41*(8), 1638-1642.
2. World Obesity Atlas 2022; World Obesity Federation, 2022. Accessed 05 July 2024.
3. Otda, T., Takamura, T., Misu, H., Ota, T., Murata, S., Hayashi, H., Takayama, H., Kikuchi, A., Kanamori, T., Shima, K.R. & Lan, F. (2013). Proteasome dysfunction mediates obesity-induced endoplasmic reticulum stress and insulin resistance in the liver. *Diabetes*, *62*(3), 811-824.
4. Lee, S. S., & Kang, S. (2015). Effects of regular exercise on obesity and type 2 diabetes mellitus in Korean children: Improvements glycemic control and serum adipokines level. *Journal of Physical Therapy Science*, *27*(6), 1903-1907.
5. Higgins, V., Asgari, S., Hamilton, J. K., Wolska, A., Remaley, A. T., Hartmann, B., Holst, J.J. & Adeli, K. (2020). Postprandial dyslipidemia, hyperinsulinemia, and impaired gut peptides/bile acids in adolescents with obesity. *The Journal of Clinical Endocrinology & Metabolism*, *105*(4), 1228-1241.
6. Chatzigeorgiou, A., Garcia-Martin, R., Chung, K. J., Alexaki, I., Klotzsche-von Ameln, A., Siegert, G., Bornstein, S., Lutgens, E. & Chavakis, T. (2014). Dual role of B7 costimulation in obesity-related non-alcoholic steatohepatitis (NASH) and metabolic dysregulation. *Experimental Clinical Endocrinology & Diabetes*, *122*(03), P165.
7. Kolb, R., Sutterwala, F. S., & Zhang, W. (2016). Obesity and Cancer: Inflammation bridges the two. *Current Opinion in Pharmacology*, *29*, 77-89.
8. Wadden, T. A., Tronieri, J. S., & Butryn, M. L. (2020). Lifestyle modification approaches for the treatment of obesity in adults. *American Psychologist*, *75*(2), 235-251.
9. Salam, R. A., Padhani, Z. A., Das, J. K., Shaikh, A. Y., Hoodbhoy, Z., Jeelani, S. M., Lassi, Z.S. & Bhutta, Z. A. (2020). Effects of lifestyle modification interventions to prevent and manage child and adolescent obesity: A systematic review and meta-analysis. *Nutrients*, *12*(8), 2208.
10. World Obesity; Causes of Obesity, 2023. Accessed 5 July 2024.
11. Bray, G. A., Kim, K. K., & Wilding, J. P. (2017). Obesity: A chronic relapsing progressive disease process. A position statement of the World Obesity Federation. *Obesity Reviews*, *18*(7), 715-723.
12. <http://www.who.int/mediacentre/factsheets/fs311/en/> (Accessed 5 July 2024).

13. http://www.who.int/childgrowth/standards/weight_for_height/en/ (Accessed 5 July 2024).
14. http://www.who.int/growthref/who2007_bmi_for_age/en/ (Accessed 5 July 2024).
15. Okorodudu, D. O., Jumean, M. F., Montori, V. M., Romero-Corral, A., Somers, V. K., Erwin, P. J., & Lopez-Jimenez, F. (2010). Diagnostic performance of body mass index to identify obesity as defined by body adiposity: A systematic review and meta-analysis. *International Journal of Obesity*, 34(5), 791-799.
16. Reilly, J. J., Kelly, J., & Wilson, D. C. (2010). Accuracy of simple clinical and epidemiological definitions of childhood obesity: Systematic review and evidence appraisal. *Obesity Reviews*, 11(9), 645-655.
17. Javed, A., Jumean, M., Murad, M. H., Okorodudu, D., Kumar, S., Somers, V. K., & Lopez-Jimenez, F. (2015). Diagnostic performance of body mass index to identify obesity as defined by body adiposity in children and adolescents: A systematic review and meta-analysis. *Pediatric Obesity*, 10(3), 234-244.
18. Consultation, W. E. (2008). Waist circumference and waist-hip ratio. *Report of a WHO Expert Consultation. Geneva: World Health Organization, 2008*, 8-11.
19. Jensen, M. D., Ryan, D. H., Apovian, C. M., Ard, J. D., Comuzzie, A. G., Donato, K. A., & Yanovski, S. Z. (2014). 2013 AHA/ACC/TOS guideline for the management of overweight and obesity in adults: A report of the American College of Cardiology/American Heart Association Task Force on Practice Guidelines and The Obesity Society. *Circulation*, 129, S102-S138.
20. Patel, D. (2015). Pharmacotherapy for the management of obesity. *Metabolism*, 64(11), 1376-1385.
21. <https://asmbs.org/patients/who-is-a-candidate-for-bariatric-surgery> (Accessed 5 July 2024).
22. Haslam, D. (2016). Weight management in obesity—past and present. *International Journal of Clinical Practice*, 70(3), 206-217.
23. Manning, S., Pucci, A., & Finer, N. (2014). Pharmacotherapy for obesity: Novel agents and paradigms. *Therapeutic Advances in Chronic Disease*, 5(3), 135-148.
24. Onakpoya, I. J., Heneghan, C. J., & Aronson, J. K. (2016). Post-marketing withdrawal of anti-obesity medicinal products because of adverse drug reactions: A systematic review. *BMC medicine*, 14, 1-11.

25. Kim, G. W., Lin, J. E., Blomain, E. S., & Waldman, S. A. (2014). Antiobesity pharmacotherapy: New drugs and emerging targets. *Clinical Pharmacology & Therapeutics*, 95(1), 53-66.
26. <https://www.Clevelandclinic.org>. Obesity: Causes, Types, Prevention & Definition (Accessed 5 July 2024).
27. nih.gov. Prescription Medications to Treat Overweight & Obesity - NIDDK (Accessed 5 July 2024).
28. <https://clinicaltrials.gov/search?cond=obesity&term=pancreatic%20lipase> (Accessed 5 July 2024).
29. Chapus, C., Rovey, M., Sarda, L., & Verger, R. (1988). Minireview on pancreatic lipase and colipase. *Biochimie*, 70(9), 1223-1233.
30. Persson, B., Bengtsson-Olivecrona, G., Enerback, S., Olivecrona, T., & Jornvall, H. (1989). Structural features of lipoprotein lipase: Lipase family relationships, binding interactions, non-equivalence of lipase cofactors, vitellogenin similarities and functional subdivision of lipoprotein lipase. *European Journal of Biochemistry*, 179(1), 39-45.
31. Yadav, N., & Paul, A. T. (2023). Synthesis of amide warhead containing coumarin derivatives as potential pancreatic lipase inhibitors: *In silico* and *in vitro* evaluation for obesity treatment. *Medicinal Chemistry Research*, 32(10), 2219-2233.
32. Lowe, M. E., Rosenblum, J. L., & Strauss, A. W. (1989). Cloning and characterization of human pancreatic lipase cDNA. *Journal of Biological Chemistry*, 264(33), 20042-20048.
33. Gullo, L., Ventrucci, M., Tomassetti, P., Migliori, M., & Pezzilli, R. (1999). Fecal elastase 1 determination in chronic pancreatitis. *Digestive Diseases and Sciences*, 44, 210-213.
34. Domínguez-Muñoz, J. E., Hieronymus, C., Sauerbruch, T., & Malfertheiner, P. (1995). Fecal elastase test: Evaluation of a new noninvasive pancreatic function test. *American Journal of Gastroenterology*, 90(10), 1834-1837.
35. Gunstone, F. D., & Gunstone, F. D. (1996). Processing: Extraction, refining, fractionation, hydrogenation and interesterification. *Fatty Acid and Lipid Chemistry*, 87-99.
36. Lowe, M. E. (1997). Structure and function of pancreatic lipase and colipase. *Annual Review of Nutrition*, 17(1), 141-158.
37. Mansbach, C. M., & Siddiqi, S. A. (2010). The biogenesis of chylomicrons. *Annual Review of Physiology*, 72, 315-333.

38. Wieloch, T., Borgström, B., Piéroni, G., Pattus, F., & Verger, R. (1981). Porcine pancreatic procolipase and its trypsin-activated form: Lipid binding and lipase activation on monomolecular films. *FEBS Letters*, *128*(2), 217-220.
39. Erlanson-Albertsson, C., & Larsson, A. (1981). Importance of the N-terminal sequence in porcine pancreatic colipase. *Biochimica et Biophysica Acta (BBA)-Lipids and Lipid Metabolism*, *665*(2), 250-255.
40. Wang, D. Q. H. (2007). Regulation of intestinal cholesterol absorption. *Annual Review of Physiology*, *69*, 221-248.
41. Shi, Y., & Cheng, D. (2009). Beyond triglyceride synthesis: The dynamic functional roles of MGAT and DGAT enzymes in energy metabolism. *American Journal of Physiology-Endocrinology and Metabolism*, *297*(1), E10-E18.
42. Goodman, B. E. (2010). Insights into digestion and absorption of major nutrients in humans. *Advances in Physiology Education*, *34*, 44-53.
43. Levy, E., Spahis, S., Sinnett, D., Peretti, N., Maupas-Schwalm, F., Delvin, E., & Lavoie, M. A. (2007). Intestinal cholesterol transport proteins: An update and beyond. *Current Opinion in Lipidology*, *18*(3), 310-318.
44. Iqbal, J., & Hussain, M. M. (2009). Intestinal lipid absorption. *American Journal of Physiology-Endocrinology and Metabolism*, *296*(6), E1183-E1194.
45. Sternby, B., Engström, Å., Hellman, U., Vihert, A. M., Sternby, N. H., & Borgström, B. (1984). The primary sequence of human pancreatic colipase. *Biochimica et Biophysica Acta (BBA)-Protein Structure and Molecular Enzymology*, *784*(1), 75-80.
46. Winkler, F. K., d'Arcy, A., & Hunziker, W. (1990). Structure of human pancreatic lipase. *Nature*, *343*(6260), 771-774.
47. <https://www.rcsb.org>. RCSB Protein Data Bank (RCSB PDB) (Accessed 5 July 2024).
48. <https://www.fda.gov/drugs/postmarket-drug-safety-information-patients-and-providers/Orlistat-marketed-alli-and-xenical-information> (Accessed 5 July 2024).
49. Guerciolini, R. (1997). Mode of action of Orlistat. *International Journal of Obesity and Related Metabolic Disorders*, *21*, S12-23.
50. Borgström, B. (1988). Mode of action of tetrahydrolipstatin: A derivative of the naturally occurring lipase inhibitor lipstatin. *Biochimica et Biophysica Acta (BBA)-Lipids and Lipid Metabolism*, *962*(3), 308-316.

51. Bénarouche, A., Point, V., Carrière, F., & Cavalier, J. F. (2014). Using the reversible inhibition of gastric lipase by Orlistat for investigating simultaneously lipase adsorption and substrate hydrolysis at the lipid-water interface. *Biochimie*, *101*, 221-231.
52. Stalder, H., Oesterhelt, G., & Borgström, B. (1992). Tetrahydrolipstatin: Degradation products produced by human carboxyl-ester lipase. *Helvetica Chimica Acta*, *75*(5), 1593-1603.
53. Stalder, H., Schneider, P. R., & Oesterhelt, G. (1990). Tetrahydrolipstatin: Thermal and hydrolytic degradation. *Helvetica Chimica Acta*, *73*(4), 1022-1036.
54. Sridhar, S. N. C., George, G., Verma, A., & Paul, A. T. (2019). Natural products-based pancreatic lipase inhibitors for obesity treatment. *Natural Bio-active Compounds: Volume 1: Production and Applications*, 149-191.
55. Hadvary, P., Lengsfeld, H., & Wolfer, H. (1988). Inhibition of pancreatic lipase *in vitro* by the covalent inhibitor tetrahydrolipstatin. *Biochemical Journal*, *256*(2), 357-361.
56. Hadvary, P., Sidler, W., Meister, W., Vetter, W., & Wolfer, H. (1991). The lipase inhibitor tetrahydrolipstatin binds covalently to the putative active site serine of pancreatic lipase. *Journal of Biological Chemistry*, *266*(4), 2021-2027.
57. Hochuli, E., Kupfer, E., Maurer, R., Meister, W., Mercadal, Y., & Schmidt, K. (1987). Lipstatin, an inhibitor of pancreatic lipase, produced by *Streptomyces toxytricini* II. Chemistry and structure elucidation. *The Journal of Antibiotics*, *40*(8), 1086-1091.
58. https://ss.pmda.go.jp/en_all/search.x?nccharset=21AF663C&q=CETILISTATILISTAT&ie=UTF-8&page=1. Pharmaceuticals Medical Devices Agency of Japan (PMDA). (Accessed 5 July 2024).
59. Tiwari, S. S., Mukesh, S., Sangamwar, A. T., & Talluri, M. K. (2020). *In vivo* metabolic investigation of Cetilistat in normal versus pseudo-germ-free rats using UPLC-QTOFMS/MS and *in silico* toxicological evaluation of its metabolites. *Biomedical Chromatography*, *34*(8), e4860-4870.

Literature Review

Gaps - Aim and Objectives

2. Literature Review

2.1. Natural products and their role in drug discovery

Natural products derived from plants are distinguished by their minimal toxicity and extensive structural diversity. Furthermore, natural resources are consumed on a daily basis by humans in the form of food, where they serve as significant reservoirs of diverse bioactive natural products. Historically, the process of discovering drugs derived from natural sources was predominately done through trial and error. Nevertheless, the present situation benefits by allowing for the integration of advanced methodologies, including computer aided drug designing, LC-MS and HPLC based fast and accurate preparative separation etc. Drug development can be expedited through the implementation of integrated and interdisciplinary strategies [1]. Significant importance is also attributed to chemical and structural modifications of natural products in the drug discovery process. As an illustration, Orlistat is a structurally modified form of lipstatin, which originates from *Streptomyces toxytricini* [2,3]. Another example, wherein chemical modification of cinchona alkaloids yielded oxautin-1, which functions as an inhibitor of autophagy [4]. The chemical constituent Khellin derived from *Ammi visnaga* has been helpful in the synthesis of cromolyn, which is used as a bronchodilator in the form of sodium cromoglycate. Galegine, that has been obtained from *Galega officinalis*, served as the prototype for the development of metformin and other antidiabetic medications of the bisguanidine class. Verapamil (an antihypertensive) derives its origin from papaverine, a natural product that was isolated from *Papaver somniferum* [5] (**Fig 2.1**). There are numerous instances in which natural products have served as precursors to the identification of new pharmaceuticals or drug candidates. In drug discovery and development, medicinal plants and the natural products derived from them have consistently been of paramount importance.

At present, the potential of natural products and its inspired analogues for the treatment of obesity still needs to be explored and might be an excellent alternative strategy for the development of safe and effective antiobesity drugs [4-6]. To date, more than 700 natural products-based PL inhibitors have been identified. These are classified under various chemical classes such as polyphenols, saponins, triterpenes, alkaloids etc. Polyphenolic compounds account for nearly 42 % of the total phytochemicals used to inhibit PL, followed by the class of saponins and the other classes [7].

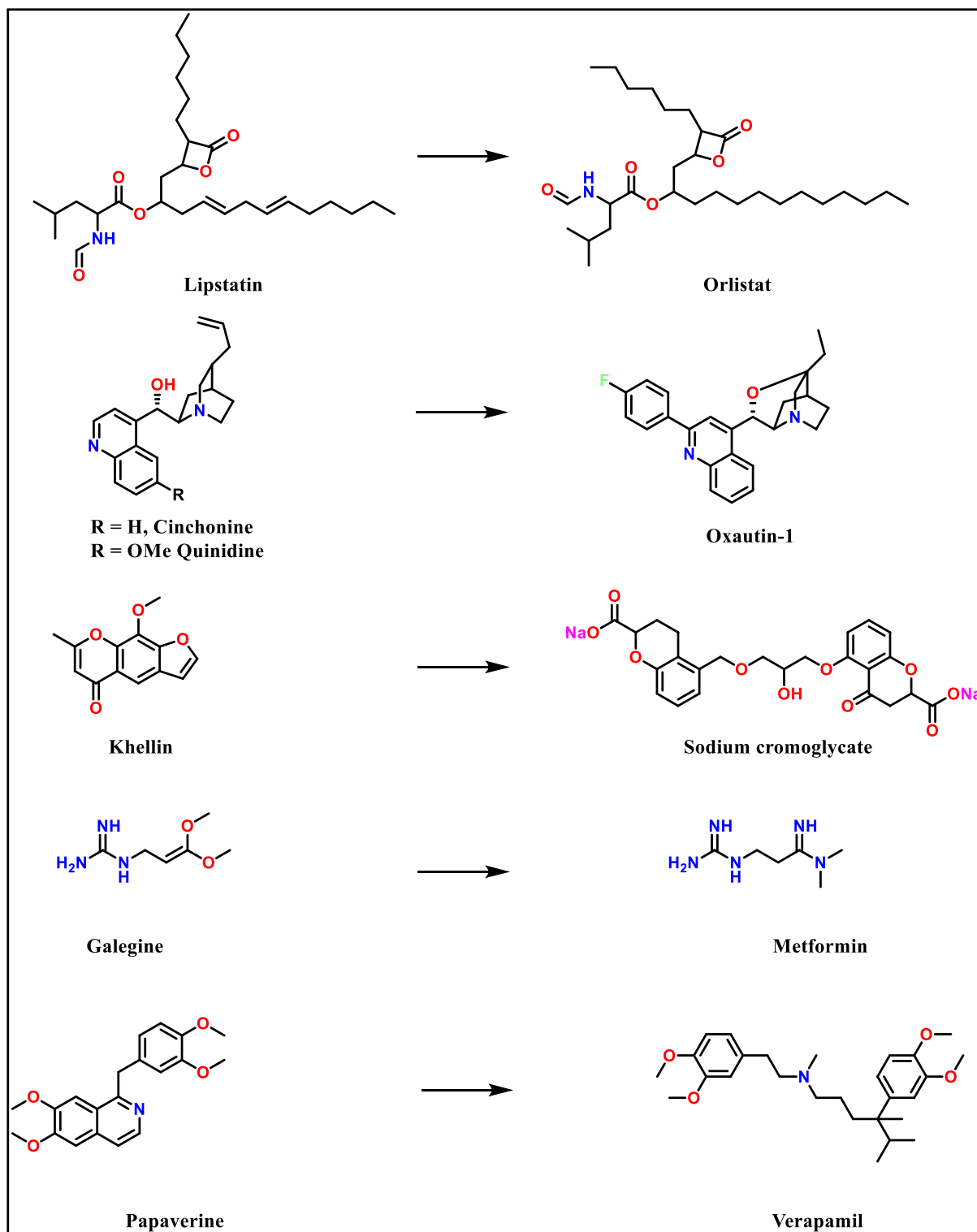


Figure 2.1. Examples of natural product leads and their corresponding synthetic products

2.2. Coumarins

Numerous biologically active phytochemicals contain heterocyclic scaffold as an integral component. Currently, the structures of numerous commercial medications also possess heterocyclic scaffolds. The majority of biologically active molecules that contain bicyclic oxygen heterocycles formed by fusion with the benzene ring are shown in **Fig 2.2**. Benzopyrone refers to the either of the two ketone derivatives of benzopyran which makes up the core skeleton of many flavonoid compounds i.e. 1-benzopyran-4-one (Chromone) and 1-benzopyran-2-one (Coumarin) [8].

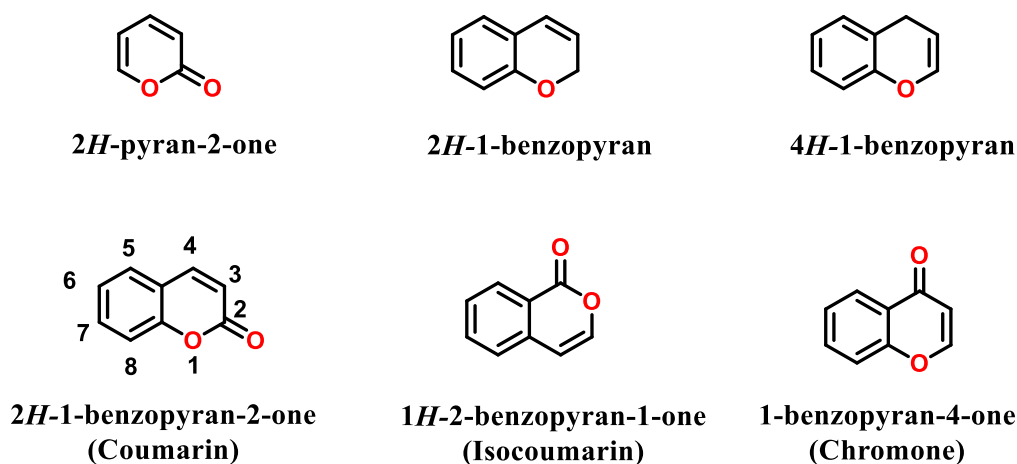


Figure 2.2. Biologically important oxygen heterocycles

Coumarins are secondary metabolites found widely in plants and represent an important class of natural and synthetic analogues of oxygen containing heterocycles. Coumarins were initially found in tonka bean (*Dipteryx odorata* Wild), which are indigenous to Brazil, Colombia, Guyana, and Venezuela. Coumarins are also found in significant quantities in various plant parts, with the highest concentrations being found in the fruits (*Aegle marmelos*, *Tetrapleura tetraptera*, bilberry, and cloudberry), seeds (*Calophyllum cerasiferum* and *Calophyllum inophyllum*), and subsequently in the roots (*Ferulago campestris*), leaves *Murraya paniculata*, *Phellodendron amurense*), and latex of the tropical rainforest tree *Calophyllum teysmannii*, green tea and other foods such as chicory. Significant concentrations of these metabolites are also found in lavender oil, cinnamon bark oil, and cassia oil. The proportion of coumarins found in different plant parts may be impacted by environmental factors and seasonal variations. Although their precise role remains obscure, coumarins have been proposed as bacteriostats, fungistats, plant growth regulators, and even waste products [9]. Approximately thirteen hundred coumarin derivatives have been identified from plants, bacteria, and fungi. In the year 1820, coumarin

CHAPTER II

was first obtained as a natural product and nearly 150 types of coumarin were found in 30 diverse plant families such as Umbelliferae, Oleaceae, Clusiaceae, Guttiferae and Rutaceae [10]. The six main classes of coumarins are furanocoumarins, dihydrofuranocoumarins, pyranocoumarins, pyrone substituted coumarins, phenylcoumarins and biscoumarins. Coumarins and their derivatives have attracted intense interest as pharmacophores and hence, a great deal of work has been directed towards the synthesis of various coumarin analogues for their application in a wide range of biological activities. Examples include warfarin, acenocoumarol (anticoagulants), carbocromen (coronary disease), scopoletin (antifungal), hymecromone (choleric and antispasmodic), armillarisin A, novobiocin [antibiotics], batoprazine (anti-aggression), ensaculin (NMDA antagonist and a 5HT1A agonist) and auraptene (Antineoplastic, Apoptosis inducer, Dopaminergic agonist, Neuroprotective, Antihypertensive, γ -secretase modulator) etc. as shown in **Fig 2.3** [9,10].

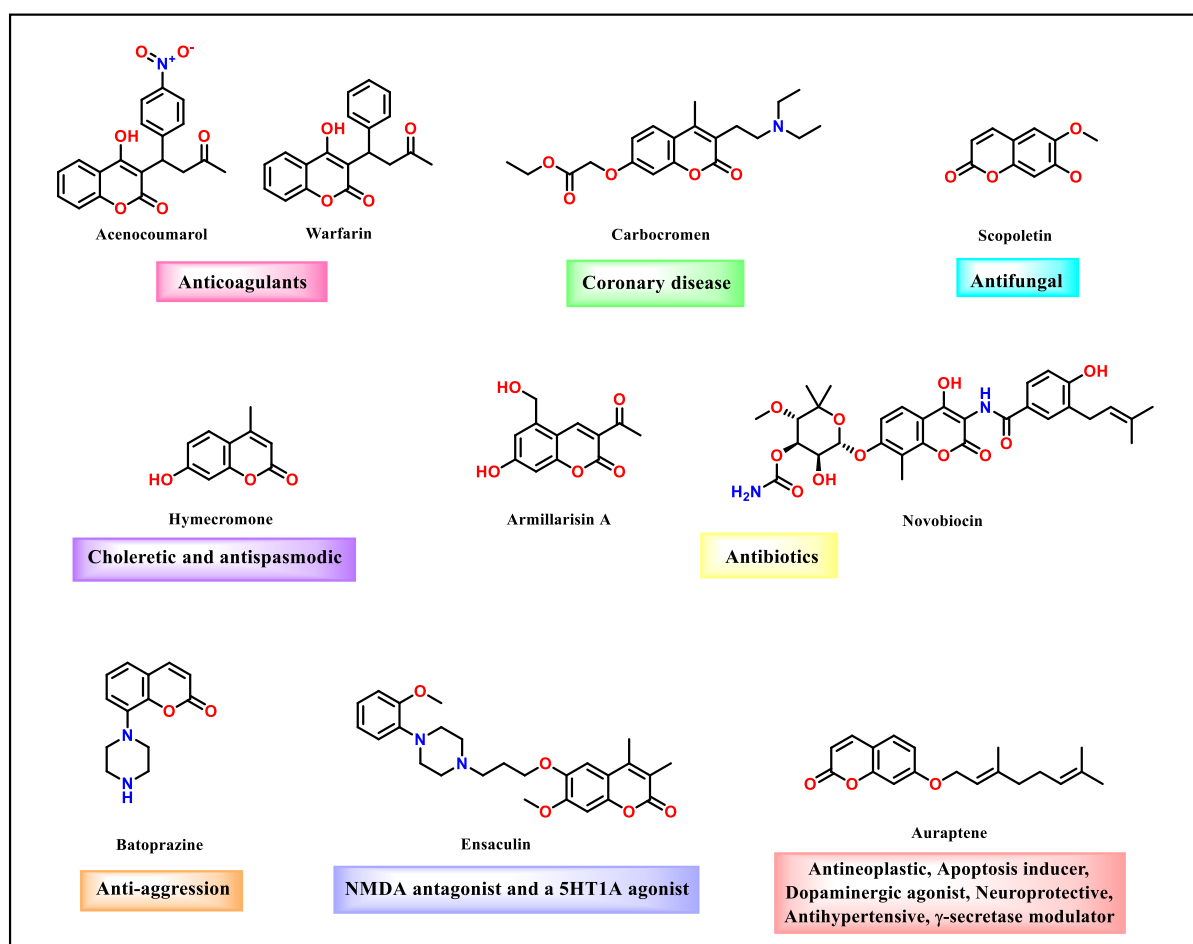


Figure 2.3. Examples of coumarin scaffold-based drugs.

Coumarin has attained a central position as a privileged structure in the design and discovery of novel drug molecules possessing high affinity and specificity to different molecular targets. The presence of several key features such as low molecular weight, planar aromatic ring fused with lactone functionality, ease of modification, stability, a readily available group for hydrogen bonding as well as for protein- ligand interaction, makes this heterocycle a unique pharmacophore in medicinal chemistry arena. Recognizing the presence of these features within coumarin scaffold, this scaffold has extensively been studied in pursuit of structurally diverse leads for drug discovery & development [11].

2.2.1. Role of Coumarins in the obesity treatment

2.2.1.1. Antiobesity activity of coumarins

Various coumarin derivatives have also been reported to possess anti-obesity activity *viz.*, Osthole and pteryxin (**Fig 2.4**) [12,13]. Osthole is an active constituent isolated from the fruit of *Cnidium monnieri* (L.) Cusson, a Chinese herbal medicine. Osthole has been found to decrease the levels of serum total cholesterol (TC), triglyceride (TG), coefficient of hepatic weight, and the hepatic tissue contents of TC and TG, and the levels of MDA and TNF- α in liver. It also increased the GSH levels in liver. Importantly, the histological evaluation of liver specimens demonstrated that osthole dramatically decreased lipid accumulation [12]. Another natural coumarin, Pteryxin, isolated from the hexane extract of the *Peucedanum japonicum* Thunb has been reported to possess anti-obesity activity [13,14]. Esculetin isolated from the stem barks of *Fraxinus rhynchophylla* (Oleaceae) has been reported to possess potent antiadipogenic activity against preadipocyte cell line, 3T3-L1 by *in vitro* assay system [15].

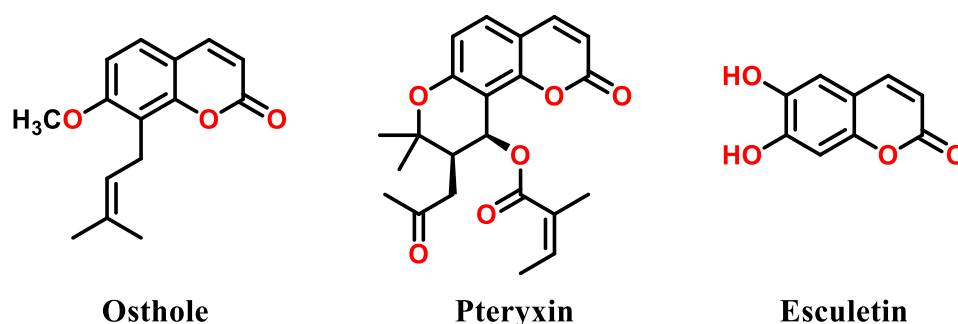


Figure 2.4. Naturally occurring coumarin possessing *in vivo* anti-obesity activity.

2.2.1.2. Coumarin scaffold-based PL inhibitors of natural origin

The potential of coumarins has been least explored in the area of PL inhibition, with very few reported to date. Examples include cleomiscosin A, cleomiscosin C and cleomiscosin B isolated from the stem barks of *F. rhynchophylla* that have exerted weak effects on PL activity (**Fig. 2.5**) [16,17].

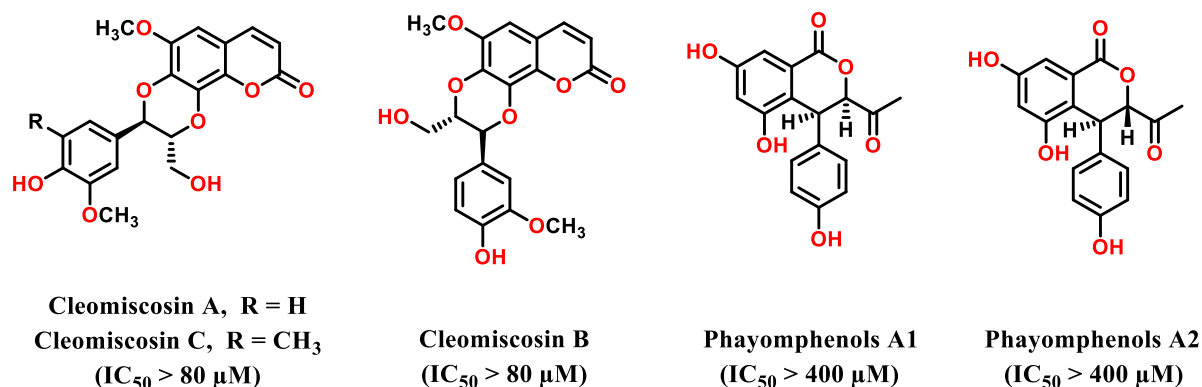


Figure 2.5. Naturally occurring coumarin and isocoumarins with PL inhibitory activity.

Similarly, the methanol extract from the bark of *Shorea roxburghii* was reported to inhibit PL activity with an IC₅₀ of 31.6 μg/mL. From the active extract, two new 3-acetyl-4-phenyl-3,4-dihydroisocoumarins, phayomphenols A₁ and A₂ were isolated. The absolute stereochemistry was elucidated as (3*R*,4*S*)- and (3*S*,4*S*)-3-acetyl-5,7-dihydroxy-4-(4-hydroxyphenyl)-3,4-dihydroisocoumarin. These isocoumarins exhibited a weak PL inhibitory activity (IC₅₀ > 400 μM) as compared with a lipase inhibitor, Orlistat (IC₅₀ = 56 nM) [18].

2.2.2. Coumarin scaffold-based PL inhibitors of synthetic origin

Nevertheless, these naturally occurring coumarins exhibited weak PL inhibitory activity. On the contrary, structural modifications that include various substitutions on the coumarin scaffold resulted in a significant enhancement in their PL inhibitory activity.

Fattah T. A et.al (2019) reported the PL inhibitory activity of various furo[3,2-*c*] coumarins (**Fig 2.6**) wherein the most potential analogue among the series exhibited (IC₅₀ value of 9.37 ± 1.36 μM as compared with the IC₅₀ values of Orlistat i.e. 0.2 ± 0.01 μM. The most potent analogue exhibited no steric clashes within the PL active site. Second best analogue displayed good PL inhibition with the IC₅₀ value of 10.21 ± 1.29 μM, while another displayed poor activity (IC₅₀ = 50.71 ± 6.4 μM) [19].

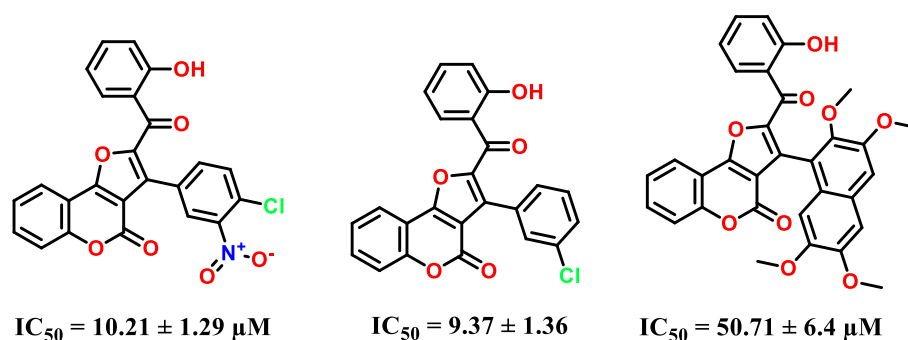


Figure 2.6. Synthetic coumarin derivatives with PL inhibitory activity.

2.3. Gaps in Existing Research

There are very few drugs which are marketed for the long-term treatment of obesity. Amongst all the drugs used clinically for management of obesity, Orlistat is the only drug which acts on PL (located peripherally). Hence it avoids the majority of systemic as well as CNS side effects. However, Orlistat is associated with some mild side effects like steatorrhea, liquid stools, fecal urgency, etc. As with the recent reports, citing severe adverse effects of the drug (hepatotoxicity, acute pancreatitis and renal injuries), there is an urgent requirement for potential and safer anti-obesity drugs. In light of these limitations in the literature, the current work attempts to design and synthesis coumarin analogues as more safe and potent PL inhibitors for obesity treatment. Coumarins exhibit a plethora of biological activities, including anti-inflammatory and anti-tumour. Molecular modeling studies have been implemented in the design of coumarin analogues with several bioactive groups to obtain analogues with better antiobesity activity. Structural modifications that include various substitutions on the coumarins have resulted in a significant enhancement in their PL inhibitory activity. Therefore, structural modification on coumarin may result in potent PL inhibitor. Also, the current research for the identification of potent PL inhibitor is mostly relying on natural products. Among the reported analogues of natural sources, very few are with greater potency. Such potential to moderate activity of these naturally isolated analogues may be due to lack of structural features that are essential for potent PL inhibition. Hence, these natural product-based analogues require synthetic modification in order to obtain potent PL inhibitors.

2.4. Aim

Considering the potential gaps in the existing research, the present thesis aims at “Design, Synthesis and Biological Evaluation of Coumarin Analogues as Potent Pancreatic Lipase Inhibitors for Obesity Treatment”

2.5. Objectives

To achieve the above aim following are the objectives:

1. To prepare extracts from the selected Indian medicinal plants and to determine their *in-vitro* inhibitory activity against pancreatic lipase
2. To perform bioassay guided fractionation of the most potent extract followed by purification and characterization of the isolated phytoconstituents(s)
3. To evaluate the isolated phytoconstituents(s) for the *in-vitro* pancreatic lipase inhibition and to identify the structural features required for the inhibitory activity using *in silico* experiments
4. To synthesize, characterize and evaluate pancreatic lipase inhibitory activity of various synthetic analogues of the identified lead(s)
5. To evaluate the *in vivo* efficacy of the most potent synthetic analogue(s) using high fat diet fed mice model

References

1. Zhang, L., Song, J., Kong, L., Yuan, T., Li, W., Zhang, W., Hou, B., Lu, Y. & Du, G. (2020). The strategies and techniques of drug discovery from natural products. *Pharmacology & Therapeutics*, 216, 107686-10799.
2. Liu, T. T., Liu, X. T., Chen, Q. X., & Shi, Y. (2020). Lipase inhibitors for obesity: A review. *Biomedicine & Pharmacotherapy*, 128, 110314-110323.
3. McNeely, W., & Benfield, P. (1998). Orlistat. *Drugs*, 56(2), 241-249.
4. Grigalunas, M., Burhop, A., Christoforow, A., & Waldmann, H. (2020). Pseudo-natural products and natural product-inspired methods in chemical biology and drug discovery. *Current Opinion in Chemical Biology*, 56, 111-118.
5. Cragg, G. M., & Newman, D. J. (2013). Natural products: A continuing source of novel drug leads. *Biochimica et Biophysica Acta*, 1830(6), 3670-3695.
6. Patwardhan, B., Warude, D., Pushpangadan, P., & Bhatt, N. (2005). Ayurveda and traditional Chinese medicine: A comparative overview. *Evidence-Based Complementary and Alternative Medicine*, 2, 465-473.
7. Patwardhan, B., Vaidya, A. D., & Chorghade, M. (2004). Ayurveda and natural products drug discovery. *Current Science*, 86(6), 789-799.
8. Szwaczko, K. (2022). Coumarins synthesis and transformation *via* C-H bond activation - A Review. *Inorganics*, 10(2), 23-53.
9. Venugopala, K. N., Rashmi, V., & Odhav, B. (2013). Review on natural coumarin lead compounds for their pharmacological activity. *BioMed Research International*, 2013, 1-14.
10. Ibrar, A., Shehzadi, S. A., Saeed, F., & Khan, I. (2018). Developing hybrid molecule therapeutics for diverse enzyme inhibitory action: Active role of coumarin-based structural leads in drug discovery. *Bioorganic & Medicinal Chemistry*, 26(13), 3731-3762.
11. Keri, R. S., Budagumpi, S., & Balappa Somappa, S. (2022). Synthetic and natural coumarins as potent anticonvulsant agents: A review with structure-activity relationship. *Journal of Clinical Pharmacy and Therapeutics*, 47(7), 915-931.
12. Sun, F., Xie, M. L., Zhu, L. J., Xue, J., & Gu, Z. L. (2009). Inhibitory effect of osthole on alcohol-induced fatty liver in mice. *Digestive and Liver Disease*, 41(2), 127-133.
13. Nugara, R. N., Inafuku, M., Iwasaki, H., & Oku, H. (2014). Partially purified *Peucedanum japonicum* Thunb extracts exert anti-obesity effects *in vitro*. *Nutrition*, 30(5), 575-583.

CHAPTER II

14. Nugara, R. N., Inafuku, M., Takara, K., Iwasaki, H., & Oku, H. (2014). Pteryxin: A coumarin in *Peucedanum japonicum* Thunb leaves exerts antiobesity activity through modulation of adipogenic gene network. *Nutrition*, 30(10), 1177-1184.
15. Shin, E., Choi, K. M., Yoo, H. S., Lee, C. K., Hwang, B. Y., & Lee, M. K. (2010). Inhibitory effects of coumarins from the stem barks of *Fraxinus rhynchophylla* on adipocyte differentiation in 3T3-L1 cells. *Biological and Pharmaceutical Bulletin*, 33(9), 1610-1614.
16. Birari, R. B., & Bhutani, K. K. (2007). Pancreatic lipase inhibitors from natural sources: Unexplored potential. *Drug Discovery Today*, 12(19-20), 879-889.
17. Ahn, J. H., Shin, E. J., Liu, Q., Kim, S. B., Choi, K. M., Yoo, H. S., Hwang, B.Y. & Lee, M. K. (2012). Lignan derivatives from *Fraxinus rhynchophylla* and inhibitory activity on pancreatic lipase. *Natural Product Sciences*, 18(2), 116-120.
18. Morikawa, T., Chaipech, S., Matsuda, H., Hamao, M., Umeda, Y., Sato, H., Tamura, H., Ninomiya, K., Yoshikawa, M., Pongpiriyadacha, Y. and Hayakawa, T. (2012). Anti-hyperlipidemic constituents from the bark of *Shorea roxburghii*. *Journal of Natural Medicines*, 66, 516-524.
19. Fattah, T. A., Saeed, A., Al-Hiari, Y. M., Kasabri, V., Almasri, I. M., Al-Alawi, S., Larik, F.A. & Channar, P. A. (2019). Functionalized furo [3, 2-c] coumarins as anti-proliferative, anti-lipolytic, and anti-inflammatory compounds: Synthesis and molecular docking studies. *Journal of Molecular Structure*, 1179, 390-400.

Materials and Methods

3. Materials and Methods

3.1. Plant material collection, processing and extraction

Azadirachta indica (NIP-NPM-CD-229) and unripe fruits of *Aegle marmelos* (NIP-NPM-CD-242) were collected from the BITS Pilani (Pilani campus). Fruits of *Emblica officinalis* (NIP-NPM-CD-252), fruits of *Piper nigrum* (NIP-NPMCD-233) and bark of *Cinnamomum zeylanicum* (NIP-NPM-CD-253), were bought from local market of Pilani. Few plants were also obtained from the local market of Chandigarh such as leaves of *Clerodendrum serratum* (NIP-NPM-CD-255), fruits of *Piper chaba* (NIPNPM-CD-226), *Piper longum* (NIP-NPM-CD-241), bark of *Sphaeranthus indicus* (NIP-NPMCD-256), bark of *Symplocos racemosa* (NIP-NPM-CD-257). Authentication of the plant material was done by Dr. A.S. Sandhu, Department of Natural Products, National Institute of Pharmaceutical Education and Research (NIPER), Mohali, S.A.S Nagar, Chandigarh. The voucher specimens have been deposited in the herbarium of the Department of Pharmacy's Natural Drug Laboratory at BITS Pilani, Pilani campus.

The collected plant was shade dried in Natural Product Laboratory. All the dried plant materials underwent processing and were screened through BSS no. 10# in order to attain the intended particle size. Three distinct extraction techniques were utilized to the powdered material (30 g each): hot percolation or soxhlation (24 h), ultrasonication (1 h), and maceration (72 h), by utilising hexane and methanol as solvents for soxhlation, maceration and ultrasonication extraction. The extracts were filtered through cotton and concentrated using a rotary evaporator.

3.2. Computational studies

The *in silico* experimental methodology used for the current research is described below. Standard procedures for molecular docking and dynamics simulations (MD) were carried out using the following resources [1-5].

Computational sources: Molegro Virtual Docker 6.0 (MVD, (CLC Bio, Denmark)) for docking; Tyrone workstation (NVIDIA RTX 2040), Ubuntu 18.04 OS for MD.

Software and version: MVD 6.0 for docking; Desmond software (Schrodinger, Academic license, Version 2020-1) for dynamics.

Results analysis: BIOVIA Discovery Studio 4.5 visualizer (Dassault Systemes Biovia, Accelrys, USA).

3.2.1. Molecular Docking

The 3D X-ray structure of the human PL (PDB ID - 1LPB, resolution - 2.46 Å with co-crystallized ligand - methoxyundecyl phosphinic acid (MUP)) was used as the protein structure for the *in silico* studies as shown in **Fig 3.1** [1,2].

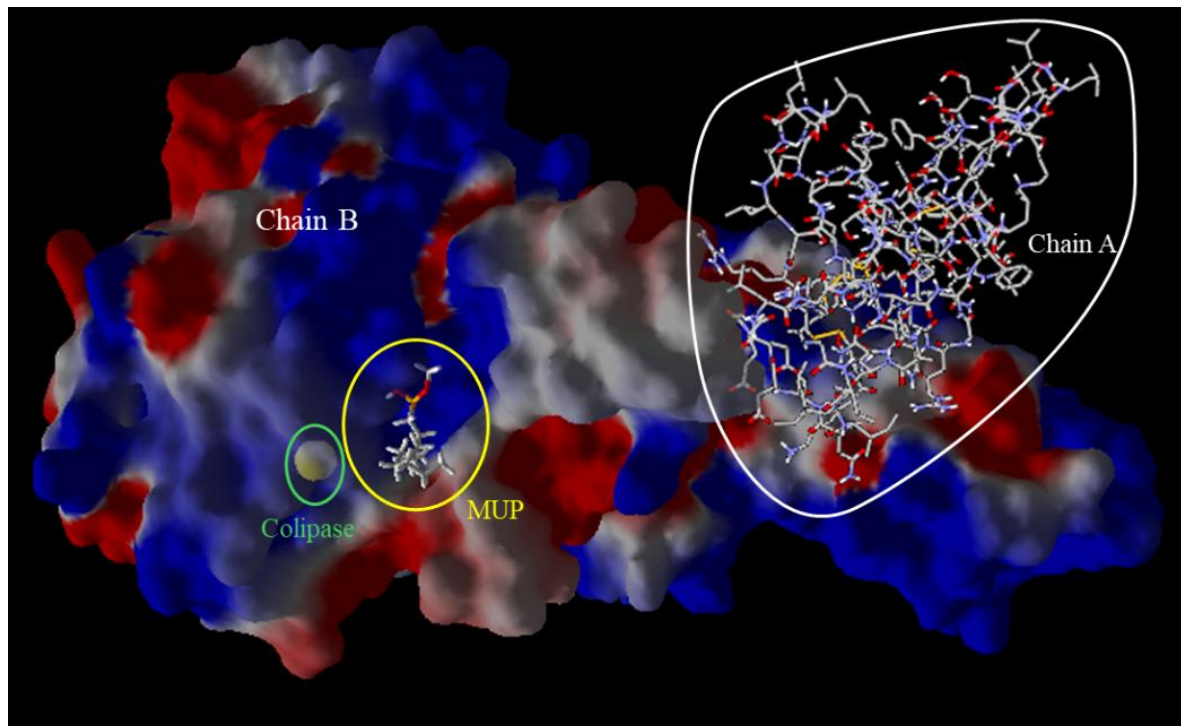


Figure 3.1. Secondary structure of the human PL-colipase complex co-crystallised with MUP at the active site (PDB Code: 1LPB).

The protein was prepared using the protein preparation wizard of MVD by removal of crystallographic water molecules and protonation, followed by repair and optimization. The grid was generated by considering the co-crystal ligand (MUP) present at active site of PL. The receptor site grid was constructed with the XYZ coordinates by using prepared protein (Chain B) as an input file for docking simulation. The coordinates for the active site were X-7.86, Y-24.91 and Z-55.11 with a 20 Å radius. The validation of the grid was performed by redocking the co-crystallised ligand (MUP, subjected to energy minimization) into the active site of PL. The redocked pose deviated from the co-crystallised pose by an RMSD of 0.99 Å (**Fig 3.2**).

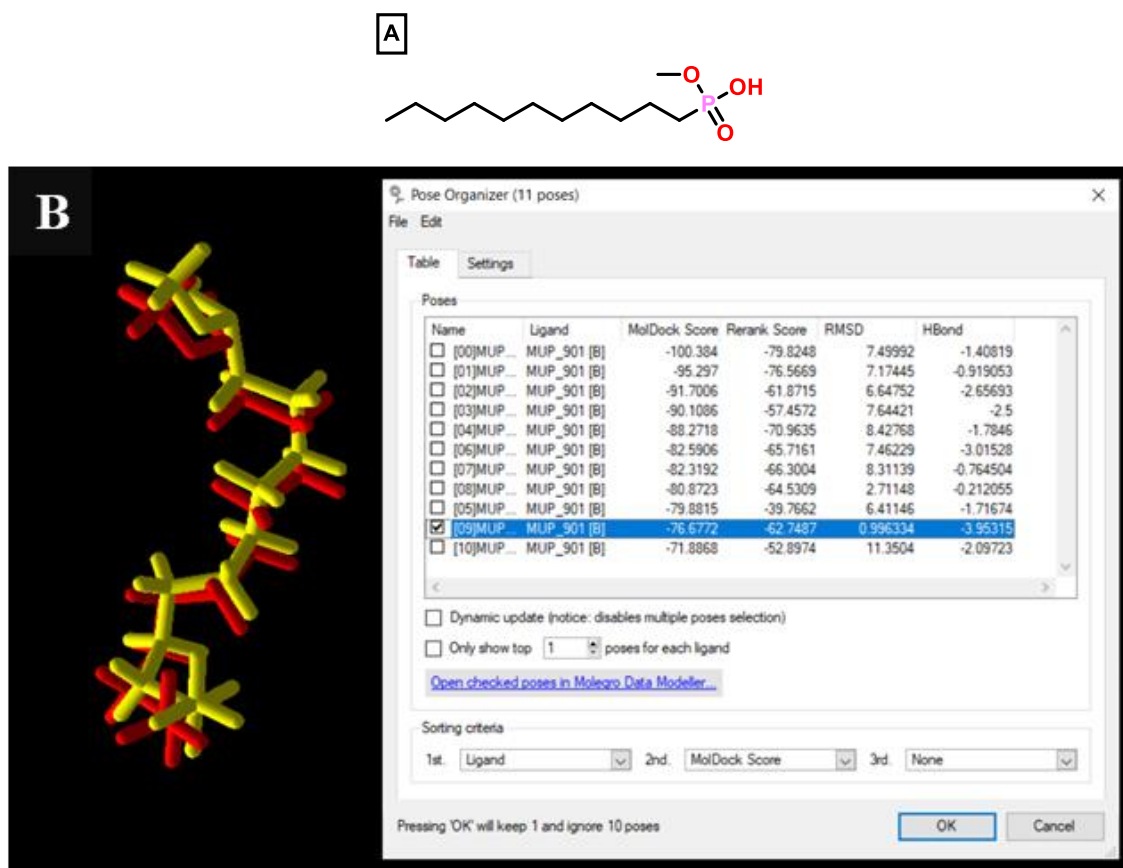


Figure 3.2. (A) Structure of MUP; (B) Superimposition of the re-docked pose of MUP (Yellow) with the co-crystallised pose (Red).

Prior to the docking, the chemical structure of the analogues were drawn using Chemdraw 2D module and the energy minimised structures were obtained using Molecular Mechanics 2 (MM2) force field in Chemdraw 3D module of ChemBioOffice v12 and v16 (PerkinElmer, USA). The MVD prepare molecules wizard was then used to prepare these analogues. During the analogue's preparation process, all potential conformations were considered. The prepared protein and analogues were then subjected to docking by using docking wizard of MVD. The obtained docked poses of the analogues were analysed for their MolDock scores (kcal/mol), while the various interactions exhibited by the analogues with the active site and hydrophobic lid domain amino acids were visualised in Discovery Studio Visualizer (Dassault Systemes Biovia, USA).

3.2.2. Molecular Dynamics (MD)

Under physiological conditions, molecular dynamics (MD) simulation aids in the visualization of the protein-ligand complex (PLC) at the binding site region of the target. The MD analysis was conducted utilizing the Desmond module of Schrodinger (Version 2020-1) [3]. Through the system's builder panel, the orthorhombic simulation box was prepared with the Simple

Point-Charge (SPC) explicit water model in such a way that the minimum distance between the protein surface and the solvent surface was 10 Å. Neutralization of the solvated system was accomplished by counterions and limiting the salt concentration in the physiological system to 0.15 M. The PLC system was designated with the Optimized Potentials for Liquid Simulations all atom (OPLS AA) force field [5]. The system was minimized using the minimization panel for 100 ps. The MD simulation was performed using the equilibrated system. For MD simulation time was set to 100 ns at 310.15 K (37°C) temperature of 1.013 bar pressure using the NPT (Isothermal-Isobaric ensemble, constant temperature, constant pressure, constant number of particles) ensemble with default parameters [6]. Utilizing the MD simulation panel, the MD simulation was executed. Furthermore, the out.cms file was used to view the trajectories. The trajectory was written with 1000 frames during the complete MD simulation. The protein backbone frames were aligned to the backbone of the initial frame to better understand the complex's stability during MD simulation. Finally, the equilibrated systems were employed to simulate a 100 ns no-restraint production run after loading the file. The radius of gyration (Rg), root mean square deviation (RMSD), root mean square fluctuation (RMSF), and the solvent accessible surface area (SASA) analysis were generated using the simulation interaction diagram panel [6].

3.3. PL inhibition assay and enzyme kinetics

The porcine pancreatic lipase (Type II), *p*-nitrophenyl butyrate (*p*-NPB), and Orlistat were purchased from Sigma-Aldrich (St. Louis, MO, USA). Sodium chloride (molecular biology grade) and Tris(hydroxymethyl) aminomethane (Tris) buffer were purchased from Sisco Research Laboratories located in Mumbai, India. Molecular biology grade dimethyl sulphoxide (DMSO) was procured from HiMedia Pvt. Ltd. (New Delhi, India). The PL inhibition assay was carried out in accordance with the standardized protocol [7,8]. The enzyme solutions were prepared just prior to use and utilized freshly.

3.3.1. PL inhibition assay

The crude porcine PL (5 mg/mL) was suspended in Tris-HCl buffer (containing 0.25 M of Tris and NaCl each, adjusted to pH 7.4 with HCl). The mixture was subjected to vigorous shaking, followed by centrifugation (4000 rpm, 10 min) and the supernatant was collected and used as an enzyme solution. At linear concentrations, stock solutions of the extract/isolated coumarins/synthesised analogues and Orlistat were prepared in DMSO. The final reaction mixture for each well comprised of 219 µL of buffer, 25 µL of enzyme, and 5 µL of analogues (varying stock concentrations). The reaction mixture was pre-incubated at 37 °C for 5 mins prior to the addition of 1.25 µL of the substrate (*p*-NPB, 10 mM in acetonitrile). The amount

of DMSO in the final concentration did not exceed 2%. After five mins, the absorbance of the final mixture was measured using a BioTek SYNERGY H1 microplate spectrophotometer at absorbance maxima of 4-nitrophenolate (405 nm) (**Fig 3.3**).

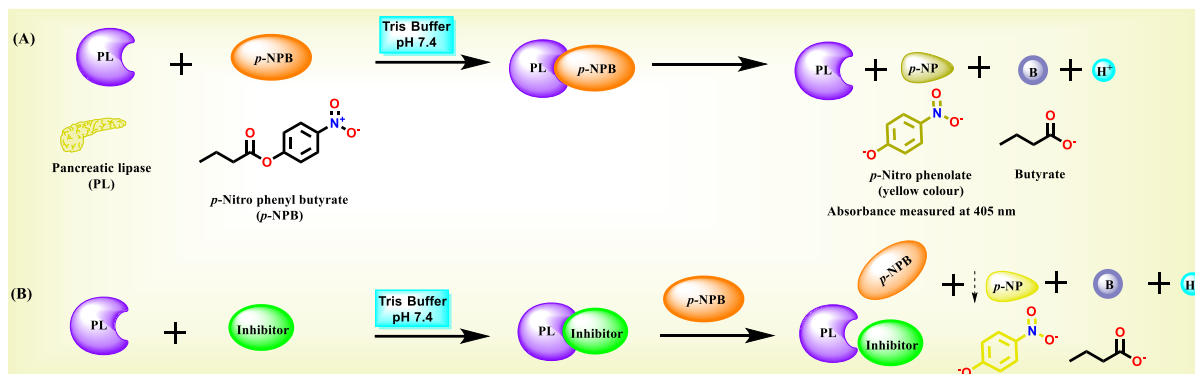


Figure 3.3. The enzymatic hydrolysis of *p*-nitrophenyl butyrate (*p*-NPB) (**A**) in the absence of an inhibitor; (**B**) in the presence of an inhibitor. (Low intensity of *p*-Nitro phenolate (**B**) indicates the presence of strong PL-inhibitor).

The assay was carried out in triplicate and the percentage of inhibition will be determined using the formula

$$\% \text{ Inhibition} = [1 - (A_T/A_E)] \times 100 \text{ ----- Formula 3.1}$$

Where A_E represents the absorbance of the enzyme control (without inhibitor), and A_T represents the difference in absorbance between the test sample with and without substrate. The IC_{50} of all the analogues was computed by plotting a linear regression curve [8].

3.3.2. Enzyme kinetics

For the inhibition kinetics, the PL inhibition assay protocol was repeated with different concentrations of the most potent analogue of each series and substrate (25, 50, 100, and 200 μ M). The absorbance of the final reaction mixture was taken in kinetic mode (16 readings for 30 mins) and the respective concentration of *p*-NPB was calculated from its calibration curve. The velocity of the reaction was then calculated as the slope of the graph for concentration V_s time. A double reciprocal Lineweaver-Burk plot with reciprocals of velocity and substrate concentration (on y-axis & x-axis, respectively) was plotted to determine the type of inhibition [9]. The inhibition constant K_i , was determined using the Cheng-Prusoff equation [10].

3.4. Synthesis and characterization

The syntheses of all the final analogues were carried out as per the procedure detailed under corresponding chapters 5-7 [11,12]. Briefly, the reactions were carried out using Spinot

(Tarson, India) magnetic hot plate. Progress of the reactions was followed by Thin Layer Chromatography (TLC) analysis (Silica gel G60 F₂₅₄, Merck). The final reaction mixture was concentrated using rotary evaporator (Heidolph, Germany). Melting points were determined with electro thermal capillary melting point apparatus. ATR spectra were recorded on a Bruker Alpha FT-IR spectrophotometer. ¹H (400 MHz) and ¹³C (100 MHz) NMR spectra were recorded on a Bruker Avance II 400 spectrometer using CD₃OD, DMSO-*d*₆ and CDCl₃ as solvents. High-resolution mass data (HRMS) were obtained on an Agilent 6545 Q-TOF LC/MS (ESI). High Performance Liquid Chromatography (HPLC) was performed for determining the purity of analogues on Dionex UltiMate 3000 UHPLC (Thermoscientific) with Diode Array detector and Chromeleon software.

3.5. Fluorescence spectroscopy

The fluorescence quenching experiment was performed using a Fluorolog-3 fluorescence spectrophotometer (Horiba Jobin Yvon Inc., France). The fluorescence quenching of the PL was assessed using the methodologies that were previously reported, with the requisite modifications [13,14]. The most active analogues from each series were dissolved in DMSO to prepare standard stock solutions (2 mg/mL). A standard solution of PL (5 mg/mL) was prepared in Tris-HCl buffer (pH 7.4). Inhibitors of varying concentrations (0.15 - 40 µg/mL) were combined with PL and transferred to a cuvette of 1.0 cm path length, and the fluorescence intensity was measured using an excitation wavelength (λ_{ex}) of 295 nm and emission wavelength (λ_{em} - a range of 300-500 nm), by keeping a slit width of 1.5 nm. The quenching mechanism of the inhibitors was identified using a linear Stern-Volmer plot. It was calculated using the following formula:

$$\frac{F}{F_0} = 1 + K_{sv}[Q] = 1 + k_q\tau_0[Q] \text{-----} \boxed{\text{Formula 3.2}}$$

where F_0 and F are the fluorescence intensities in the absence and presence of the quencher, k_q is the bimolecular quenching rate constant, $[Q]$ is the concentration K_{sv} and τ_0 were used to calculate the bimolecular quenching constant k_q in both scenarios. The τ_0 in this study was equivalent to that of human PL (1.59 ns) due to the fact that the porcine PL sequence is 94% homologous to human PL and all tryptophan residues were conserved. The following modified Stern-Volmer equation was used to determine the number of binding sites:

$$\log \frac{(F_0 - F)}{F} = \log K + n[Q] \text{-----} \boxed{\text{Formula 3.3}}$$

where $[Q]$ was the analytical quencher concentration, K is the binding constant, F_0 is the protein fluorescence in the absence of solute, and F is the protein fluorescence at a specific solute concentration [13,14].

References

1. Thomsen, R., & Christensen, M. H. (2006). MolDock: A new technique for high-accuracy molecular docking. *Journal of Medicinal Chemistry*, 49(11), 3315-3321.
2. Egloff, M. P., Marguet, F., Buono, G., Verger, R., Cambillau, C., & van Tilbeurgh, H. (1995). The 2.46 Å resolution structure of the pancreatic lipase-colipase complex inhibited by a C11 alkyl phosphonate. *Biochemistry*, 34(9), 2751-2762.
3. D. E. Shaw Research, New York, NY. (2020). Schrodinger Release 2020-4: Desmond Molecular Dynamics System, Maestro-Desmond Interoperability Tools, Schrodinger.
4. Mark, P., & Nilsson, L. (2001). Structure and dynamics of the TIP3P, SPC, and SPC/E water models at 298 K. *The Journal of Physical Chemistry A*, 105(43), 9954-9960.
5. Jorgensen, W. L., Maxwell, D. S., & Tirado-Rives, J. (1996). Development and testing of the OPLS all-atom force field on conformational energetics and properties of organic liquids. *Journal of American Chemical Society*, 118(45), 11225-11236.
6. Yadav, N., & Paul, A. T. (2023). Synthesis of amide warhead containing coumarin derivatives as potential pancreatic lipase inhibitors: *In silico* and *in vitro* evaluation for obesity treatment. *Medicinal Chemistry Research*, 32(10), 2219-2233.
7. Bustanji, Y., Al-Masri, I. M., Mohammad, M., Hudaib, M., Tawaha, K., Tarazi, H., & AlKhatib, H. S. (2011). Pancreatic lipase inhibition activity of trilactone terpenes of *Ginkgo biloba*. *Journal of Enzyme Inhibition and Medicinal Chemistry*, 26(4), 453-459.
8. Sridhar, S. N. C., Palawat, S., & Paul, A. T. (2020). Design, synthesis, biological evaluation and molecular modelling studies of conophylline inspired novel indolyl oxoacetamides as potent pancreatic lipase inhibitors. *New Journal of Chemistry*, 44(28), 12355-12369.
9. Lineweaver, H., & Burk, D. (1934). The determination of enzyme dissociation constants. *Journal of the American Chemical Society*, 56(3), 658-666.
10. Burlingham, B. T., & Widlanski, T. S. (2003). An intuitive look at the relationship of K_i and IC_{50} : A more general use for the Dixon plot. *Journal of Chemical Education*, 80(2), 214-218.
11. Brahmachari, G. (2015). Room temperature one-pot green synthesis of coumarin-3-carboxylic acids in water: A practical method for the large-scale synthesis. *ACS Sustainable Chemistry & Engineering*, 3(9), 2350-2358.
12. Chan, L. C., & Cox, B. G. (2007). Kinetics of amide formation through carbodiimide/*N*-hydroxybenzotriazole (HOBt) couplings. *The Journal of Organic Chemistry*, 72(23), 8863-8869.

CHAPTER III

13. Li, S., Pan, J., Hu, X., Zhang, Y., Gong, D., & Zhang, G. (2020). Kaempferol inhibits the activity of pancreatic lipase and its synergistic effect with orlistat. *Journal of Functional Foods*, 72, 104041.
14. Li, Y. Q., Yang, P., Gao, F., Zhang, Z. W., & Wu, B. (2011). Probing the interaction between 3 flavonoids and pancreatic lipase by methods of fluorescence spectroscopy and enzymatic kinetics. *European Food Research and Technology*, 233, 63-69.

Identification of Natural Product Lead from
Aegle marmelos

4. Identification of Natural Product Lead from *Aegle marmelos*

4.1. Preliminary Screening

Natural Products especially from plant origin have been an effective source for the treatment of various diseases and are known to produce lesser adverse effects. We have screened a set of flora for *in vitro* PL inhibition assay. The study highlighted the methanol extract of unripe fruits *Aegle marmelos* (AM) obtained through ultrasonic extraction to exhibit potential PL inhibitory activity with an IC₅₀ value of 13.02 µg/mL as compared to other plants (**Table 4.1**).

Table 4.1: PL inhibition of selected plants using different extraction techniques with hexane and methanol

No.	Plant (Part)	Solvent	IC ₅₀ (µg/mL)		
			Ultrasonication	Soxhlation	Maceration
1	<i>Cinnamomum zeylanicum</i> (bark)	Hexane	38.01 ± 0.97	32.6 ± 0.57	40.79 ± 1.89
2		Methanol	21.35 ± 0.47	14.07 ± 0.15	23.54 ± 0.46
3	<i>Azadirachta indica</i> (leaves)	Hexane	41.68 ± 1.91	51.25 ± 1.23	84.85 ± 0.46
4		Methanol	28.28 ± 0.76	31.09 ± 0.27	55.24 ± 0.98
5	<i>Piper nigrum</i> (fruits)	Hexane	31.16 ± 2.40	38.76 ± 1.16	47.84 ± 2.64
6		Methanol	21.23 ± 0.44	29.67 ± 0.49	23.75 ± 1.73
7	<i>Piper chaba</i> (fruits)	Hexane	42.74 ± 0.69	33.11 ± 0.92	51.99 ± 6.03
8		Methanol	25.85 ± 2.05	31.10 ± 1.94	45.12 ± 1.40
9	<i>Piper longum</i> (fruits)	Hexane	51.40 ± 1.12	42.97 ± 1.47	99.87 ± 1.28
10		Methanol	14.10 ± 0.70	26.30 ± 0.96	56.49 ± 3.98
11	<i>Cleodendrum serratum</i> (leaves)	Hexane	35.63 ± 1.22	35.48 ± 0.18	49.05 ± 5.20
12		Methanol	28.59 ± 0.31	28.69 ± 1.65	49.86 ± 4.04
13	<i>Aegle marmelos</i> (unripe fruits)	Hexane	29.23 ± 0.75	35.35 ± 2.52	35.13 ± 1.94
14		Methanol	13.02 ± 1.05	43.58 ± 1.98	37.15 ± 5.00
15	<i>Sphaeranthus indicus</i> (bark)	Hexane	31.43 ± 1.54	34.09 ± 0.56	39.07 ± 0.97
16		Methanol	23.99 ± 0.60	21.40 ± 0.98	31.78 ± 0.45
17	<i>Symplocos racemose</i> (bark)	Hexane	34.66 ± 0.07	32.12 ± 0.43	48.09 ± 1.87
18		Methanol	28.37 ± 0.35	34.75 ± 1.64	39.06 ± 0.56
19	<i>Embllica officinalis</i> (fruits)	Hexane	32.87 ± 3.21	49.91 ± 5.03	32.37 ± 3.37
20		Methanol	49.97 ± 3.92	55.45 ± 5.24	64.77 ± 5.01

* All experiments were performed in triplicate and the values are expressed as mean ± SEM.

There are several plausible explanations for the potential enzyme inhibition exhibited by the aforementioned plant extracts. The phytoconstituents serve as the principal determinant, while the solvent and extraction technique utilized are secondary factors. The phytoconstituents of these medicinal plants are distinguished by a substantial molecular volume that facilitates interaction with the active site and the presence of a reactive carbonyl functional group that may engage in an interaction with Ser 152 of PL. Based on the potential activity for PL inhibition, AM was selected for further study.

4.2. Literature Review of *Aegle marmelos*

4.2.1. Description of the plant

AM (L.) Correa belongs to family Rutaceae and it is a small to medium-sized tree or deciduous shrub that may reach a height of 13 meters and has drooping, thin branches and a tangled crown. It is found throughout India (except Jammu & Kashmir, Himachal Pradesh, Sikkim, Arunachal Pradesh), Sri Lanka, Nepal, Bangladesh, Myanmar, Vietnam, Indonesia, Malaysia, Thailand, Pakistan, Ceylon, Laos, Java, Egypt, Tibet, Philippines, Fiji, China, Tropical Africa and the United States. It ascends to an altitude of 1200 meters as it is a subtropical plant. It is commonly referred to as Bael (unripe fruit)/Bel/Bili/Shivapala, Bilva in Sanskrit, Sirphal/Siri-phal/Kooralam in Hindi, and Bael Fruit/Indian Bael/Holy Fruit/Golden Apple in English [1,2]. Various parts of the plant are depicted in **Fig 4.1**.

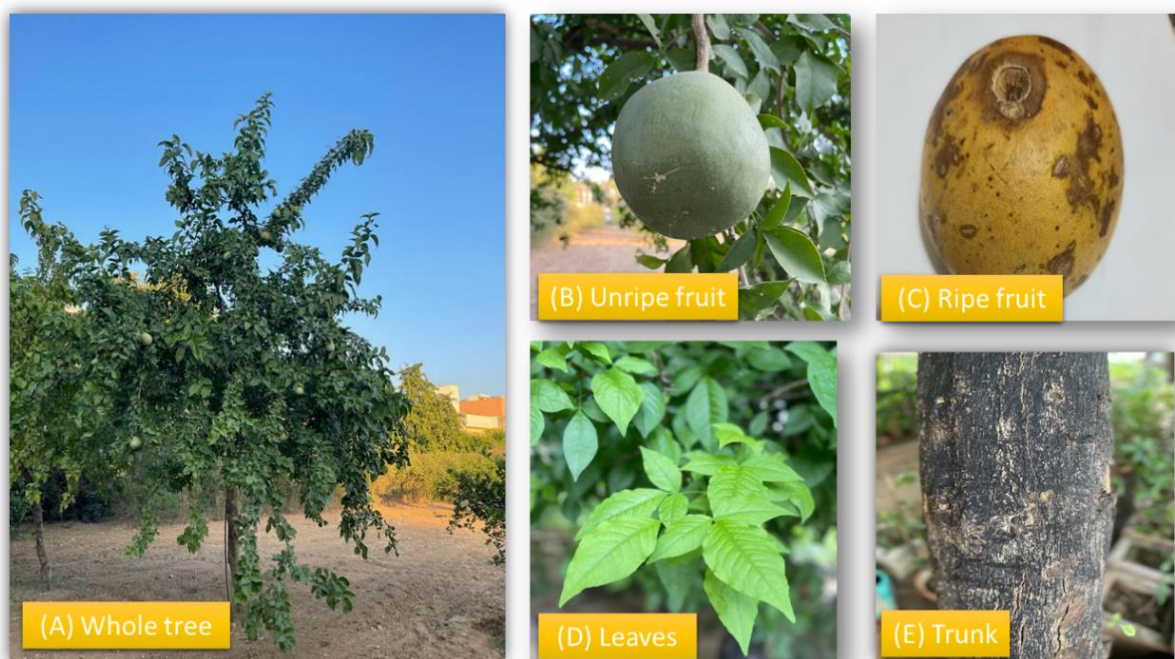


Figure 4.1. *Aegle marmelos*, (A) The whole tree, (B) unripe fruit, (C) ripe fruit, (D) leaves and (E) trunk

Typically, planting occurs during the monsoon season, flowering occurs from April to June, and fruit development occurs at the end of May and continues till July. A detailed taxonomical classification of AM is summarized in **Table 4.2** [2].

Table 4.2. Taxonomical classification of AM

Taxonomical classification of AM	
Kingdom	Plantae
Subkingdom	Tracheobionta
Super division	Spermatophyta
Division	Magnoliophyta
Class	Magnoliopsida
Subclass	Rosidae
Order	Sapindales
Family	Rutaceae
Genus	<i>Aegle</i>
Species	<i>Aegle marmelos</i>

AM plant has a long history of use in India, especially its leaves and fruits are considered holy because they are dedicated to Hindu deities, notably Lord Shiva. Consequently, it is frequently referred to as "Shiva druma" or the Shiva tree in historical literature. The root bark, leaves, and fruit (that are just starting to ripen) are used in medicinal preparations.

According to *Ayurveda*, AM fruit powder has a hot potency, a bitter taste, is dry, light, and astringent, and helps to enhance digestive capacity and rekindle the digestive fire. The gum extracted from immature fruits of AM is edible and has been recommended in ancient medical systems for medicinal purposes. Coumarins, alkaloids, flavonoids, carotenoids, phenolics, pectins, tannins, and terpenoids have been reported to be present in the unripe fruits of AM [3]. The fruits have been recommended as an antiamebic and antihistamine [4]. The unripe fruit possesses antipyretic, anti-mycobacterial, antioxidant, cytoprotective, antiproliferative, apoptotic, anticancer and anti-microbial activity [5-8]. The fruit is also reported as inhibitor for CYP450 and urease [9]. The AM fruit gum has a higher concentration of *d*-galactose (54.26 % w/w) and glucouronic acid (20.8 % w/w) than other commonly used gums [10].

4.2.2. Phytoconstituents and their Pharmacological activities

Oral administration (250 mg/kg) of the aqueous extract of bael fruits and seeds significantly lowered the serum and tissue lipid profile in streptozotocin-induced diabetic rats [11]. Ethanolic extract of AM leaves also inhibited the elevation of serum cholesterol and triglycerides level in Triton WR 1339 treated hyperlipidemic rat [12].

Furthermore, an assessment was conducted on the lipolytic activity of the dichloromethane extract derived from the leaves of AM. The results indicated a glycerol release of 44.63 ± 4.5 (12 h) nmol/mL and 62.05 ± 3.2 (24 h) nmol/mL, respectively, at a concentration of 100 $\mu\text{g/mL}$ ($p < 0.008$). The lipolytic activity was found to be greatest in the coumarin class of compounds, followed by furanocoumarins and alkaloids. As the most active compound at a concentration of 100 μM , umbelliferone induced a glycerol release of 148 ± 3.2 nmol/mL. Esculetin followed it with a glycerol release of 143.23 ± 3.2 nmol/mL. Serum TG, TC, and glucose levels were reduced as a result of umbelliferone and esculetin treatment in rats. [13]. Esculetin was additionally documented to induce apoptosis and inhibit adipogenesis in 3T3-L1. Consequently, esculetin possessed the capacity to combat obesity through the dual mechanism of adipogenesis inhibition and adipolysis enhancement [14].

As characteristic chemical constituents, more than thirty alkaloids have been extracted and identified from AM. But only six have been reported to be isolated from the fruits of AM as illustrated in **Fig. 4.2**. Aegeline, isolated from AM, exhibited antihistamine, antidyslipidemic and anti-bacterial activity [13-18]. Its inspired analogues exhibited anti-hyperlipidaemic and anti-adipogenic activity [19-20]. Aegeline and 2-*O*-methyl aegeline isolated from the unripe fruits of AM have been reported to act as a urease inhibitor [5]. Aegeline, has shown good antihyperglycemic activity and also antidyslipidemic property. It reduced plasma triglyceride, total cholesterol and free fatty acids accompanied with increase in high density lipoprotein in dyslipidemic hamster model at the dose of 50 mg/kg body weight [21].

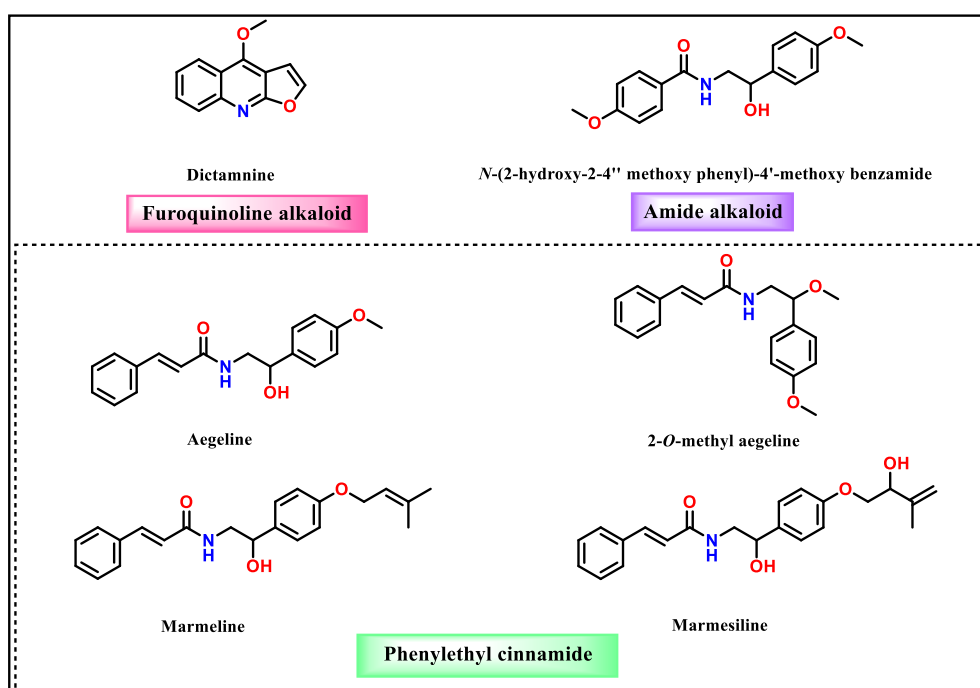


Figure 4.2. Alkaloids identified and isolated from the fruits of AM.

CHAPTER IV

Till date, a total of fifty-five coumarins have been isolated from AM, predominantly from its fruits and bark [6,7,9,22-30]. Approximately 24 coumarins out of 55 have been isolated from the fruits of AM. The predominant types of coumarins isolated from AM fruits are simple coumarins and furanocoumarins, as illustrated in **Fig 4.3**.

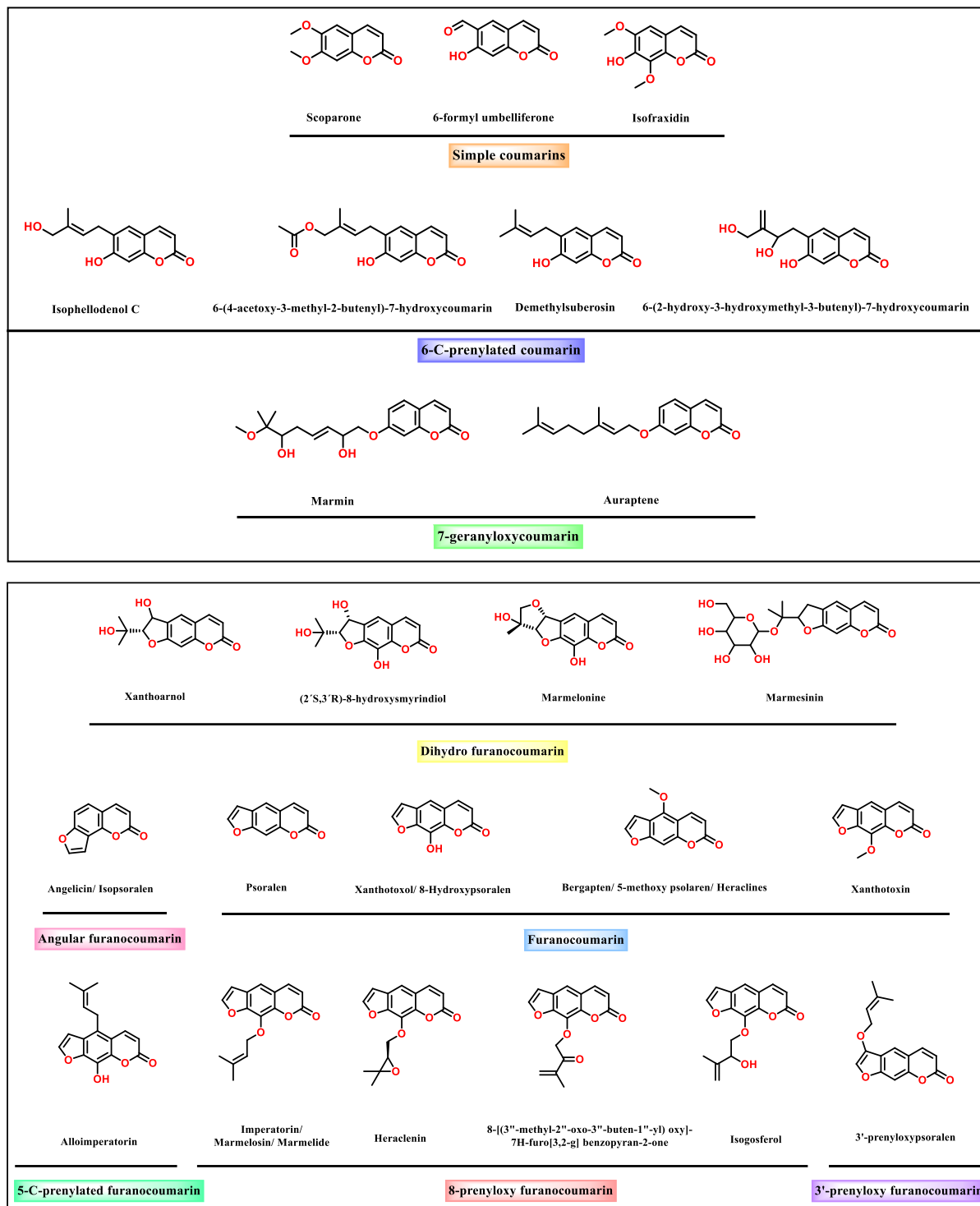


Figure 4.3. Coumarins identified and isolated from the fruits of AM.

A multitude of pharmacological activities have been documented for coumarin scaffolds containing phytoconstituents isolated from AM. For example, Marmin isolated from the roots, stem bark, leaves and fruits of AM has been reported to have anti-inflammatory, anti-histamine, anti-oxidant and anti-mycobacterial activities [6,15,30-32]. Marmin, 7'-O-methylmarmin, xanthotoxol, marmesin and alloimperatorin have been evaluated for urease inhibitory activity [5]. Amongst all these alloimperatorin exhibited the lowest IC₅₀ value of 27.5 μM. 5-methoxypsoralen reported to inhibit *in vitro* cell growth of human K562 cells [33]. Xanthotoxol, marmesinin and imperatorin from the fruits of AM have been reported as CYPs inhibitor [7], while marmesinin from leaves of AM was found to possess anti-oxidant activity [27]. Marmelosin has been evaluated for antioxidant, cytoprotective property, antiproliferative, apoptotic, anticancer activity, anti-diabetic, anti-mycobacterial and antiviral activity [6,8,35,36]. From the raw fruit of AM 3'-prenyloxypsoralen was isolated and evaluated for cytotoxic activity against normal cell line (HEK293) and cancer cell line (HeLa, MCF7, and HT29) [29]. Heraclenin identified from fruits of AM was tested against *Xanthomonas oryzae* and *Colletotrichum lindemuthianum* for anti-microbial activity [8]. Thus, the inherent coumarins derived from AM exhibit considerable promise as scaffold for the drug discovery and development against various pharmacological targets (**Table 4.3**). However, there is a lack of literature regarding the phytoconstituents identified from the unripe fruits of AM for PL inhibition. Therefore, the methanolic extract that demonstrated potential inhibitory activity against PL was selected for investigation to ascertain the class of phytoconstituents responsible for the observed PL inhibition and thus antiobesity activity.

Table 4.3. Summary of various coumarins and their pharmacological properties reported from AM

Sr. No.	Phytoconstituents	Plant Part	Activity	Results	References
1.	Umbelliferone/7-hydroxy coumarin	Stem barks and leaves	Anti-oxidant	Trolox equivalent antioxidant capacity (TEAC) mg TE/ g - 2,2-diphenyl-1-picrylhydrazyl (DPPH) - 187.09 ± 3.33 - 2,2'-Azino-bis(3-ethylbenzthiozoline-6-sulfonic acid) decolorization (ABTS) - 92.10 ± 20.73 - Cupric reducing antioxidant capacity (CUPRAC) - 217.01 ± 33.41 - Ferric reducing antioxidant power (FRAP) - 13.04 ± 2.71	[32]
		Leaves	Anti-obesity	- Glycerol release of 148 ± 3.2 nmol/mL at 100 μ M concentration - Lowered plasma TC levels to 98.3 ± 2.8 mg/dL as compared to TC levels of 117.8 ± 1.2 in HFD control group - Lowered plasma TG levels to 132.1 ± 1.9 mg/dL as compared to TG levels of 178.3 ± 3.9 mg/dL in HFD control group - Lowered plasma glucose levels to 101.3 ± 1.3 mg/dL as compared to glucose levels of 117.9 ± 4.2 mg/dL in HFD control group - <i>In vivo</i> activity has no discernible effect on food intake suggesting that it does not impede the function of the satiety centre - Lowered the increased body weight of the rats	[13]
2.	Esculetin	Leaves	Anti-obesity	- Glycerol release of 143.23 ± 3.2 nmol/mL at 100 μ M concentration - Decreased the TC levels significantly ($p < 0.05$) to 92.3 ± 3.6 mg/dL as compared to TC levels of 117.8 ± 1.2 in HFD control group - Decreased the TG levels significantly ($p < 0.05$) to 136.1 ± 2.3 mg/dL as compared to TG levels of 178.3 ± 3.9 mg/dL in HFD control group	[13]

CHAPTER IV

				<ul style="list-style-type: none"> - Decreased the glucose levels significantly ($p < 0.05$) to 100.0 ± 2.9 mg/dL as compared to glucose levels of 117.9 ± 4.2 mg/dL in HFD control group - <i>In vivo</i> activity has no discernible effect on food intake suggesting that it does not impede the function of the satiety centre - Lowered the increase in body weight of the rats 	
3.	Scopolectin/ Scopoletin	Leaves	Anti-thyroid, Anti-oxidative, Anti-hyperglycemic	<ul style="list-style-type: none"> - Inhibited hepatic lipid peroxidation and increased the activity of antioxidants, superoxide dismutase and catalase - Exhibited a superior therapeutic activity, compared with the standard antithyroid drug, (propylthiouracil (PU)) - Inhibited hepatic lipid peroxidation 	[37]
4.	Scoparone	Leaves	Lipolysis	Glycerol release of 126.28 ± 3.2 nmol/mL at 100 μ M concentration	[13]
5.	Marmin	Root	Anti-inflammatory	Exhibit anti-inflammatory effect in carrageenan induced inflammation in rats	[30]
		Root & stem bark	Anti-histamine/ anti-allergy	<ul style="list-style-type: none"> - Abrogated the contraction of tracheal smooth muscle induced by compound 48/80 - Inhibited CaCl_2-induced contraction in Ca^{2+} free Krebs solution - Inhibited two phases of contraction that were consecutively induced by metacholine and CaCl_2 in Ca^{2+} free Krebs solution 	[15]
		Root & stem bark	Anti-histamine/ anti-allergy	<ul style="list-style-type: none"> - Inhibited the contraction of guinea pig tracheal (GPT) induced immunologically by ovalbumin - Relaxed the precontraction of GPT induced by 3×10^{-5} M histamine - The value of EC_{50} of marmin was 4.42 ± 0.02 	[31]
		Bark and fresh root	Anti-histamine/ anti-allergy	<ul style="list-style-type: none"> - Inhibited the histamine release by $17.0 \pm 5.0\%$ and $94.6 \pm 1.0\%$ at 10 and 100 μM - Inhibited the synthesis of histamine in RBL-2H3 cells induced by DNP-BSA by $62.37 \pm 2.19\%$ at concentration 	[15]

CHAPTER IV

				of 100 μM	
		Bark and fresh root	Anti-histamine/ anti-allergy	<ul style="list-style-type: none"> - Inhibited the histamine release in rat basophilic leukemia (RBL-2H3) cell lines induced by dinitro-phenylated bovine serum albumin (DNP-BSA), thapsigargin or ionomycin - Suppressed Ca^{2+} influx on RBL-2H3 cell line induced by thapsigargin - Inhibited the histamine release from rat peritoneal mast cells (RPMCs) induced by thapsigargin - Showed weak inhibitory effects on the histamine release from RPMCs induced by compound 48/80, phorbol myristate acetate (PMA) or ionomycin - Showed low inhibitory effect when histamine was stimulated by ionomycin 	[15]
		Stem barks and leaves	Anti-oxidant	TEAC mg TE/ g <ul style="list-style-type: none"> - DPPH - 218.90 ± 15.00 - ABTS - 62.78 ± 10.98 - CUPRAC - 266.93 ± 6.51 - FRAP - 117.02 ± 10.85 	[32]
		Fruit	Anti-mycobacterial & antimicrobial	<ul style="list-style-type: none"> - Antimycobacterium activity against <i>M. tuberculosis</i> H37Ra with an $\text{IC}_{50} = 4.31 \mu\text{g/mL}$ whereas, 82.4% growth inhibition of <i>M. bovis</i> at $100 \mu\text{g/mL}$ - At $100 \mu\text{g/mL}$, showed growth inhibition, 18.4%, 26.7% and 10.9% of <i>S. aureus</i>, <i>E. coli</i> and <i>B. subtilis</i> 	[6]
		Unripe fruits	Urease inhibition	IC_{50} values for thiourea and marmin against urease $21.5 \pm 0.09 \mu\text{M}$ & $89.4 \pm 0.18 \mu\text{M}$, respectively	[9]
6.	7'-O-methylmarmin	Unripe fruits	Urease inhibition	IC_{50} values for thiourea and 7'-O-methylmarmin against urease were $21.5 \pm 0.09 \mu\text{M}$ & $152.8 \pm 0.09 \mu\text{M}$, respectively	[9]
7.	5-methoxypsolaren	Stem barks	Anticancer	It was able to induce K562 differentiation when used at concentrations lower than that causing 50% inhibition of K562 cell growth	[33]
8.	Xanthotoxol/8-	Unripe fruits	Urease	Inhibited urease with IC_{50} value of $65.4 \pm 0.24 \mu\text{M}$ & 21.5	[9]

CHAPTER IV

	hydroxy psoralen		inhibition	$\pm 0.09 \mu\text{M}$ for xanthotoxol & thiourea	
		Fruit	CYPs inhibition	- Inhibition of CYP1A2 with IC_{50} value of $42.0 \pm 2.8 \mu\text{M}$ - No significant inhibition of recombinant CYP2D6, 2C9, and 2C19 observed	[7]
9.	Marmesin	Unripe fruits	Urease inhibition	Inhibited urease with IC_{50} value of $82.8 \pm 0.14 \mu\text{M}$ as compared to thiourea ($21.5 \pm 0.09 \mu\text{M}$)	[9]
10.	Marmesinin	Fruits	CYPs inhibitor	- Inhibited CYP3A4 and 1A2 with IC_{50} value of 39.0 ± 1.2 and $21.2 \pm 0.1 \mu\text{M}$, respectively -No significant inhibition of recombinant CYP2D6, 2C9, and 2C19 was observed	[7]
		Leaves	Anti-oxidant and the membrane effects during experimental myocardial injury	- At a dose of 200 mg/kg (p.o.), demonstrated a decrease in serum enzyme levels and restored the electrocardiographic changes towards normalcy - Oral treatment for 2 days before and during isoproterenol administration decreased the effect of lipid peroxidation. - Exhibited membrane stabilizing action by inhibiting the release of β -glucuronidase from the subcellular fractions	[27]
11.	Alloimperatorin	Unripe fruits	Urease inhibition	Inhibited urease with IC_{50} value $27.5 \mu\text{M}$	[9]
12.	Imperatorin/ Marmelosin/ Marmelide	Fruits	CYP450 enzyme inhibition	- Competitive and time-dependent inhibition of CYP3A4 with IC_{50} value of $4.0 \pm 0.3 \mu\text{M}$ - Reversible and non-competitive inhibition was observed for CYP1A2 with IC_{50} value of $0.40 \pm 0.02 \mu\text{M}$ - Time-dependent inhibition of CYP3A4 was not affected by the addition of reduced glutathione - No significant inhibition of recombinant CYP2D6, 2C9, and 2C19 was observed	[7]
13.		Fruits	Antioxidant, cytoprotective, antiproliferative, apoptotic,	- Antioxidant activity with IC_{50} of $\sim 15.4 \pm 0.32 \mu\text{M}$ as opposed to standard - gallic acid (IC_{50} $1.1 \pm 0.08 \mu\text{M}$) - Antiproliferative activity with IC_{50} of $\sim 6.24 \pm 0.16 \mu\text{M}$ as opposed to deferoxamine ($\sim 10.8 \pm 0.28 \mu\text{M}$) and	[8]

CHAPTER IV

			anticancer	protected cells against cellular/DNA damage - Anti-inflammatory property was evident with significant reduction in the release of NO (~3.9 fold) and TNF- α (~3.4 fold), in addition to the inhibition of NF κ B (~2.7 fold), a transcription factor in RAW 264.7 cells -Marked down regulation of galectin-3 (~5.5 folds) and tyrosinase (~11.1 folds) by gene expression analysis substantiated by tyrosinase inhibition (IC ₅₀ - 20.3 \pm 1.26 μ M Vs. Kojic acid - IC ₅₀ - 24.1 \pm 1.41 μ M) -Induced apoptotic bodies, chromatin condensation and nuclear blebbing in RAW 264.7 cells	
		Fruits	Anti-mycobacterial	-Exhibited antimycobacterium activity against <i>M. tuberculosis</i> H37Ra with an IC ₅₀ value of 12.46 μ g/mL whereas, at 100 μ g/mL, 62.5% growth inhibition of <i>M. bovis</i> was observed - At 100 μ g/mL, exhibited 64.6% and 74.9% growth inhibition of <i>E. coli</i> and <i>B. subtilis</i> respectively	[6]
		Fruits	Antiviral	- Demonstrated IC ₅₀ of 62.5 μ g/mL in plaque inhibition assay at 96 h -Exhibited cytotoxicity at concentrations of 500 μ g/mL (marmelide) and 4000 μ g/mL (ribavirin) at 96 h - It is a virucidal agent that interfere with early events of its replicative cycle like adsorption, penetration, at various steps in single cycle growth curve and effect of time of addition in the case of human coxsackie viruses	[36]
		Leaves	Lipolysis	Glycerol release of 130.48 \pm 3.2 nmol/mL at 100 μ M concentration	[13]
14.	Iso-imperatorin	Leaves	Lipolysis	Glycerol release of 115.84 \pm 3.2 nmol/ml at 100 μ M with $p < 0.001$	[13]
15.	3'-prenyloxypsoralen	Raw fruits	Cytotoxic	- Inhibited Normal cell line (HEK293) with IC ₅₀ value of 31.2 μ g/mL - Inhibited Cancer cell line (HeLa, MCF7, and HT29) with	[29]

CHAPTER IV

				IC ₅₀ values of 44.8, 36.3 and > 50.0 µg/mL	
16.	Heraclenin	Fruit	Anti-microbial	At 3000 & 6000 ppm of heraclenin exhibited significant inhibition of <i>Xanthomonas oryzae</i> & <i>Colletotrichum lindemuthianum</i> as compared to control	[8]
17.	(+)-4-(2'-hydroxy-3'-methylbut-3'-enyloxy)-8H-[1,3]dioxolo[4,5-h]chromen-8-one	Seeds	Anti-fungal	- Antifungal activity against <i>A. fumigatus</i> , <i>Candida albicans</i> , <i>T. mentagrophytes</i> and <i>Cryptococcus neoformans</i> with MICs of 6.25 µg/mL, 31.25 µg/mL and 31.25 µg/mL disc diffusion assay (DDA), broth microdilution assay (BMA) and percent spore germination inhibition assay (PSGIA) respectively - Found inactive against <i>Sporothrix schenckii</i>	[38]

Abbreviations: Trolox equivalent antioxidant capacity (TEAC), 2,2-diphenyl-1-picrylhydrazyl (DPPH), 2,2'-Azino-bis(3-ethylbenzthiozoline-6-sulfonic acid) decolorization (ABTS), Cupric reducing antioxidant capacity (CUPRAC), Ferric reducing antioxidant power (FRAP), Total Cholesterol (TC), Triglycerides (TG), High Fat Diet (HFD), propylthiouracil (PU), guinea pig tracheal (GPT), dinitro-phenylated bovine serum albumin (DNP-BSA), rat peritoneal mast cells (RPMCs), phorbol myristate acetate (PMA), Cytochrome (CYP), Deoxyribonucleic acid (DNA), Tumor necrosis factor alpha (TNF- α), Nuclear factor kappa-light-chain-enhancer of activated B cells (NF κ B), macrophage cell line (RAW 264.7), Mycobacterium tuberculosis strain (H37Ra), immortalized human embryonic kidney cells (HEK293), Henrietta's Lacks (HeLa), breast cancer cell line (MCF7), human colorectal adenocarcinoma cell line (HT29), disc diffusion assay (DDA), broth microdilution assay (BMA) and percent spore germination inhibition assay (PSGIA)

4.3. Column chromatography and Bioassay-guided fractionation of AM extract

Considering the potential of methanol extract of AM for PL inhibition, column chromatography was performed using the parameters detailed in **Table 4.4**.

Table 4.4. Column dimensions and other parameters used in column chromatography.

Parameter	Condition	Parameter	Condition
Stationary phase	Silica gel 60-120#	Gradient	Hexane → DCM (at 10% increment) DCM → Ethyl acetate (at 10% increment) Ethyl acetate → Methanol (at 10% increment) Methanol : Formic acid (99:1 %) for final wash
Sample loaded	130 g		
Column dimensions	100 cm (L) x 6 cm (D)		
Column packed	40 cm (600 g Silica)		
Elution method	Gradient		
Fraction volume	250 mL		
Total no of fractions	120		

A total of 120 fractions were obtained, that were pooled based on the TLC profiles to obtain 13 fractions (F1-F13) as illustrated in **Fig. 4.4**.

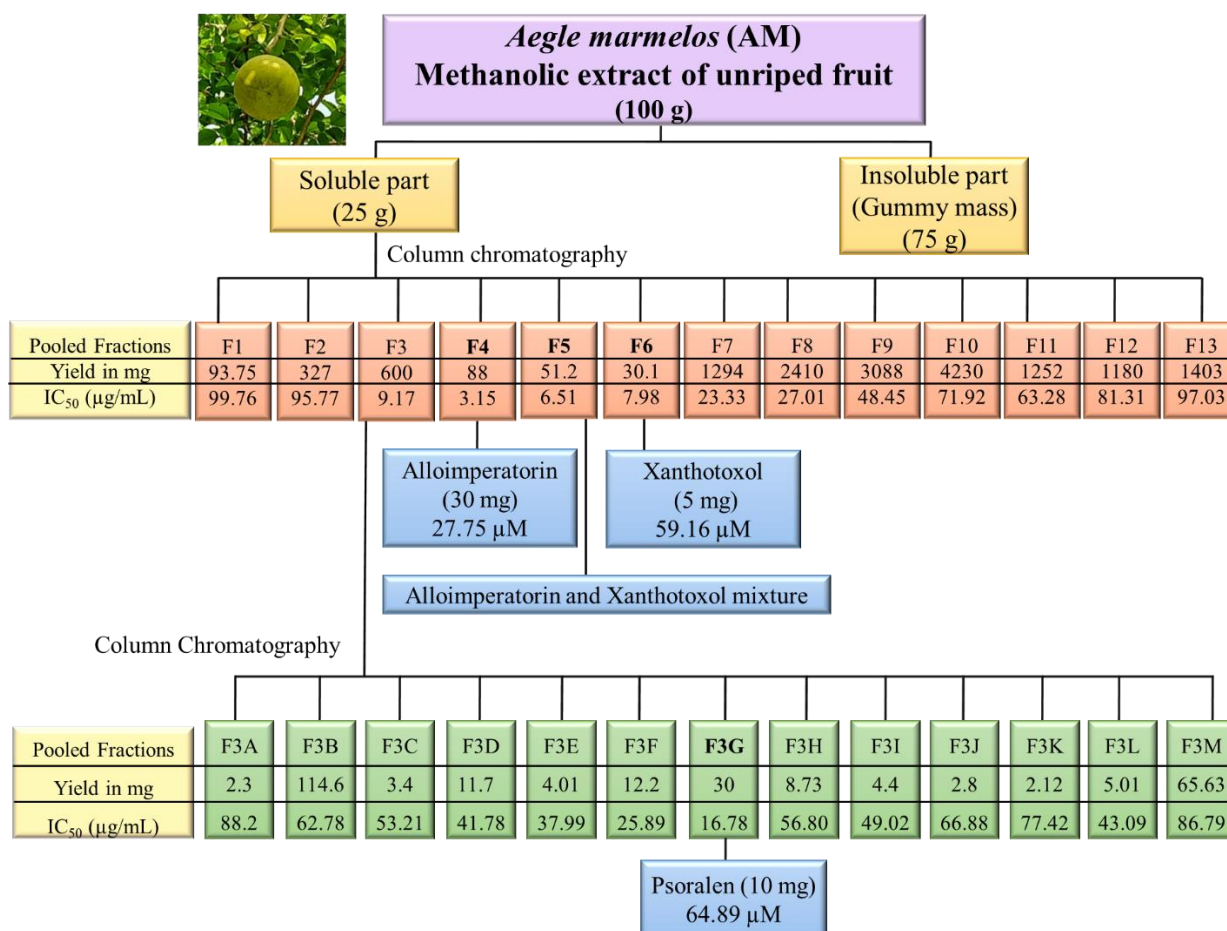


Figure 4.4. Schematic flow of bioassay guided fractionation of methanolic extract of AM.

All these fractions were evaluated for PL inhibition assay. As summarized in **Fig. 4.4**, fractions F4, F5, F6 and F3 exhibited potential PL inhibition with an IC_{50} value of 3.15, 6.51, 7.98 and 9.17 $\mu\text{g/mL}$, respectively.

To develop TLC profiles of fractions, three mobile phase compositions; a) Toluene: Ethyl acetate (7.5:2.5 % v/v), b) Toluene: Ethyl acetate: Glacial acetic acid (7:3:0.1% v/v/v); c) Toluene: Ethyl acetate: Formic acid (6:4:0.1 % v/v/v) were used. An overall better profile of the fractions was obtained with mobile phase Toluene: Ethyl acetate: Glacial acetic acid (7:3:0.1 % v/v/v), that was run on a 10 cm length TLC plate. An HPTLC analysis of all the collected fractions was done as illustrated in **Fig. 4.5**. HPTLC analysis highlighted the presence of a coumarin as the major constituent in **F-4**. Further **F-4** was purified by solvent washing (hexane, dichloromethane, ethyl acetate and methanol) to give amorphous light yellow color powder (30 mg). An NMR (^1H , ^{13}C , DEPT, HMQC, HMBS and COSY) analysis indicated the compound to be alloimperatorin. A HPTLC analysis of **F-6** highlighted the presence of one coumarins as the major constituent. Further **F-6** was purified by solvent washing (hexane, diethyl ether, dichloromethane, chloroform, acetone, ethyl acetate and methanol) to give white color powder (5 mg). An NMR (^1H , ^{13}C , DEPT, HMQC, HMBS and COSY) and mass analysis indicated the compound to be xanthotoxol. Further column chromatography of **F3** resulted in 13 subfractions (**F3(A-M)**), wherein subfraction **F3G** exerted the highest PL inhibitory potential ($IC_{50} = 16.78 \mu\text{g/mL}$). A white colored natural product was obtained from this subfraction. The natural product was further purified by solvent washing (hexane, diethyl ether, dichloromethane, chloroform, acetone, ethyl acetate and methanol),and recrystallization. Further it was identified as psoralen by using spectroscopic techniques such as 1D, 2D NMR, HRMS and by comparing with previously published data [5]. A HPTLC analysis of **F-5** highlighted the mixture of two phytoconstituents namely, xanthotoxol and alloimperatorin as the major constituents.

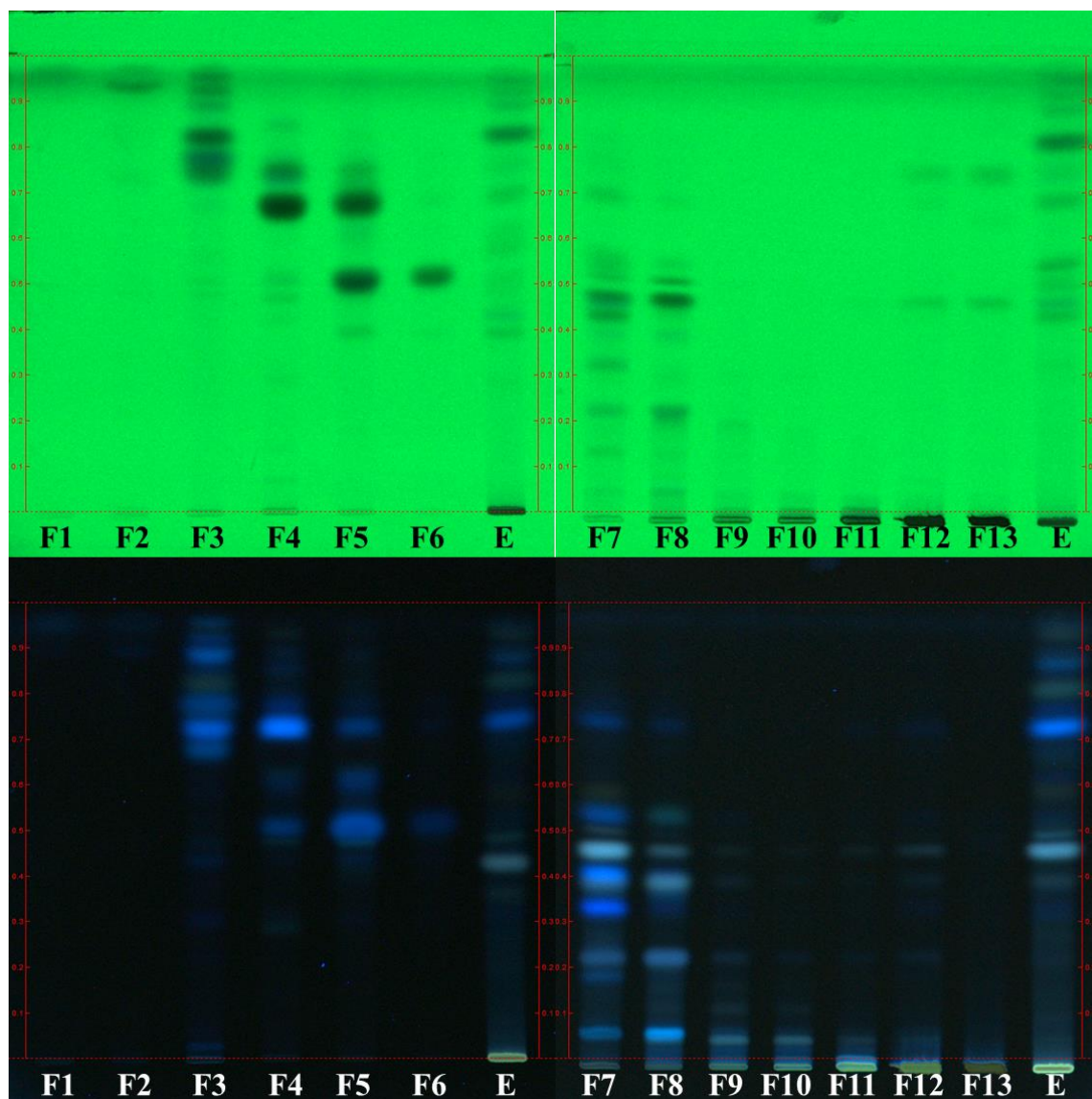


Figure 4.5. HPTLC of all the AM fractions (Mobile phase - Toluene: Ethyl acetate: Glacial acetic acid (7:3:0.1 % v/v/v)).

4.4. Analytical data of isolated phytoconstituents

9-hydroxy-4-(3-methylbut-2-en-1-yl)-7H-furo[3,2-g]chromen-7-one (Alloimperatorin)

Yellow solid; m.p: 230-233 °C; ¹H NMR (400 MHz, DMSO-*d*₆) δ 8.17 (d, *J* = 9.9 Hz, 1H), 7.98 (d, *J* = 2.3 Hz, 1H), 7.05 (d, *J* = 2.3 Hz, 1H), 6.38 (d, *J* = 9.9 Hz, 1H), 5.08 (t, 1H), 3.68 (d, *J* = 6.9 Hz, 2H), 1.77 (s, 3H), 1.60 (s, 3H). ¹³C NMR (100 MHz, DMSO-*d*₆) δ 160.57, 147.36, 145.33, 142.76, 140.82, 132.21, 128.49, 125.28, 123.22, 122.72, 114.05, 113.66, 106.50, 27.53, 25.79, 18.30. HRMS (ESI+) Calculated for C₁₆H₁₄O₄ [M + H]⁺, 271.0965; Found 271.0961 [9].

9-hydroxy-7H-furo[3,2-g]chromen-7-one (Xanthoxol)

White solid; m.p: 251-252 °C; ¹H NMR (400 MHz, CD₃OD) δ 7.91 (d, *J* = 9.5 Hz, 1H), 7.74 (d, *J* = 2.2 Hz, 1H), 7.26 (s, 1H), 6.81 (d, *J* = 2.2 Hz, 1H), 6.25 (d, *J* = 9.6 Hz, 1H). ¹³C NMR (100 MHz, CD₃OD) δ 161.58, 149.20, 146.87, 145.64, 139.66, 130.32, 125.93, 116.39, 113.21, 109.81, 106.48. HRMS (ESI+) Calculated for C₁₁H₆O₄ [M + H]⁺, 203.0337; Found 203.0338 [9].

7H-furo[3,2-g]chromen-7-one (Psoralen)

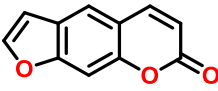
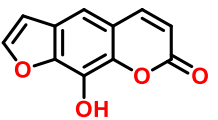
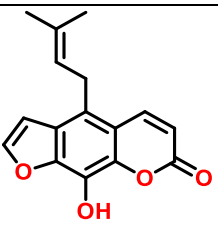
White solid; m.p: 158-161 °C ; ¹H NMR (400 MHz, CDCl₃) δ 7.80 (d, *J* = 9.5 Hz, 1H), 7.70 (d, *J* = 2.3 Hz, 1H), 7.69 (s, 1H), 7.48 (d, *J* = 0.9 Hz, 1H), 6.83 (dd, *J* = 2.3, 1.0 Hz, 1H), 6.38 (d, *J* = 9.6 Hz, 1H). ¹³C NMR (100 MHz, CDCl₃) δ 161.00, 156.44, 152.07, 146.91, 144.04, 124.88, 119.82, 115.44, 114.70, 106.37, 99.91. HRMS (ESI+) Calculated for C₁₁H₆O₃ [M+], 186.0317; Found 186.0311 [39].

All the three isolated phytoconstituents namely, alloimperatorin, xanthoxol and psoralen exhibited potential to moderate PL inhibitory activity (IC₅₀ = 27.75 ± 0.67, 59.16 ± 0.71 and 64.89 ± 0.83 μM) as compared Orlistat (IC₅₀ = 0.97 ± 0.31 μM) that was used as positive control.

4.5. Molecular docking studies

In order to comprehend the interaction between the phytoconstituent and PL, molecular docking studies were conducted utilizing the isolated and identified phytoconstituents from AM using Molegro Virtual Docker 6.0. As represented in **Table 4.5**, alloimperatorin exhibited a higher MolDock score of -110.296 kcal/mol as compared to xanthotoxol and psoralen.

Table 4.5. Docking scores and interactions exhibited by isolated phytoconstituents from AM.

Isolated constituents with their structures	MolDock Score (kcal/mol)	H-bond	C-H bond	π - π T shaped	π - π interactions/ π alkyl	π -cation
 Psoralen	-84.6327	Phe 77, Gly 76, His 151	-	Phe 77	Ala 178	His 263
 Xanthotoxol	-87.1329	Phe 77, Gly 76, His 151, Leu 153	Ser 152	-	Ala 178	His 263
 Alloimperatorin	-110.296	Gly 76, Phe 77, His 151, Ser 152, Leu 153	-	-	Ile 78, Ala 178, Ala 259, Ala 260, Ile 209	His 263

To summarize, the present chapter focused on the identification of natural product lead that would exhibit potent PL inhibition. The methanol extract from the unripe fruits of AM was subjected to bioassay guided fractionation, owing to its potential PL inhibition. Coumarin rich fractions were found to be responsible for potential PL inhibition activity. Further studies that involved column chromatography and fractionation resulted in the isolation and identification of alloimperatorin as potential natural product lead, that exhibited an IC_{50} value of $27.75 \pm 0.67 \mu\text{M}$ with comparable to the standard drug, orlistat ($IC_{50} = 0.97 \mu\text{M}$). Further *in silico* investigation result in understanding that the coumarin scaffold proceed the desired interactions with PL but requires structural modification/optimization to impart potent activity properties.

References

1. Ghosh, S., Kumar, A., Sachan, N., & Chandra, P. (2020). Bioactive compounds and distinctive pharmacological activity guided review of *Aegle marmelos*: A miraculous plant of indigenous medicine system. *Current Bioactive Compounds*, 16(7), 965-977.
2. Bhar, K., Mondal, S., & Suresh, P. (2019). An eye-catching review of *Aegle marmelos* L.(Golden Apple). *Pharmacognosy Journal*, 11(2), 207-224.
3. Charoensiddhi, S., & Anprung, P. (2008). Bioactive compounds and volatile compounds of Thai bael fruit (*Aegle marmelos* (L.) Correa) as a valuable source for functional food ingredients. *International Food Research Journal*, 15(3), 287-295.
4. Baliga, M. S., Bhat, H. P., Pereira, M. M., Mathias, N., & Venkatesh, P. (2010). Radioprotective effects of *Aegle marmelos* (L.) Correa (Bael): A concise review. *The Journal of Alternative and Complementary Medicine*, 16(10), 1109-1116.
5. Chinchansure, A. A., Shamnani, N. H., Arkile, M., Sarkar, D., & Joshi, S. P. (2015). Antimycobacterium activity of coumarins from fruit Pulp of *Aegle marmelos* (L.) Correa. *International Journal of Basic and Applied Chemical Sciences*, 5(3), 39-44.
6. Manda, V. K., Avula, B., Chittiboyina, A. G., Khan, I. A., Walker, L. A., & Khan, S. I. (2016). Inhibition of CYP3A4 and CYP1A2 by *Aegle marmelos* and its constituents. *Xenobiotica*, 46(2), 117-125.
7. Pynam, H., & Dharmesh, S. M. (2018). Antioxidant and anti-inflammatory properties of marmelosin from Bael (*Aegle marmelos* L.); Inhibition of TNF- α mediated inflammatory/tumor markers. *Biomedicine & Pharmacotherapy*, 106, 98-108.
8. P Santhana Krishnan, V., Karthikeyan, G., Janaki, P., Poonkodi, B., & Sathya, R. (2016). Isolation of Heraclenin from *Aegle marmelos* correa and screening for its antimicrobial activity through *in vitro* & *in silico* studies. *The Natural Products Journal*, 6(2), 134-141.
9. Ali, M. S., Ahmed, G., Pervez, M. K., Lateef, M., Afza, N., & Iqbal, L. (2011). Allo-imperatorin: A potent urease inhibitor from fresh unripe fruits of *Aegle marmelos* (Rutaceae). *Journal of the Chemical Society of Pakistan*, 33(6), 960-964.
10. Mandal, P. K., & Mukherjee, A. K. (1980). Structural investigations on bael exudate gum. *Carbohydrate Research*, 84(1), 147-159.
11. Kesari, A. N., Gupta, R. K., Singh, S. K., Diwakar, S., & Watal, G. (2006). Hypoglycemic and antihyperglycemic activity of *Aegle marmelos* seed extract in normal and diabetic rats. *Journal of Ethnopharmacology*, 107(3), 374-379.

12. Vijaya, C., Ramanathan, M., & Suresh, B. (2009). Lipid lowering activity of ethanolic extract of leaves of *Aegle marmelos* (Linn.) in hyperlipidaemic models of Wistar albino rats. *Indian Journal of Experimental Biology*, 47, 182-185.
13. Karmase, A., Birari, R., & Bhutani, K. K. (2013). Evaluation of anti-obesity effect of *Aegle marmelos* leaves. *Phytomedicine*, 20(10), 805-812.
14. Yang, J. Y., Della-Fera, M. A., Hartzell, D. L., Nelson-Dooley, C., Hausman, D. B., & Baile, C. A. (2006). Esculetin induces apoptosis and inhibits adipogenesis in 3T3-L1 cells. *Obesity*, 14(10), 1691-1699.
15. Nugroho, A. E., Riyanto, S., Sukari, M. A., & Maeyama, K. (2011). Effects of aegeline, a main alkaloid of *Aegle marmelos* Correa leaves, on the histamine release from mast cells. *Pakistan Journal of Pharmaceutical Sciences*, 24(3), 359-367.
16. Gautam, S., Ishrat, N., Singh, R., Narender, T., & Srivastava, A. K. (2015). Aegeline from *Aegle marmelos* stimulates glucose transport via Akt and Rac1 signaling and contributes to a cytoskeletal rearrangement through PI3K/Rac1. *European Journal of Pharmacology*, 762, 419-429.
17. Phuwapraisirisan, P., Puksasook, T., Jong-Aramruang, J., & Kokpol, U. (2008). Phenylethyl cinnamides: A new series of α -glucosidase inhibitors from the leaves of *Aegle marmelos*. *Bioorganic & Medicinal Chemistry Letters*, 18(18), 4956-4958.
18. Faizi, S., Farooqi, F., Zikr-Ur-Rehman, S., Naz, A., Noor, F., Ansari, F., Ahmad, A. & Khan, S. A. (2009). Shahidine, a novel and highly labile oxazoline from *Aegle marmelos*: The parent compound of aegeline and related amides. *Tetrahedron*, 65(5), 998-1004.
19. Rajan, S., Satish, S., Shankar, K., Pandeti, S., Varshney, S., Srivastava, A., Kumar, D., Gupta, A., Gupta, S., Choudhary, R. and Balaramnavar, V.M. (2018). Aegeline inspired synthesis of novel β 3-AR agonist improves insulin sensitivity *in vitro* and *in vivo* models of insulin resistance. *Metabolism*, 85, 1-13.
20. Satish, S., Srivastava, A., Yadav, P., Varshney, S., Choudhary, R., Balaramnavar, V. M., Narender, T. & Gaikwad, A. N. (2018). Aegeline inspired synthesis of novel amino alcohol and thiazolidinedione hybrids with antiadipogenic activity in 3T3-L1 cells. *European Journal of Medicinal Chemistry*, 143, 780-791.
21. Narender, T., Shweta, S., Tiwari, P., Reddy, K. P., Khaliq, T., Prathipati, P., Puri, A., Srivastava, A.K., Chander, R., Agarwal, S.C. & Raj, K. (2007). Antihyperglycemic and antidyslipidemic agent from *Aegle marmelos*. *Bioorganic & Medicinal Chemistry Letters*, 17(6), 1808-1811.

22. Gajbhiye, N., Makasana, J., & Thorat, T. (2012). Simultaneous determination of marmin, skimmianine, umbelliferone, psoralene, and imperatorin in the root bark of *Aegle marmelos* by high performance thin layer chromatography. *JPC-Journal of Planar Chromatography-Modern TLC*, 25(4), 306-313.
23. Chakthong, S., Wearyee, P., Puangphet, P., Mahabusarakam, W., Plodpai, P., Voravuthikunchai, S. P., & Kanjana Opas, A. (2012). Alkaloid and coumarins from the green fruits of *Aegle marmelos*. *Phytochemistry*, 75, 108-113.
24. Sastry, A. V. S., Girija Sastry, V., Naga Sandhya, G., & Srinivas, K. (2011). Phytochemical investigations and hepatoprotective effects of aqueous fruit extract of *Aegle marmelos* Corr. *International Journal of Chemical Sciences*, 9(2), 900-910.
25. Ohashi, K., Watanabe, H., Ohi, K., Arimoto, H., & Okumura, Y. (1995). Two new 7-geranyloxycoumarins from the bark of *Aegle marmelos*, an Indonesian medicinal Plant. *Chemistry Letters*, 24(10), 881-882.
26. Laphookhieo, S., Phungpanya, C., Tantapakul, C., Techa, S., Tha-in, S., & Narmdorkmai, W. (2011). Chemical constituents from *Aegle marmelos*. *Journal of the Brazilian Chemical Society*, 22, 176-178.
27. Vimal, V., & Devaki, T. (2004). Linear furanocoumarin protects rat myocardium against lipidperoxidation and membrane damage during experimental myocardial injury. *Biomedicine & Pharmacotherapy*, 58(6-7), 393-400.
28. Shinde, P. B., & Laddha, K. S. (2015). Simultaneous quantification of furanocoumarins from *Aegle marmelos* fruit pulp extract. *Journal of Chromatographic Science*, 53(4), 576-579.
29. Radchatawedchakoon, W., Bamrungsuk, S., Namwijit, S., Apiratikul, N., Sakee, U., & Yingyongnarongkul, B. E. (2015). A new 3'-prenyloxypsoralen from the raw fruits of *Aegle marmelos* and its cytotoxic activity. *Natural Product Communications*, 10(11), 1973-1975.
30. Pitre, S., & Srivastava, S. K. (1988). Pharmacological, microbiological and phytochemical studies on roots of *Aegle marmelos*. *Journal of Ethnopharmacology*, 23(2-3), 194-197.
31. Nugroho, A. E., Wibowo, J. T. R. I., & Riyanto, S. U. G. E. N. G. (2012). Marmin, a compound from *Aegle marmelos* Corr., relaxes the ovalbumin-induced contraction of trachea. *International Journal of Pharmacy and Pharmaceutical Sciences*, 4(1), 479-484.
32. Ng, R. C., Kassim, N. K., Yeap, Y. S., Ee, G. C. L., Yazan, S. L., & Musa, K. H.

- (2018). Isolation of carbazole alkaloids and coumarins from *Aegle marmelos* and *Murraya koenigii* and their antioxidant properties. *Sains Malaysiana*, 47(8), 1749-1756.
33. Lampronti, I., Martello, D., Bianchi, N., Borgatti, M., Lambertini, E., Piva, R., & Gambari, R. (2003). *In vitro* antiproliferative effects on human tumor cell lines of extracts from the Bangladeshi medicinal plant *Aegle marmelos* Correa. *Phytomedicine*, 10(4), 300-308.
34. Li, H., Chao, X., He, C. L., Wang, X. M., Liang, M., & Dong, C. H. (2016). Alloimperatorin and its epoxide derivative exhibit *in vitro* antitumor activity in HL-60 acute myeloid leukemia cancer cells *via* inducing apoptosis, cell cycle disruption and inhibition of cell migration. *Bangladesh Journal of Pharmacology*, 11(1), 194-199.
35. Ram, P. P., Varun, G., Balram, S., Deepak, C., Veerma, R., & Anil, B. (2012). Extraction and isolation of marmelosin from *Aegle marmelos*, synthesis and evaluation of their derivative as antidiabetic agent. *Der Pharmacia Lettre*, 4(4), 1085-1092.
36. Badam, L., Bedekar, S. S, Sonavane, K. B., & Joshi, S. P. (2002). *In vitro* antiviral activity of bael (*Aegle marmelos* Corr) upon human coxsackieviruses B1-B6. *Journal of Communicable Diseases*, 34(2), 88-99.
37. Panda, S., & Kar, A. (2006). Evaluation of the antithyroid, antioxidative and antihyperglycemic activity of scopoletin from *Aegle marmelos* leaves in hyperthyroid rats. *Phytotherapy Research*, 20(12), 1103-1105.
38. Mishra, B. B., Kishore, N., Tiwari, V. K., Singh, D. D., & Tripathi, V. (2010). A novel antifungal anthraquinone from seeds of *Aegle marmelos* Correa (Rutaceae). *Fitoterapia*, 81(2), 104-107.
39. Mahajan, N., Koul, B., Kaur, J., Bishnoi, M., Gupta, P., Kumar, A., Shah, B.A., Mubeen, I., Rai, A.K., Prasad, R. & Singh, J. (2022). Antiobesity potential of bioactive constituents from dichloromethane extract of *Psoralea corylifolia* L. seeds. *BioMed Research International*, 2022, 9504787.

Synthesis of Series I

5. Synthesis of Coumarin Analogues - Series I

5.1. Rationale

Bioassay guided fractionation of the most active methanolic extract from AM fruits resulted in the isolation and identification of coumarins (psoralen, xanthotoxol and alloimperatorin) as potential NP leads for PL inhibition. Nevertheless, molecular modelling studies of these leads (present in AM) in the active site of Human PL highlighted, favourable interactions for the coumarin scaffold. As represented in **Fig 5.1**, psoralen, xanthotoxol and alloimperatorin possessed a coumarin scaffold. This can be further confirmed with the previous literature on the PL inhibitory activity of coumarins *viz.*, coumarinolignans (**Fig 5.1**) namely, cleomiscosin A, C, and B from *Fraxinus rhynchophylla* stem barks. These coumarins have been reported to inhibit PL activity [1], with moderate to low potential as they did not contain an ester or ester mimicking group (amide/ketoamide) essential for potential PL inhibition (**Fig 5.1**).

Nevertheless, coumarins have been least explored for the PL inhibition and those reported exhibit moderate PL inhibitory activity. On the contrary, structural modifications that include various substitutions on the coumarins have resulted in a significant enhancement in their PL inhibitory activity. For example, the most potent analogue of furo[3,2-*c*]coumarins inhibited PL with the potent IC_{50} value of $9.37 \pm 1.36 \mu\text{M}$, as compared with orlistat ($0.2 \mu\text{M}$) [2]. In recent years, a variety of tripeptides have been reported to inhibit the PL enzyme. The primary reason for the effectiveness of all of these tripeptide's inhibitors was their amidic linkages [3,4]. Similarly, Sridhar *et al.* has previously synthesized and reported 2-thioxo-thiazolidin-4-one acetic acid derivatives for their potent PL inhibitory potential (IC_{50} 5.16 μM , 9.34 μM , and 10.64 μM , respectively), which were comparable to that of Orlistat (0.99 μM). The molecular docking studies confirmed that the carbonyl group of the amide linkage in the rhodanine moiety interacted with Ser 152. This group's presence facilitated the interaction with lid domain amino acids, thereby increasing the potency of the molecule [5].

CHAPTER V

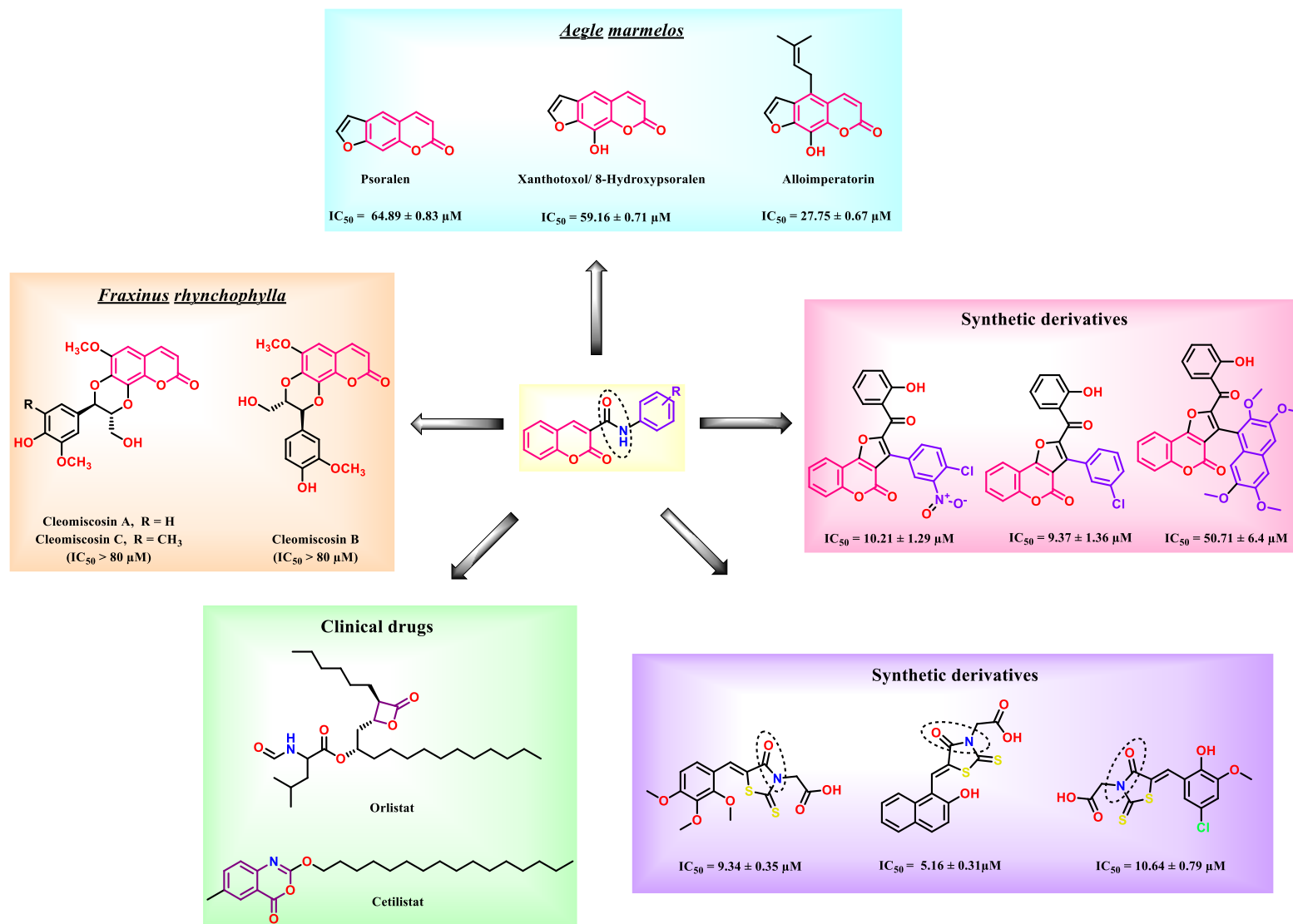


Figure 5.1. Rationale for selecting coumarin analogues as PL inhibitors

Further Orlistat and alloimperatorin exhibited a MolDock Scores of -139.41 kcal/mol and -110.296 kcal/mol, respectively (**Fig 5.2**). Potential chemical functionalities having an ability to interact with Ser 152 are essential requirement for the PL inhibition. Orlistat possessed a highly reactive β -lactone, while alloimperatorin contained a furanocoumarin ring. The furan ring's presence may be the reason for the diminished PL inhibitory potential of the furanocoumarins, as it did not exhibit any interaction with the critical amino acids (catalytic/hydrophobic) of the PL. Thus, to develop potent PL inhibitors various structural modifications such as the reducing the structural rigidity, incorporation of the reactive functionalities and various essential pharmacophoric features that are required for PL inhibition were proposed.

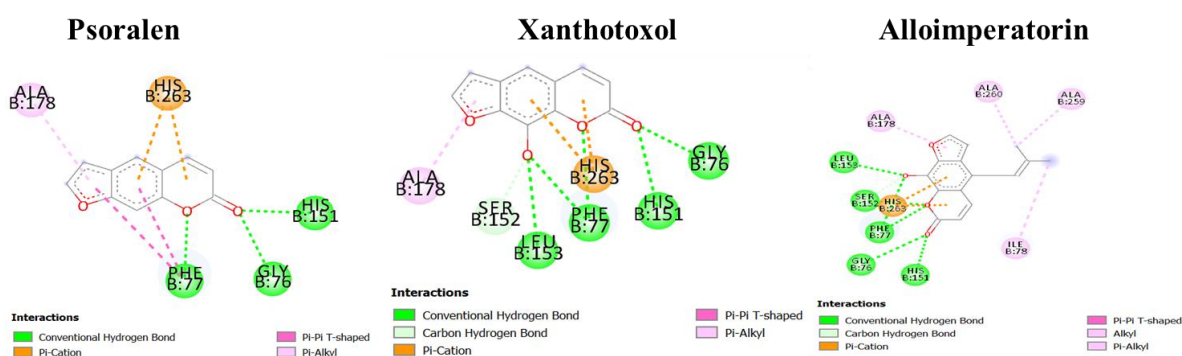


Figure 5.2. 2D pose of psoralen, xanthotoxol and alloimperatorin in the active site of PL.

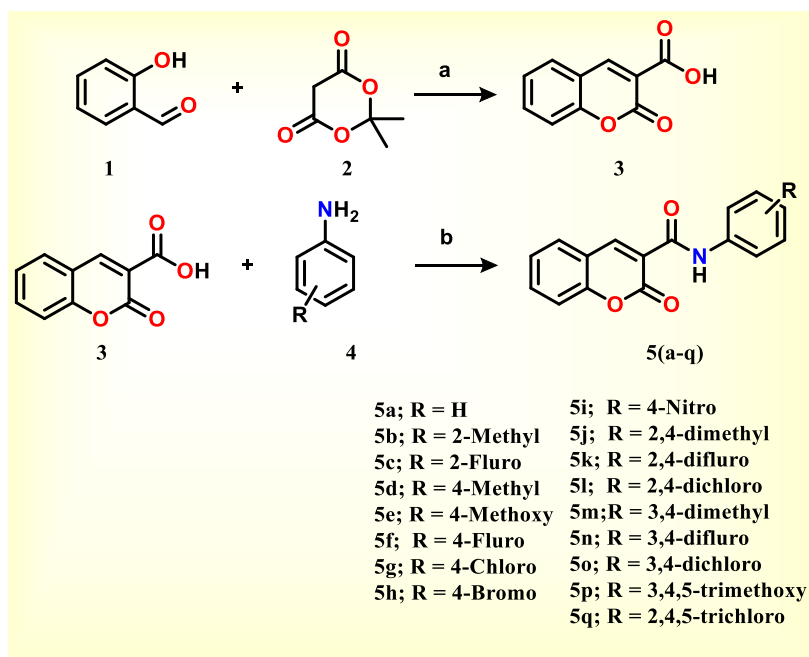
Based on the above literature, we hypothesized the design of coumarin inspired amide warhead containing analogues to possess potential PL inhibitory activity (**Fig 5.1**). These analogues can be considered as pharmacophoric hybrid of the coumarin scaffold and amide functionality, present in a single molecule. These analogues were designed with an aim to achieve the required amino acid interaction important for PL and as well as to include the reactive carbonyl group. A series of 17 amide warhead containing coumarin analogues were synthesised and evaluated for their PL inhibitory activity.

5.2. Synthesis and Characterization

The syntheses of all the final compounds **5a-5q** (**Table 5.1**) were carried out as per the procedure detailed in **Scheme 5.1**. Initially, Meldrum's acid (**2**; 1 equiv) and K_2CO_3 (0.60 equiv) were allowed to react in the presence of water at room temperature. In this basic reaction media, Meldrum's conjugate base was generated. After 10 to 15 mins, salicylaldehyde (**1**; 1 equiv) was added to the reaction mixture. The conjugate base of Meldrum's acid was engaged in a nucleophilic attack on the electron-deficient carbonyl carbon of salicylaldehyde, producing a Knoevenagel intermediate. In the subsequent step, the

geometrically favourable phenolic group within the intermediate underwent a ring-closure reaction *via* a nucleophilic attack on the carbonyl carbon of the acidic portion of Meldrum's intermediate, resulting in the formation of coumarin-3-carboxylate and the elimination of an acetone molecule. The salt's acidification liberated coumarin-3-carboxylic acid (**3**). After 20 h, 92% of the expected coumarin-3-carboxylic acid (2-oxo-2*H*-chromene-3-carboxylic acid; **3**) was produced [6].

To a solution of coumaric-3-carboxylic acid (1 equiv) in DMF at 0°C, EDC.HCl (1.10 equiv) was added and the mixture was allowed to react for 10 mins, resulting in the creation of O-acylisourea. HOBt (1.10 equiv) was introduced to this reaction mixture, which reacted with acid (**3**) to produce HOBt ester and urea as a by-product. Then substituted anilines (1 equiv) were added to the reaction mixture, followed by DIPEA (0.60 equiv). In the acid aniline coupling reaction, two by-products, EDC-derived urea and HOBt, were produced. Therefore, the reaction was catalytic in HOBt but stoichiometric in EDC, which was transformed into urea. The reaction mixture was agitated at room temperature for 15-20 h in presence of nitrogen, resulting in the production of the desired products (**5a-5q**). The solvent was removed in a vacuum, and the water-soluble residues were easily eliminated in an aqueous work-up. Using silica gel-based column chromatography, purification was further achieved [7]. Spectroscopic techniques such as IR, NMR (¹H and ¹³C), HRMS and HPLC were utilised to characterise all synthesized analogues.



Scheme 5.1. Reagents and conditions: (a) K₂CO₃, H₂O, RT, 20 h; (b) DMF, 0 °C, EDC.HCl, HOBt, Ar-NH₂, DIPEA, 20-30 °C, 15-20 h.

5.2.1. General procedure for the synthesis of coumarin-3-carboxylic acid derivatives

Synthetic route for the preparation of coumarin-3-carboxylic acid derivatives is summarized in **Scheme 5.1**. Meldrum's acid (**2**; 1 equiv), distilled water (5 mL), and K_2CO_3 (0.20 equiv) were added to a 50 mL RBF. After 10-15 mins, salicylaldehyde (**1**; 1 equiv) was added to the reaction mixture. The mixture was then aggressively agitated at room temperature for 20 h to complete the conversion. Upon completion, the resultant solution was acidified with 1N HCl, and the solid mass was precipitated, filtered, and thoroughly washed with water to provide a nearly pure product of coumarin-3-carboxylic acid (**3**). It was crystallised using ethyl acetate for further purification [6].

5.2.2. General Procedure of synthesis of coumarin-3-carboxamide derivatives (5a-q)

A solution of coumaric-3-carboxylic acid (**3**; 1 equiv) in DMF at 0 °C was progressively treated with EDC.HCl (1.10 equiv) and HOBT (1.10 equiv). Various substituted anilines (**4**; 1 equiv) were dissolved in DMF and added to the reaction mixture after 10 mins, followed by the addition of DIPEA (0.60 equiv). The reaction was stirred at room temperature for 15 to 20 h. After the reaction was complete, water was used for the work up. The precipitated solid mass was filtered, carefully washed with water, and then air-dried. To achieve a pure product, column chromatography was performed using a gradient of ethyl acetate/hexane as the eluent and silica (#100-200) as the stationary phase. NMR, HRMS, ATR and HPLC were used to characterize the synthesized analogues (**5a-5q**) [7].

5.2.3. Analytical data of synthesized analogues**2-oxo-N-phenyl-2H-chromene-3-carboxamide (5a)**

Yield: 85 %; white solid; mp = 250-252 °C; 1H NMR (400 MHz, $CDCl_3$) δ 10.86 (s, 1H), 9.05 (s, 1H), 7.79 - 7.70 (m, 4H), 7.50 - 7.34 (m, 4H), 7.19 (t, J = 7.4 Hz, 1H). ^{13}C NMR (100 MHz, $CDCl_3$) δ 161.84, 159.31, 154.52, 148.96, 137.68, 134.37, 129.96, 129.08, 125.49, 124.84, 120.60, 118.74, 118.69, 116.74. IR (ATR) ν 3841.67, 3746.91, 3611.09, 3031.76, 2919.21, 2470.42, 1691.61, 1591.48, 1541.44, 1429.76, 1312.95, 1241.44, 1194.24, 1118.72, 1019.02, 967.53, 899, 729.95, 681.49, 638.07 cm^{-1} . HRMS (ESI+) calculated for $C_{16}H_{11}NO_3$ $[M + H]^+$, 266.0818; found 266.0783. HPLC purity: 99.71 %, t_R = 7.257 min.

2-oxo-N-(o-tolyl)-2H-chromene-3-carboxamide (5b)

Yield: 88 %; off-white solid; mp = 229-231 °C; 1H NMR (400 MHz, $CDCl_3$) δ 10.81 (s, 1H), 9.07 (s, 1H), 8.28 (d, J = 8.2 Hz, 1H), 7.77 (d, J = 6.1 Hz, 1H), 7.73 (t, J = 7.9 Hz, 1H), 7.51 - 7.40 (m, 2H), 7.30 (d, J = 7.4 Hz, 1H), 7.26 (d, J = 7.6 Hz, 1H), 7.12 (t, J = 6.8 Hz, 1H), 2.45 (s, 3H). ^{13}C NMR (100 MHz, $CDCl_3$) δ 161.99, 159.28, 154.49, 148.95, 136.14, 134.33, 130.50, 129.95, 128.62, 126.74, 125.48, 124.98, 121.94, 118.88, 118.76, 116.74, 18.10. IR

(ATR) ν 3851.79, 3744.88, 3613.27, 3030.27, 2371.08, 2310.12, 1706.76, 1604.53, 1548.36, 1450.28, 1374.02, 1312.13, 1253.93, 1203.95, 1116.69, 1034.12, 974.00, 927.08, 745.73, 644.46 cm^{-1} . HRMS (ESI+) calculated for $\text{C}_{17}\text{H}_{13}\text{NO}_3$ $[\text{M} + \text{H}]^+$, 280.0974; found 280.0914. HPLC purity: 99.31 %, $t_R = 8.840$ min.

***N*-(2-fluorophenyl)-2-oxo-2*H*-chromene-3-carboxamide (5c)**

Yield: 80 %; off-white solid; mp = 260-262 °C; ^1H NMR (400 MHz, CDCl_3) δ 11.14 (s, 1H), 9.03 (s, 1H), 8.52 – 8.47 (m, 1H), 7.78 - 7.70 (m, 2H), 7.50 - 7.41 (m, 2H), 7.23 - 7.10 (m, 3H). ^{13}C NMR (100 MHz, CDCl_3) δ 161.64, 159.49, 154.61, 151.95, 149.08, 134.51, 129.99, 125.49, 125.06, 124.51, 122.26, 118.64, 118.51, 116.82, 115.16, 114.98. IR (ATR) ν 3851.20, 3743.53, 3672.32, 3613.19, 3030.61, 2311.61, 1703.46, 1610.45, 1543.42, 1448.06, 1321.17, 1256.66, 1197.69, 1130.59, 1027.16, 969.90, 925.84, 789.47, 742.09, 641.53 cm^{-1} . HRMS (ESI+) calculated for $\text{C}_{16}\text{H}_{10}\text{FNO}_3$ $[\text{M} + \text{H}]^+$, 284.0724; found 284.0709. HPLC purity: 98.55 %, $t_R = 8.343$ min.

2-oxo-*N*-(*p*-tolyl)-2*H*-chromene-3-carboxamide (5d)

Yield: 89 %; lemon yellow solid; mp = 330-333 °C; ^1H NMR (400 MHz, CDCl_3) δ 10.78 (s, 1H), 9.03 (s, 1H), 7.79 - 7.67 (m, 2H), 7.64 (d, $J = 8.1$ Hz, 2H), 7.50 - 7.39 (m, 2H), 7.20 (d, $J = 8.0$ Hz, 2H), 2.36 (s, 3H). ^{13}C NMR (100 MHz, CDCl_3) δ 161.83, 159.13, 154.48, 148.76, 135.16, 134.50, 134.27, 129.92, 129.58, 125.45, 120.54, 118.76, 116.72, 20.97. IR (ATR) ν 3851.95, 3743.42, 3672.70, 3613.27, 3023.80, 2368.08, 2314.64, 1916.31, 1700.97, 1603.64, 1541.36, 1409.12, 1317.33, 1247.35, 1201.32, 1128.51, 1028.17, 926.20, 801.08, 754.40 cm^{-1} . HRMS (ESI+) calculated for $\text{C}_{17}\text{H}_{13}\text{NO}_3$ $[\text{M} + \text{H}]^+$, 280.0974; found 280.0949. HPLC purity: 99.57 %, $t_R = 9.467$ min.

***N*-(4-methoxyphenyl)-2-oxo-2*H*-chromene-3-carboxamide (5e)**

Yield: 91 %; yellow solid; mp = 352-355 °C; ^1H NMR (400 MHz, CDCl_3) δ 10.73 (s, 1H), 9.02 (s, 1H), 7.79 - 7.62 (m, 4H), 7.49 - 7.38 (m, 2H), 6.96 - 6.88 (m, 2H), 3.83 (s, 3H). ^{13}C NMR (100 MHz, CDCl_3) δ 161.84, 159.04, 156.75, 154.46, 148.63, 134.24, 130.91, 129.90, 125.45, 122.11, 118.77, 118.75, 116.71, 114.22, 55.50. IR (ATR) ν 3852.16, 3743.16, 3672.56, 3612.89, 3273.59, 3273.59, 3052.48, 2928.36, 2314.21, 1696.14, 1600.02, 1543.28, 1509.44, 1455.51, 1300.26, 1226.64, 1028.32, 799.90, 758.92, 718.06, 638.62 cm^{-1} . HRMS (ESI+) calculated for $\text{C}_{17}\text{H}_{13}\text{NO}_4$ $[\text{M} + \text{H}]^+$, 296.0924; found 296.0895. HPLC purity: 99.34 %, $t_R = 6.457$ min.

***N*-(4-fluorophenyl)-2-oxo-2*H*-chromene-3-carboxamide (5f)**

Yield: 82 %; off-white solid; mp = 224-228 °C; ^1H NMR (400 MHz, CDCl_3) δ 10.85 (s, 1H), 9.04 (s, 1H), 7.89 - 7.60 (m, 4H), 7.59 - 7.35 (m, 2H), 7.10 (t, $J = 8.4$ Hz, 2H). ^{13}C NMR (100

MHz, CDCl₃) δ 161.87, 159.32, 154.52, 149.03, 134.47, 133.76, 129.98, 125.55, 122.23, 118.70, 118.50, 116.78, 115.87, 115.64. IR (ATR) ν 3852.62, 3743.87, 3672.92, 3613.03, 3027.43, 2922.77, 2847.70, 2372.12, 2312.46, 1917.45, 1840.12, 1746.41, 1688.83, 1543.38, 1398.42, 1194.88, 1051.44, 827.37, 791.12, 746.78 cm⁻¹. HRMS (ESI+) calculated for C₁₆H₁₀FNO₃ [M + H]⁺, 284.0724; found 284.0695. HPLC purity: 99.49 %, t_R = 7.477 min.

***N*-(4-chlorophenyl)-2-oxo-2*H*-chromene-3-carboxamide (5g)**

Yield: 86 %; off-white solid; mp = 228-230 °C; ¹H NMR (400 MHz, CDCl₃) δ 10.91 (s, 1H), 9.04 (s, 1H), 7.81 - 7.67 (m, 4H), 7.53 - 7.34 (m, 4H). ¹³C NMR (100 MHz, CDCl₃) δ 161.86, 159.39, 154.54, 149.16, 136.28, 134.55, 130.02, 129.12, 125.59, 121.78, 118.68, 118.40, 116.79, 115.88. IR (ATR) ν 3851.51 3742.74, 3672.56, 3612.95, 3182.79, 3047.22, 2927.12, 2853.93, 2313.29, 1693.98, 1594.00, 1394.51, 1198.53, 1125.56, 1076.56, 1006.31, 924.92, 823.75, 749.00 cm⁻¹. HRMS (ESI+) calculated for C₁₆H₁₀ClNO₃ [M + H]⁺, 300.0428; found 300.0379. HPLC purity: 99.60 %, t_R = 11.140 min.

***N*-(4-bromophenyl)-2-oxo-2*H*-chromene-3-carboxamide (5h)**

Yield: 79 %; yellow solid; mp = 220-225°C; ¹H NMR (400 MHz, CDCl₃) δ 10.91 (s, 1H), 9.04 (s, 1H), 7.80 - 7.71 (m, 2H), 7.71 - 7.65 (m, 2H), 7.55 - 7.43 (m, 4H). ¹³C NMR (100 MHz, CDCl₃) δ 161.85, 159.40, 154.54, 149.19, 136.77, 134.57, 132.07, 130.02, 125.60, 122.10, 118.68, 118.39, 117.49, 116.80. IR (ATR) ν 3851.47, 3742.96, 3672.30, 3037.89, 2924.02, 2311.88, 1840.35, 1748.73, 1688.24, 1521.97, 1452.87, 1389.08, 1178.09, 1110.73, 1046.92, 972.96, 922.57, 817.73, 743.98 cm⁻¹. HRMS (ESI+) calculated for C₁₆H₁₀BrNO₃ [M + H]⁺, 343.9923; found 343.9916. HPLC purity: 99.74 %, t_R = 12.640 min.

***N*-(4-nitrophenyl)-2-oxo-2*H*-chromene-3-carboxamide (5i)**

Yield: 60 %; yellow solid; mp = 240-242 °C; ¹H NMR (400 MHz, DMSO-*d*₆) δ 10.21 (s, 1H), 9.18 (s, 1H), 7.93 (d, *J* = 72.2 Hz, 4H), 7.69 - 7.41 (m, 4H). ¹³C NMR (100 MHz, DMSO-*d*₆) δ 161.29, 155.37, 151.43, 136.35, 135.77, 127.52, 126.88, 125.58, 124.28, 118.31, 118.30, 118.28, 117.58, 116.82. IR (ATR) ν 3851.63, 3743.47, 3613.25, 3316.83, 2927.32, 2851.85, 1717.75, 1636.84, 1537.29, 1452.72, 1367.14, 1272.74, 1123.37, 1069.71, 966.26, 859.67, 747.05, 698.10, 642.46 cm⁻¹. HRMS (ESI+) calculated for C₁₆H₁₀N₂O₅ [M + H]⁺, 311.0669; found 311.0717. HPLC purity: 92.74 %, t_R = 7.633 min.

***N*-(2,4-dimethylphenyl)-2-oxo-2*H*-chromene-3-carboxamide (5j)**

Yield: 78 %; yellow solid; mp = 241-243 °C; ¹H NMR (400 MHz, CDCl₃) δ 10.72 (s, 1H), 9.05 (s, 1H), 8.11 (d, *J* = 8.0 Hz, 1H), 7.80 - 7.67 (m, 2H), 7.50 - 7.39 (m, 2H), 7.12 - 7.05 (m, 2H), 2.40 (s, 3H), 2.34 (s, 3H). ¹³C NMR (100 MHz, CDCl₃) δ 161.98, 159.19, 154.47, 148.77, 134.68, 134.23, 133.52, 131.18, 129.91, 128.72, 127.22, 125.44, 122.06, 118.95,

118.78, 116.72, 20.92, 18.00. IR (ATR) ν 3851.18, 3743.32, 3672.61 3612.93, 3037.30, 2915.58, 2365.39, 2316.01, 1702.60, 1604.07, 1541.97, 1443.83, 1371.94, 1312.10, 1204.08, 1158.12, 1031.77, 927.49, 754.22, 641.34 cm^{-1} . HRMS (ESI+) calculated for $\text{C}_{18}\text{H}_{15}\text{NO}_3$ [$\text{M} + \text{H}$] $^+$, 294.1131; found 294.1117. HPLC purity: 99.44 %, $t_R = 11.907$ min.

***N*-(2,4-difluorophenyl)-2-oxo-2*H*-chromene-3-carboxamide (5k)**

Yield: 83 %; white solid; mp = 214-217 °C; ^1H NMR (400 MHz, CDCl_3) δ 11.06 (s, 1H), 9.02 (s, 1H), 8.44 (td, $J = 9.6, 9.2, 6.0$ Hz, 1H), 7.75 (ddd, $J = 16.0, 8.3, 1.6$ Hz, 2H), 7.50 - 7.41 (m, 2H), 6.94 (ddq, $J = 11.6, 4.8, 2.9$ Hz, 2H). ^{13}C NMR (100 MHz, CDCl_3) δ 161.66, 159.51, 154.60, 151.97, 149.15, 134.60, 130.01, 125.54, 123.25, 123.14, 118.60, 118.30, 116.84, 111.23, 111.02, 104.06. IR (ATR) ν 3851.32, 3742.89, 3672.73, 3613.04, 3038.89, 2362.46, 2316.70, 1704.31, 1612.13, 1545.31, 1435.25, 1293.42, 1201.76, 1128.13, 1031.41, 955.61, 847.48, 847.48, 791.99, 751.89, 641.99 cm^{-1} . HRMS (ESI+) calculated for $\text{C}_{16}\text{H}_9\text{F}_2\text{NO}_3$ [$\text{M} + \text{H}$] $^+$, 302.0629; found 302.0626. HPLC purity: 99.63 %, $t_R = 9.033$ min.

***N*-(2,4-dichlorophenyl)-2-oxo-2*H*-chromene-3-carboxamide (5l)**

Yield: 84 %; white solid; mp = 200-204 °C; ^1H NMR (400 MHz, $\text{DMSO-}d_6$) δ 11.33 (s, 1H), 9.12 (s, 1H), 8.56 (s, 1H), 8.41 - 7.98 (m, 2H), 7.81 (d, $J = 17.3$ Hz, 2H), 7.57 (d, $J = 30.2$ Hz, 2H). IR (ATR) ν 3851.68, 3741.69, 3672.09, 3612.70, 3054.77, 2318.09, 1695.26, 1584.02, 1526.10, 1456.95, 1385.08, 1303.60, 1199.13, 1162.29, 1116.09, 1023.75, 971.09, 870.67, 755.95, 693.66 cm^{-1} . HRMS (ESI+) calculated for $\text{C}_{16}\text{H}_9\text{Cl}_2\text{NO}_3$ [$\text{M} + \text{H}$] $^+$, 334.0038; found 334.0041. HPLC purity: 98.93 %, $t_R = 21.827$ min.

* ^{13}C NMR - could not be recorded due to solubility issue.

***N*-(3,4-dimethylphenyl)-2-oxo-2*H*-chromene-3-carboxamide (5m)**

Yield: 80 %; white solid; mp = 200-202 °C; ^1H NMR (400 MHz, CDCl_3) δ 10.74 (s, 1H), 9.02 (s, 1H), 7.78 - 7.67 (m, 2H), 7.55 - 7.40 (m, 4H), 7.15 (d, $J = 8.0$ Hz, 1H), 2.30 (s, 3H), 2.27 (s, 3H). ^{13}C NMR (100 MHz, CDCl_3) δ 161.82, 159.08, 154.46, 148.69, 137.30, 135.41, 134.24, 133.25, 130.06, 129.92, 125.44, 121.80, 118.77, 118.04, 116.70, 19.93, 19.30. IR (ATR) ν 3851.18, 3743.32, 3672.61 3612.93, 3037.30, 2915.58, 2365.39, 2316.01, 1702.60, 1604.07, 1541.97, 1443.83, 1371.94, 1312.10, 1204.08, 1158.12, 1031.77, 926.20, 801.08, 754.40 cm^{-1} . HRMS (ESI+) calculated for $\text{C}_{18}\text{H}_{15}\text{NO}_3$ [$\text{M} + \text{H}$] $^+$, 294.1131; found 294.1118. HPLC purity: 99.43 %, $t_R = 12.347$ min.

***N*-(3,4-difluorophenyl)-2-oxo-2*H*-chromene-3-carboxamide (5n)**

Yield: 77 %; white solid; mp = 193-195 °C; ^1H NMR (400 MHz, $\text{DMSO-}d_6$) δ 10.77 (s, 1H), 8.92 (s, 1H), 8.03 (d, $J = 5.8$ Hz, 1H), 7.96 (s, 1H), 7.79 (d, $J = 8.7$ Hz, 1H), 7.59 - 7.53 (m, 1H), 7.53 - 7.39 (m, 3H). IR (ATR) ν 3851.74, 3742.48, 3613.10, 3056.89, 2362.78, 2318.10,

1694.90, 1608.48, 1555.93, 1509.97, 1439.23, 1283.19, 1203.27, 1119.54, 1033.29, 969.57, 869.91, 792.81, 753.93, 644.12 cm^{-1} . HRMS (ESI+) calculated for $\text{C}_{16}\text{H}_9\text{F}_2\text{NO}_3$ $[\text{M} + \text{H}]^+$, 302.0629; found 302.0580. HPLC purity: 99.62 %, $t_R = 9.077$ min.

^{13}C NMR – could not be recorded due to solubility issue.

***N*-(3,4-dichlorophenyl)-2-oxo-2*H*-chromene-3-carboxamide (5o)**

Yield: 75 %; off-white solid; mp = 202-203 °C; ^1H NMR (400 MHz, $\text{DMSO-}d_6$) δ 10.82 (s, 1H), 8.92 (s, 1H), 8.17 (s, 1H), 8.03 (d, $J = 7.7$ Hz, 1H), 7.79 (d, $J = 8.0$ Hz, 1H), 7.67 (d, $J = 6.0$ Hz, 2H), 7.57 (d, $J = 8.5$ Hz, 1H), 7.50 (d, $J = 7.5$ Hz, 1H). IR (ATR) ν 3851.68, 3741.69, 3672.09, 3612.70, 3054.77, 2318.09, 1695.26, 1526.10, 1456.95, 1385.08, 1303.60, 1199.13, 1162.29, 1116.09, 1023.75, 971.09, 870.67, 755.95, 693.66 cm^{-1} . HRMS (ESI+) calculated for $\text{C}_{16}\text{H}_9\text{Cl}_2\text{NO}_3$ $[\text{M} + \text{H}]^+$, 334.0038; found 333.9980. HPLC purity: 93.37 %, $t_R = 4.303$ min. ^{13}C NMR – could not be recorded due to solubility issue.

2-oxo-*N*-(3,4,5-trimethoxyphenyl)-2*H*-chromene-3-carboxamide (5p)

Yield: 92 %; lemon yellow solid; mp = 180-183 °C; ^1H NMR (400 MHz, CDCl_3) δ 10.81 (s, 1H), 9.02 (s, 1H), 7.76 - 7.70 (m, 2H), 7.50 - 7.40 (m, 2H), 7.08 (s, 2H), 3.92 (s, 6H), 3.86 (s, 3H). ^{13}C NMR (100 MHz, CDCl_3) δ 161.89, 159.26, 154.47, 153.35, 148.89, 135.07, 134.49, 133.77, 129.97, 125.58, 118.72, 118.53, 116.76, 98.05, 61.01, 56.18. IR (ATR) ν 3852.05, 3742.81, 3672.73, 3613.11, 2929.68, 1701.14, 1607.49, 1557.81, 1505.97, 1456.02, 1413.83, 1312.23, 1232.19, 1178.77, 1014.69, 794.18, 748.52, 658.08 cm^{-1} . HRMS (ESI+) calculated for $\text{C}_{16}\text{H}_9\text{Cl}_2\text{NO}_3$ $[\text{M} + \text{H}]^+$, 356.1135; found 356.1112. HPLC purity: 96.84 %, $t_R = 5.490$ min.

2-oxo-*N*-(2,4,5-trichlorophenyl)-2*H*-chromene-3-carboxamide (5q)

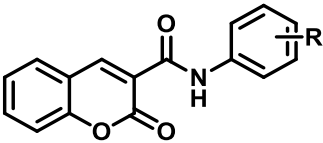
Yield: 91 %; lemon yellow solid; mp = 131-134 °C; ^1H NMR (400 MHz, CDCl_3) δ 12.76 (s, 1H), 8.62 (s, 1H), 7.62 (s, 1H), 7.51 - 7.42 (m, 2H), 7.38 (s, 1H), 7.07 (d, $J = 8.2$ Hz, 1H), 7.01 (t, 1H). ^{13}C NMR (100 MHz, CDCl_3) δ 164.34, 161.46, 144.86, 134.44, 132.85, 131.84, 131.23, 130.82, 128.47, 120.48, 119.44, 118.73, 117.65. IR (ATR) ν 3852.22, 3742.74, 3672.93, 3612.89, 2359.68, 1701.94, 1611.10, 1558.14, 1451.07, 1390.43, 1347.87, 1278.87, 1231.29, 1191.62, 1130.59, 1068.49, 875.99, 791.68, 758.08, 676.79 cm^{-1} . HRMS (ESI+) calculated for $\text{C}_{16}\text{H}_8\text{Cl}_3\text{NO}_3$ $[\text{M} + \text{NH}_4]^+$, 384.9970; found 384.9899. HPLC purity: 96.98 %, $t_R = 5.770$ min.

5.3. Pancreatic lipase inhibition assay

The PL inhibitory activity of all synthesised coumarin analogues (**5a-5q**) was performed according to standard protocol described in chapter 3 [8,9]. The enzyme used was Porcine PL (Type II) with 4-nitrophenyl butyrate as the substrate. As described in **Table 5.1**, the analogue

5a, which lacked any substitutions on either the coumarin or phenyl ring, exhibited poor PL inhibitory activity ($IC_{50} = 61.86 \pm 3.65 \mu\text{M}$). The impact of different halogen substituents (F, Cl, Br) on the *ortho*, *meta* and *para* positions of the phenyl ring was also explored. Surprisingly, fluorine on the *ortho* position of the phenyl ring increased the PL inhibitory potency of **5c** ($IC_{50} = 24.90 \pm 0.44 \mu\text{M}$). The activity of analogues containing fluoro, chloro and bromo substituents at the *para* position of the phenyl ring (**5f**, **5g**, **5h**) was shown to decrease activity ($IC_{50} = 44.29 \pm 2.44$, 58.63 ± 4.80 and $42.89 \pm 2.59 \mu\text{M}$ respectively). The substitution of fluoro groups at both the *ortho* and *para* positions of the phenyl ring inhibited PL effectively (**5k**, $IC_{50} = 21.30 \pm 1.81 \mu\text{M}$). **5q**, a trisubstituted chloro analogue, was found to be a potential PL inhibitor ($IC_{50} = 19.41 \pm 2.63 \mu\text{M}$). These findings demonstrated the significance of substituent (halogen) locations on the phenyl ring for PL inhibitory action. These investigations revealed that the position of electron-donating and electron-withdrawing substituents on the phenyl ring was crucial for PL inhibition.

Table 5.1. *In vitro* PL inhibitory activity of the synthesized analogues (**5a-5q**)

					
Code	R	$IC_{50} (\mu\text{M})^*$	Code	R	$IC_{50} (\mu\text{M})^*$
5a	-H	61.86 ± 3.65	5j	2,4-di- CH_3	39.78 ± 2.66
5b	2- CH_3	33.85 ± 1.16	5k	2,4-di-F	21.30 ± 1.81
5c	2-F	24.90 ± 0.44	5l	2,4-di-Cl	NS
5d	4- CH_3	50.19 ± 3.25	5m	3,4-di CH_3	37.30 ± 2.05
5e	4- OCH_3	37.20 ± 2.05	5n	3,4-di-F	NS
5f	4-F	44.29 ± 2.44	5o	3,4-di-Cl	NS
5g	4-Cl	58.63 ± 4.80	5p	3,4,5-tri- OCH_3	32.21 ± 0.55
5h	4-Br	42.89 ± 2.59	5q	2,4,5-tri-Cl	19.41 ± 2.63
5i	4- NO_2	40.61 ± 3.76		Orlistat	0.97 ± 0.31

*All experiments were performed in triplicate and the values are expressed in Mean \pm S.E.M.
NS = not soluble in DMSO

5.4. Enzyme kinetics

In order to comprehend the nature of inhibition (competitive, uncompetitive and non-competitive), the enzyme kinetics of the most potent analogues **5q** was analysed (**Table 5.2**). For the same, a three-concentration range of inhibitor (0, 0.3125, and 2.5 μM) was applied to four distinct substrate concentrations (25, 50, 100, and 200 μM). As depicted in **Fig 5.3**, the Lineweaver-Burk plot converged at the y-intercept ($1/V_{max}$), whereas K_m rose proportionally to inhibitor concentration [10].

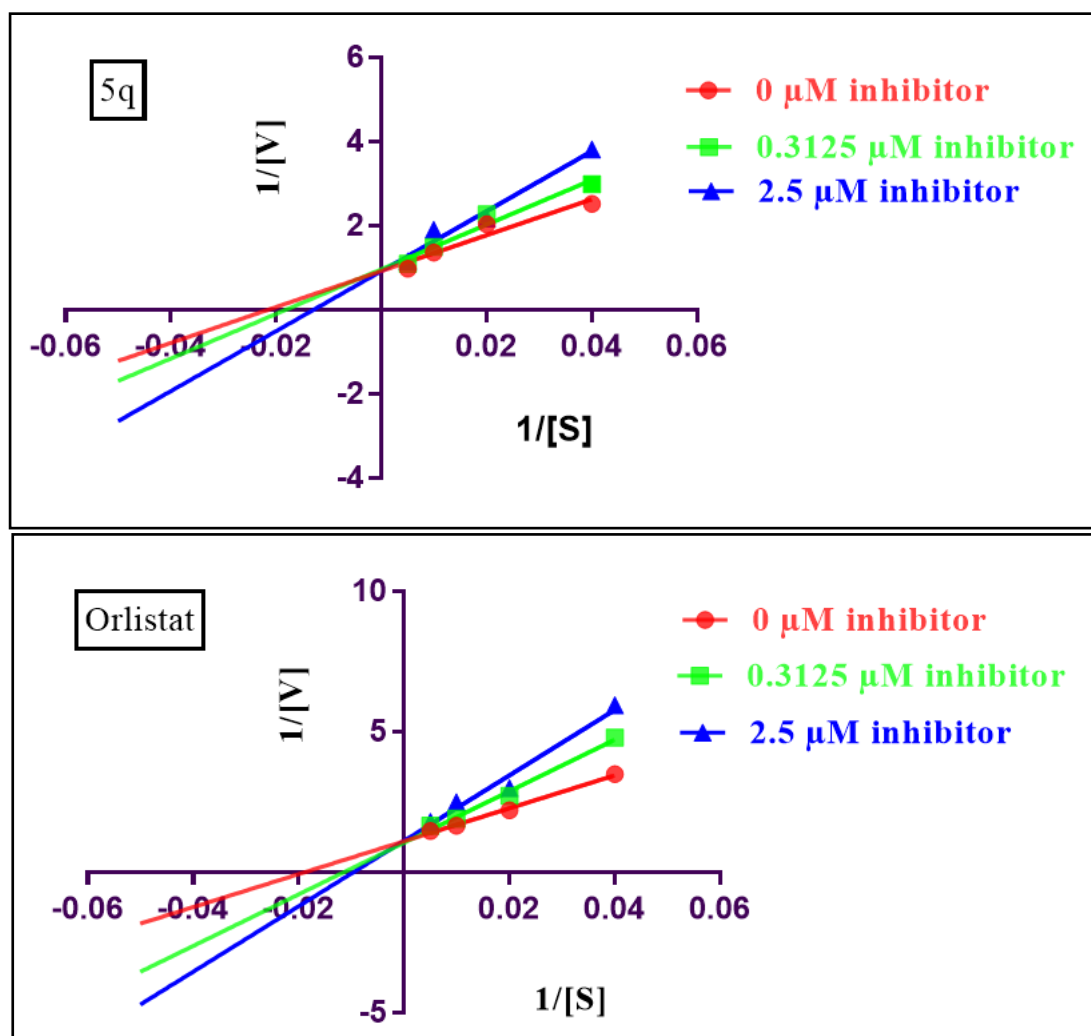


Figure 5.3. Double reciprocal Lineweaver-Burk plots of **5q** and Orlistat.

The apparent K_m value increased proportionally with increasing substrate concentration; however, the V_{max} was unchanged by substrate concentration, showing the extent of reversible inhibition. Using the Cheng-Prusoff equation, the inhibition constant (K_i) was also determined, and analogues **5q** were found to have K_i values of $10.386 \mu\text{M}$, respectively (Table 5.2). With a K_i value of $0.588 \mu\text{M}$, orlistat (positive control) likewise exhibited competitive inhibition [11].

Table 5.2. K_m , V_{max} and K_i values of **5q** and orlistat retrieved from the PL enzyme kinetics.

Code	K_m (apparent) at different concentration (μM)			V_{max} ($\mu\text{M}/\text{min}$)	K_i (μM)	Nature of inhibition
	$0 \mu\text{M}$	$0.3125 \mu\text{M}$	$2.5 \mu\text{M}$			
5q	45.806	54.409	76.617	1.058	10.386	Competitive
Orlistat	52.435	86.501	102.971	0.907	0.588	Competitive

5.5. Structure activity relationship

For depicting SAR, substituents on the phenyl ring of coumarin analogues were studied. According to **Table 5.1**, the IC_{50} for analogue with an unsubstituted phenyl ring (**5a**) was 61.86 μM . The replacement of halogens at various positions on the phenyl ring enhanced the inhibitory activity of PL. Halogen (F) on *ortho* position of **5c** analogue ($IC_{50} = 24.90 \mu\text{M}$) inhibited PL more effectively than its *para*-substituted **5f** analogue ($IC_{50} = 44.29 \mu\text{M}$) counterpart. Amongst the *para* substituents the bromo substituted analogue **5h** ($IC_{50} = 42.89 \mu\text{M}$) was marginally more active than the fluoro **5f** ($IC_{50} = 44.29 \mu\text{M}$) and chloro **5g** ($IC_{50} = 58.63 \mu\text{M}$) substituted analogues. The disubstituted fluoro analogue (**5k**, $IC_{50} = 21.30 \mu\text{M}$) had the second highest PL inhibitory activity in this series. The trisubstituted chloro analogue **5q** was the most potent PL inhibitor ($IC_{50} = 19.41 \mu\text{M}$). The **5e** analogue with a methoxy substituent at the *para* position of the phenyl ring had an IC_{50} value of 37.20 μM , however the **5p** counterpart with three methoxy groups on the phenyl ring had better IC_{50} value of 32.21 μM than **5e**. Analogue **5b** ($IC_{50} = 33.85 \mu\text{M}$) with *ortho*-substitution as methyl group on phenyl ring was more active than **5d** analogues with methyl group in *para* position ($IC_{50} = 50.19 \mu\text{M}$). The di-substitution of methyl at the (2nd,4th) and (3rd,4th) positions inhibited PL activity substantially ($IC_{50} = 39.78$ and $37.30 \mu\text{M}$, respectively). This investigation revealed the significance of substituents position on the phenyl ring for PL inhibition. **Fig 5.4** depicts a summary of the structure activity relationship (SAR) analysis, illustrating the effects of various substituents on PL inhibitory activity.

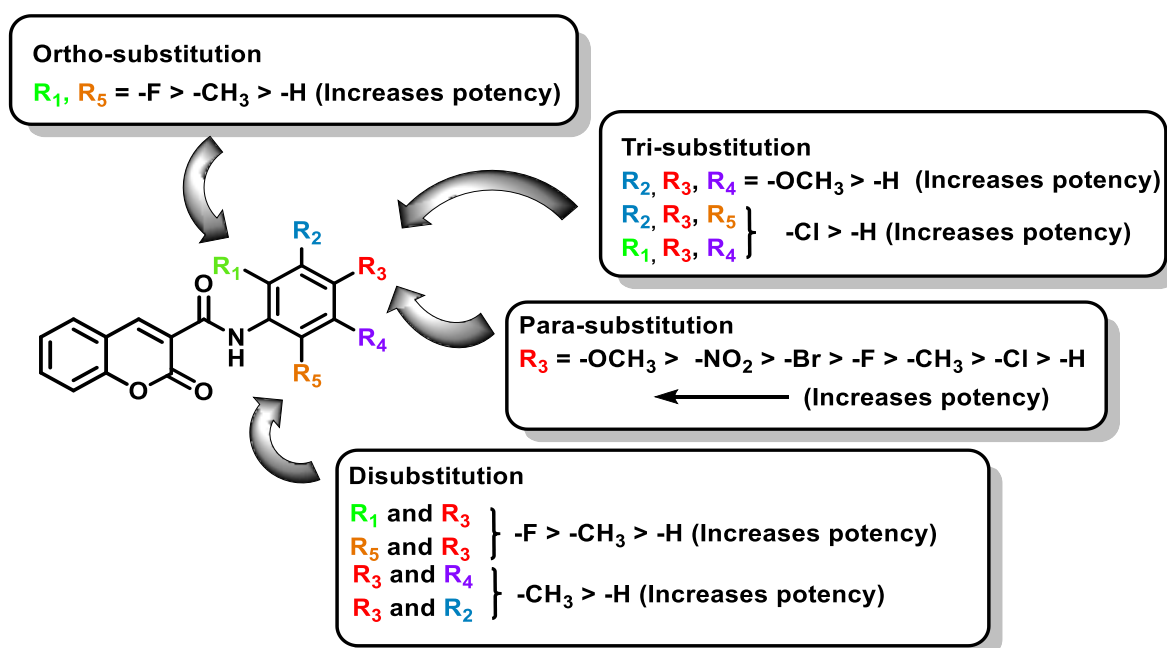


Figure 5.4. SAR study of coumarin analogues (Series I).

5.6. Fluorescence Quenching Measurements with PL

Phenylalanine (Phe), tyrosine (Tyr), and tryptophan (Trp) are the aromatic amino acids that contribute to the fluorescence property of PL. Fluorescence emission may be attributed to the presence of 25 Phe residues, 16 Tyr residues, and 7 Trp residues in PL. The Trp residues (Trp 17, Trp 30, Trp 86, Trp 107, Trp 253, Trp 339, and Trp 403) are the primary contributors to the intrinsic fluorescence, as the quantum yield for Phe is extremely low. Additionally, the structural and dynamic properties of an analogue are observed to affect the emission spectra of tryptophan. Consequently, intrinsic fluorescence spectroscopy can be employed to investigate the association reaction between a bioactive analogue and PL [12,13].

The previously reported method with the necessary modifications [12] was used to evaluate the effects of the synthesized analogues (**5q**) on the fluorescence quenching of PL. The results are summarized in **Fig 5.5**.

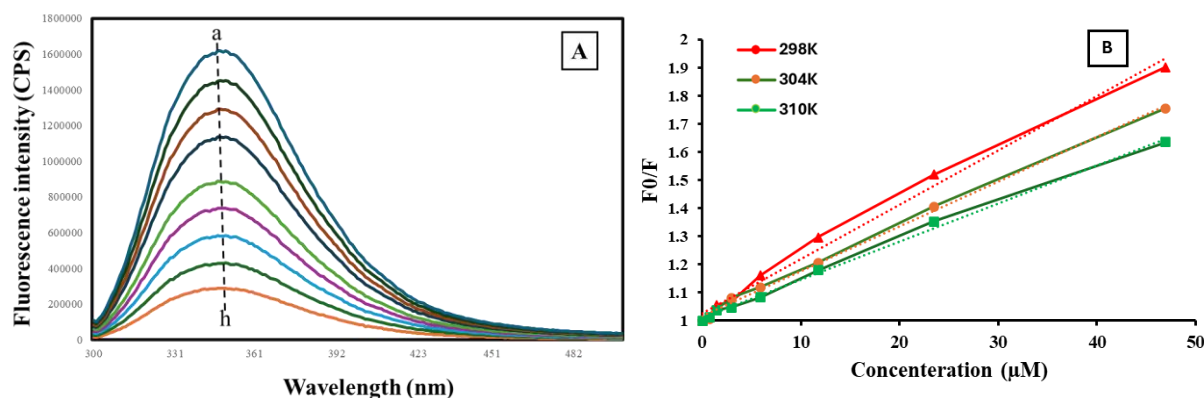


Figure 5.5. (A) The fluorescence spectra of PL in the presence of **5q** at various concentrations (pH 7.4, T = 298 K, a to h in increasing concentrations); (B) Stern-Volmer plot for the quenching of **5q** on the PL.

As illustrated in **Fig. 5.5.**, the PL fluorescence was quenched by **5q**. Additionally, the fluorescence intensity decreased as the concentration of quencher (**5q**) increased, suggesting the formation of PL-quencher complexes. The above fluorescence quenching was mainly due to static or dynamic mechanism. To identify the underlying mechanism of quenching, Stern-Volmer equation was utilized and the values were determined as per **Formula 3.3** (chapter 3). Fluorescence quenching can be classified into two categories: static quenching and dynamic quenching. Dynamic quenching is the term used to describe the process by which the quencher molecule in solution deactivates the excited state fluorophore, whereas static quenching is the term used to describe the formation of a non-fluorescent ground state complex of fluorophores and quencher. The dynamic quenching is emphasized by a direct

correlation between the quenching constant and the temperature, whereas static quenching is represented by a diminished quenching constant as the temperature increases [12,13].

Table 5.3. Bimolecular quenching constant (k_q), binding constant (K_b) and the number of binding sites (n) at different temperatures for **5q**.

#	T (K)	$K_{sv}/10^4$ (L/mol)	$k_q/10^{12}$ (L/mol sec)	R^2	$K_b/10^5$ (L/mol)	n	R^2
5q	298	1.6	1.09	0.9919	3.02	0.850	0.9899
	304	1.4	7.92	0.9955	2.62	0.846	0.9931
	310	1.1	6.20	0.9994	2.11	0.820	0.9929

As represented in **Table 5.3**, an inverse correlation between the K_{sv} and temperature suggested that the quenching effects on the PL may be mainly attributed due to static quenching rather than dynamic quenching.

The values of 'n' at the corresponding temperature were in the range of 0.820 to 0.850 (closer to 1), that indicated the presence of only one binding site in PL. This result further supported the competitive inhibition on the enzyme kinetics of PL. Additionally, the ' K_b ' values were in the range of 2.11 to 3.02 x 10⁵ L/mol indicating the strong binding forces of **5q** with PL.

5.7. Molecular docking analysis

The energy-minimized structures of the analogues (**5a-5q**) were docked into the crystal structure of human PL (PDB ID: 1LPB, resolution: 2.46 Å) with validated grid parameters using Molegro Virtual Docker 6.0. At the active site of the PL enzyme, there is an extremely restricted catalytic triad composed of Ser 152, Asp 176, and His 263 that is surrounded by a hydrophobic lid domain (Gly 76 - Lys 80 and Leu 213 - Met 217). This hydrophobic lid domain is opened during triglyceride hydrolysis by an activating process at the interface. The coumarin scaffold of the analogue exhibited hydrophobic interactions and π - π stacking with the lid domain, resulting in the lid domain's opening. The amide functionality was necessary for interaction with Ser 152. Additionally, the phenyl ring was substituted so that the electron-rich moiety effectively interacted with Arg 256.

As depicted in **Fig 5.6**, the potent analogue **5q** and Orlistat were found to bind at the active site of PL. **Table 5.4** depicts the MolDock score and docking interactions of all the analogues. All analogues were found to interact with hydrophobic amino acids in the lid domain, including Phe 77, Gly 76, and Ile 78, via π - π T-shaped and π -alkyl interactions. The unsubstituted coumarin analogue **5a** demonstrated a MolDock score of -97.688 kcal/mol. The substitution of a methyl group at the *ortho* position (**5b**) of the phenyl ring resulted in a

MolDock score -98.688 kcal/mol. Surprisingly, the *ortho*-substitution of the fluoro group on the phenyl ring did not raise the MolDock score for **5c** (-97.466 kcal/mol) but it did result in significant PL inhibition activity. The *ortho* and *para* substitutions improved the MolDock score for **5k** (-105.421 kcal/mol) and PL inhibition activity. This may be a result of the additional halogen interaction seen by analogues **5c** and **5k** with Phe 77 and Asp 79.

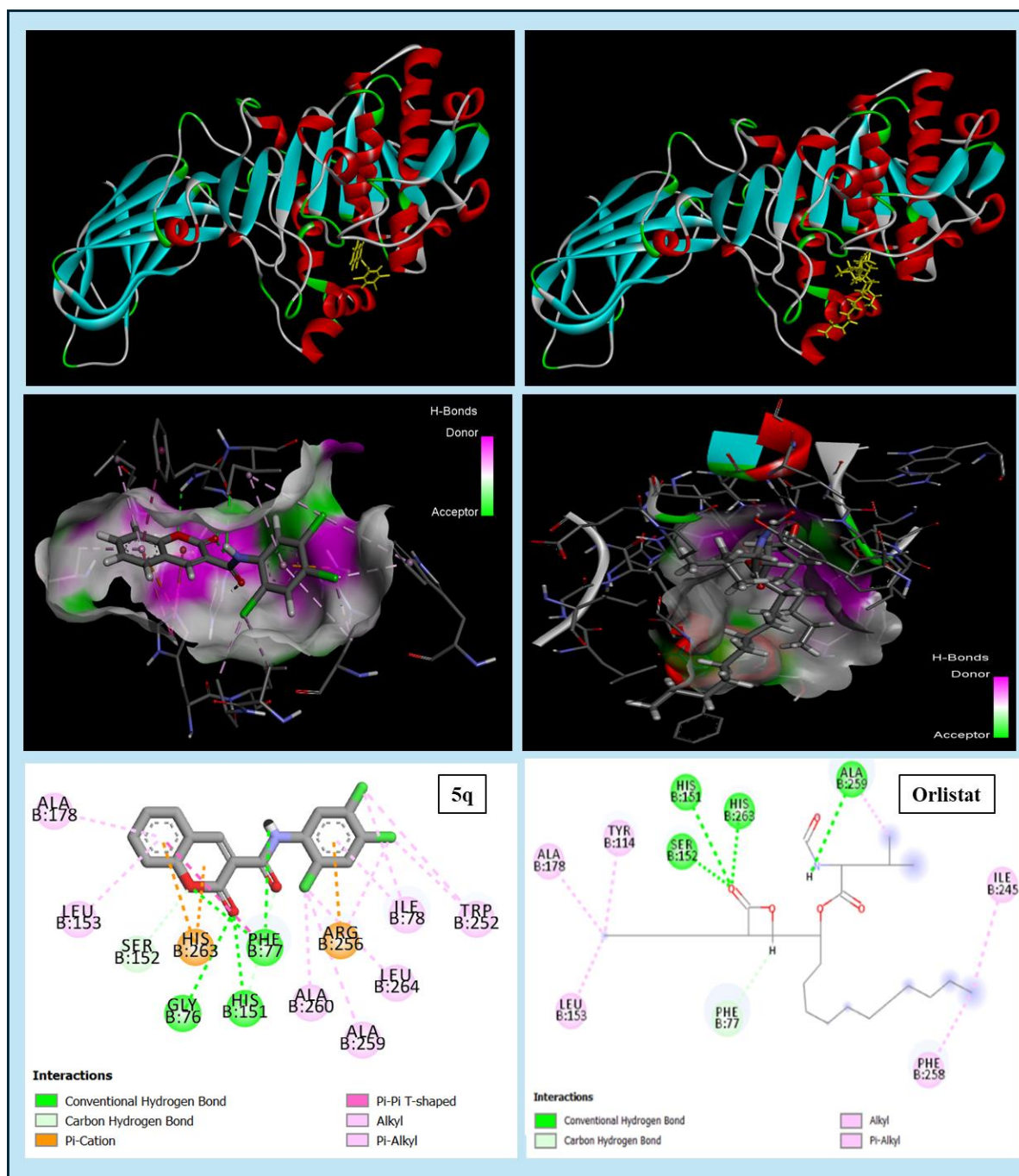


Figure 5.6. 2D and 3D interaction diagram of **5q** and Orlistat in the active site of PL (1LPB)

The analogues (**5f**, **5g** and **5h**) with only one halogen atom on the *para* position of the phenyl ring had a MolDock score between -100.744 and -101.351 kcal/mol. Halogen disubstitution on the phenyl ring improved the MolDock score from -97.688 to -106.401 kcal/mol. The MolDock score for monosubstituted methyl group on phenyl ring of **5b** (-98.688 kcal/mol) and **5d** (101.368 kcal/mol) analogue was less as compared to the MolDock score of disubstituted analogues with methyl group on phenyl ring i.e. **5j** (-105.561 kcal/mol) and **5m** (-106.388 kcal/mol). The MolDock score of the **5e** analogue with a methoxy group on the *para* position of the phenyl group was -105.71 kcal/mol. Trimethoxy-substituted **5p** analogue docking score was not significantly different (-106.055 kcal/mol) from **5e**. The MolDock score for **5i** (-105.843 kcal/mol) was due to the presence of an electron-withdrawing nitro group. The analogue with three chloro groups at the second, fourth, and fifth positions of phenyl ring **5q** had a MolDock score of -113.845 kcal/mol. Orlistat, a commonly used PL inhibitor, was also shown to have comparable interactions with a MolDock score of -139.41 kcal/mol. These docking investigations shed light on the substituents crucial for binding interactions (Table 5.4), which are required for PL inhibitory activity.

Table 5.4. MolDock score (kcal/mol) and interaction summary of **5a-5q** analogues at the active site of the PL.

Code	R	MolDock Score (kcal/mol)	H-bond	π - π T shaped	π -cation	π - π alkyl/ Alkyl	Halogen
5a	-H	-97.688	Phe 77, Gly 76, His 151	Phe 77	Arg 256, His 263	Ile 78, Leu 153, Ala 178	-
5b	2-CH ₃	-98.688	Phe 77, Gly 76, His 151	Phe 77	Arg 256, His 263	Ile 78, Leu 264, Ala 178, Ala 259, Ala 260	-
5c	2-F	-97.466	Phe 77, Gly 76, His 151	Phe 77	Arg 256, His 263	Leu 153, Ala 178, Ala 259, Ala 260, Leu 264	Phe 77, Asp 79
5d	4-CH ₃	-101.368	Phe 77, Gly 76, His 151	Phe 77	Arg 256, His 263	Ile 78, Leu 153, Ala 178, Trp 252	-
5e	4-OCH ₃	-105.71	Phe 77, Gly 76, His 151	Phe 77	Arg 256, His 263	Ile 78, Ala 178,	-

CHAPTER V

5f	4-F	-101.351	Phe 77, Gly 76, His 151	Phe 77	Arg 256, His 263	Ile 78, Leu 153, Ala 178	-
5g	4-Cl	-101.232	Phe 77, Gly 76, His 151	Phe 77	Arg 256, His 263	Ile 78, Leu 153, Ala 178, Trp 252	-
5h	4-Br	-100.744	Phe 77, Gly 76, His 151	Phe 77	Arg 256, His 263	Ile 78, Leu 153, Ala 178, Trp 252	-
5i	4-NO ₂	-105.843	Phe 77, Gly 76, Ser 152, Leu 153	-	His 263	Ile 78, Ala 178, Pro 180	-
5j	2,4-di- CH ₃	-105.561	Phe 77, Gly 76, His 151	Phe 77	Arg 256, His 263	Ile 78, Leu 264, Ala 178, Trp 252, Ala 260	-
5k	2,4-di-F	-105.421	Phe 77, His 151	-	Arg 256, His 263	Ile 78, Leu 153, Ala 178, Ala 259	Phe 77, Asp 79
5l	2,4-di- Cl	-106.401	Phe 77, Gly 76, His 151	Phe 77	Arg 256, His 263	Ile 78, Leu 153, Ala 178, Trp 252, Leu 264, Ala 259, Ala 260	-
5m	3,4- diCH ₃	-106.388	Phe 77, Gly 76, His 151, Ser152	-	Arg 256, His 263	Ile 78, Leu 153, Ala 178, Trp 252, Ala 259	-
5n	3,4-di-F	-105.411	Phe 77, Gly 76, His 151, Ser152		Arg 256, His 263	Ile 78, Leu 153, Ala 178	Arg 256
5o	3,4-di- Cl	-105.561	Phe 77, Gly 76, His 151	Phe 77	Arg 256, His 263	Ile 78, Leu 153, Ala 178, Trp 252, Ala 259	-
5p	3,4,5-tri- OCH ₃	-106.055	Phe 77, Gly 76, His 151, Arg 256	Phe 77	His 263	Leu 153, Ala 178	-

5q	2,4,5-tri-Cl	-113.845	Phe 77, Gly 76, His 151	Phe 77	Arg 256, His 263	Ile 78, Leu 153, Ala 178, Trp 252, Leu 264, Ala 259, Ala 260	-
	Orlistat	-139.41	Ser 152, His 151, His 263, Ala 259	-	-	Leu 153, Ala 178, Tyr 114, Ile 245, Phe 258	-

5.8. Molecular dynamics simulations

Molecular docking studies revealed the significance of key amino acid interactions, including lid domain amino acids Gly 76 - Lys 80, Leu 213 - Met 217, Ser 152, Asp 176, Arg 256, His 263, and others. In order to better comprehend the significance of the aforementioned interactions, a 100 ns simulation of the protein-ligand complex of the potent analogue **5q** was conducted using molecular dynamics. Using the specified protocol (Chapter 3), the simulation was executed, and the results were examined. The protein-ligand root mean square deviation (RMSD) and protein-ligand contacts were examined to comprehend the stability of the complex and depict the time span of the effective amino acid interactions under dynamic conditions.

RMSD denotes the average displacement of an atom from a particular frame with regard to a reference frame. The RMSD of protein-ligand (**5q**) oscillated between 3 and 4.5 Å during 100 ns runs, indicating the overall stability of the complex (protein-ligand). As seen in **Fig 5.7 (A)**, the RMSD of the backbone remains steady during the run. In addition, a time-dependent shift in the ligand RMSD was observed. Until 60 ns, the ligand RMSD was 2.5 Å; after 60 ns, it initially drops from 2.5 Å and a sharp deflection in the RMSD occurs at 95 ns and found to deviate up to 20 Å. A smaller RMSD value for the ligand compared to the protein indicated the stability of the ligand in relation to the protein and binding pockets. Root Mean Square Fluctuation (RMSF) is a valuable method for predicting changes in the local environment of proteins. As depicted in **Fig 5.7 (B)**, amino acid fluctuations in the catalytic triad and lid domain were less than 5 Å, indicating the likelihood of these amino acids remaining intact in a dynamic environment [14].

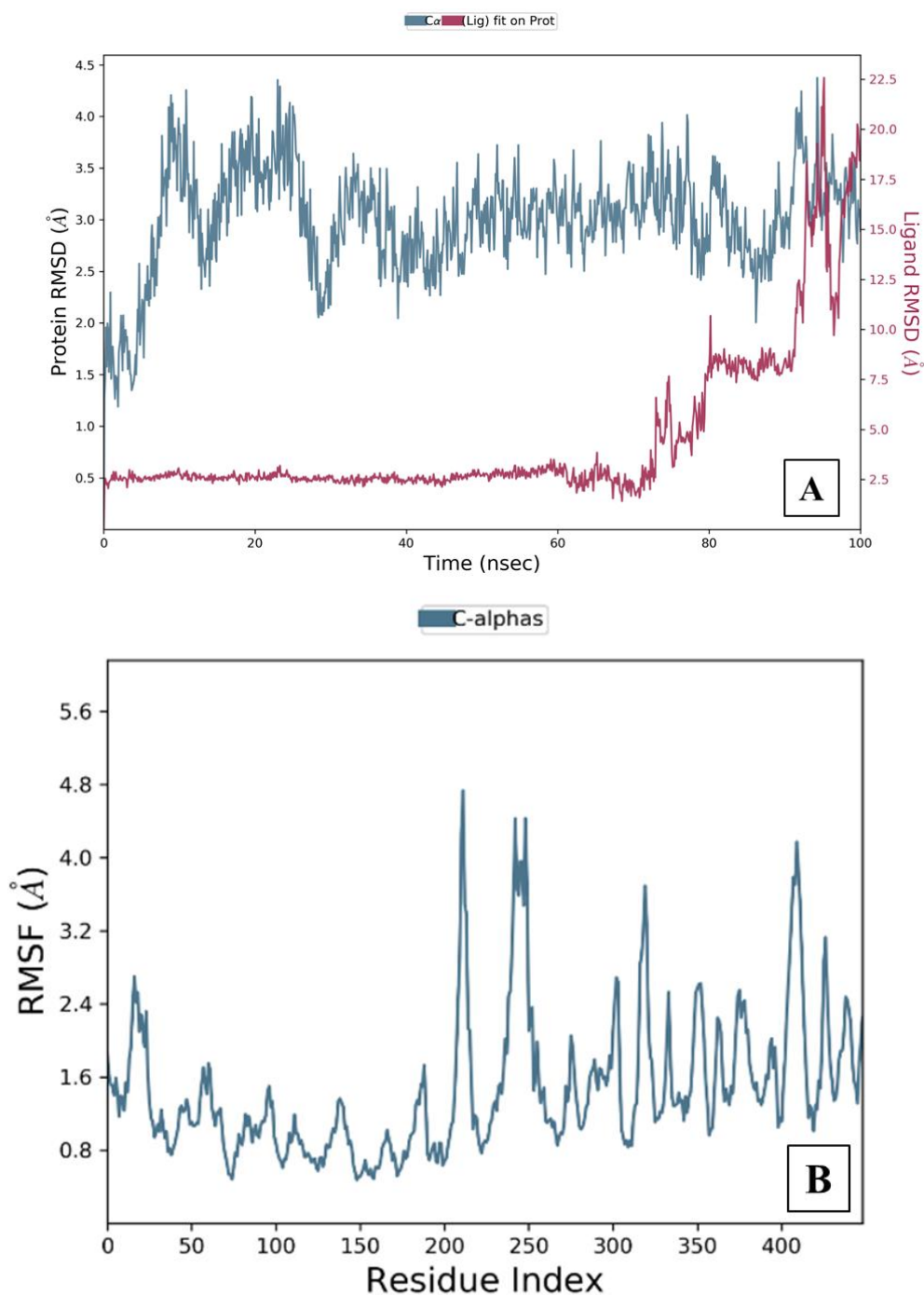


Figure 5.7. (A) RMSD plot of the protein-ligand (**5q**) complex (PDB ID: 1LPB); (B) Protein RMSF plot

The protein-ligand complex exhibited multiple forms of interactions like H-bonds, hydrophobic bonds, ionic bonds, and others. As the catalytic triad of PL is encased in a hydrophobic domain, the opening of this lid domain is necessary for PL inhibition. As depicted in **Fig 5.8 (A)**, the simulation uncovered a prominent hydrophobic interaction between the lid-domain amino acids (Gly 76, Phe 77, Ile 78, Asp 79, Tyr 114 and Phe 215) and ligand, suggesting the potential of designed analogues in the opening of the lid domains,

thereby enhancing the inhibitory properties. Timeline representation was further reinforced by these facts, in which a substantial interaction with the lid domain and catalytic triad amino acids were visible **Fig 5.8 (B)** [15].

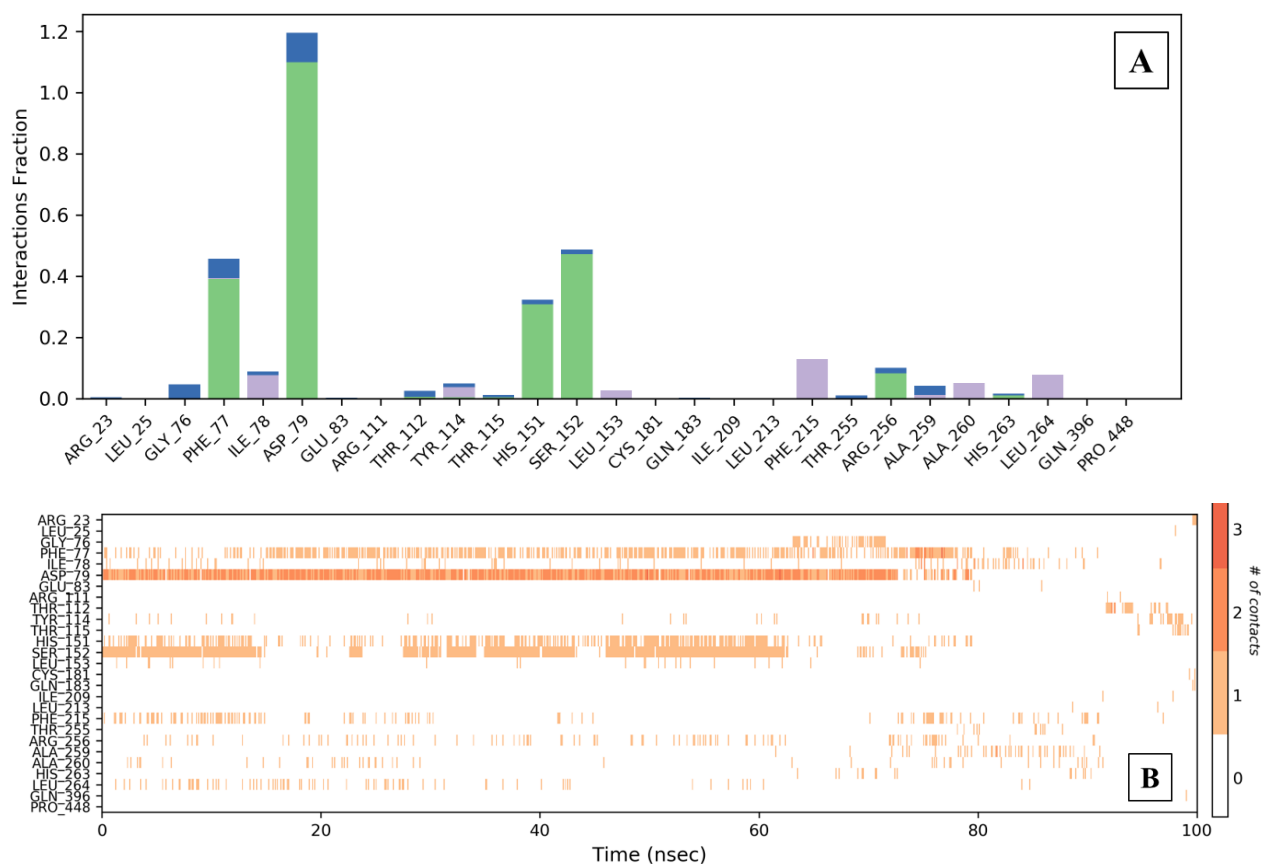


Figure 5.8. (A) Protein-ligand (**5q**) interaction bar charts stacked vertically (PDB ID: 1LPB); (B) Protein-ligand contact timeline (H-bonds, hydrophobic, ionic, water bridges).

In conclusion, a series of 17 coumarin analogues were designed and synthesised, and their PL inhibitory activity was then evaluated. These analogues were synthesised by coupling a coumarin scaffold with substituted phenyl rings *via* an amide warhead. Synthesized analogues were characterized using various spectroscopic techniques (NMR, ATR, HRMS and HPLC). Analogue **5q** shown potential PL inhibitory activity ($IC_{50} = 19.41 \mu M$) amongst all the analogues. Enzyme inhibition kinetic study of **5q** resulted in competitive inhibition ($K_i = 10.386 \mu M$), indicating a stable binding conformation of the molecule in the enzyme. The inhibitory character of these analogues was further validated by molecular modelling studies such as docking and dynamic simulation. Molecular dynamic methods indicated that **5q** was stable in dynamic environments.

References

1. Ahn, J. H., Shin, E. J., Liu, Q., Kim, S. B., Choi, K. M., Yoo, H. S., Hwang, B.Y. & Lee, M. K. (2012). Lignan derivatives from *Fraxinus rhynchophylla* and inhibitory activity on pancreatic lipase. *Natural Product Sciences*, 18(2), 116-120.
2. Fattah, T. A., Saeed, A., Al-Hiari, Y. M., Kasabri, V., Almasri, I. M., AlAlawi, S., Larik, F.A. & Channar, P. A. (2019). Functionalized furo [3, 2-c] coumarins as anti-proliferative, anti-lipolytic, and anti-inflammatory compounds: Synthesis and molecular docking studies. *Journal of Molecular Structure*, 1179, 390-400.
3. Stefanucci, A., Dimmito, M. P., Zengin, G., Luisi, G., Mirzaie, S., Novellino, E., & Mollica, A. (2019). Discovery of novel amide tripeptides as pancreatic lipase inhibitors by virtual screening. *New Journal of Chemistry*, 43(7), 3208-3217.
4. Stefanucci, A., Luisi, G., Zengin, G., Macedonio, G., Dimmito, M. P., Novellino, E., & Mollica, A. (2019). Discovery of arginine-containing tripeptides as a new class of pancreatic lipase inhibitors. *Future Medicinal Chemistry*, 11(1), 5-19.
5. Chauhan, D., George, G., Sridhar, S. N. C., Bhatia, R., Paul, A. T., & Monga, V. (2019). Design, synthesis, biological evaluation, and molecular modeling studies of rhodanine derivatives as pancreatic lipase inhibitors. *Archiv der Pharmazie*, 352(10), 1900029.
6. Brahmachari, G. (2015). Room temperature one-pot green synthesis of coumarin-3-carboxylic acids in water: A practical method for the large-scale synthesis. *ACS Sustainable Chemistry & Engineering*, 3(9), 2350-2358.
7. Chan, L. C., & Cox, B. G. (2007). Kinetics of amide formation through carbodiimide/N-hydroxybenzotriazole (HOBt) couplings. *The Journal of Organic Chemistry*, 72(23), 8863-8869.
8. Sridhar, S. N. C., Ginson, G., Reddy, P. V., Tantak, M. P., Kumar, D., & Paul, A. T. (2017). Synthesis, evaluation and molecular modelling studies of 2-(carbazol-3-yl)-2-oxoacetamide analogues as a new class of potential pancreatic lipase inhibitors. *Bioorganic & Medicinal Chemistry*, 25(2), 609-620.
9. Sridhar, S. N. C., Bhurta, D., Kantiwal, D., George, G., Monga, V., & Paul, A. T. (2017). Design, synthesis, biological evaluation and molecular modelling studies of novel diaryl substituted pyrazolyl thiazolidinediones as potent pancreatic lipase inhibitors. *Bioorganic & Medicinal Chemistry Letters*, 27(16), 3749-3754.
10. Lineweaver, H., & Burk, D. (1934). The determination of enzyme dissociation constants. *Journal of the American Chemical Society*, 56(3), 658-666.

11. Burlingham, B. T., & Widlanski, T. S. (2003). An intuitive look at the relationship of K_i and IC_{50} : A more general use for the Dixon plot. *Journal of Chemical Education*, 80(2), 214-218.
12. Li, S., Pan, J., Hu, X., Zhang, Y., Gong, D., & Zhang, G. (2020). Kaempferol inhibits the activity of pancreatic lipase and its synergistic effect with orlistat. *Journal of Functional Foods*, 72, 104041.
13. Li, Y. Q., Yang, P., Gao, F., Zhang, Z. W., & Wu, B. (2011). Probing the interaction between 3 flavonoids and pancreatic lipase by methods of fluorescence spectroscopy and enzymatic kinetics. *European Food Research and Technology*, 233, 63-69.
14. George, G., Yadav, N., Auti, P. S., & Paul, A. T. (2023). Molecular modelling, synthesis and *in vitro* evaluation of quinazolinone hybrid analogues as potential pancreatic lipase inhibitors. *Journal of Biomolecular Structure and Dynamics*, 41(19), 9583-9601.
15. Yadav, N., & Paul, A. T. (2023). Synthesis of amide warhead containing coumarin derivatives as potential pancreatic lipase inhibitors: *In silico* and *in vitro* evaluation for obesity treatment. *Medicinal Chemistry Research*, 32(10), 2219-2233.

Synthesis of Series II

6. Synthesis of Coumarin Analogues - Series II

6.1. Rationale

The synthesized coumarin analogues (**Series I**) exhibited a potential PL inhibition with the most active analogue from the series, **5q** that exhibited an IC_{50} value of 19.41 μ M. Further molecular modelling analysis of Orlistat and **5q** revealed that the latter possessed greater interaction distance between the reactive carbonyl group of amide group and Ser 152 of the active site (**Fig. 6.1**). This might be the probable reason for a lesser PL inhibitory potential.

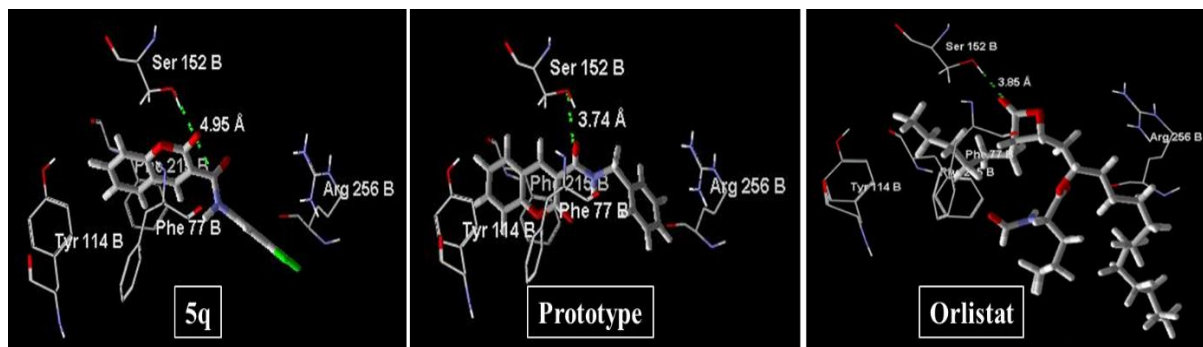
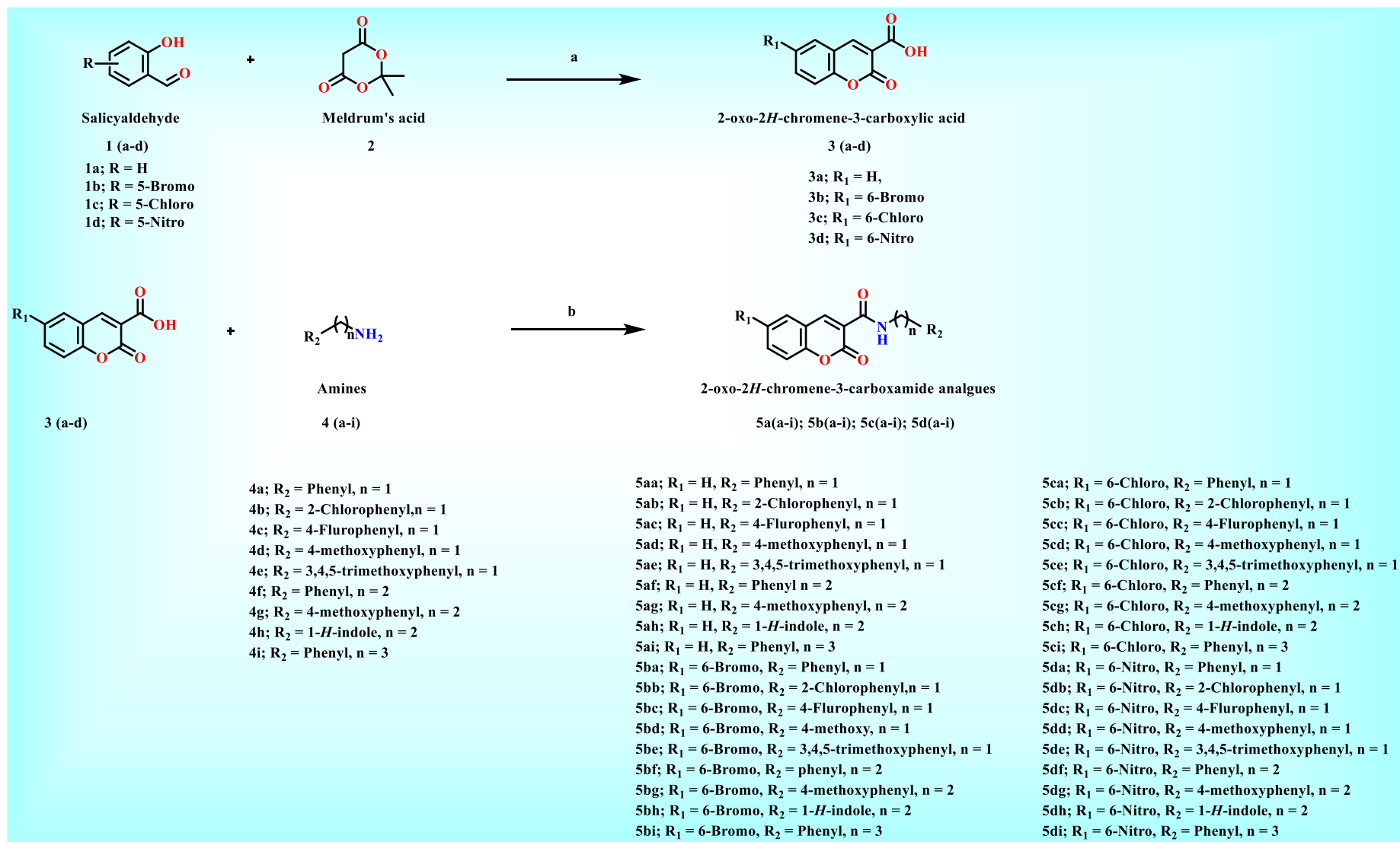


Figure 6.1. Rationale for designing series II coumarin analogues as PL inhibitors. The interaction distance has reduced from 4.95 Å in **5q** to 3.74 Å by the incorporation of an additional carbon linker (Prototype).

Thus, the present chapter was focused on understanding the effect of linker groups between the amide and aromatic groups. A preliminary molecular modelling study highlighted that the incorporation of an additional carbon atom between the amide group and phenyl ring might be helpful for the reduction of the interaction distance of the carbonyl group from Ser 152 (**Fig. 6.1**) Accordingly, a series of 36 coumarin analogues were designed, synthesized, characterized and evaluated for their *in-vitro* PL inhibitory potential.

6.2. Synthesis and Characterization

The syntheses of all the final analogues (**5a(a-i)**, **5b(a-i)**, **5c(a-i)** and **5d(a-i)**) were carried out as per the procedure detailed in **Scheme 6.1**. Synthesis and characterization of final analogues was performed in the same manner as discussed in the previous chapter (Chapter 5).



Scheme 6.1. Reagents and conditions: (a) K₂CO₃, H₂O, RT, 20 h; (b) DMF, 0 °C, EDC.HCl, HOBT, Ar-(CH₂)_n-NH₂, DIPEA, 20-30 °C, 15-20 h.

6.2.1. General procedure for the synthesis of coumarin-3-carboxylic acid derivatives (3a-3d)

A brief description of the synthetic pathway utilized in the synthesis of coumarin-3-carboxylic acid analogues is presented in **Scheme 6.1**. In a 50 mL RBF, K₂CO₃ (0.20 equiv), distilled water (5 mL), and 2,2-dimethyl-1,3-dioxane-4,6-dione (**2**; 1 equiv) were added. Salicylaldehyde (**1a-1d**; 1 equiv) was added to the reaction mixture after 15 mins. Following this, the mixture underwent 20 h of continuous stirring at room temperature in order to complete the conversion. Upon completion, the solution was acidified using 1N HCl (20 mL). The resulting solid mass was subsequently precipitated, filtered, and meticulously rinsed with water in order to obtain coumarin-3-carboxylic acid (**3a-3d**), which was nearly pure. For additional purification, the compounds (**3a-3d**) were crystallized from ethyl acetate [9].

6.2.2. General Procedure of synthesis of coumarin-3-carboxamide derivatives (5(a-i), 5b(a-i), 5c(a-i) and 5d(a-i))

A solution of coumarin-3-carboxylic acid (**3a-3d**; 1 equiv) in DMF at 0 °C was gradually treated with EDC.HCl (1.10 equiv) and HOBT (1.10 equiv). Amines with various substitutions (**4a-4i**; 1 equiv) were dissolved in DMF and added to the reaction mixture. After 10 mins, DIPEA (0.60 equiv) was added. The reaction was agitated at ambient temperature (25-30 °C) for a duration of 15 to 20 h. Following the completion of the reaction, water was utilized for work up. The solid material that formed was separated by filtration, thoroughly rinsed with water, and subsequently dried by exposure to air. In order to get a product that is free from impurities, column chromatography was employed that utilized a mixture of ethyl acetate and hexane as the eluent, and silica (#100-200) as the stationary phase. The synthesized analogues (**5(a-i)**, **5b(a-i)**, **5c(a-i)** and **5d(a-i)**) were characterized using NMR, HRMS, and ATR techniques [10,11].

6.2.3. Analytical Data for the final analogues (5a(a-i), 5b(a-i), 5c(a-i) and 5d(a-i))

N-benzyl-2-oxo-2*H*-chromene-3-carboxamide (**5aa**)

Yield: 89%; off white solid; mp = 320-322 °C; ¹H NMR (400 MHz, CDCl₃) δ 9.20 (t, J = 6.4 Hz, 1H), 8.98 (s, 1H), 7.76-7.64 (m, 2H), 7.46-7.28 (m, 7H), 4.69 (d, J = 5.9 Hz, 2H). ¹³C NMR (100 MHz, CDCl₃) δ 161.54, 161.42, 154.48, 148.57, 137.93, 134.09, 129.83, 128.73, 127.72, 127.48, 125.31, 118.66, 118.47, 116.66, 43.87. IR (ATR) ν 3841.49, 3743.78, 3613.15, 3315.28, 3039.94, 2926.59, 2309.12, 1697.30, 1656.14, 1607.31, 1522.18, 1445.60, 1357.75, 1230.25, 1160.45, 1029.90, 964.51, 756.76, 697.69, 633.79 cm⁻¹. HRMS (ESI+) calculated for C₁₇H₁₃NO₃ [M + H]⁺, 280.0974; found 280.0968. HPLC purity: 100.00 %, t_R = 5.54 min.

***N*-(2-chlorobenzyl)-2-oxo-2*H*-chromene-3-carboxamide (5ab)**

Yield: 83%; white solid; mp = 363-364 °C; ¹H NMR (400 MHz, CDCl₃) δ 9.31 (t, 1H), 8.95 (s, 1H), 7.74-7.66 (m, 2H), 7.48-7.37 (m, 4H), 7.30-7.24 (m, 2H), 4.77 (d, J = 6.0 Hz, 2H). ¹³C NMR (100 MHz, CDCl₃) δ 161.64, 161.41, 154.49, 148.63, 135.33, 134.15, 133.73, 129.84, 129.82, 129.61, 128.90, 127.03, 125.32, 118.62, 118.36, 116.68, 41.80. IR (ATR) ν 3841.14, 3744.83, 3672.40, 3613.39, 3328.39, 3053.13, 2390.91, 2307.12, 1705.60, 1661.03, 1612.04, 1522.48, 1456.74, 1360.47, 1244.62, 1128.74, 1033.69, 972.00, 798.15 753.28 cm⁻¹. HRMS (ESI+) calculated for C₁₇H₁₃NO₃ [M + H]⁺, 314.0585; found 314.0576. HPLC purity: 99.77 %, t_R = 7.25 min.

***N*-(4-fluorobenzyl)-2-oxo-2*H*-chromene-3-carboxamide (5ac)**

Yield: 88%; white solid; mp = 333-335 °C; ¹H NMR (400 MHz, CDCl₃) δ 9.18 (t, 1H), 8.97 (s, 1H), 7.74-7.66 (m, 2H), 7.45-7.33 (m, 4H), 7.08-7.01 (m, 2H), 4.65 (d, J = 5.9 Hz, 2H). ¹³C NMR (100 MHz, CDCl₃) δ 163.41, 161.59, 154.47, 148.69, 134.20, 129.86, 129.49, 125.37, 118.62, 118.33, 116.68, 115.66, 115.45, 43.15. IR (ATR) ν 3851.38, 3741.79, 3613.99, 3327.43, 3049.33, 2391.00, 2308.50, 1702.57, 1654.84, 1608.45, 1516.09, 1444.58, 1351.47, 1218.84, 1154.58, 1054.75, 966.46, 808.71, 753.24, 676.71 cm⁻¹. HRMS (ESI+) calculated for C₁₇H₁₂FNO₃ [M + H]⁺, 298.088; found 298.0872. HPLC purity: 99.67 %, t_R = 5.67 min.

***N*-(4-methoxybenzyl)-2-oxo-2*H*-chromene-3-carboxamide (5ad)**

Yield: 87%; off white solid; mp = 366-368 °C; ¹H NMR (400 MHz, CDCl₃) δ 9.12 (s, 1H), 8.96 (s, 1H), 7.75-7.64 (m, 2H), 7.46-7.36 (m, 2H), 7.31 (d, J = 8.6 Hz, 2H), 6.90 (d, J = 8.6 Hz, 2H), 4.62 (d, J = 5.8 Hz, 2H), 3.82 (s, 3H). ¹³C NMR (100 MHz, CDCl₃) δ 161.41, 159.02, 154.46, 148.50, 134.07, 130.06, 129.82, 129.14, 125.30, 118.66, 118.51, 116.65, 114.12, 55.32, 43.37. IR (ATR) ν 3839.44, 3744.44, 3613.47, 3320.68, 3042.42, 2934.46, 2842.43, 1696.79, 1606.63, 1519.94, 1443.74, 1356.08, 1303.61, 1235.78, 1168.74, 1028.30, 958.88, 824.21, 747.01, 642.13 cm⁻¹. HRMS (ESI+) calculated for C₁₈H₁₅NO₄ [M + H]⁺, 310.1080; found 310.1079. HPLC purity: 99.23 %, t_R = 5.24 min.

2-oxo-*N*-(3,4,5-trimethoxybenzyl)-2*H*-chromene-3-carboxamide (5ae)

Yield: 75%; off white solid; mp = 458-460 °C; ¹H NMR (400 MHz, CDCl₃) δ 9.19 (s, 1H), 8.98 (s, 1H), 7.77-7.66 (m, 2H), 7.47-7.38 (m, 2H), 6.61 (s, 2H), 4.62 (d, J = 5.8 Hz, 2H), 3.89 (s, 6H), 3.86 (s, 3H). ¹³C NMR (100 MHz, CDCl₃) δ 161.52, 154.48, 153.47, 148.66, 134.19, 133.63, 129.86, 125.38, 118.65, 118.43, 116.69, 104.84, 60.85, 56.16, 44.16. IR (ATR) ν 3849.50, 3745.43, 3611.48, 3319.78, 2935.73, 2306.81, 1706.51, 1655.96, 1595.71, 1513.29, 1457.61, 1354.45, 1237.34, 1117.26, 987.80, 922.75, 829.57, 763.46, 716.60,

638.84 cm^{-1} . HRMS (ESI+) calculated for $\text{C}_{20}\text{H}_{19}\text{NO}_6$ $[\text{M} + \text{H}]^+$, 370.1291; found 370.1284. HPLC purity: 99.56 %, $t_{\text{R}} = 4.34$ min.

2-oxo-*N*-phenethyl-2-chromene-3-carboxamide (5af)

Yield: 90%; white solid; mp = 331-333 °C; ^1H NMR (400 MHz, CDCl_3) δ 8.93 (s, 1H), 8.90 (s, 1H), 7.75-7.64 (m, 2H), 7.44-7.29 (m, 6H), 7.28-7.24 (m, 1H), 3.75 (q, 2H), 2.97 (t, $J = 7.2$ Hz, 2H). ^{13}C NMR (100 MHz, CDCl_3) δ 161.47, 161.39, 154.42, 148.26, 138.81, 134.01, 129.80, 128.80, 128.65, 126.56, 125.28, 118.66, 118.49, 116.63, 41.36, 35.67. IR (ATR) ν 3851.53, 3742.35, 3672.92, 3613.50, 3321.51, 1704.16, 1653.58, 1611.10, 1519.40, 1455.09, 1362.24, 1291.58, 1241.30, 1156.11, 1065.19, 1023.07, 979.06, 795.98, 747.65, 694.65 cm^{-1} . HRMS (ESI+) calculated for $\text{C}_{18}\text{H}_{15}\text{NO}_3$ $[\text{M} + \text{H}]^+$, 294.1131; found 294.1124. HPLC purity: 99.77 %, $t_{\text{R}} = 6.22$ min.

***N*-(4-methoxyphenethyl)-2-oxo-2*H*-chromene-3-carboxamide (5ag)**

Yield: 80%; white solid; mp = 377-379 °C; ^1H NMR (400 MHz, CDCl_3) δ 8.92 (s, 1H), 8.88 (s, 1H), 7.73-7.65 (m, 2H), 7.44-7.36 (m, 2H), 7.20 (d, $J = 8.6$ Hz, 2H), 6.88 (d, $J = 8.6$ Hz, 2H), 3.81 (s, 3H), 3.70 (q, 2H), 2.90 (t, $J = 7.2$ Hz, 2H). ^{13}C NMR (100 MHz, CDCl_3) δ 161.43, 161.39, 158.31, 154.42, 148.23, 133.99, 130.84, 129.80, 129.74, 125.27, 118.67, 118.52, 116.62, 114.06, 55.25, 41.57, 34.76. IR (ATR) ν 3851.84, 3742.33, 3672.87, 3613.25, 3346.19, 3048.03, 2941.62, 2309.86, 1711.30, 1647.93, 1519.51, 1455.92, 1366.84, 1295.65, 1237.82, 1164.28, 1038.74, 989.40, 753.09, 670.56 cm^{-1} . HRMS (ESI+) calculated for $\text{C}_{19}\text{H}_{17}\text{NO}_4$ $[\text{M} + \text{H}]^+$, 324.1237; found 324.1228. HPLC purity: 99.18 %, $t_{\text{R}} = 5.77$ min.

***N*-(2-(1*H*-indol-3-yl)ethyl)-2-oxo-2*H*-chromene-3-carboxamide (5ah)**

Yield: 91%; off white solid; mp = 389-391 °C; ^1H NMR (400 MHz, CDCl_3) δ 8.95 (s, 1H), 8.93 (s, 1H), 8.19 (s, 1H), 7.72-7.63 (m, 3H), 7.43-7.36 (m, 3H), 7.26-7.11 (m, 3H), 3.83 (q, $J = 6.7$ Hz, 2H), 3.13 (t, $J = 7.0$ Hz, 2H). ^{13}C NMR (100 MHz, CDCl_3) δ 161.45, 161.39, 154.39, 148.19, 136.44, 133.96, 129.80, 127.27, 125.26, 122.22, 122.13, 119.42, 118.78, 118.68, 118.58, 116.60, 112.92, 111.25, 40.29, 25.26. IR (ATR) ν 3851.31, 3742.39, 3671.55, 3613.03, 3401.43, 3354.15, 2930.56, 1695.27, 1650.22, 1604.49, 1517.13, 1447.65, 1359.00, 1285.81, 1225.16, 1138.09, 1023.54, 971.67, 729.90, 638.78 cm^{-1} . HRMS (ESI+) calculated for $\text{C}_{20}\text{H}_{16}\text{N}_2\text{O}_3$ $[\text{M} + \text{H}]^+$, 333.1240; found 333.1233. HPLC purity: 100.00 %, $t_{\text{R}} = 5.11$ min.

2-oxo-*N*-(3-phenylpropyl)-2*H*-chromene-3-carboxamide (5ai)

Yield: 90%; white solid; mp = 343-345 °C; ^1H NMR (400 MHz, CDCl_3) δ 8.94 (s, 1H), 8.89 (s, 1H), 7.76-7.65 (m, 2H), 7.47-7.37 (m, 2H), 7.35-7.28 (m, 2H), 7.27-7.17 (m, 3H), 3.52 (q, 2H), 2.75 (t, 2H), 2.00 (p, $J = 7.4$ Hz, 2H). ^{13}C NMR (100 MHz, CDCl_3) δ 161.52, 161.50, 154.44, 148.25, 141.32, 133.99, 129.80, 128.46, 128.43, 125.98, 125.29, 118.70, 118.57,

116.64, 39.37, 33.24, 30.96. IR (ATR) ν 3848.78, 3738.03, 3619.71, 3329.31, 3043.68, 2432.74, 2354.35, 2175.34, 2112.14, 1699.90, 1610.36, 1516.80, 1449.70, 1355.70, 1232.27, 878.36, 748.98, 690.13 cm^{-1} . HRMS (ESI+) calculated for $\text{C}_{19}\text{H}_{17}\text{NO}_3$ $[\text{M} + \text{H}]^+$, 308.1287; found 308.1228. HPLC purity: 100.00 %, $t_{\text{R}} = 7.77$ min.

***N*-benzyl-6-bromo-2-oxo-2*H*-chromene-3-carboxamide (5ba)**

Yield: 80%; off white solid; mp = 392-393 °C; ^1H NMR (400 MHz, $\text{DMSO-}d_6$) δ 9.11 (s, 1H), 8.84 (s, 1H), 8.27 (s, 1H), 7.90 (d, $J = 8.8$ Hz, 1H), 7.50 (d, $J = 8.8$ Hz, 1H), 7.40-7.23 (m, 5H), 4.55 (d, $J = 6.0$ Hz, 2H). ^{13}C NMR (100 MHz, $\text{DMSO-}d_6$) δ 159.11, 158.98, 152.07, 136.77, 134.00, 130.00, 128.87, 127.88, 126.53, 124.84, 119.71, 119.53, 118.07, 114.09, 43.70. IR (ATR) ν 3852.25, 3742.63, 3672.80, 3612.74, 3335.08, 3038.14, 2359.96, 1708.32, 1650.79, 1539.30, 1411.29, 1352.46, 1237.36, 1201.03, 1149.03, 1055.39, 971.30, 792.66, 714 cm^{-1} . HRMS (ESI+) calculated for $\text{C}_{17}\text{H}_{12}\text{BrNO}_3$ $[\text{M} + \text{H}]^+$, 358.00796; found 358.0057. HPLC purity: 99.04 %, $t_{\text{R}} = 5.93$ min.

6-bromo-*N*-(2-chlorobenzyl)-2-oxo-2*H*-chromene-3-carboxamide (5bb)

Yield: 86%; off white solid; mp = 435-437 °C; ^1H NMR (400 MHz, $\text{DMSO-}d_6$) δ 9.18 (s, 1H), 8.84 (s, 1H), 8.27 (s, 1H), 7.91 (d, $J = 8.1$ Hz, 1H), 7.50 (d, $J = 9.6$ Hz, 2H), 7.46-7.25 (m, 3H), 4.62 (d, $J = 6.0$ Hz, 2H). ^{13}C NMR (100 MHz, $\text{DMSO-}d_6$) δ 161.67, 159.43, 155.16, 146.79, 136.79, 136.23, 132.99, 132.61, 130.83, 129.69, 129.42, 127.74, 120.83, 118.94, 117.13, 114.17, 38.50. IR (ATR) ν 3852.36, 3742.50, 3672.90, 3613.26, 3326.73, 2359.57, 1708.63, 1654.54, 1611.68, 1540.80, 1414.86, 1351.39, 1240.29, 1203.89, 1153.06, 1044.35, 976.69, 793.42, 748.59, 651.29 cm^{-1} . HRMS (ESI+) calculated for $\text{C}_{17}\text{H}_{11}\text{BrClNO}_3$ $[\text{M} + \text{H}]^+$, 391.9689; found 391.9668. HPLC purity: 99.44 %, $t_{\text{R}} = 8.24$ min.

6-bromo-*N*-(4-fluorobenzyl)-2-oxo-2*H*-chromene-3-carboxamide (5bc)

Yield: 85%; off white solid; mp = 406-408 °C; ^1H NMR (400 MHz, $\text{DMSO-}d_6$) δ 9.13 (s, 1H), 8.83 (s, 1H), 8.27 (s, 1H), 7.90 (d, $J = 8.8$ Hz, 1H), 7.49 (d, $J = 9.1$ Hz, 1H), 7.43-7.36 (m, 2H), 7.21-7.12 (m, 2H), 4.52 (d, $J = 6.0$ Hz, 2H). ^{13}C NMR (100 MHz, $\text{DMSO-}d_6$) δ 161.50, 161.44, 160.24, 153.40, 146.65, 136.70, 132.56, 129.98, 129.90, 120.79, 118.91, 117.09, 115.65, 115.44, 42.54. IR (ATR) ν 3851.48, 3741.94, 3672.57, 3612.81, 3337.51, 3043.05, 2359.13, 1713.53, 1652.09, 1609.80, 1548.00, 1510.87, 1417.43, 1355.38, 1221.31, 1156.15, 1063.02, 977.67, 794.61, 650.86 cm^{-1} . HRMS (ESI+) calculated for $\text{C}_{17}\text{H}_{11}\text{BrFNO}_3$ $[\text{M} + \text{H}]^+$, 375.9985; found 375.9960. HPLC purity: 99.02 %, $t_{\text{R}} = 8.06$ min.

6-bromo-*N*-(4-methoxybenzyl)-2-oxo-2*H*-chromene-3-carboxamide (5bd)

Yield: 85%; off white solid; mp = 438-440 °C; ^1H NMR (400 MHz, CDCl_3) δ 9.05 (s, 1H), 8.88 (s, 1H), 7.85 (d, $J = 2.4$ Hz, 1H), 7.76 (dd, $J = 8.8, 2.3$ Hz, 1H (due to meta coupling)),

7.32 (d, $J = 3.0$ Hz, 1H), 7.30 (d, $J = 2.6$ Hz, 2H), 6.90 (d, $J = 8.6$ Hz, 2H), 4.61 (d, $J = 5.8$ Hz, 2H), 3.82 (s, 3H). ^{13}C NMR (100 MHz, CDCl_3) δ 160.86, 160.74, 159.09, 153.22, 147.11, 136.77, 131.83, 129.85, 129.16, 120.12, 119.58, 118.37, 117.96, 114.16, 55.32, 43.47. IR (ATR) ν 3852.41, 3742.67, 3672.81, 3613.62, 3042.41, 2359.72, 2320.34, 1916.88, 1705.16, 1656.05, 1516.85, 1416.47, 1307.66, 1240.83, 1175.90, 1034.67, 972.92, 919.98, 794.33, 641.68 cm^{-1} . HRMS (ESI+) calculated for $\text{C}_{18}\text{H}_{14}\text{BrNO}_4$ $[\text{M} + \text{H}]^+$, 388.0185; found 388.0170. HPLC purity: 99.01 %, $t_{\text{R}} = 7.56$ min.

6-bromo-2-oxo-*N*-(3,4,5-trimethoxybenzyl)-2*H*-chromene-3-carboxamide (5be)

Yield: 89%; off white solid; mp = 530-532 °C; ^1H NMR (400 MHz, $\text{DMSO-}d_6$) δ 9.04 (t, $J = 5.9$ Hz, 1H), 8.81 (s, 1H), 8.26 (d, $J = 2.4$ Hz, 1H), 7.89 (dd, $J = 8.8, 2.4$ Hz, 1H), 7.49 (d, $J = 8.9$ Hz, 1H), 6.70 (s, 2H), 4.47 (d, $J = 6.0$ Hz, 2H), 3.76 (s, 6H), 3.64 (s, 3H). ^{13}C NMR (100 MHz, $\text{DMSO-}d_6$) δ 161.51, 160.25, 153.37, 153.33, 146.36, 136.98, 136.65, 134.92, 132.52, 121.11, 120.86, 118.91, 117.10, 105.35, 60.46, 56.32, 43.45. IR (ATR) ν 3852.01, 3742.62, 3672.97, 3613.39, 2927.83, 2832.88, 2359.71, 1715.93, 1652.21, 1546.47, 1511.61, 1460.28, 1421.04, 1343.19, 1236.20, 1128.28, 1068.51, 986.00, 794.51, 649.83 cm^{-1} . HRMS (ESI+) calculated for $\text{C}_{20}\text{H}_{18}\text{BrNO}_6$ $[\text{M} + \text{H}]^+$, 448.0396; found 448.0359. HPLC purity: 99.73 %, $t_{\text{R}} = 5.92$ min.

6-bromo-2-oxo-*N*-phenethyl-2*H*-chromene-3-carboxamide (5bf)

Yield: 94%; off white solid; mp = 404-405 °C; ^1H NMR (400 MHz, CDCl_3) δ 8.84 (s, 1H), 8.82 (t, $J = 7.9$ Hz, 1H), 7.84 (d, $J = 2.3$ Hz, 1H), 7.75 (dd, $J = 8.8, 2.3$ Hz, 1H), 7.37-7.25 (m, 6H), 3.74 (q, 2H), 2.96 (t, $J = 7.2$ Hz, 2H). ^{13}C NMR (100 MHz, CDCl_3) δ 160.92, 160.73, 153.18, 146.88, 138.69, 136.70, 131.83, 128.78, 128.67, 126.61, 120.13, 119.54, 118.34, 117.92, 41.41, 35.60. IR (ATR) ν 3852.25, 3742.63, 3672.80, 3612.74, 3335.08, 3038.14, 2359.96, 1708.32, 1650.79, 1539.30, 1411.29, 1352.46, 1237.36, 1201.03, 1149.03, 1055.39, 971.30, 792.66, 714.75, 647.44 cm^{-1} . HRMS (ESI+) calculated for $\text{C}_{18}\text{H}_{14}\text{BrNO}_3$ $[\text{M} + \text{H}]^+$, 372.0236; found 372.0208. HPLC purity: 99.60 %, $t_{\text{R}} = 9.25$ min.

6-bromo-*N*-(4-methoxyphenethyl)-2-oxo-2*H*-chromene-3-carboxamide (5bg)

Yield: 90%; off white solid; mp = 450-451 °C; ^1H NMR (400 MHz, CDCl_3) δ 8.84 (s, 1H), 8.80 (s, 1H), 7.84 (d, $J = 2.3$ Hz, 1H), 7.76 (dd, $J = 8.8, 2.3$ Hz, 1H), 7.30 (d, $J = 8.8$ Hz, 1H), 7.20 (d, $J = 8.6$ Hz, 2H), 6.88 (d, $J = 8.6$ Hz, 2H), 3.81 (s, 3H), 3.70 (q, 2H), 2.90 (t, $J = 7.2$ Hz, 2H). ^{13}C NMR (100 MHz, CDCl_3) δ 160.90, 160.74, 158.34, 153.18, 146.86, 136.69, 131.82, 130.71, 129.73, 120.13, 119.57, 118.34, 117.92, 114.08, 55.26, 41.63, 34.69. IR (ATR) ν 3852.25, 3742.63, 3672.80, 3612.74, 3335.08, 3038.14, 2860.11, 2359.96, 1708.32, 1650.79, 1539.30, 1411.29, 1352.46, 1237.36, 1201.03, 1149.03, 1055.39, 971.30, 792.66,

714.75, 647.44 cm^{-1} . HRMS (ESI+) calculated for $\text{C}_{19}\text{H}_{16}\text{BrNO}_4$ $[\text{M} + \text{H}]^+$, 402.0341; found 402.0312. HPLC purity: 99.07 %, $t_{\text{R}} = 8.51$ min.

***N*-(2-(1*H*-indol-3-yl)ethyl)-6-bromo-2-oxo-2*H*-chromene-3-carboxamide (5bh)**

Yield: 92%; off white solid; mp = 486-488 °C; ^1H NMR (400 MHz, $\text{DMSO-}d_6$) δ 10.86 (s, 1H), 8.84 (s, 1H), 8.80 (t, $J = 5.7$ Hz, 1H), 8.25 (d, $J = 2.4$ Hz, 1H), 7.87 (dd, $J = 8.9, 2.4$ Hz, 1H), 7.62 (d, $J = 7.9$ Hz, 1H), 7.46 (d, $J = 8.9$ Hz, 1H), 7.35 (d, $J = 8.1$ Hz, 1H), 7.22 (d, $J = 2.4$ Hz, 1H), 7.08 (t, $J = 8.1$ Hz, 1H), 6.99 (t, $J = 8.0$ Hz, 1H), 3.64 (q, $J = 7.1$ Hz, 2H), 2.97 (t, $J = 7.2$ Hz, 2H). ^{13}C NMR (100 MHz, $\text{DMSO-}d_6$) δ 161.15, 160.36, 153.34, 146.61, 136.78, 136.65, 132.56, 127.60, 123.31, 121.46, 120.84, 120.51, 118.85, 118.83, 118.73, 117.11, 111.88, 111.86, 40.63, 25.43. IR (ATR) ν 3852.25, 3742.63, 3672.80, 3612.74, 3335.08, 3038.14, 2860.11, 2359.96, 1708.32, 1650.79, 1539.30, 1411.29, 1352.46, 1237.36, 1201.03, 1149.03, 1055.39, 943.70, 882.58, 804.95, 735.43, 669.26 cm^{-1} . HRMS (ESI+) calculated for $\text{C}_{20}\text{H}_{15}\text{BrN}_2\text{O}_3$ $[\text{M} + \text{H}]^+$, 411.0345; found 411.0323. HPLC purity: 100.00 %, $t_{\text{R}} = 7.31$ min.

6-bromo-2-oxo-*N*-(3-phenylpropyl)-2*H*-chromene-3-carboxamide (5bi)

Yield: 91%; off white solid; mp = 415-417 °C; ^1H NMR (400 MHz, CDCl_3) δ 8.85 (s, 1H), 8.82 (t, $J = 5.9$ Hz, 1H), 7.85 (d, $J = 2.3$ Hz, 1H), 7.76 (dd, $J = 8.8, 2.3$ Hz, 1H), 7.32 (d, $J = 8.2$ Hz, 2H), 7.29 (d, $J = 2.9$ Hz, 1H), 7.26–7.20 (m, 3H), 3.51 (q, $J = 6.8$ Hz, 2H), 2.74 (t, $J = 7.7$ Hz, 2H), 2.00 (p, $J = 7.3$ Hz, 2H). ^{13}C NMR (100 MHz, CDCl_3) δ 160.95, 160.87, 153.18, 146.89, 141.24, 136.70, 131.84, 128.48, 128.42, 126.02, 120.15, 119.58, 118.36, 117.95, 39.45, 33.23, 30.90. IR (ATR) ν 3851.15, 3740.52, 3671.81, 3608.84, 3331.08, 3040.14, 2359.96, 1708.32, 1649.79, 1538.30, 1421.29, 1351.46, 1237.36, 1201.03, 1149.03, 1051.39, 971.30, 792.66, 714.79, 646.41 cm^{-1} . HRMS (ESI+) calculated for $\text{C}_{19}\text{H}_{16}\text{BrNO}_3$ $[\text{M} + \text{H}]^+$, 386.0392; found 386.0373. HPLC purity: 99.64 %, $t_{\text{R}} = 11.96$ min.

***N*-benzyl-6-chloro-2-oxo-2*H*-chromene-3-carboxamide (5ca)**

Yield: 85%; off white solid; mp = 363-365 °C; ^1H NMR (400 MHz, CDCl_3) δ 9.13 (s, 1H), 8.90 (s, 1H), 7.70 (d, $J = 2.4$ Hz, 1H), 7.63 (dd, $J = 8.9, 2.5$ Hz, 1H), 7.40–7.37 (m, 4H), 7.35–7.28 (m, 2H), 4.69 (d, $J = 5.9$ Hz, 2H). ^{13}C NMR (100 MHz, CDCl_3) δ 161.03, 160.84, 152.77, 147.31, 137.72, 134.02, 130.74, 128.77, 127.75, 127.57, 119.62, 119.54, 118.13, 43.97. IR (ATR) ν 3846.36, 3741.59, 3674.62, 3618.66, 3034.32, 2357.89, 2175.94, 2112.85, 1919.55, 1707.81, 1652.65, 1525.65, 1415.91, 1348.46, 1233.95, 965.95, 830.98, 793.59, 714.10, 639.61 cm^{-1} . HRMS (ESI+) calculated for $\text{C}_{17}\text{H}_{12}\text{ClNO}_3$ $[\text{M} + \text{H}]^+$, 314.0584; found 314.0558. HPLC purity: 98.82 %, $t_{\text{R}} = 7.51$ min.

6-chloro-*N*-(2-chlorobenzyl)-2-oxo-2*H*-chromene-3-carboxamide (5cb)

Yield: 91%; off white solid; mp = 405-407 °C; ¹H NMR (400 MHz, DMSO-*d*₆) δ 9.17 (t, J = 6.1 Hz, 1H), 8.83 (s, 1H), 8.12 (d, J = 2.5 Hz, 1H), 7.78 (dd, J = 8.9, 2.6 Hz, 1H), 7.56 (d, J = 8.8 Hz, 1H), 7.51-7.45 (m, 1H), 7.44-7.39 (m, 1H), 7.37-7.29 (m, 2H), 4.61 (d, J = 6.1 Hz, 2H). ¹³C NMR (100 MHz, DMSO-*d*₆) δ 161.69, 160.41, 153.03, 146.87, 136.21, 134.05, 129.70, 129.60, 129.44, 129.35, 129.31, 127.75, 124.03, 120.32, 118.70, 114.17, 41.34. IR (ATR) ν 3845.81, 3741.01, 3389.50, 2357.83, 2256.84, 2124.61, 1656.32, 1522.09, 1346.55, 1230.28, 992.11, 820.79 cm⁻¹. HRMS (ESI+) calculated for C₁₇H₁₁Cl₂NO₃ [M + H]⁺, 348.0195; found 348.0169. HPLC purity: 97.62 %, t_R = 10.19 min.

6-chloro-*N*-(4-fluorobenzyl)-2-oxo-2*H*-chromene-3-carboxamide (5cc)

Yield: 93%; off white solid; mp = 376-377 °C; ¹H NMR (400 MHz, DMSO-*d*₆) δ 9.14 (t, J = 6.1 Hz, 1H), 8.83 (s, 1H), 8.12 (d, J = 2.5 Hz, 1H), 7.78 (dd, J = 8.9, 2.5 Hz, 1H), 7.55 (d, J = 8.8 Hz, 1H), 7.44-7.36 (m, 2H), 7.22-7.12 (m, 2H), 4.52 (d, J = 6.1 Hz, 2H). ¹³C NMR (100 MHz, DMSO-*d*₆) δ 162.93, 161.52, 160.29, 152.99, 146.74, 135.62, 133.96, 129.90, 129.55, 129.27, 120.82, 118.66, 115.66, 115.45, 42.54. IR (ATR) ν 3846.89, 3741.49, 3674.09, 3618.91, 3338.66, 3045.04, 2359.40, 2176.61, 1717.77, 1655.80, 1514.21, 1424.66, 1352.79, 1225.73, 1084.35, 975.87, 895.13, 825.29, 746.36, 654.50 cm⁻¹. HRMS (ESI+) calculated for C₁₇H₁₁ClFNO₃ [M + H]⁺, 332.0490; found 332.0459. HPLC purity: 99.07 %, t_R = 7.70 min.

6-chloro-*N*-(4-methoxybenzyl)-2-oxo-2*H*-chromene-3-carboxamide (5cd)

Yield: 85%; off white solid; mp = 409-411 °C; ¹H NMR (400 MHz, CDCl₃) δ 9.06 (s, 1H), 8.89 (s, 1H), 7.69 (d, J = 2.5 Hz, 1H), 7.63 (dd, J = 8.8, 2.5 Hz, 1H), 7.37 (d, J = 8.9 Hz, 1H), 7.33-7.29 (m, 2H), 6.94-6.86 (m, 2H), 4.61 (d, J = 5.7 Hz, 2H), 3.82 (s, 3H). ¹³C NMR (100 MHz, CDCl₃) δ 160.89, 160.81, 159.07, 152.75, 147.23, 133.98, 130.71, 129.85, 129.17, 128.76, 119.62, 119.58, 118.12, 114.15, 55.32, 43.46. IR (ATR) ν 3847.10, 3741.12, 3674.16, 3618.69, 3345.15, 3039.08, 2885.68, 2357.21, 2176.31, 2112.05, 1919.68, 1701.22, 1512.29, 1351.18, 1235.11, 891.58, 824.85, 665.80 cm⁻¹. HRMS (ESI+) calculated for C₁₈H₁₄ClNO₄ [M + H]⁺, 344.0690; found 344.0653. HPLC purity: 98.79 %, t_R = 7.08 min.

6-chloro-2-oxo-*N*-(3,4,5-trimethoxybenzyl)-2*H*-chromene-3-carboxamide (5ce)

Yield: 92%; off white solid; mp = 501-503 °C; ¹H NMR (400 MHz, CDCl₃) δ 9.11 (t, J = 5.9 Hz, 1H), 8.90 (s, 1H), 7.71 (d, J = 2.5 Hz, 1H), 7.63 (dd, J = 8.8, 2.5 Hz, 1H), 7.38 (d, J = 8.9 Hz, 1H), 6.60 (s, 2H), 4.61 (d, J = 5.8 Hz, 2H), 3.88 (s, 6H), 3.85 (s, 3H). ¹³C NMR (100 MHz, CDCl₃) δ 160.99, 160.89, 153.47, 152.76, 147.38, 137.39, 134.10, 133.43, 130.78, 128.80, 119.59, 119.48, 118.15, 104.84, 60.86, 56.16, 44.25. IR (ATR) ν 3847.07, 3741.12, 3675.51, 3617.78, 3350.99, 3044.38, 2823.90, 2356.99, 2175.70, 2110.72, 1718.15, 1655.47,

1513.93, 1424.83, 1344.89, 1237.86, 1130.75, 988.47, 815.43, 647.05 cm^{-1} . HRMS (ESI+) calculated for $\text{C}_{20}\text{H}_{18}\text{ClNO}_6$ $[\text{M} + \text{H}]^+$, 404.0901; found 404.0877. HPLC purity: 97.36 %, $t_{\text{R}} = 5.59$ min.

6-chloro-2-oxo-*N*-phenethyl-2*H*-chromene-3-carboxamide (5cf)

Yield: 88%; off white solid; mp = 374-376 °C; ^1H NMR (400 MHz, CDCl_3) δ 8.85 (s, 1H), 8.83 (s, 1H), 7.69 (d, $J = 2.4$ Hz, 1H), 7.62 (dd, $J = 8.9, 2.4$ Hz, 1H), 7.40-7.29 (m, 4H), 7.28-7.22 (m, 2H), 3.79-3.70 (m, 2H), 2.96 (t, $J = 7.2$ Hz, 2H). ^{13}C NMR (100 MHz, CDCl_3) δ 160.96, 160.80, 152.72, 147.00, 138.69, 133.92, 130.68, 128.79, 128.76, 128.67, 126.62, 119.62, 119.55, 118.09, 77.36, 77.05, 76.73, 41.42, 35.60. IR (ATR) ν 3847.31, 3741.24, 3674.84, 3618.56, 3344.80, 3044.09, 22356.66, 2176.53, 2111.47, 1919.86, 1702.79, 1521.30, 1348.77, 1236.81, 1071.76, 892.06, 836.28, 729.86, 676.15 cm^{-1} . HRMS (ESI+) calculated for $\text{C}_{18}\text{H}_{14}\text{ClNO}_3$ $[\text{M} + \text{H}]^+$, 328.0741; found 328.0718. HPLC purity: 99.03 %, $t_{\text{R}} = 8.62$ min.

6-chloro-*N*-(4-methoxyphenethyl)-2-oxo-2*H*-chromene-3-carboxamide (5cg)

Yield: 93%; off white solid; mp = 420-422 °C; ^1H NMR (400 MHz, CDCl_3) δ 8.85 (s, 1H), 8.81 (t, $J = 5.3$ Hz, 1H), 7.69 (d, $J = 2.4$ Hz, 1H), 7.62 (dd, $J = 8.9, 2.5$ Hz, 1H), 7.37 (d, $J = 8.9$ Hz, 1H), 7.24-7.16 (m, 2H), 6.92-6.82 (m, 2H), 3.81 (s, 3H), 3.75-3.66 (m, 2H), 2.90 (t, $J = 7.2$ Hz, 2H). ^{13}C NMR (100 MHz, CDCl_3) δ 160.92, 160.80, 158.33, 152.71, 146.97, 133.90, 130.71, 130.67, 129.73, 128.75, 119.63, 119.58, 118.09, 114.08, 55.26, 41.63, 34.69. IR (ATR) ν 3848.01, 3741.40, 3674.78, 3618.39, 3345.92, 3046.80, 2359.91, 2176.93, 1706.58, 1659.49, 1526.62, 1353.42, 1244.83, 1071.81, 1031.19, 974.15, 882.95, 813.82, 749.91, 669.53 cm^{-1} . HRMS (ESI+) calculated for $\text{C}_{19}\text{H}_{16}\text{ClNO}_4$ $[\text{M} + \text{H}]^+$, 358.0846; found 358.0821. HPLC purity: 99.31 %, $t_{\text{R}} = 7.94$ min.

***N*-(2-(1*H*-indol-3-yl)ethyl)-6-chloro-2-oxo-2*H*-chromene-3-carboxamide (5ch)**

Yield: 94%; off white solid; mp = 486-488 °C; ^1H NMR (400 MHz, $\text{DMSO-}d_6$) δ 10.87 (s, 1H), 8.85 (s, 1H), 8.81 (t, $J = 5.7$ Hz, 1H), 8.13 (d, $J = 2.6$ Hz, 1H), 7.77 (dd, $J = 8.9, 2.6$ Hz, 1H), 7.62 (d, $J = 7.9$ Hz, 1H), 7.54 (d, $J = 8.8$ Hz, 1H), 7.35 (d, $J = 8.1$ Hz, 1H), 7.22 (d, $J = 2.4$ Hz, 1H), 7.08 (t, $J = 7.5$ Hz, 1H), 6.99 (t, $J = 7.3$ Hz, 1H), 3.64 (q, $J = 6.8$ Hz, 2H), 2.97 (t, $J = 7.2$ Hz, 2H). ^{13}C NMR (100 MHz, $\text{DMSO-}d_6$) δ 161.17, 160.41, 152.94, 146.69, 136.77, 133.91, 129.56, 129.27, 127.59, 123.31, 121.46, 120.58, 120.36, 118.84, 118.74, 118.62, 111.88, 111.86, 25.42. IR (ATR) ν 3845.84, 3741.25, 3674.50, 3618.55, 3276.91, 3039.00, 2358.06, 2176.20, 1708.21, 1653.64, 1533.10, 1349.57, 1230.34, 1084.39, 1004.32, 943.70, 882.58, 804.95, 735.43, 669.26 cm^{-1} . HRMS (ESI+) calculated for $\text{C}_{20}\text{H}_{15}\text{ClN}_2\text{O}_3$ $[\text{M} + \text{H}]^+$, 367.0850; found 367.0824. HPLC purity: 98.36 %, $t_{\text{R}} = 6.87$ min.

6-chloro-2-oxo-N-(3-phenyl propyl)-2H-chromene-3-carboxamide (5ci)

Yield: 92%; off white solid; mp = 385-387 °C; ¹H NMR (400 MHz, CDCl₃) δ 8.86 (s, 1H), 8.82 (s, 1H), 7.70 (d, J = 2.5 Hz, 1H), 7.63 (dd, J = 8.8, 2.5 Hz, 1H), 7.38 (d, J = 8.9 Hz, 1H), 7.34-7.29 (m, 2H), 7.25-7.21 (m, 2H), 7.19 (t, J = 1.5 Hz, 1H), 3.51 (td, J = 7.1, 5.8 Hz, 2H), 2.79-2.71 (m, 2H), 2.00 (p, J = 7.4 Hz, 2H). ¹³C NMR (100 MHz, CDCl₃) δ 160.98, 160.94, 152.72, 147.01, 141.24, 133.92, 130.70, 128.76, 128.49, 128.42, 126.03, 119.65, 119.60, 118.11, 39.45, 33.23, 30.90. IR (ATR) ν 3843.76, 3614.81, 3553.62, 3450.60, 3329.07, 2706.48, 2435.75, 2092.09, 1711.56, 1652.25, 1531.62, 1409.60, 1344.85, 1240.06, 1146.29, 1061.26, 976.75, 896.74, 798.44, 682.59 cm⁻¹. HRMS (ESI+) calculated for C₁₉H₁₆ClNO₃ [M + H]⁺, 342.0897; found 342.0874. HPLC purity: 91.74 %, t_R = 11.07 min.

N-benzyl-6-nitro-2-oxo-2H-chromene-3-carboxamide (5da)

Yield: 80%; off white solid; mp = 363-365 °C; ¹H NMR (400 MHz, CDCl₃) δ 9.15 (d, J = 6.1 Hz, 1H), 8.89 (s, 1H), 7.60 (d, J = 8.7 Hz, 1H), 7.41-7.33 (m, 4H), 7.30 (dd, J = 8.4, 2.2 Hz, 1H), 6.95 (dd, J = 8.7, 2.4 Hz, 1H), 6.88 (d, J = 2.4 Hz, 1H), 4.68 (d, J = 5.9 Hz, 2H). ¹³C NMR (100 MHz, CDCl₃) δ 164.91, 162.10, 161.82, 156.70, 148.52, 138.11, 130.97, 128.69, 127.70, 127.40, 114.73, 114.07, 112.43, 100.32, 43.78. IR (ATR) ν 3851.25, 3742.64, 3612.83, 3343.49, 2924.85, 2396.08, 2306.63, 1697.76, 1606.77, 1523.00, 1360.48, 1213.36, 1122.84, 1018.19, 968.74, 829.77, 777.10, 703.32 cm⁻¹. HRMS (ESI+) calculated for C₁₇H₁₂N₂O₅ [M]⁺, 324.0741; found 324.0746. HPLC purity: 99.80 %, t_R = 5.83 min.

6-nitro-N-(2-chlorobenzyl)-2-oxo-2H-chromene-3-carboxamide (5db)

Yield: 77%; off white solid; mp = 405-407 °C; ¹H NMR (400 MHz, DMSO-*d*₆) δ 9.09 (t, J = 6.0 Hz, 1H), 8.84 (s, 1H), 7.90 (d, J = 8.8 Hz, 1H), 7.44-7.35 (m, 2H), 7.20-7.13 (m, 2H), 7.11 (d, J = 2.4 Hz, 1H), 7.04 (dd, J = 8.7, 2.4 Hz, 1H), 4.52 (d, J = 6.0 Hz, 2H). ¹³C NMR (100 MHz, DMSO-*d*₆) δ 162.06, 161.25, 160.50, 156.68, 148.44, 135.82, 135.80, 132.04, 129.96, 129.88, 115.66, 115.45, 115.37, 114.12, 112.61, 100.78, 42.45, 40.62, 40.41, 40.20, 39.99, 39.78, 39.57, 39.36. IR (ATR) ν 3850.81, 3742.20, 3616.53, 3352.71, 2391.22, 2308.28, 1697.47, 1651.25, 1515.44, 1361.89, 1212.16, 1115.02, 1022.14, 790.04, 741.36 cm⁻¹. HRMS (ESI+) calculated for C₁₇H₁₁ClN₂O₅ [M + H]⁺, 359.0429; found 359.0499. HPLC purity: 99.70 %, t_R = 7.68 min.

6-nitro-N-(4-fluorobenzyl)-2-oxo-2H-chromene-3-carboxamide (5dc)

Yield: 75%; off white solid; mp = 376-379 °C; ¹H NMR (400 MHz, DMSO-*d*₆) δ 9.15 (s, 1H), 8.86 (s, 1H), 7.93 (d, J = 8.7 Hz, 1H), 7.49-7.31 (m, 4H), 7.16-7.04 (m, 2H), 4.65-4.58 (m, 2H). ¹³C NMR (100 MHz, DMSO-*d*₆) δ 165.00, 162.20, 162.07, 161.36, 148.59, 136.44, 132.59, 132.10, 129.68, 129.44, 129.28, 127.74, 114.18, 100.79, 41.26, 40.62, 40.41, 40.20,

39.99, 39.78, 39.58, 39.37. IR (ATR) ν 3850.22, 3742.19, 3617.12, 3339.07, 2925.31, 2386.41, 2309.12, 1695.19, 1518.34, 1361.44, 1212.70, 1119.80, 1010.61, 817.55, 714.21 cm^{-1} . HRMS (ESI+) calculated for $\text{C}_{17}\text{H}_{11}\text{FN}_2\text{O}_5$ $[\text{M} + \text{H}] + [-\text{H}_2\text{O}]$, 325.0590; found 325.0619. HPLC purity: 99.66 %, $t_{\text{R}} = 5.97$ min.

6-nitro-*N*-(4-methoxybenzyl)-2-oxo-2*H*-chromene-3-carboxamide (5dd)

Yield: 80%; off white solid; mp = 409-411 °C; ^1H NMR (400 MHz, CDCl_3) δ 9.07 (s, 1H), 8.88 (s, 1H), 7.60 (d, $J = 8.7$ Hz, 1H), 7.33-7.28 (m, 2H), 6.95 (dd, $J = 8.7, 2.4$ Hz, 1H), 6.91-6.82 (m, 3H), 4.60 (d, $J = 5.8$ Hz, 2H), 3.81 (s, 3H). ^{13}C NMR (100 MHz, CDCl_3) δ 164.87, 161.97, 161.79, 158.96, 156.68, 148.43, 130.94, 130.25, 129.09, 114.80, 114.09, 114.04, 112.43, 100.31, 55.30, 43.27. IR (ATR) ν 3850.89, 3741.58, 3616.67, 3337.78, 2930.91, 2389.14, 2308.58, 1702.20, 1649.62, 1611.95, 1519.39, 1459.07, 1370.63, 1229.55, 1136.62, 1032.32, 977.15, 816.03, 749.10, 672.73 cm^{-1} . HRMS (ESI+) calculated for $\text{C}_{18}\text{H}_{14}\text{N}_2\text{O}_6$ $[\text{M} + \text{H}]^+$, 393.0490; found 393.0483. HPLC purity: 99.29 %, $t_{\text{R}} = 5.50$ min.

6-nitro-2-oxo-*N*-(3,4,5-trimethoxybenzyl)-2*H*-chromene-3-carboxamide (5de)

Yield: 82%; off white solid; mp = 501-503 °C; ^1H NMR (400 MHz, CDCl_3) δ 9.13 (t, $J = 5.9$ Hz, 1H), 8.88 (s, 1H), 7.60 (d, $J = 8.8$ Hz, 1H), 6.96 (dd, $J = 8.7, 2.4$ Hz, 1H), 6.87 (d, $J = 2.2$ Hz, 1H), 6.60 (s, 2H), 4.59 (d, $J = 5.8$ Hz, 2H), 3.87 (s, 6H), 3.84 (s, 3H). ^{13}C NMR (100 MHz, CDCl_3) δ 164.97, 162.06, 161.87, 156.71, 153.42, 148.57, 137.27, 133.84, 130.99, 114.67, 114.10, 112.41, 104.79, 100.33, 60.84, 56.14, 44.06. IR (ATR) ν 3850.52, 3741.67, 3616.49, 3332.07, 2380.76, 2310.51, 1697.28, 1640.84, 1515.21, 1460.63, 1368.55, 1231.28, 1121.51, 1002.79, 786.22 cm^{-1} . HRMS (ESI+) calculated for $\text{C}_{20}\text{H}_{18}\text{N}_2\text{O}_8$ $[\text{M} + \text{Na}]^+$, 437.0955; found 437.0941. HPLC purity: 99.26 %, $t_{\text{R}} = 4.52$ min.

6-nitro-2-oxo-*N*-phenethyl-2*H*-chromene-3-carboxamide (5df)

Yield: 87%; off white solid; mp = 374-375 °C; ^1H NMR (400 MHz, CDCl_3) δ 8.85 (s, 1H), 8.85 (s, 1H), 7.59 (d, $J = 8.7$ Hz, 1H), 7.37 – 7.29 (m, 3H), 7.28 – 7.21 (m, 2H), 6.95 (dd, $J = 8.7, 2.4$ Hz, 1H), 6.86 (d, $J = 2.2$ Hz, 1H), 3.76 – 3.70 (m, 2H), 2.96 (t, $J = 7.3$ Hz, 2H). ^{13}C NMR (100 MHz, CDCl_3) δ 164.81, 162.01, 161.79, 156.64, 148.21, 138.92, 130.93, 128.81, 128.62, 126.51, 114.81, 113.99, 112.43, 100.30, 41.29, 35.74. IR (ATR) ν 3849.67, 3741.76, 3616.01, 3340.48, 2383.43, 2309.97, 1703.75, 1620.41, 1519.35, 1367.74, 1283.22, 1213.63, 1123.19, 1016.88, 830.17, 751.97, 704.05 cm^{-1} . HRMS (ESI+) calculated for $\text{C}_{18}\text{H}_{14}\text{N}_2\text{O}_5$ $[\text{M} + \text{H}]^+$, 339.0975; found 339.0995. HPLC purity: 99.65 %, $t_{\text{R}} = 6.51$ min.

6-nitro-*N*-(4-methoxyphenethyl)-2-oxo-2*H*-chromene-3-carboxamide (5dg)

Yield: 86%; off white solid; mp = 420-422 °C; ^1H NMR (400 MHz, CDCl_3) δ 8.84 (s, 1H), 8.82 (s, 1H), 7.59 (d, $J = 8.7$ Hz, 1H), 7.20 (d, $J = 8.5$ Hz, 2H), 6.95 (dd, $J = 8.8, 2.4$ Hz, 1H),

6.88 (d, $J = 8.8$ Hz, 3H), 3.80 (s, 3H), 3.69 (q, $J = 7.1$ Hz, 2H), 2.89 (t, $J = 7.2$ Hz, 2H). ^{13}C NMR (100 MHz, CDCl_3) δ 164.80, 161.97, 161.77, 158.28, 156.63, 148.15, 130.96, 130.91, 129.73, 114.88, 114.04, 113.95, 112.45, 100.32, 56.00, 41.49, 34.83. IR (ATR) ν 3849.88, 3741.57, 3616.67, 3339.25, 2924.38, 2385.99, 2309.57, 1700.45, 1636.18, 1518.05, 1365.55, 1214.80, 1113.01, 1015.96, 824.50, 706.39 cm^{-1} . HRMS (ESI+) calculated for $\text{C}_{19}\text{H}_{16}\text{N}_2\text{O}_6$ $[\text{M} + \text{Na}]^+$, 391.8877; found 392.0892. HPLC purity: 99.49 %, $t_{\text{R}} = 6.04$ min.

***N*-(2-(1H-indol-3-yl)ethyl)-6-nitro-2-oxo-2H-chromene-3-carboxamide (5dh)**

Yield: 91%; off white solid; mp = 486-488 °C; ^1H NMR (400 MHz, $\text{DMSO}-d_6$) δ 10.87 (s, 1H), 8.84 (s, 1H), 8.78 (t, $J = 5.7$ Hz, 1H), 7.89 (d, $J = 8.7$ Hz, 1H), 7.62 (d, $J = 7.9$ Hz, 1H), 7.35 (d, $J = 8.1$ Hz, 1H), 7.22 (d, $J = 2.3$ Hz, 1H), 7.12-6.94 (m, 4H), 3.63 (q, $J = 6.9$ Hz, 2H), 2.97 (t, $J = 7.2$ Hz, 2H). ^{13}C NMR (100 MHz, $\text{DMSO}-d_6$) δ 164.84, 161.76, 161.31, 156.59, 148.24, 136.78, 131.98, 127.61, 123.28, 121.45, 118.85, 118.72, 115.27, 114.08, 112.60, 111.97, 111.85, 100.70, 40.31, 25.52. IR (ATR) ν 3849.08, 3741.48, 3616.17, 3220.49, 3059.50, 2930.54, 2390.54, 2308.57, 1701.91, 1604.39, 1536.66, 1453.83, 1370.48, 1223.04, 1142.05, 1019.58, 965.94, 869.83, 796.59, 737.88 cm^{-1} . HRMS (ESI-) calculated for $\text{C}_{20}\text{H}_{15}\text{N}_3\text{O}_5$ $[\text{M} - \text{H}]^+$, 376.0939; found 376.0914. HPLC purity: 98.40 %, $t_{\text{R}} = 5.24$ min.

6-nitro-2-oxo-*N*-(3-phenylpropyl)-2H-chromene-3-carboxamide (5di)

Yield: 77%; off white solid; mp = 385-387 °C; ^1H NMR (400 MHz, CDCl_3) δ 8.86 (s, 1H), 8.83 (s, 1H), 7.60 (dd, $J = 8.8, 1.1$ Hz, 1H), 7.35-7.29 (m, 2H), 7.25-7.16 (m, 3H), 6.95 (ddd, $J = 8.6, 2.4, 1.1$ Hz, 1H), 6.88 (s, 1H), 3.50 (q, $J = 6.4$ Hz, 2H), 2.74 (t, $J = 7.7$ Hz, 2H), 1.99 (p, $J = 7.3$ Hz, 2H). ^{13}C NMR (100 MHz, CDCl_3) δ 164.81, 162.04, 161.91, 156.64, 148.20, 141.39, 130.92, 128.44, 125.95, 114.88, 114.01, 112.46, 100.31, 39.27, 33.24, 31.03. IR (ATR) ν 3852.00, 3741.59, 3616.52, 3336.56, 3044.66, 2927.29, 2854.49, 2393.62, 2308.22, 1694.17, 1594.72, 1513.90, 1365.99, 1215.15, 1114.71, 1014.92, 803.32, 743.47, 693.42 cm^{-1} . HRMS (ESI+) calculated for $\text{C}_{19}\text{H}_{16}\text{N}_2\text{O}_6$ $[\text{M} + \text{H}]^+$, 353.1132; found 353.1186. HPLC purity: 99.59 %, $t_{\text{R}} = 8.20$ min.

6.3. Pancreatic lipase inhibition assay

The PL inhibitory activity of the synthesized coumarin analogues **5a(a-i)**, **5b(a-i)**, **5c(a-i)** and **5d(a-i)** was evaluated utilizing the assay protocol that was standardized within our laboratory [12]. The Type II porcine PL enzyme was used, with *p*-NPB as the substrate. Each inhibitor concentration was prepared utilizing DMSO (2%). Before calculating IC_{50} values, the absorbance of the resultant mixture was measured at 405 nm using a microplate reader in order to determine the percentage of inhibition. It was determined that the IC_{50} values of all analogues was within the range of 9.20-60.51 μM (Table 6.1). A significant number of the

analogues (**5cb**, **5cd**, **5ce**, **5ch**, **5db**, **5dc**, **5dd**, **5de**, **5dg**, **5dh**) exhibited good PL inhibitory activity (9.20-20.12 μM). Conversely, a set of the analogues (**5bh**, **5cc**, **5cf**, **5cg**, **5ci**, **5da**, **5df**, **5di**, **5be**, **5ag**, **5ah**, **5bb**, **5bc**, **5bd**, **5bg**, **5ca**) showed moderate activity range (21.24-40.35 μM). A limited number of analogues (**5ad**, **5ae**, **5ai**, **5ba**, **5bf**, **5bi**, **5aa**, **5ab**, **5ac**, **5af**) exhibited poor inhibitory activity, (ranging from 41.94-60.51 μM). **5dh** and **5de** were identified as the most potent inhibitory analogues of PL among all the analogues ($\text{IC}_{50} = 9.20$ and 11.4 μM , respectively). Orlistat (standard drug) exhibited a significant PL inhibition with IC_{50} value of 0.97 μM .

Table 6.1. *In vitro* PL inhibitory activity of the synthesized analogues (**5a(a-i)**, **5b(a-i)**, **5c(a-i)** and **5d(a-i)**).

Code	IC_{50} (μM)	Code	IC_{50} (μM)
5aa	60.51 \pm 2.83	5ca	40.04 \pm 2.21
5ab	51.29 \pm 1.16	5cb	20.12 \pm 1.30
5ac	57.69 \pm 1.37	5cc	24.60 \pm 1.25
5ad	47.47 \pm 1.11	5cd	20.01 \pm 0.46
5ae	44.12 \pm 2.3	5ce	17.96 \pm 0.28
5af	56.82 \pm 2.35	5cf	30.74 \pm 1.10
5ag	40.35 \pm 2.19	5cg	24.35 \pm 1.54
5ah	34.44 \pm 1.99	5ch	15.98 \pm 1.79
5ai	49.93 \pm 3.00	5ci	24.42 \pm 1.97
5ba	48.42 \pm 0.81	5da	28.17 \pm 0.17
5bb	31.31 \pm 3.03	5db	14.67 \pm 0.88
5bc	36.33 \pm 0.94	5dc	18.18 \pm 0.20
5bd	33.73 \pm 1.60	5dd	13.04 \pm 0.44
5be	30.80 \pm 1.05	5de	11.4 \pm 0.08
5bf	41.94 \pm 1.01	5df	21.24 \pm 1.01
5bg	31.04 \pm 1.69	5dg	19.19 \pm 1.33
5bh	29.04 \pm 1.16	5dh	9.20 \pm 0.84
5bi	47.05 \pm 0.05	5di	24.11 \pm 1.08
Orlistat			0.97 \pm 0.31

*All experiments were performed in triplicate and the values are expressed in Mean \pm S.E.M.

6.4. Enzyme kinetics

To comprehend the nature of inhibition (competitive, uncompetitive and non-competitive), the enzyme kinetics of the most potent analogues **5dh** was analysed (**Fig. 6.2**). For the same, a three-concentration range of inhibitor (0, 0.3125, and 2.5 μM) was utilized along with the four distinct substrate concentrations (25, 50, 100, and 200 μM).

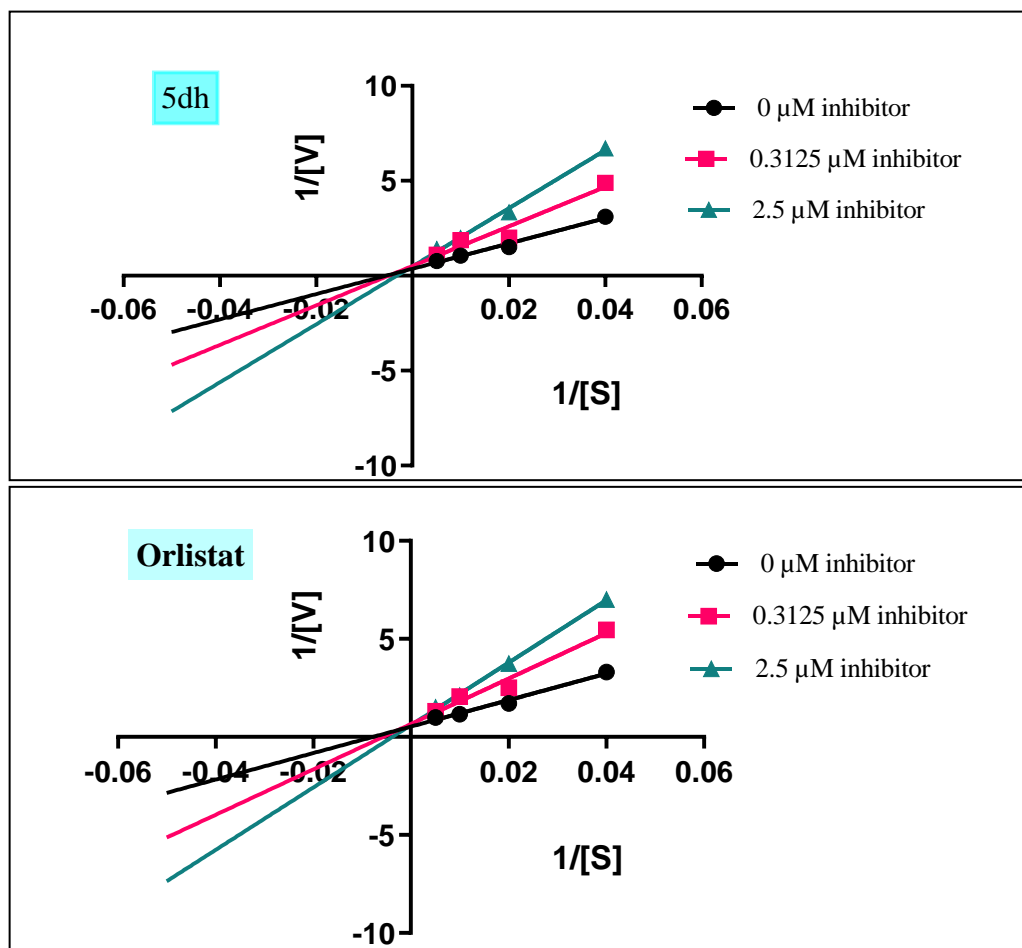


Figure 6.2. Double reciprocal Lineweaver-Burk plots of **5dh** and Orlistat.

As depicted in **Fig 6.2**, the Lineweaver-Burk plot converged at the y-intercept ($1/V_{max}$), whereas K_m rose proportionally to inhibitor concentration [13]. The analogue **5dh** bind to the active site of PL and inhibited PL competitively. The apparent K_m value increased proportionally with increasing substrate concentration; however, the V_{max} was unchanged by substrate concentration, explaining the extent of reversible inhibition. Using the Cheng-Prusoff equation, the inhibition constant (K_i) was also determined, and analogue **5dh** was found to have K_i values of 4.504 μM , respectively (**Table 6.2**). With a K_i value of 0.588 μM , Orlistat (positive control) likewise exhibited competitive inhibition [14].

Table 6.2. K_m , V_{max} and K_i values of **5dh** and Orlistat retrieved from the PL enzyme kinetics

Code	K_m (apparent) at different concentration (μM)			V_{max} ($\mu\text{M}/\text{min}$)	K_i (μM)	Nature of inhibition
	0 μM	0.3125 μM	2.5 μM			
5dh	42.951	45.338	56.666	1.279	4.504	Competitive
Orlistat	52.435	86.501	102.971	0.907	0.588	Competitive

6.5. Structure activity relationship (SAR)

The PL inhibitory activities of the coumarin analogues that were synthesized (**5a(a-i)**, **5b(a-i)**, **5c(a-i)** and **5d(a-i)**) were utilized to generate the preliminary SAR. The SAR component was categorized into three groups, as illustrated in **Fig 6.3**: 1) Impact of substituted coumarin ring (R_1 substitution); 2) Impact of substituted aromatic ring (R_2 substitution). 3) Impact of carbon linker ($n=1,2,3$). As seen in **Table 6.1**, the analogue **5aa**, which did not have any modifications on either the coumarin or phenyl ring, demonstrated weak inhibitory activity against PL ($\text{IC}_{50} = 60.51 \pm 2.83 \mu\text{M}$). The influence of several electron-withdrawing substituents (chlorine, bromine and nitro) on the sixth position of the coumarin ring was investigated. The analogues containing nitro substitution (R_1) exhibited better inhibition of PL as compared to the analogues without substitution and those substituted with halogens (Cl and Br). The impact of several substituted aromatic amines was examined on R_2 position. In the context of aromatic substitution, it was found that electron-donating groups (EDG) were more effective than electron-withdrawing groups (EWG) in R_2 position. Among the EDG (trimethoxy, & methoxy), the analogue with 3,4,5-trimethoxy substitution showed better activity (**5de**; $\text{IC}_{50} = 11.4 \pm 0.08 \mu\text{M}$) and was identified as the second most potent analogue in the series. When comparing with analogues containing electron-withdrawing groups (EWG) such as chloro and fluoro, it was observed that the substitution of chloro on the 2nd position of the phenyl ring (**5db**) exhibited better activity with an IC_{50} value of $14.67 \pm 0.88 \mu\text{M}$. Analogues containing fluoro substituent (**5ac**, **5bc**, **5cc** & **5dc**; $\text{IC}_{50} = 57.69 \pm 1.37$, 36.33 ± 0.94 , 24.60 ± 1.25 and $18.18 \pm 0.20 \mu\text{M}$ respectively) showed lower activity as compared to analogues containing methoxy (**5ad**, **5bd**, **5cd** & **5dd**; $\text{IC}_{50} = 47.47 \pm 1.11$, 33.73 ± 1.60 , 20.01 ± 0.46 and $13.04 \pm 0.44 \mu\text{M}$ respectively) at the *para* position of the phenyl ring. The analogue with a *p*-methoxy substitution had comparatively lower activity (**5dd**; $\text{IC}_{50} = 13.04 \pm 0.44 \mu\text{M}$) as compared to the analogue with trimethoxy substitution (**5de**). The impact of several carbon linkers on PL inhibition was examined, and the analogue with two carbon linker substitutions (**5dh**) exhibited the best inhibition with an IC_{50} of $9.20 \pm 0.84 \mu\text{M}$.

The analogue with three carbon chain **5di** ($IC_{50} = 24.11 \pm 1.08 \mu\text{M}$) exhibited lower inhibitory potential against PL as compared to **5df** ($IC_{50} = 21.24 \pm 1.01 \mu\text{M}$) with two carbon linkers. From the above SAR, it was clear that the impact of substituents on the R_1 , R_2 groups, and carbon linker are crucial in developing a promising PL inhibitor. **Fig. 6.3** presents a concise overview of the SAR analysis, demonstrating the impact of different substituents on the inhibitory activity of PL.

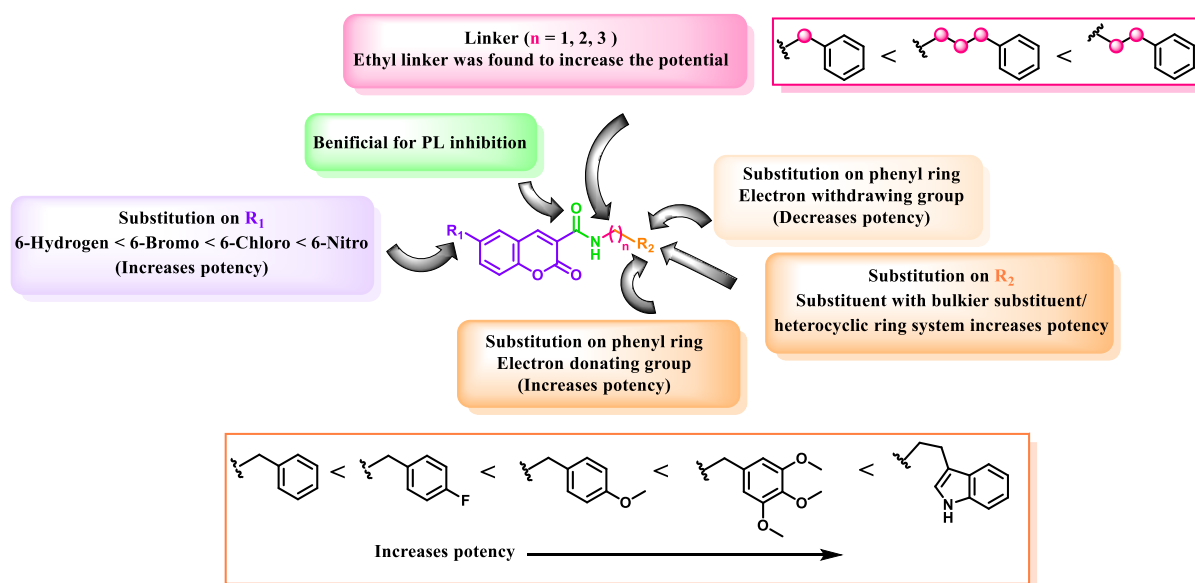


Figure 6.3. SAR study of coumarin analogues (**Series II**).

6.6. Fluorescence Quenching Measurements with PL

The effect of the **5dh** analogue on the fluorescence quenching of PL was evaluated (See chapter 3) and the results are depicted in **Fig. 6.4** and **Table 6.3**. The **5dh** analogue exerted a concentration-dependent quenching effect to the PL fluorescence.

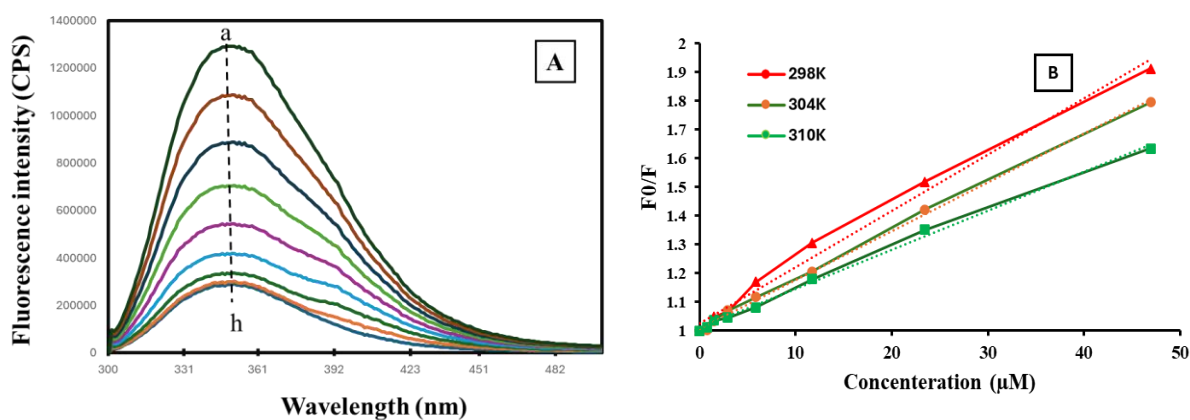


Figure 6.4. (A) The fluorescence spectra of PL in the presence of **5dh** at various concentrations (pH 7.4, $T = 298 \text{ K}$, a to h in increasing concentrations); (B) Stern-Volmer plot for the quenching of **5dh** on the PL.

As illustrated in **Fig. 6.4.**, the PL fluorescence was quenched by the analogue **5dh**. Additionally, the fluorescence intensity decreased as the concentration of quencher (**5dh**) increased, suggesting the formation of PL-quencher complexes. The above fluorescence quenching is mainly due to static or dynamic mechanism. To identify the underlying mechanism of quenching, Stern-Volmer equation was utilized and the values were determined as per **Formula 3.3** (chapter 3).

Table 6.3. Bimolecular quenching constant (k_q), binding constant (K_b) and the number of binding sites (n) at different temperatures for **5dh**.

#	T (K)	$K_{SV}/10^4$ (L/mol)	$k_q/10^{12}$ (L/mol sec)	R^2	$K_b/10^5$ (L/mol)	n	R^2
5dh	298	1.88	1.24	0.9953	2.98	0.891	0.9991
	304	1.41	9.62	0.9967	2.22	0.888	0.9932
	310	1.21	7.73	0.9978	1.66	0.871	0.9955

As represented in **Table 6.3**, an inverse correlation between the K_{sv} and temperature suggested that the quenching effects on the PL was mainly attributed to static quenching rather than dynamic quenching.

The values of 'n' at the corresponding temperature were closer to 1, indicating the presence of only one binding site in PL. This result further supported the competitive inhibition that was observed in the enzyme kinetics study. Additionally, the ' K_b ' values were in the range of 1.66 to 2.98 x 10⁵ L/mol indicating the strong binding forces of **5dh** with PL.

6.7. Molecular docking analysis

The energy-minimized structures of the **5a(a-i)**, **5b(a-i)**, **5c(a-i)** and **5d(a-i)** were docked into the crystal structure of human PL (PDB ID: 1LPB, resolution: 2.46 Å) with validated grid parameters using Molegro Virtual Docker 6.0. According to the literature, it has been verified that the active region of the PL enzyme is composed of a hydrophobic lid domain (Gly 76-Lys 80, Tyr 114, and Leu 213 - Met 217) that encloses the tightly confined catalytic triad consisting of Ser 152 - Asp 176 - His 263 amino acids. The crystal structure of PL was examined to see if the side chains of the lid domain have a role in the hydrophobic groove for substrate contact [15]. In order for an inhibitor molecule to access the catalytic triad, it must engage in interactions with the hydrophobic lid domain, namely through alkyl or aromatic contacts, to facilitate its opening. Through careful examination of these facts, analogues were designed that facilitated the interactions between the coumarin scaffold and the amino acids in the lid domain (*via* π - π interactions), which help in the opening of the lid domain. In addition, we have included an amide warhead to facilitate the interaction with the active site

amino acid residue. The aromatic part of amines possessed an electron-rich aryl/heteroaryl group that can interact with an important amino acid, namely Arg 256, through a π -cation interaction. The various substituted coumarin analogues were designed, subjected to docking, and the resulting docking data were analysed. The MolDock scores of all the coumarin analogues ranged from -100.974 to -140.251 kcal/mol as depicted in **Table 6.4**. The analogue **5dh** had the highest MolDock score of -140.251 kcal/mol. Additionally, the docking poses of analogue **5dh** was examined for various docking interactions.

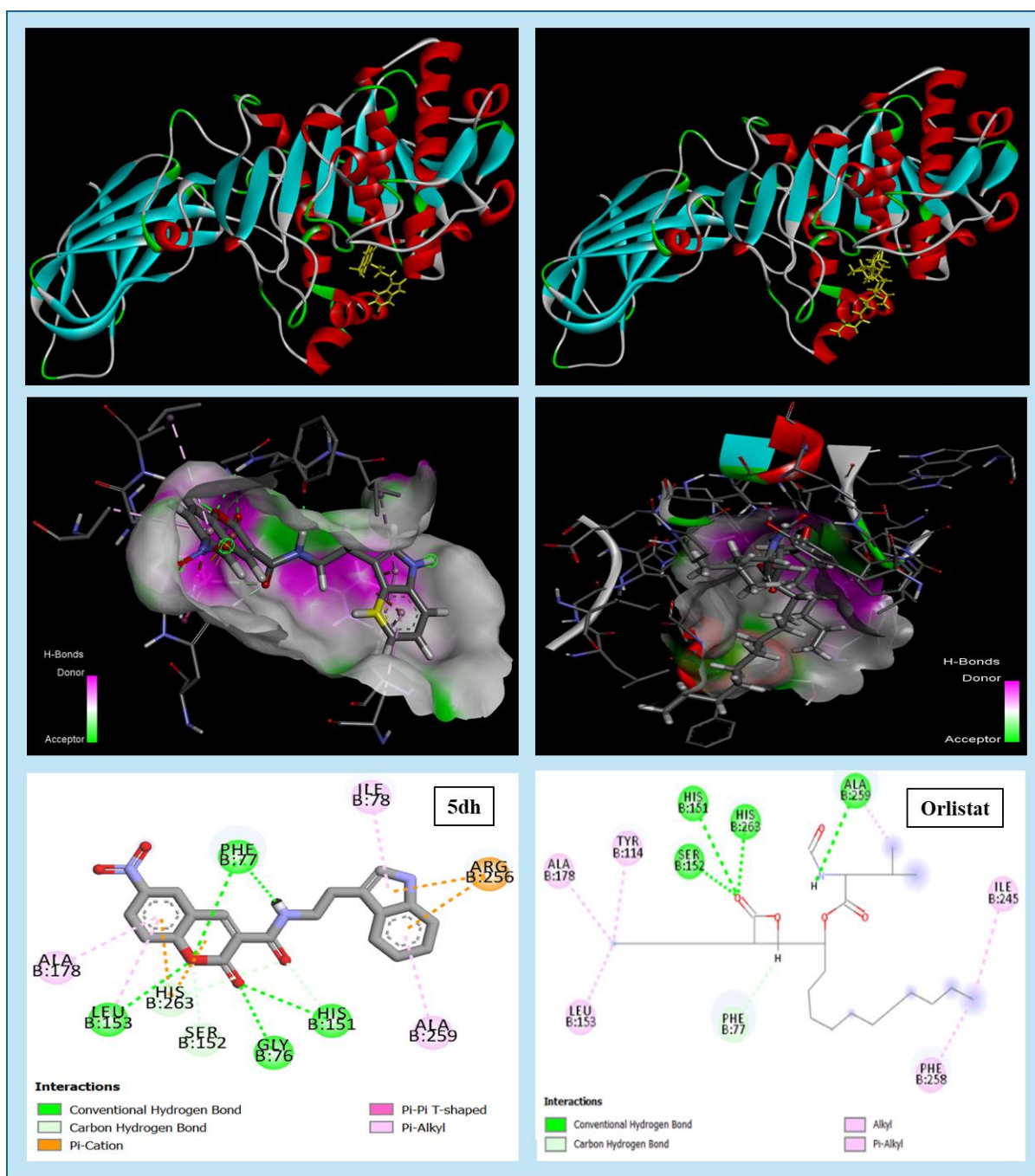


Figure 6.5. 2D and 3D interaction diagram of **5dh** and Orlistat in the active site of PL.

CHAPTER VI

As depicted in **Fig 6.5**, the analog **5dh** exhibited several essential interactions with the amino acids present in the active site. The indole ring exhibited π -cation interaction with Arg 256. Hydrogen bonding interactions were observed between the amide warhead and Phe 77. The coumarin scaffold exhibited hydrogen bonding with Gly 76, Phe 77, His 151, and Leu 153. Additionally, it displayed π -cation interactions with His 263, and π -alkyl interaction with Ala 178 and Leu 153. The carbonyl oxygen of coumarin participated in the creation of hydrogen bonding interactions between Gly 76 and His 151.

Table 6.4. MolDock score (kcal/mol) and interaction summary of analogues (**5a(a-i)**, **5b(a-i)**, **5c(a-i)** and **5d(a-i)**) at the active site of the PL.

Code	R ₁	R ₂	n	Mol Dock Score (kcal/mol)	H-bond	π - π interactions	π -cation	π -alkyl
5aa	H	-H	1	-100.974	Phe 77, Ser 152	Phe 77, Tyr 114	Asp 79, Arg 256	Ile 78, Leu 264, Ala 178, Pro180
5ab		2-Cl	1	-101.322	Phe 77, Ser 152, Leu 153, His 263	Phe 77	Arg 256, His 263	Ile 78, Leu 264, Ala 178, Ala 260
5ac		4-F	1	-111.179	Phe 77, Ser 152, Leu 153, His 263	Phe 77	Asp 79, Arg 256, His 263	Ile 78, Ala 178, Leu 264
5ad		4-OCH ₃	1	-115.012	Phe 77, Ser 152, Arg 256	Phe 77, Tyr 114	Asp 79, Arg 256	Leu 264, Ala 178, Pro180
5ae		3,4,5-tri-OCH ₃	1	-115.011	His 151, Ser 152	Phe 215	Arg 256, His 263	Ile 78, Leu 153, Ala 178
5af		-H	2	-111.634	Phe 77, Ser 152	Tyr 114, His 263	-	Ala 178, Ala 259, Ala 260, Arg 256
5ag		4-OCH ₃	2	-118.309	Phe 77, Ser 152	Tyr 114	Asp 79, Arg 256	Ile 78, Leu 264, Ala 178, Pro 180
5ah		1- <i>H</i> -indole	2	-128.564	Phe 77, Ser 152	Tyr 114, Phe 215	Arg 256, His 263	Ile 78, Ala 178, Pro 180, Ala 259, Ala 260
5ai		H	3	-111.564	His 151, Ser 152	-	Arg 256, His 263	Ile 78, Leu 153, Ala 178
5ba	Br	-H	1	-108.13	Phe 77, Leu 153, His 263	Tyr 114, Phe 215	-	Tyr 114, Ala 178, Pro 180, Ala 260
5bb		2-Cl	1	-112.369	Phe 77, Ser 152, Leu 153	Phe 215, Tyr 114	-	Tyr 114, Pro 180, Phe 215, Ala 178, Ala 260, His 263

CHAPTER VI

5bc		4-F	1	-116.705	Phe 77, Ser 152, Leu 153	Tyr 114, Phe 215	-	Tyr 114, Ala 178, Pro 180
5bd		4-OCH ₃	1	-117.43	Phe 77, Leu 153, His 263	Tyr 114, Phe 215	-	Tyr 114, Ala 178, Pro 180, Leu 264
5be		3,4,5-tri- OCH ₃	1	-119.469	Phe 77, Leu 153	Phe 215	His 263	Tyr 114, Ala 178, Pro 180, Ala 260, Leu 264
5bf		-H	2	-114.093	Gly 76, Phe 77, His 151	Phe 77	Arg 256, His 263	Tyr 114, Ala 178, Phe 215, Pro 180, Ala 259, Leu 153
5bg		4-OCH ₃	2	-121.561	Phe 77, Ser 152, Leu 153, His 263	Tyr 114, Phe 215	-	Tyr 114, Ala 178, Pro 180, Ala 260
5bh		1- <i>H</i> -indole	2	-129.174	Gly 76, Phe 77, His 151	-	Arg 256, His 263	Ile 78, Tyr 114, Leu 153, Ala 178, Phe 215, Pro 180, Ala 259, Arg 256
5bi		H	3	-120.428	Phe 77, Ser 152, Leu 153	Tyr 114, Phe 215	-	Tyr 114, Ala 178, Pro 180, Ala 259, Ala 260, Arg 256
5ca	Cl	-H	1	-108.557	Phe 77, Leu 153, His 263	Tyr 114, Phe 215	-	Tyr 114, Ala 178, Pro 180, Ala 260
5cb		2-Cl	1	-112.632	Phe 77, Ser 152, Leu 153	Tyr 114, Phe 215	-	Tyr 114, Phe 215, Ala 178, Pro 180, Ala 260, His 263
5cc		4-F	1	-113.29	Phe 77, Leu 153, His 263	Tyr 114, Phe 215	-	Tyr 114, Ala 178, Pro 180, Leu 264
5cd		4-OCH ₃	1	-118.501	Phe 77, Ser 152, Leu 153, His 263	Tyr 114, Phe 215	-	Tyr 114, Ala 178, Pro 180, Leu 264
5ce		3,4,5-tri- OCH ₃	1	-113.907	Phe 77, Ser 152, Leu 153, His 151	Phe 77, Phe 215	His 263	Ile 78, Phe 215
5cf		-H	2	-114.039	Gly 76, Phe 77, His 151	-	His 263, Arg 256	Tyr 114, Ala 178, Phe 215, Leu 153, Pro 180, Ala 259
5cg		4-OCH ₃	2	-117.248	Gly 76, Phe 77,	-	His 263	Tyr 114, Ala 178, Phe 215,

CHAPTER VI

					His 151			Leu 153, Pro 180, Ala 259, Arg 256
5ch		1- <i>H</i> -indole	2	-128.272	Asp 79, Phe 77, Ser 152, His 153	Tyr 114, Phe 215	-	Tyr 114, Ala 178, Pro 180, Ala 259, Ala 260
5ci		H	3	-120.233	Phe 77, Leu 153, His 263	Tyr 114, Phe 215	-	Tyr 114, Ala 178, Pro 180, Ala 259, Ala 260, Arg 256
5da	NO ₂	-H	1	-113.292	Gly 76, Phe 77, His 151	Phe 77	His 263	Ala 178, Ala 259, Ala 260, Leu 153, Leu 264, Arg 256
5db		2-Cl	1	-118.498	Gly 76, Phe 77, His 151	Phe 77	His 263	Ile 78, Ala 178, Ala 259, Ala 260, Arg 256
5dc		4-F	1	-122.203	Ser 152, His 263, His 151, Arg 256	Tyr 115	Arg 256	Ile 78, Ala 178, Ala 260, Leu 264
5dd		4-OCH ₃	1	-122.679	Phe 77, Leu 153, His 263	Tyr 114, Phe 215	-	Ala 178, Pro 180, Leu 264
5de		3,4,5-tri- OCH ₃	1	-122.731	Gly 76, Ser 152, His 151, Arg 256	Phe 77, Trp 252	His 263	Ile 78, Ala 259
5df		-H	2	-124.516	Gly 76, Phe 77, His 151	Phe 77	His 263, Arg 256	Ala 178, Ala 259, Leu 153
5dg		4-OCH ₃	2	-132.132	Gly 76, Phe 77, His 151	-	Arg 256, His 263	Ala 178, Ala 259, Leu 153
5dh		1-<i>H</i>- indole	2	-140.251	Gly 76, Phe 77, His 151, Leu 153	-	Arg 256, His 263	Ile 78, Ala 178, Ala 259, Leu 153
5di		-H	3	-132.628	Phe 77, His 263, Leu 153	Tyr 115, Phe 215	-	Ala 178, Pro 180, Ala 260
Orlistat		-	-139.41	Phe 77, Ser 152, His 263, His 151, Ala 259	-	-	Tyr 114, Leu 153, Ala 178, Phe 258, Ile 245	

6.8. Molecular dynamics simulations

While molecular docking analysis provides initial insights into docking interactions, it is incapable of forecasting the magnitude of such interactions under dynamic conditions. Given the perpetual state of flux exhibited by all proteins within the human body, it becomes imperative to forecast the ligand's behaviour under such dynamic physiological conditions. The ligand-protein complex of the highest-scoring analogue **5dh**, was therefore simulated using MD for 100 ns. Following MD simulation, the outcomes were evaluated by considering protein-ligand Root Mean Square Deviation (RMSD) and contacts between proteins and ligands to comprehend the stability of the complex and depict the time span of the effective amino acid interactions under dynamic conditions. The RMSD measures the average displacement of a selected group of atoms in a certain frame relative to a reference frame. The protein maintained its stability throughout the simulation, as illustrated in **Fig 6.6. (A)**. The ligand's RMSD remained below 7.5 Å until 65 ns. Following this time interval, the RMSD shifts from 7.5 Å to 12 Å, with a significant deflection occurring at 75 ns (below 5.4 Å). Subsequently, the RMSD stabilizes at a value below 7.5 Å. The Root Mean Square Fluctuation (RMSF) is a valuable tool for identifying localized variations along the protein chain. As depicted in **Fig 6.6. (B)**, amino acid fluctuations in the catalytic triad and lid domain were less than 3Å, indicating the likelihood of these amino acids remaining intact in a dynamic environment.

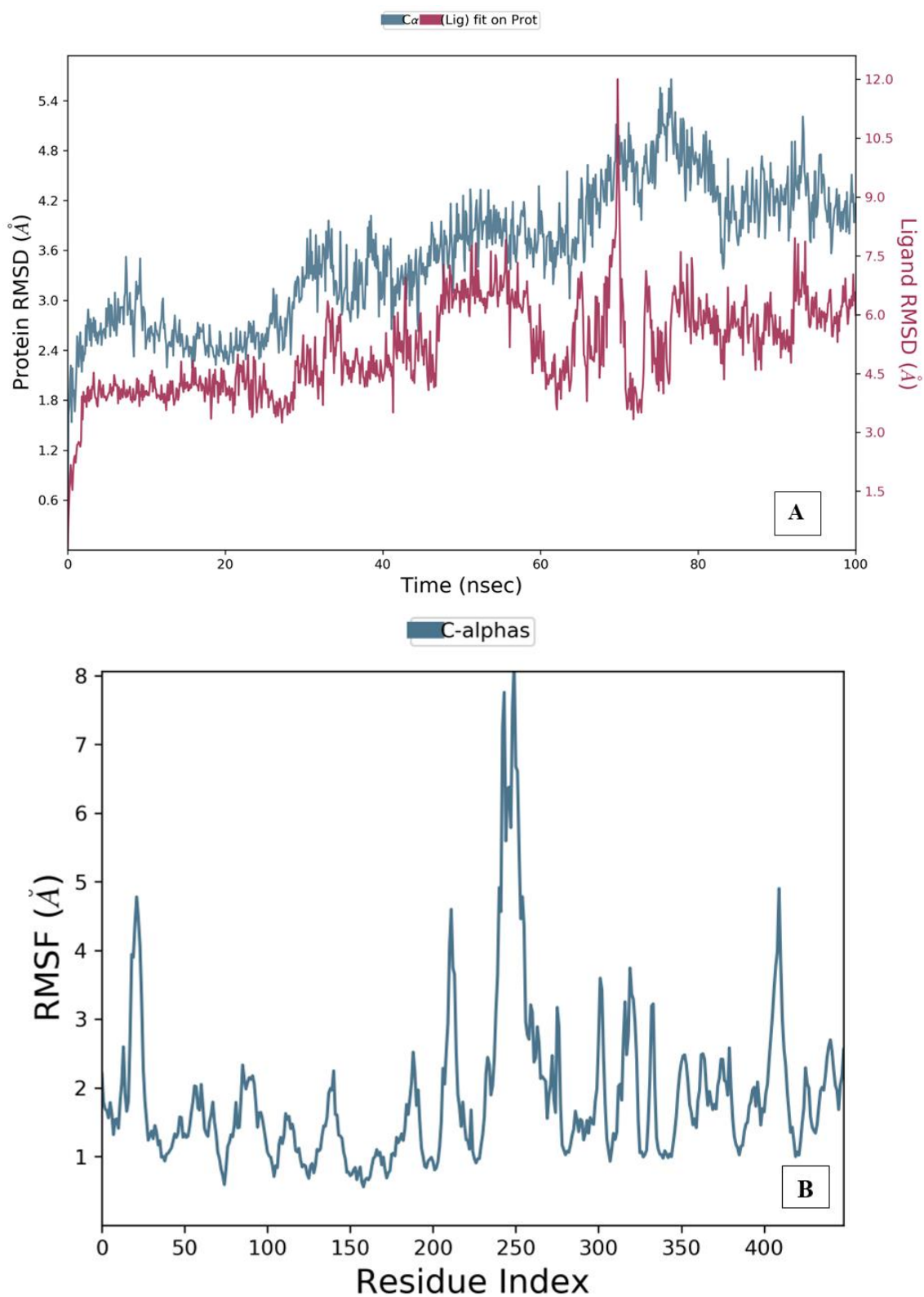


Figure 6.6. (A) RMSD plot of the protein-ligand (**5dh**) complex (PDB ID: 1LPB);
(B) Protein RMSF plot.

A variety of interactions, including hydrogen, hydrophobic and ionic bonds, were observed within the protein-ligand complex. The hydrophobic domain encasing the catalytic triad of PL ensures that PL inhibition requires the opening of this lid domain. The data presented in **Fig 6.7 (A)** indicated that Phe 77 was engaged in multiple interactions (including hydrophobic, hydrogen bonding, as well as water bridges) for a fraction of time greater than 0.5. Through hydrophobic interaction and the formation of water bridges, Tyr 114 and Phe 215 were also observed to interact for greater than 0.8 and 1.0 fractions of time, respectively. Additionally, prolonged interaction durations with the amino acids Tyr 114, Phe 215; Ala 259; His 263 are illustrated in **Fig 6.7 (A)**. The interaction with the catalytic triad (Ser 152 & His 263) and hydrophobic lid domain (Phe 77, Ile 78, Asp 79, Tyr 114 & Phe 215) amino acid demonstrated the efficacy of the designed analogue **5dh**. A temporal depiction of the contacts and interactions (hydrophobic, ionic, and water bridges) are outlined in **Fig 6.7 (B)**. As depicted in the **Fig 6.7 (B)** the total number of specific contacts between the protein and the ligand throughout the trajectory is displayed in the upper panel. The residues that interact with the ligand in each trajectory frame are displayed in the bottom panel. Certain residues established multiple specific contacts with the ligand were denoted by a darker hue of orange on the scale located to the right of the plot.

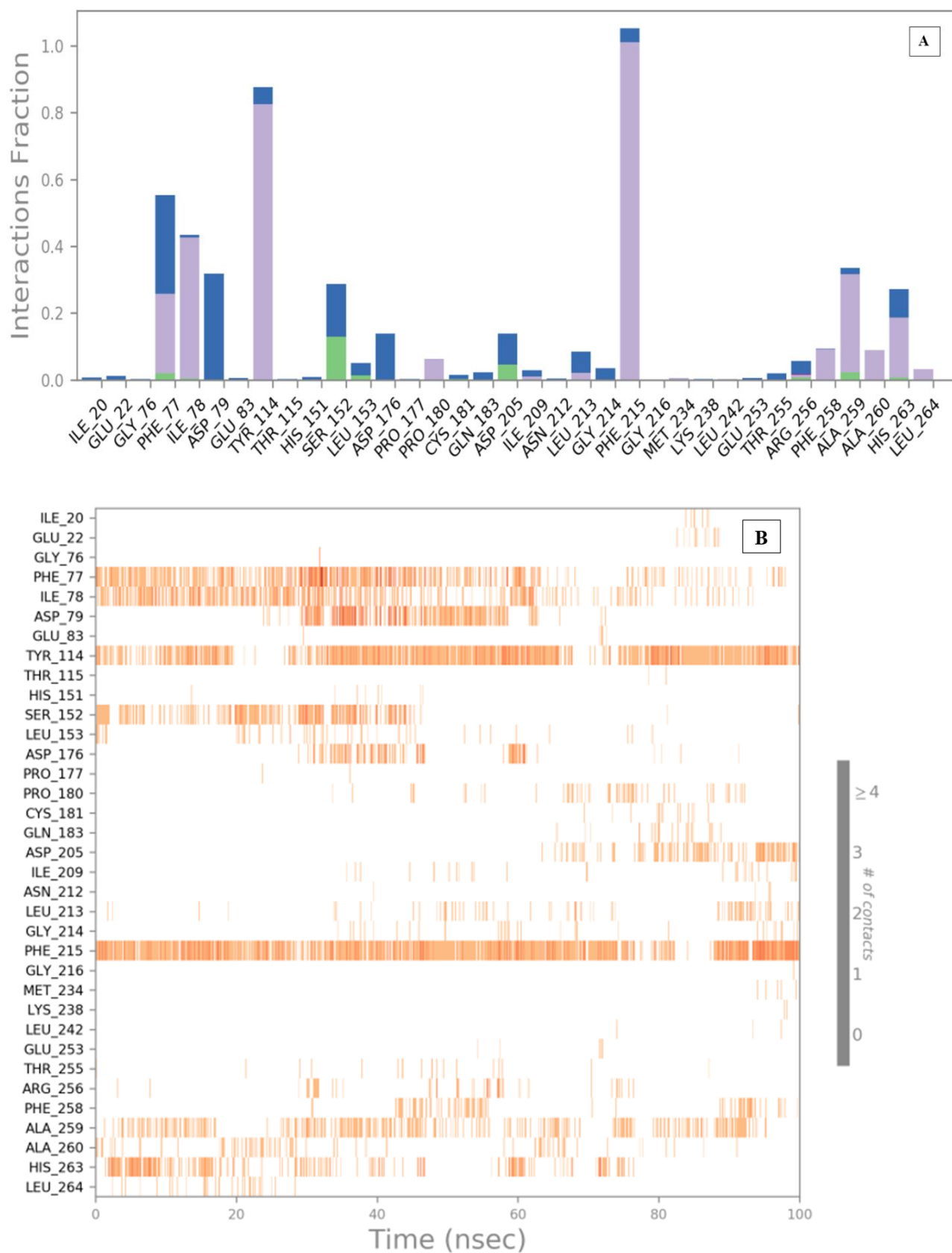


Figure 6.7. (A) Protein-ligand (**5dh**) interaction bar charts stacked vertically (PDB ID: 1LPB); (B) Protein-ligand contact timeline (H-bonds, hydrophobic, ionic, water bridges).

In conclusion, a series of thirty-six coumarin analogues were designed and synthesized through a suitable chemical reaction scheme, followed by characterization *via* various spectroscopic techniques. The PL inhibitory assay was performed to screen these analogues for PL inhibitory potential and a total of two analogues namely, **5dh** and **5de** were found to be potent ($IC_{50} = 9.20$ and $11.4 \mu\text{M}$, respectively). The SAR was obtained by observing the IC_{50} values of various substituted analogues. The 6-nitro substituent on coumarin was found to be effective in inhibiting the PL enzyme, while non-substituted groups on the 6th position of coumarin was found to show less PL inhibitory potential. The substitution of an indole ring *via* a two carbon linker was found to be effective in PL inhibition. Also, analogue **5dh** was found to competitively inhibit the PL enzyme with K_i values of $4.504 \mu\text{M}$, respectively. Many of the analogues were found to interact with the active site amino acid residues (Phe 77, Tyr 114, Ser 152, Phe 215, Arg 256, His 263, etc.) that were comparable to Orlistat. Furthermore, molecular dynamic simulation revealed that the protein-ligand complex of the most potent analogue **5dh** remained stable at the PL active site for 100 ns under physiological conditions. While the PL inhibition of the synthesized analogues was potentially greater than that of series I, it was believed that additional structural modifications could enhance the PL inhibition. This is elaborated in the next chapter.

References

1. Umezawa, H., Aoyagi, T., Uotani, K., Hamada, M., Takeuchi, T., & Takahashi, S. (1980). Ebelactone, an inhibitor of esterase, produced by *Actinomycetes*. *The Journal of Antibiotics*, 33(12), 1594-1596.
2. Mutoh, M., Nakada, N., Matsukuma, S., Ohshima, S., Yoshinri, K., Watanabe, J., & Arisawa, M. (1994). Panclitics, novel pancreatic lipase inhibitors I. Taxonomy, fermentation, isolation and biological activity. *The Journal of Antibiotics*, 47(12), 1369-1375.
3. Chen, H. P., Zhao, Z. Z., Li, Z. H., Dong, Z. J., Wei, K., Bai, X., Zhang, L., Wen, C.N., Feng, T. & Liu, J. K. (2016). Novel natural oximes and oxime esters with a vibrallactone backbone from the basidiomycete *Boreostereum vibrans*. *ChemistryOpen*, 5(2), 142-149.
4. Wei, K., Wang, G. Q., Bai, X., Niu, Y. F., Chen, H. P., Wen, C. N., Li, Z.H., Dong, Z.J., Zuo, Z.L., Xiong, W.Y. & Liu, J. K. (2015). Structure-based optimization and biological evaluation of pancreatic lipase inhibitors as novel potential antiobesity agents. *Natural Products and Bioprospecting*, 5, 129-157.
5. Kim, J. H., Kim, H. J., Kim, C., Jung, H., Kim, Y. O., Ju, J. Y., & Shin, C. S. (2007).

- Development of lipase inhibitors from various derivatives of *Monascus* pigment produced by *Monascus* fermentation. *Food Chemistry*, 101(1), 357-364.
- Kim, J. H., Kim, H. J., Park, H. W., Youn, S. H., Choi, D. Y., & Shin, C. S. (2007). Development of inhibitors against lipase and α -glucosidase from derivatives of *Monascus* pigment. *FEMS Microbiology Letters*, 276(1), 93-98.
 - Ahn, J. H., Shin, E. J., Liu, Q., Kim, S. B., Choi, K. M., Yoo, H. S., Hwang, B.Y. & Lee, M. K. (2012). Lignan derivatives from *Fraxinus rhynchophylla* and inhibitory activity on pancreatic lipase. *Natural Product Sciences*, 18(2), 116-120.
 - Fattah, T. A., Saeed, A., Al-Hiari, Y. M., Kasabri, V., Almasri, I. M., Al-Alawi, S., Larik, F.A. & Channar, P. A. (2019). Functionalized furo [3, 2-*c*] coumarins as anti-proliferative, anti-lipolytic, and anti-inflammatory compounds: Synthesis and molecular docking studies. *Journal of Molecular Structure*, 1179, 390-400.
 - Brahmachari, G. (2015). Room temperature one-pot green synthesis of coumarin-3-carboxylic acids in water: A practical method for the large-scale synthesis. *ACS Sustainable Chemistry & Engineering*, 3(9), 2350-2358.
 - Chan, L. C., & Cox, B. G. (2007). Kinetics of amide formation through carbodiimide/N-hydroxybenzotriazole (HOBt) couplings. *The Journal of Organic Chemistry*, 72(23), 8863-8869.
 - Yadav, N., & Paul, A. T. (2023). Synthesis of amide warhead containing coumarin derivatives as potential pancreatic lipase inhibitors: *In silico* and *in vitro* evaluation for obesity treatment. *Medicinal Chemistry Research*, 32(10), 2219-2233.
 - George, G., Yadav, N., Auti, P. S., & Paul, A. T. (2023). Molecular modelling, synthesis and *in vitro* evaluation of quinazolinone hybrid analogues as potential pancreatic lipase inhibitors. *Journal of Biomolecular Structure and Dynamics*. 41(19), 9583-9601.
 - Lineweaver, H., & Burk, D. (1934). The determination of enzyme dissociation constants. *Journal of the American Chemical Society*, 56(3), 658-666.
 - Burlingham, B. T., & Widlanski, T. S. (2003). An intuitive look at the relationship of K_i and IC_{50} : A more general use for the Dixon plot. *Journal of Chemical Education*, 80(2), 214-218.
 - Pandey, V., Adhikrao, P. A., Motiram, G. M., Yadav, N., Jagtap, U., Kumar, G., & Paul, A. (2024). Biaryl carboxamide-based peptidomimetics analogs as potential pancreatic lipase inhibitors for treating obesity. *Archiv der Pharmazie*, 357(4), e2300503.

Synthesis of Series III

7. Synthesis of Coumarin Analogues - Series III

7.1. Rationale

The synthesized coumarin analogues (**Series II**) exhibited a potential PL inhibition with the most active analogue from the series, **5dh** and **5de** that exhibited an IC_{50} value of 9.20 and 11.40 μ M, respectively. In order to determine the optimal position on the coumarin scaffold for further substitution, additional molecular modeling analyses were performed (**Fig 7.1**).

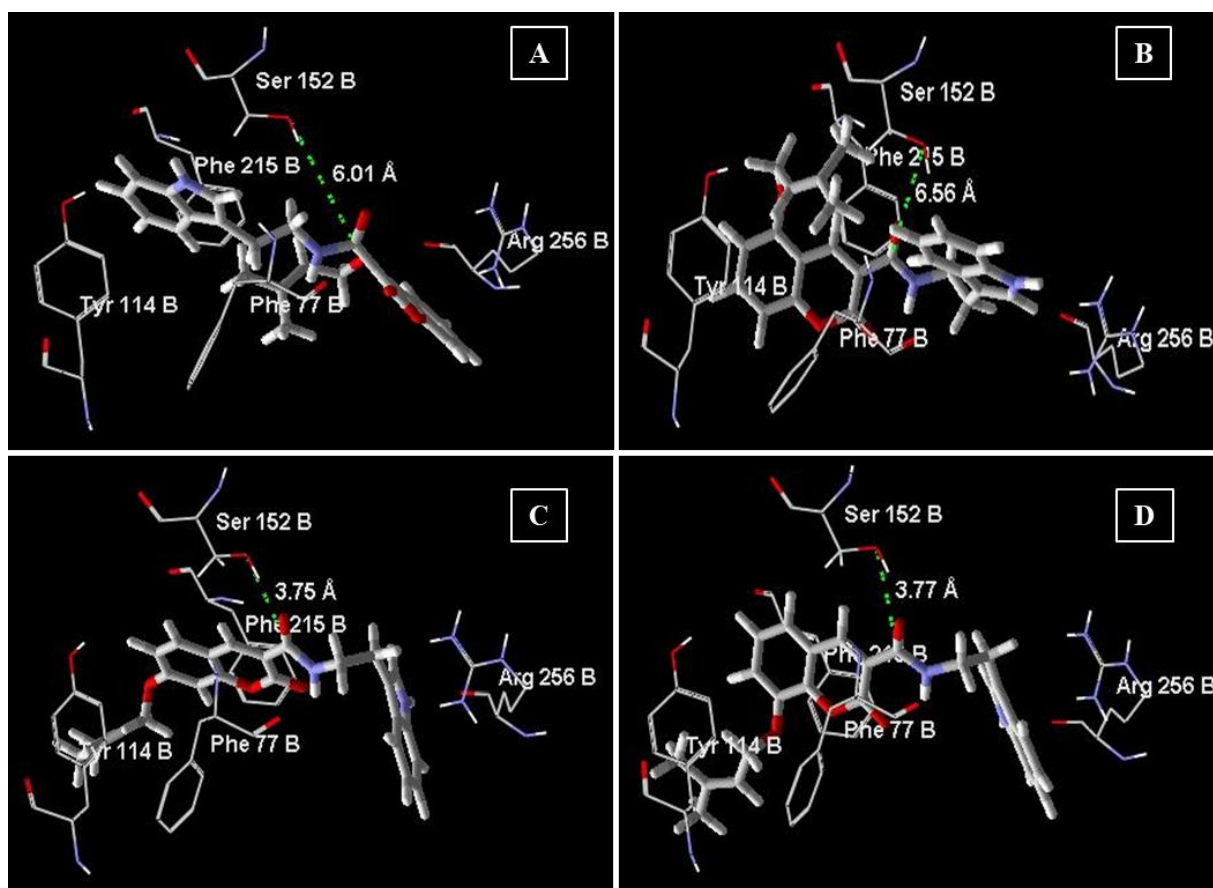


Figure 7.1. Rationale for designing series III coumarin analogues as PL inhibitors. The interaction distance between the reactive carbonyl and Ser 152 at 4th position (**A**) was found 6.01 Å; 5th position (**B**) 6.56 Å; 7th position (**C**) 3.75 Å; and 8th position (**D**) 3.77 Å.

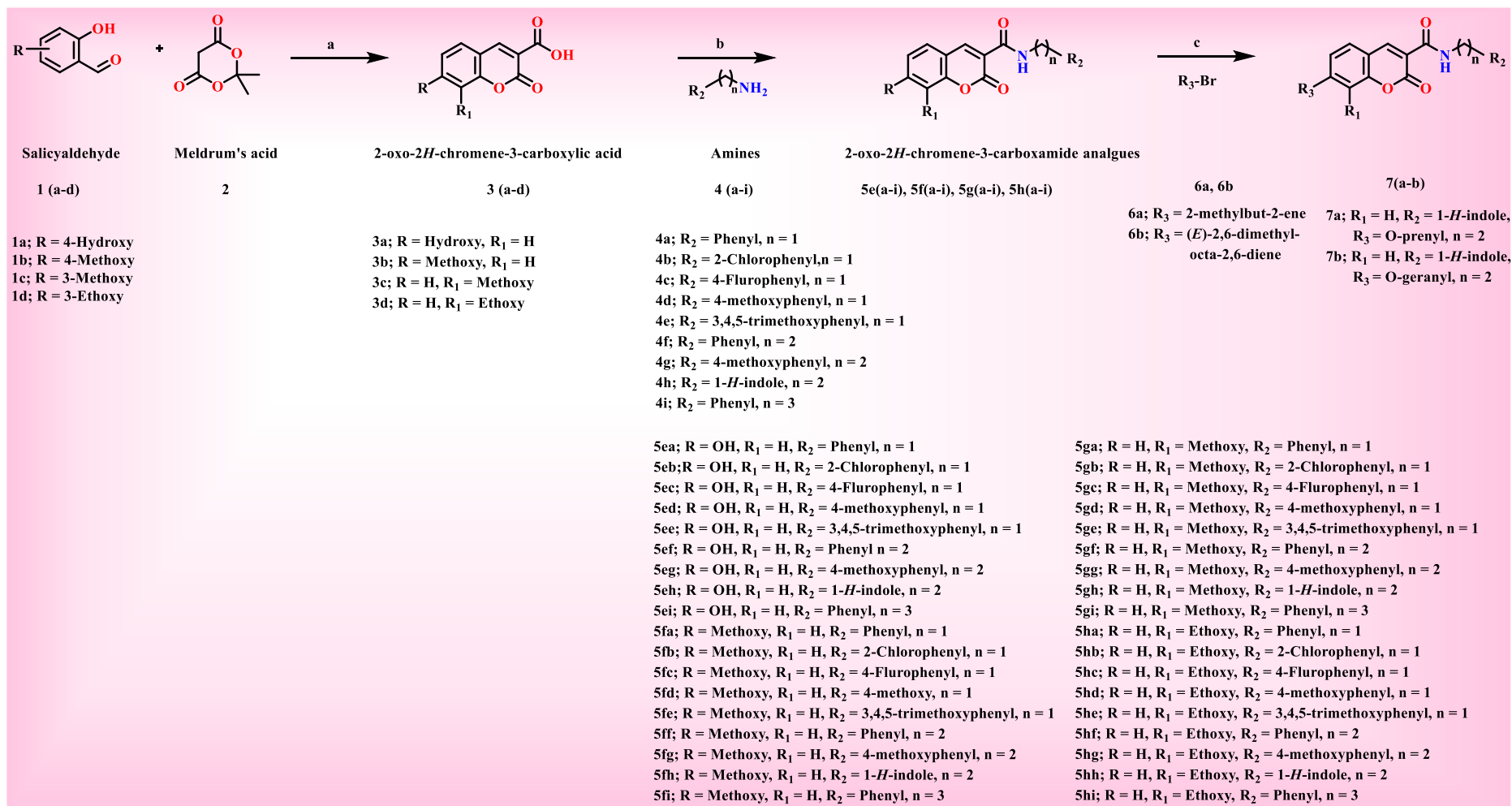
Preliminary molecular modelling study highlighted that the incorporation of an alkyl linker on the seventh and eight positions of coumarin scaffold might be helpful for the reduction of the interaction distance of the carbonyl group from Ser 152 (**Fig 7.1**) As a result, we further started exploring seventh and eighth position of the designing of coumarin analogues that can display promising inhibitory activity against PL (**Fig 7.1**). Accordingly, a series of 36 coumarin analogues were designed, synthesized, characterized and evaluated for their *in-vitro* PL inhibitory potential.

The current investigation involved the development of a series of coumarin analogues that possessed a range of crucial pharmacophoric characteristics necessary to potentially inhibit PL. The pharmacophore comprised of four characteristics: (I) R₁/R₃ on the seventh and eighth position of coumarin scaffold to enhance the hydrophobicity on the coumarin scaffold *via* *O*-alkyl functionalities; (II) amide warhead to interact with Ser 152; and (III) linker (n=1-3), a structural framework that facilitates the attainment of appropriate conformational flexibility to ensure a proper interaction with the active site amino acid and the lid domain; (IV) R₂, (either a simple or heterocyclic aromatic ring) to form a π -cation interaction with Arg 256. We hypothesised that the incorporation of these structural characteristics onto a coumarin scaffold would lead to an increase in its inhibitory potential for PL [1-2].

7.2. Synthesis and Characterization

The syntheses of all the final analogues **5e(a-i)**, **5f(a-i)**, **5g(a-i)**, **5h(a-i)** and **7(a-b)** were carried out as per the procedure detailed in **Scheme 7.1**. Synthesis and characterization of final analogues were performed in the same manner as discussed in the previous chapter (Chapter 5) [3-4].

CHAPTER VII



Scheme 7.1. Reagents and conditions: (a) K₂CO₃, H₂O, RT, 20 h; (b) DMF, 0 °C, EDC.HCl, HOBT, Ar-(CH₂)_n-NH₂, DIPEA, 20-30 °C, 15-20 h
(c) K₂CO₃, acetone, alkyl halides, reflux 60 °C.

7.2.1. General procedure for the synthesis of coumarin-3-carboxylic acid derivatives**3a-3d**

50 mL RBF was supplemented with distilled water (5 mL), K_2CO_3 (0.20 equiv), and 2,2-dimethyl-1,3-dioxane-4,6-dione (**2**; 1 equiv). Following a 15 mins interval, salicylaldehyde **1a-1d** (1 equiv) was introduced into the reaction mixture. After that, the mixture was stirred continuously at room temperature for a duration of 20 h to facilitate the completion of the conversion. After the process was finished, the solution was acidified with 1N HCl. Following these steps, the solid mass that was produced was filtered, precipitated, and thoroughly cleansed with water to obtain coumarin-3-carboxylic acid **3a-3d**. Further purification of the analogues **3a-3d** was done by crystallization using ethyl acetate as the solvent [3].

7.2.2. General Procedure for synthesis of coumarin-3-carboxamide derivatives (5e(a-i), 5f(a-i), 5g(a-i), 5h(a-i) and 7(a-b))

Under a controlled temperature of 0 °C, a solution of **3a-3d** (1 equiv) in DMF was systematically treated with 1.10 equiv of EDC.HCl and HOBt. Amines with a range of substitutions **4a-4i** (1 equiv) were dissolved in DMF before being introduced into the reaction mixture. N-diisopropylethylamine (DIPEA) (0.60 equiv) was introduced after a duration of 10 mins. The chemical reaction was stirred at room temperature for a period of 15-20 h to get the desired products (**5e(a-i)**, **5f(a-i)**, **5g(a-i)** and **5h(a-i)**) [3,4]. Further, the *O*-substitution of prenyl/geranyl moieties on **5eh** was carried out at 60°C in the presence of K_2CO_3 (3 equiv), prenyl/geranyl bromides (1.5 equiv) and acetone to yield **7(a-b)** [5]. After the reaction was fully completed, water was used to facilitate the work-up process. The resultant solid substance was filtered out, followed by a comprehensive rinsing with water and subsequent air drying. To obtain an impurity-free product, column chromatography was utilized (eluent was a mixture of hexane and ethyl acetate; the stationary phase was silica (#100-200). Using NMR, HRMS, ATR and HPLC techniques, the synthesized analogues (**5e(a-i)**, **5f(a-i)**, **5g(a-i)**, **5h(a-i)** and **7(a-b)**) were characterized.

7.2.3. Analytical Data for the final analogues (5e(a-i), 5f(a-i), 5g(a-i), 5h(a-i) and 7(a-b))***N*-benzyl-7-hydroxy-2-oxo-2*H*-chromene-3-carboxamide (5ea)**

Yield: 93%; off white solid; mp = 432-433 °C; 1H NMR (400 MHz, $DMSO-d_6$) δ 11.08 (s, 1H), 9.06 (t, $J = 6.0$ Hz, 1H), 8.81 (d, $J = 0.7$ Hz, 1H), 7.82 (d, $J = 8.6$ Hz, 1H), 7.34 (d, $J = 4.4$ Hz, 4H), 7.29 - 7.23 (m, 1H), 6.88 (dd, $J = 8.6, 2.2$ Hz, 1H), 6.80 (d, $J = 2.2$ Hz, 1H), 4.54 (d, $J = 6.0$ Hz, 2H). ^{13}C NMR (100 MHz, $DMSO-d_6$) δ 164.15, 162.16, 161.50, 156.77, 148.66, 139.55, 132.47, 128.86, 127.84, 127.40, 114.81, 114.13, 111.60, 102.27, 43.13. IR

(ATR) ν 3853.54, 3744.50, 3735.89, 3711.50, 3649.81, 2360.04, 1734.52, 1717.31, 1684.31, 1652.75, 1647.01, 1506.41, 1457.63, 1032.97, 794.81, 668.56 cm^{-1} . HRMS (ESI+) calculated for $\text{C}_{17}\text{H}_{13}\text{NO}_4$ $[\text{M} + \text{H}]^+$, 296.0917; found 296.0946. HPLC purity: 99.91 %, t_R - 3.313 min.

***N*-(2-chlorobenzyl)-7-hydroxy-2-oxo-2*H*-chromene-3-carboxamide (5eb)**

Yield: 91%; off white solid; mp = 474-476 °C; ^1H NMR (400 MHz, $\text{DMSO-}d_6$) δ 11.10 (s, 1H), 9.13 (t, J = 6.1 Hz, 1H), 8.80 (s, 1H), 7.82 (d, J = 8.6 Hz, 1H), 7.49 - 7.27 (m, 4H), 6.88 (dd, J = 8.6, 2.3 Hz, 1H), 6.81 (d, J = 2.2 Hz, 1H), 4.60 (d, J = 6.0 Hz, 2H). ^{13}C NMR (100 MHz, $\text{DMSO-}d_6$) δ 164.21, 162.33, 161.52, 156.82, 148.80, 136.48, 132.58, 132.53, 129.66, 129.41, 129.25, 127.73, 114.83, 113.94, 111.60, 102.29, 41.22. IR (ATR) ν 3215.11, 1707.26, 1645.57, 1618.31, 1596.79, 1542.28, 1506.41, 1447.59, 1418.89, 1367.25, 1334.25, 1301.25, 1263.95, 1114.74, 1043.01, 992.79, 964.79, 737.42, 715.90, 672.86, 641.30 cm^{-1} . HRMS (ESI+) calculated for $\text{C}_{17}\text{H}_{12}\text{ClNO}_4$ $[\text{M} + \text{H}]^+$, 330.0528; found 330.0539. HPLC purity: 99.90 %, t_R - 3.963 min.

***N*-(4-fluorobenzyl)-7-hydroxy-2-oxo-2*H*-chromene-3-carboxamide (5ec)**

Yield: 88%; off white solid; mp = 445-447 °C; ^1H NMR (400 MHz, $\text{DMSO-}d_6$) δ 11.08 (s, 1H), 9.08 (t, J = 6.1 Hz, 1H), 8.79 (s, 1H), 7.81 (d, J = 8.6 Hz, 1H), 7.42 - 7.33 (m, 2H), 7.20 - 7.10 (m, 2H), 6.88 (dd, J = 8.6, 2.2 Hz, 1H), 6.80 (d, J = 2.2 Hz, 1H), 4.51 (d, J = 6.0 Hz, 2H). ^{13}C NMR (100 MHz, $\text{DMSO-}d_6$) δ 164.17, 162.90, 162.20, 161.43, 160.49, 156.78, 148.67, 135.86, 132.46, 129.93, 115.64, 115.43, 114.81, 114.09, 111.58, 102.27, 42.42. IR (ATR) ν 3377.22, 3261.02, 1702.96, 1615.44, 1563.80, 1500.67, 1456.19, 1433.24, 1372.98, 1291.21, 1243.86, 1159.22, 1096.09, 735.99, 707.29, 593.96 cm^{-1} . HRMS (ESI+) calculated for $\text{C}_{17}\text{H}_{12}\text{FNO}_4$ $[\text{M} + \text{H}]^+$, 314.0823; found 314.0836. HPLC purity: 99.98 %, t_R - 3.340 min.

7-hydroxy-*N*-(4-methoxybenzyl)-2-oxo-2*H*-chromene-3-carboxamide (5ed)

Yield: 89%; off white solid; mp = 478-480 °C; ^1H NMR (400 MHz, $\text{DMSO-}d_6$) δ 11.07 (s, 1H), 8.97 (t, J = 5.9 Hz, 1H), 8.81 (s, 1H), 7.82 (d, J = 8.6 Hz, 1H), 7.31 - 7.23 (m, 2H), 6.94 - 6.85 (m, 3H), 6.80 (d, J = 2.2 Hz, 1H), 4.45 (d, J = 5.9 Hz, 2H), 3.73 (s, 3H). ^{13}C NMR (100 MHz, $\text{DMSO-}d_6$) δ 164.11, 161.97, 161.51, 158.81, 156.75, 148.62, 132.46, 131.42, 129.32, 114.80, 114.28, 114.16, 111.62, 102.27, 55.52, 42.61. IR (ATR) ν 3646.94, 3304.06, 2834.92, 1763.22, 1612.57, 1537.97, 1510.71, 1450.46, 1374.42, 1246.73, 1219.47, 1170.69, 1142.00, 1030.10, 852.20, 738.86, 641.30 cm^{-1} . HRMS (ESI+) calculated for $\text{C}_{18}\text{H}_{15}\text{NO}_5$ $[\text{M} + \text{H}]^+$, 326.1028; found 326.1023. HPLC purity: 99.51 %, t_R - 3.210 min.

7-hydroxy-2-oxo-*N*-(3,4,5-trimethoxybenzyl)-2*H*-chromene-3-carboxamide (5ee)

Yield: 91%; off white solid; mp = 570-572 °C; ^1H NMR (400 MHz, $\text{DMSO-}d_6$) δ 11.09 (s, 1H), 9.00 (t, J = 6.0 Hz, 1H), 8.80 (s, 1H), 7.82 (d, J = 8.6 Hz, 1H), 6.88 (d, J = 8.6 Hz, 1H),

6.81 (s, 1H), 6.68 (s, 2H), 4.46 (d, $J = 5.8$ Hz, 2H), 3.75 (s, 6H), 3.63 (s, 3H). ^{13}C NMR (100 MHz, DMSO- d_6) δ 164.10, 162.16, 161.47, 156.74, 153.32, 148.52, 136.91, 135.15, 132.44, 114.80, 114.33, 111.61, 105.31, 102.27, 60.44, 56.28, 43.38. IR (ATR) ν 3358.57, 3263.89, 1760.35, 1645.57, 1611.14, 1581.01, 1558.06, 1533.67, 1507.84, 1460.50, 1434.67, 1418.89, 1350.03, 1299.82, 1262.51, 1240.99, 1202.26, 1119.05, 994.23, 968.41, 737.42, 714.47, 669.99, 581.04, 516.48 cm^{-1} . HRMS (ESI+) calculated for $\text{C}_{20}\text{H}_{19}\text{NO}_7$ $[\text{M} + \text{H}]^+$, 386.1240; found 386.1234. HPLC purity: 99.85 %, t_R - 2.860 min.

7-hydroxy-2-oxo-*N*-phenethyl-2*H*-chromene-3-carboxamide (5ef)

Yield: 89%; off white solid; mp = 443-444 °C; ^1H NMR (400 MHz, DMSO- d_6) δ 11.05 (s, 1H), 8.78 (s, 1H), 8.70 (t, $J = 5.8$ Hz, 1H), 7.81 (d, $J = 8.6$ Hz, 1H), 7.35 - 7.17 (m, 5H), 6.88 (dd, $J = 8.6, 2.2$ Hz, 1H), 6.79 (d, $J = 2.2$ Hz, 1H), 3.61 - 3.51 (m, 2H), 2.84 (t, $J = 7.3$ Hz, 2H). ^{13}C NMR (100 MHz, DMSO- d_6) δ 164.10, 162.40, 161.50, 156.62, 148.50, 139.41, 132.35, 129.03, 128.81, 126.68, 114.90, 113.47, 111.39, 102.12, 41.06, 35.20. IR (ATR) ν 3513.52, 3324.14, 3031.47, 2831.05, 2605.37, 2385.86, 1569.53, 1496.37, 1451.89, 1431.81, 1365.81, 1319.90, 1296.95, 1200.82, 1061.66, 991.36, 965.54, 860.80, 829.24, 793.38, 754.64, 727.38 cm^{-1} . HRMS (ESI+) calculated for $\text{C}_{18}\text{H}_{15}\text{NO}_4$ $[\text{M} + \text{H}]^+$, 310.1074; found 310.1098. HPLC purity: 99.60 %, t_R - 3.573 min.

7-hydroxy-*N*-(4-methoxyphenethyl)-2-oxo-2*H*-chromene-3-carboxamide (5eg)

Yield: 94%; off white solid; mp = 489-491 °C; ^1H NMR (400 MHz, DMSO- d_6) δ 11.07 (s, 1H), 8.78 (s, 1H), 8.68 (t, $J = 5.7$ Hz, 1H), 7.81 (d, $J = 8.6$ Hz, 1H), 7.21 - 7.13 (m, 2H), 6.89 (d, $J = 2.2$ Hz, 1H), 6.88 - 6.84 (m, 2H), 6.79 (d, $J = 2.8$ Hz, 1H), 3.72 (s, 3H), 3.56 - 3.46 (m, 2H), 2.77 (t, $J = 7.2$ Hz, 2H). ^{13}C NMR (100 MHz, DMSO- d_6) δ 164.09, 161.88, 161.50, 158.20, 156.71, 148.50, 132.46, 131.52, 130.09, 114.80, 114.28, 114.01, 111.59, 102.24, 55.43, 41.29, 34.64. IR (ATR) ν 3714.37, 3679.94, 3654.12, 3593.86, 2438.95, 2400.21, 2308.39, 2226.62, 2169.23, 1943.98, 1652.75, 1558.06, 1540.84, 793.38, 532.26 cm^{-1} . HRMS (ESI+) calculated for $\text{C}_{19}\text{H}_{17}\text{NO}_5$ $[\text{M} + \text{H}]^+$, 340.1179; found 340.1207. HPLC purity: 99.64 %, t_R - 3.400 min.

***N*-(2-(1*H*-indol-3-yl)ethyl)-7-hydroxy-2-oxo-2*H*-chromene-3-carboxamide (5eh)**

Yield: 90%; off white solid; mp = 513-515 °C; ^1H NMR (400 MHz, DMSO- d_6) δ 11.07 (s, 1H), 10.86 (s, 1H), 8.81 (s, 1H), 8.77 (t, $J = 5.7$ Hz, 1H), 7.81 (d, $J = 8.7$ Hz, 1H), 7.61 (d, $J = 7.8$ Hz, 1H), 7.35 (d, $J = 8.1$ Hz, 1H), 7.21 (d, $J = 2.3$ Hz, 1H), 7.12 - 7.03 (m, 1H), 7.02 - 6.94 (m, 1H), 6.88 (dd, $J = 8.6, 2.3$ Hz, 1H), 6.80 (d, $J = 2.2$ Hz, 1H), 3.62 (q, $J = 7.2$ Hz, 2H), 2.96 (t, $J = 7.2$ Hz, 2H). ^{13}C NMR (100 MHz, DMSO- d_6) δ 164.07, 161.92, 161.48, 156.71, 148.47, 136.77, 132.43, 127.61, 123.28, 121.45, 118.85, 118.72, 114.79, 114.13,

111.98, 111.85, 111.61, 102.25, 40.28, 25.54. IR (ATR) ν 3173.50, 1698.66, 1644.14, 1614.01, 1589.62, 1451.89, 1430.37, 1374.42, 1335.68, 1256.78, 1170.69, 1120.48, 1008.58, 981.32, 813.46, 711.60, 609.74, 542.31 cm^{-1} . HRMS (ESI+) calculated for $\text{C}_{20}\text{H}_{16}\text{N}_2\text{O}_4$ $[\text{M} + \text{H}]^+$, 349.1183; found 349.1192. HPLC purity: 100 %, t_R - 3.223 min.

7-hydroxy-2-oxo-*N*-(3-phenylpropyl)-2*H*-chromene-3-carboxamide (5ei)

Yield: 92%; off white solid; mp = 454-456 °C; ^1H NMR (400 MHz, $\text{DMSO-}d_6$) δ 11.06 (s, 1H), 8.77 (s, 1H), 8.68 (t, J = 5.8 Hz, 1H), 7.81 (d, J = 8.6 Hz, 1H), 7.31 - 7.13 (m, 5H), 6.88 (dd, J = 8.6, 2.3 Hz, 1H), 6.80 (d, J = 2.2 Hz, 1H), 3.33 (q, J = 6.7 Hz, 2H), 2.63 (t, J = 7.6 Hz, 2H), 1.83 (p, J = 7.6 Hz, 2H). ^{13}C NMR (100 MHz, $\text{DMSO-}d_6$) δ 164.07, 162.01, 161.53, 156.70, 148.33, 141.96, 132.40, 128.77, 128.74, 126.24, 114.78, 114.28, 111.59, 102.25, 39.06, 32.98, 31.19. IR (ATR) ν 3219.41, 1705.83, 1648.44, 1614.01, 1583.88, 1450.46, 1371.55, 1335.68, 1261.08, 1172.13, 1149.17, 1120.48, 1025.72, 972.71, 847.89, 820.63, 791.94, 774.72, 757.51, 717.34, 645.60, 638.43, 579.61, 526.53 cm^{-1} . HRMS (ESI+) calculated for $\text{C}_{19}\text{H}_{17}\text{NO}_4$ $[\text{M} + \text{H}]^+$, 324.1230; found 324.1261. HPLC purity: 100 %, t_R - 4.193 min.

***N*-benzyl-7-methoxy-2-oxo-2*H*-chromene-3-carboxamide (5fa)**

Yield: 90%; off white solid; mp = 366-368 °C; ^1H NMR (400 MHz, CDCl_3) δ 9.15 (s, 1H), 8.90 (s, 1H), 7.60 (d, J = 8.7 Hz, 1H), 7.40 - 7.29 (m, 5H), 6.96 (dd, J = 8.7, 2.4 Hz, 1H), 6.88 (d, J = 2.4 Hz, 1H), 4.68 (d, J = 5.8 Hz, 2H), 3.93 (s, 3H). ^{13}C NMR (100 MHz, CDCl_3) δ 164.90, 162.08, 161.82, 156.71, 148.51, 138.12, 130.96, 128.69, 127.71, 127.40, 114.77, 114.06, 112.44, 100.33, 56.03, 43.78. IR (ATR) ν 3843, 3744, 3613, 3349, 1700, 1609, 1531, 1367, 1222, 1134, 1024, 831, 708, 636, 425 cm^{-1} . HRMS (ESI+) calculated for $\text{C}_{18}\text{H}_{15}\text{NO}_4$ $[\text{M} + \text{H}]^+$, 310.1080; found 310.1088. HPLC purity: 99.50 %, t_R - 6.013 min.

***N*-(2-chlorobenzyl)-7-methoxy-2-oxo-2*H*-chromene-3-carboxamide (5fb)**

Yield: 89%; off white solid; mp = 409-411 °C; ^1H NMR (400 MHz, CDCl_3) δ 9.26 (s, 1H), 8.88 (s, 1H), 7.60 (d, J = 8.8 Hz, 1H), 7.48 - 7.44 (m, 1H), 7.43 - 7.38 (m, 1H), 7.27 - 7.21 (m, 2H), 6.96 (dd, J = 8.7, 2.4 Hz, 1H), 6.89 (d, J = 2.4 Hz, 1H), 4.77 (d, J = 6.1 Hz, 2H), 3.94 (s, 3H). ^{13}C NMR (100 MHz, CDCl_3) δ 164.94, 162.18, 161.81, 156.75, 148.56, 135.53, 133.70, 130.97, 129.76, 129.57, 128.80, 127.00, 114.67, 114.09, 112.41, 100.33, 56.04, 41.69. IR (ATR) ν 3844, 3743, 3613, 2313, 1699, 1516, 1366, 1216, 1119, 1025, 744, 627 cm^{-1} . HRMS (ESI+) calculated for $\text{C}_{18}\text{H}_{14}\text{ClNO}_4$ $[\text{M} + \text{H}]^+$, 344.0684; found 344.0702. HPLC purity: 99.45 %, t_R - 7.717 min.

***N*-(4-fluorobenzyl)-7-methoxy-2-oxo-2*H*-chromene-3-carboxamide (5fc)**

Yield: 88%; off white solid; mp = 379-380 °C; ¹H NMR (400 MHz, CDCl₃) δ 9.14 (s, 1H), 8.89 (s, 1H), 7.60 (d, J = 8.8 Hz, 1H), 7.40 - 7.30 (m, 2H), 7.09 - 6.99 (m, 2H), 6.96 (dd, J = 8.7, 2.4 Hz, 1H), 6.88 (d, J = 2.4 Hz, 1H), 4.63 (d, J = 5.9 Hz, 2H), 3.93 (s, 3H). ¹³C NMR (100 MHz, CDCl₃) δ 164.97, 162.12, 161.85, 156.73, 148.59, 133.99, 130.98, 129.45, 129.37, 115.61, 115.40, 114.64, 114.11, 112.41, 100.34, 56.04, 43.05. IR (ATR) ν 3845, 3742, 3617, 3345, 2315, 1708, 1620, 1525, 1372, 1220, 1130, 1019, 831, 753, 705, 632, 502 cm⁻¹. HRMS (ESI+) calculated for C₁₈H₁₄FNO₄ [M + H]⁺, 328.0985; found 328.0995. HPLC purity: 99.56 %, *t_R* - 5.997 min.

7-methoxy-*N*-(4-methoxybenzyl)-2-oxo-2*H*-chromene-3-carboxamide (5fd)

Yield: 91%; off white solid; mp = 412-413 °C; ¹H NMR (400 MHz, CDCl₃) δ 9.07 (t, J = 5.8 Hz, 1H), 8.89 (s, 1H), 7.60 (d, J = 8.7 Hz, 1H), 7.33 - 7.29 (m, 2H), 6.95 (dd, J = 8.7, 2.4 Hz, 1H), 6.92 - 6.85 (m, 3H), 4.60 (d, J = 5.8 Hz, 2H), 3.93 (s, 3H), 3.82 (s, 3H). ¹³C NMR (100 MHz, CDCl₃) δ 164.39, 161.95, 158.97, 156.69, 148.42, 130.94, 130.27, 129.10, 114.83, 114.09, 114.03, 112.44, 100.32, 56.02, 55.31, 43.27. IR (ATR) ν 3845, 3742, 3617, 3309, 2313, 1701, 1609, 1520, 1457, 1372, 1232, 1027, 828, 720, 443 cm⁻¹. HRMS (ESI+) calculated for C₁₉H₁₇NO₅ [M + H]⁺, 340.1179; found 340.1198. HPLC purity: 98.27 %, *t_R* - 5.520 min.

7-methoxy-2-oxo-*N*-(3,4,5-trimethoxybenzyl)-2*H*-chromene-3-carboxamide (5fe)

Yield: 90%; off white solid; mp = 504-505 °C; ¹H NMR (400 MHz, CDCl₃) δ 9.12 (t, J = 5.8 Hz, 1H), 8.89 (s, 1H), 7.61 (d, J = 8.7 Hz, 1H), 6.96 (dd, J = 8.7, 2.4 Hz, 1H), 6.88 (d, J = 2.4 Hz, 1H), 6.61 (s, 2H), 4.60 (d, J = 5.8 Hz, 2H), 3.93 (s, 3H), 3.88 (s, 6H), 3.85 (s, 3H). ¹³C NMR (100 MHz, CDCl₃) δ 164.97, 162.05, 161.87, 156.72, 153.43, 148.56, 137.30, 133.84, 130.98, 114.71, 114.10, 112.42, 104.81, 100.34, 60.84, 56.15, 56.04, 44.06. IR (ATR) ν 3845, 3742, 3617, 2314, 1698, 1526, 1225, 549, 457 cm⁻¹. HRMS (ESI+) calculated for C₂₁H₂₁NO₇ [M + H]⁺, 400.1391; found 400.1411. HPLC purity: 99.44 %, *t_R* - 4.497 min.

7-methoxy-2-oxo-*N*-phenethyl-2*H*-chromene-3-carboxamide (5ff)

Yield: 93%; off white solid; mp = 377-379 °C; ¹H NMR (400 MHz, CDCl₃) δ 8.85 (s, 2H), 7.59 (d, J = 8.7 Hz, 1H), 7.38 - 7.29 (m, 3H), 7.29 - 7.23 (m, 2H), 6.95 (dd, J = 8.7, 2.4 Hz, 1H), 6.86 (d, J = 2.4 Hz, 1H), 3.93 (s, 3H), 3.78 - 3.68 (m, 2H), 2.96 (t, J = 7.3 Hz, 2H). ¹³C NMR (100 MHz, CDCl₃) δ 164.81, 161.99, 161.77, 156.64, 148.18, 138.92, 130.92, 128.80, 128.61, 126.51, 114.85, 113.97, 112.44, 100.31, 56.02, 41.28, 35.74. IR (ATR) ν 3847, 3742, 3617, 2315, 1706, 1632, 1523, 1373, 1230, 1024, 829, 460 cm⁻¹. HRMS (ESI+) calculated for C₁₉H₁₇NO₄ [M + H]⁺, 324.1236; found 324.1247. HPLC purity: 99.60 %, *t_R* - 6.487 min.

7-methoxy-*N*-(4-methoxyphenethyl)-2-oxo-2*H*-chromene-3-carboxamide (5fg)

Yield: 89%; off white solid; mp = 423-425 °C; ¹H NMR (400 MHz, CDCl₃) δ 8.85 (s, 1H), 8.84 (s, 1H), 7.63 - 7.55 (m, 1H), 7.23 - 7.16 (m, 2H), 6.99 - 6.92 (m, 1H), 6.91 - 6.82 (m, 3H), 3.92 (s, 3H), 3.81 (s, 3H), 3.69 (q, J = 7.5 Hz, 2H), 2.89 (t, J = 7.3 Hz, 2H). ¹³C NMR (100 MHz, CDCl₃) δ 164.80, 161.96, 161.77, 158.28, 156.64, 148.15, 130.97, 130.91, 129.73, 114.89, 114.04, 113.95, 112.45, 100.32, 56.01, 55.25, 41.48, 34.83. IR (ATR) ν 3845, 3742, 3617, 3406, 2316, 1708, 1634, 1532, 1375, 1227, 1134, 1017, 753, 562 cm⁻¹. HRMS (ESI+) calculated for C₂₀H₁₉NO₅ [M + H]⁺, 354.1336; found 354.1336. HPLC purity: 99.14 %, *t_R* - 6.013 min.

***N*-(2-(1*H*-indol-3-yl)ethyl)-7-methoxy-2-oxo-2*H*-chromene-3-carboxamide (5fh)**

Yield: 88%; off white solid; mp = 529-531 °C; ¹H NMR (400 MHz, CDCl₃) δ 8.89 (t, J = 5.8 Hz, 1H), 8.86 (s, 1H), 8.19 (s, 1H), 7.69 (d, J = 7.8 Hz, 1H), 7.58 (d, J = 8.7 Hz, 1H), 7.39 (d, J = 8.2 Hz, 1H), 7.25 - 7.12 (m, 3H), 6.95 (dd, J = 8.7, 2.4 Hz, 1H), 6.85 (d, J = 2.4 Hz, 1H), 3.92 (s, 3H), 3.87 - 3.77 (m, 2H), 3.12 (t, J = 7.0 Hz, 2H). ¹³C NMR (100 MHz, CDCl₃) δ 164.78, 161.98, 161.79, 156.61, 148.14, 136.43, 130.92, 127.32, 122.18, 122.09, 119.39, 118.80, 114.95, 113.95, 113.04, 112.46, 111.22, 100.30, 56.01, 40.20, 25.32. IR (ATR) ν 3330.52, 2911.53, 2864.50, 2360.14, 1713.14, 1644.36, 1609.26, 1573.26, 1531.07, 1464.10, 1354.21, 1279.14, 1240.80, 1160.16, 1100.82, 965.09, 791.36, 742.81, 706.22 cm⁻¹. HRMS (ESI+) calculated for C₂₁H₁₈N₂O₄ [M + H]⁺, 363.1339; found 363.1352. HPLC purity: 99.76 %, *t_R* - 5.230 min.

7-methoxy-2-oxo-*N*-(3-phenylpropyl)-2*H*-chromene-3-carboxamide (5fi)

Yield: 91%; off white solid; mp = 389-390 °C; ¹H NMR (400 MHz, CDCl₃) δ 8.87 (s, 1H), 8.84 (s, 1H), 7.61 (d, J = 8.7 Hz, 1H), 7.31 (t, J = 7.5 Hz, 2H), 7.28 - 7.16 (m, 3H), 6.96 (dd, J = 8.7, 2.4 Hz, 1H), 6.89 (d, J = 2.4 Hz, 1H), 3.94 (s, 3H), 3.51 (q, J = 6.7 Hz, 2H), 2.75 (t, J = 7.7 Hz, 2H), 1.99 (p, J = 7.4 Hz, 2H). ¹³C NMR (100 MHz, CDCl₃) δ 164.81, 162.03, 161.92, 156.64, 148.20, 141.40, 130.92, 128.44, 125.95, 114.90, 114.02, 112.47, 100.32, 56.03, 39.27, 33.24, 31.04. IR (ATR) ν 3845, 3742, 3617, 2314, 1698, 1526, 1225, 549, 457 cm⁻¹. HRMS (ESI+) calculated for C₂₀H₁₉NO₄ [M + H]⁺, 338.1387; found 338.1397. HPLC purity: 99.69 %, *t_R* - 8.190 min.

***N*-benzyl-8-methoxy-2-oxo-2*H*-chromene-3-carboxamide (5ga)**

Yield: 89%; off white solid; mp = 366-368 °C; ¹H NMR (400 MHz, CDCl₃) δ 9.22 (t, J = 5.8 Hz, 1H), 8.94 (s, 1H), 7.39 - 7.27 (m, 7H), 7.21 (dd, J = 7.8, 1.7 Hz, 1H), 4.69 (d, J = 5.8 Hz, 2H), 4.01 (s, 3H). ¹³C NMR (100 MHz, CDCl₃) δ 161.60, 160.95, 148.79, 147.07, 144.11, 137.95, 128.70, 127.75, 127.45, 125.18, 120.94, 119.30, 118.60, 115.56, 56.37, 43.86. IR

(ATR) ν 3348.33, 2924.79, 1703.57, 1652.89, 1608.56, 1570.62, 1529.80, 1468.99, 1360.19, 1269.26, 1244.22, 1196.01, 1152.21, 1102.61, 1066.72, 951.80, 790.53, 725.89, 696.01, 662.66 cm^{-1} . HRMS (ESI+) calculated for $\text{C}_{18}\text{H}_{15}\text{NO}_4$ $[\text{M} + \text{H}]^+$, 310.1074; found 310.1064. HPLC purity: 98.92 %, t_R - 5.417 min.

***N*-(2-chlorobenzyl)-8-methoxy-2-oxo-2*H*-chromene-3-carboxamide (5gb)**

Yield: 89%; off white solid; mp = 409-411 °C; ^1H NMR (400 MHz, CDCl_3) δ 9.32 (t, J = 5.8 Hz, 1H), 8.92 (s, 1H), 7.48 - 7.38 (m, 2H), 7.34 - 7.24 (m, 4H), 7.21 (dd, J = 7.8, 1.7 Hz, 1H), 4.77 (d, J = 6.1 Hz, 2H), 4.01 (s, 3H). ^{13}C NMR (100 MHz, CDCl_3) δ 161.69, 160.94, 148.83, 147.08, 144.14, 135.33, 133.69, 129.74, 129.59, 128.85, 127.01, 125.19, 120.94, 119.26, 118.49, 115.64, 56.38, 41.77. IR (ATR) ν 3329.03, 2920.87, 2854.91, 1702.35, 1661.08, 1606.65, 1532.05, 1463.05, 1412.46, 1356.49, 1272.44, 1204.42, 1149.09, 1103.40, 1044.85, 955.92, 795.50, 743.93, 677.95, 635.54 cm^{-1} . HRMS (ESI+) calculated for $\text{C}_{18}\text{H}_{14}\text{ClNO}_4$ $[\text{M} + \text{H}]^+$, 344.0684; found 344.0654. HPLC purity: 98.52 %, t_R - 7.010 min.

***N*-(4-fluorobenzyl)-8-methoxy-2-oxo-2*H*-chromene-3-carboxamide (5gc)**

Yield: 89%; off white solid; mp = 379-380 °C; ^1H NMR (400 MHz, CDCl_3) δ 9.22 (t, J = 5.8 Hz, 1H), 8.94 (s, 1H), 7.37 - 7.29 (m, 3H), 7.27 (d, J = 1.7 Hz, 1H), 7.22 (dd, J = 7.8, 1.7 Hz, 1H), 7.09 - 6.99 (m, 2H), 4.64 (d, J = 6.0 Hz, 2H), 4.01 (s, 3H). ^{13}C NMR (100 MHz, CDCl_3) δ 163.40, 161.63, 160.98, 148.90, 147.08, 144.11, 133.82, 133.79, 129.51, 129.43, 125.23, 120.95, 119.27, 118.49, 115.63, 115.42, 56.37, 43.14. IR (ATR) ν 3326.18, 2929.20, 1710.59, 1657.01, 1605.92, 1510.07, 1472.25, 1442.13, 1354.37, 1268.42, 1216.41, 1151.94, 1101.48, 1052.59, 960.18, 825.36, 790.00, 739.19, 704.53, 667.76 cm^{-1} . HRMS (ESI+) calculated for $\text{C}_{18}\text{H}_{14}\text{FNO}_4$ $[\text{M} + \text{H}]^+$, 328.098; found 328.0973. HPLC purity: 99.36 %, t_R - 5.543 min.

8-methoxy-*N*-(4-methoxybenzyl)-2-oxo-2*H*-chromene-3-carboxamide (5gd)

Yield: 89%; off white solid; mp = 412-413 °C; ^1H NMR (400 MHz, CDCl_3) δ 9.14 (t, J = 5.8 Hz, 1H), 8.93 (s, 1H), 7.36 - 7.29 (m, 3H), 7.26 (d, J = 1.8 Hz, 1H), 7.20 (dd, J = 7.8, 1.7 Hz, 1H), 6.93 - 6.85 (m, 2H), 4.61 (d, J = 5.8 Hz, 2H), 4.00 (s, 3H), 3.81 (s, 3H). ^{13}C NMR (100 MHz, CDCl_3) δ 161.45, 160.90, 158.99, 148.70, 147.05, 144.09, 130.10, 129.15, 125.15, 120.92, 119.30, 118.66, 115.51, 114.09, 56.36, 55.31, 43.35. IR (ATR) ν 3309.89, 2923.85, 2855.35, 1709.13, 1651.24, 1607.51, 1573.18, 1522.99, 1466.09, 1357.25, 1247.24, 1183.21, 1145.38, 1105.17, 1038.79, 948.95, 846.68, 795.98, 720.45, 658.18 cm^{-1} . HRMS (ESI+) calculated for $\text{C}_{19}\text{H}_{17}\text{NO}_5$ $[\text{M} + \text{H}]^+$, 340.1179; found 340.1172. HPLC purity: 98.63 %, t_R - 5.137 min.

8-methoxy-2-oxo-*N*-(3,4,5-trimethoxybenzyl)-2*H*-chromene-3-carboxamide (5ge)

Yield: 88%; off white solid; mp = 504-506 °C; ¹H NMR (400 MHz, CDCl₃) δ 9.20 (t, J = 6.1 Hz, 1H), 8.94 (s, 1H), 7.35 - 7.29 (m, 1H), 7.27 (d, J = 1.7 Hz, 1H), 7.22 (dd, J = 7.8, 1.7 Hz, 1H), 6.61 (s, 2H), 4.61 (d, J = 5.9 Hz, 2H), 4.01 (s, 3H), 3.87 (s, 6H), 3.85 (s, 3H). ¹³C NMR (100 MHz, CDCl₃) δ 161.55, 161.00, 153.43, 148.85, 147.07, 144.09, 137.29, 133.66, 125.24, 120.93, 119.28, 118.56, 115.59, 104.77, 60.85, 56.36, 56.14, 44.11. IR (ATR) ν 3347.22, 2922.48, 2856.72, 2358.64, 1713.67, 1652.20, 1603.76, 1520.37, 1462.06, 1361.65, 1237.75, 1115.53, 996.74, 964.91, 839.02, 783.63, 722.41, 674.90 cm⁻¹. HRMS (ESI+) calculated for C₂₁H₂₁NO₇ [M + H]⁺, 400.1391; found 400.1386. HPLC purity: 98.68 %, *t_R* - 4.277 min.

8-methoxy-2-oxo-*N*-phenethyl-2*H*-chromene-3-carboxamide (5gf)

Yield: 90%; off white solid; mp = 377-378 °C; ¹H NMR (400 MHz, CDCl₃) δ 8.92 (t, J = 6.1 Hz, 1H), 8.89 (s, 1H), 7.36 - 7.26 (m, 6H), 7.23 (t, J = 1.6 Hz, 1H), 7.20 (dd, J = 7.8, 1.7 Hz, 1H), 4.00 (s, 3H), 3.77 - 3.68 (m, 2H), 2.96 (t, J = 7.3 Hz, 2H). ¹³C NMR (100 MHz, CDCl₃) δ 161.48, 160.90, 148.43, 147.05, 144.06, 138.83, 128.81, 128.63, 126.53, 125.13, 120.90, 119.30, 118.65, 115.46, 56.35, 41.40, 35.68. IR (ATR) ν 3359.07, 2922.40, 2855.44, 2357.11, 1707.13, 1654.26, 1606.76, 1572.76, 1524.97, 1467.03, 1359.34, 1273.77, 1243.21, 1206.80, 1105.10, 1059.33, 963.33, 788.74, 738.37, 701.47 cm⁻¹. HRMS (ESI+) calculated for C₁₉H₁₇NO₄ [M + H]⁺, 324.1230; found 324.1228. HPLC purity: 99.24 %, *t_R* - 6.063 min.

8-methoxy-*N*-(4-methoxyphenethyl)-2-oxo-2*H*-chromene-3-carboxamide (5gg)

Yield: 94%; off white solid; mp = 423-424 °C; ¹H NMR (400 MHz, CDCl₃) δ 8.91 (t, J = 5.2 Hz, 1H), 8.89 (s, 1H), 7.36 - 7.29 (m, 1H), 7.28 - 7.24 (m, 1H), 7.22 - 7.17 (m, 3H), 6.91 - 6.83 (m, 2H), 4.00 (s, 3H), 3.80 (s, 3H), 3.74 - 3.64 (m, 2H), 2.90 (t, J = 7.3 Hz, 2H). ¹³C NMR (100 MHz, CDCl₃) δ 161.45, 160.90, 158.29, 148.40, 147.05, 144.06, 130.86, 129.75, 125.12, 120.90, 119.31, 118.68, 115.43, 114.05, 56.35, 55.25, 41.60, 34.77. IR (ATR) ν 2924.28, 2855.82, 1708.02, 1656.23, 1609.76, 1571.59, 1520.65, 1466.92, 1363.34, 1241.79, 1204.28, 1179.86, 1105.37, 1070.34, 1030.01, 831.60, 791.77, 741.22, 723.43, 705.93 cm⁻¹. HRMS (ESI+) calculated for C₂₀H₁₉NO₅ [M + H]⁺, 354.1336; found 354.1342. HPLC purity: 98.96 %, *t_R* - 5.637 min.

***N*-(2-(1*H*-indol-3-yl)ethyl)-8-methoxy-2-oxo-2*H*-chromene-3-carboxamide (5gh)**

Yield: 88%; off white solid; mp = 519-521 °C; ¹H NMR (400 MHz, CDCl₃) δ 8.97 (t, J = 5.7 Hz, 1H), 8.89 (s, 1H), 8.22 (s, 1H), 7.72 - 7.65 (m, 1H), 7.43 - 7.36 (m, 1H), 7.35 - 7.21 (m, 3H), 7.20 (d, J = 1.5 Hz, 1H), 7.17 (dd, J = 4.5, 1.4 Hz, 1H), 7.13 (d, J = 1.1 Hz, 1H), 3.99 (s, 3H), 3.87 - 3.77 (m, 2H), 3.13 (t, J = 7.0 Hz, 2H). ¹³C NMR (100 MHz, CDCl₃) δ 161.47,

160.92, 148.36, 147.02, 144.04, 136.44, 127.28, 125.11, 122.28, 122.08, 120.91, 119.39, 119.31, 118.76, 118.74, 115.43, 112.88, 111.25, 56.34, 40.33, 25.25. IR (ATR) ν 3332.52, 2921.53, 2854.50, 2358.14, 1712.14, 1648.36, 1607.26, 1571.26, 1530.07, 1468.10, 1351.21, 1274.14, 1239.80, 1158.16, 1100.82, 965.09, 791.36, 742.81, 706.22 cm^{-1} . HRMS (ESI+) calculated for $\text{C}_{21}\text{H}_{18}\text{N}_2\text{O}_4$ $[\text{M} + \text{H}]^+$, 363.1339; found 363.1338. HPLC purity: 98.08 %, t_R - 5.027 min.

8-methoxy-2-oxo-*N*-(3-phenylpropyl)-2*H*-chromene-3-carboxamide (5gi)

Yield: 90%; off white solid; mp = 389-390 °C; ^1H NMR (400 MHz, CDCl_3) δ 8.93 (s, 1H), 8.91 (s, 1H), 7.34 - 7.18 (m, 8H), 4.02 (s, 3H), 3.58 - 3.43 (m, 2H), 2.74 (t, $J = 7.6$ Hz, 2H), 2.00 (p, $J = 7.7$ Hz, 2H). ^{13}C NMR (100 MHz, CDCl_3) δ 161.52, 161.04, 148.43, 147.07, 144.08, 141.34, 128.45, 128.43, 125.97, 125.15, 120.91, 119.34, 118.70, 115.46, 56.37, 39.38, 33.24, 30.97. IR (ATR) ν 3845, 3742, 3617, 2314, 1698, 1526, 1225, 549, 457 cm^{-1} . HRMS (ESI+) calculated for $\text{C}_{20}\text{H}_{19}\text{NO}_4$ $[\text{M} + \text{H}]^+$, 338.1387; found 338.1382. HPLC purity: 98.72 %, t_R - 7.470 min.

***N*-benzyl-8-ethoxy-2-oxo-2*H*-chromene-3-carboxamide (5ha)**

Yield: 89%; off white solid; mp = 377-379 °C; ^1H NMR (400 MHz, CDCl_3) δ 9.24 (s, 1H), 8.94 (s, 1H), 7.42 - 7.25 (m, 7H), 7.20 (dd, $J = 7.6, 2.0$ Hz, 1H), 4.70 (d, $J = 5.9$ Hz, 2H), 4.23 (q, $J = 7.0$ Hz, 2H), 1.54 (t, $J = 7.0$ Hz, 3H). ^{13}C NMR (100 MHz, CDCl_3) δ 161.67, 161.13, 148.86, 146.44, 144.33, 137.99, 128.70, 127.70, 127.43, 125.15, 120.87, 119.40, 118.49, 116.79, 65.15, 43.83, 14.71. IR (ATR) ν 3324.89, 3028.21, 2923.52, 2858.62, 2358.03, 1703.20, 1645.25, 1604.33, 1519.07, 1457.97, 1355.53, 1243.51, 1154.21, 1098.60, 1060.41, 1015.52, 964.86, 787.31, 734.35, 666.90 cm^{-1} . HRMS (ESI+) calculated for $\text{C}_{19}\text{H}_{17}\text{NO}_4$ $[\text{M} + \text{H}]^+$, 324.1230; found 324.1226. HPLC purity: 99.71 %, t_R - 6.863 min.

***N*-(2-chlorobenzyl)-8-ethoxy-2-oxo-2*H*-chromene-3-carboxamide (5hb)**

Yield: 90%; off white solid; mp = 420-422 °C; ^1H NMR (400 MHz, CDCl_3) δ 9.36 (t, $J = 6.1$ Hz, 1H), 8.91 (s, 1H), 7.48 - 7.43 (m, 1H), 7.42 - 7.37 (m, 1H), 7.32 - 7.23 (m, 4H), 7.20 (dd, $J = 7.7, 1.8$ Hz, 1H), 4.77 (d, $J = 6.1$ Hz, 2H), 4.22 (q, $J = 7.0$ Hz, 2H), 1.54 (t, $J = 7.0$ Hz, 3H). ^{13}C NMR (100 MHz, CDCl_3) δ 161.75, 161.12, 148.90, 146.45, 144.35, 135.37, 133.69, 129.71, 129.59, 128.84, 127.00, 125.16, 120.88, 119.35, 118.38, 116.88, 65.17, 41.76, 14.71. IR (ATR) ν 2923.42, 2856.79, 2358.11, 1709.30, 1660.67, 1607.65, 1571.32, 1526.22, 1466.37, 1360.88, 1277.38, 1242.44, 1200.83, 1101.61, 1056.82, 1020.76, 965.95, 790.23, 737.42, 653.97 cm^{-1} . HRMS (ESI+) calculated for $\text{C}_{19}\text{H}_{17}\text{NO}_4$ $[\text{M} + \text{H}]^+$, 358.0847; found 358.0838. HPLC purity: 99.18 %, t_R - 9.190 min.

8-ethoxy-*N*-(4-fluorobenzyl)-2-oxo-2*H*-chromene-3-carboxamide (5hc)

Yield: 88%; off white solid; mp = 390-392 °C; ¹H NMR (400 MHz, CDCl₃) δ 9.24 (s, 1H), 8.93 (s, 1H), 7.39 - 7.29 (m, 3H), 7.28 - 7.23 (m, 1H), 7.21 (dd, J = 7.7, 1.9 Hz, 1H), 7.08 - 7.00 (m, 2H), 4.65 (d, J = 5.9 Hz, 2H), 4.23 (q, J = 7.0 Hz, 2H), 1.54 (t, J = 7.0 Hz, 3H). ¹³C NMR (100 MHz, CDCl₃) δ 163.39, 161.71, 161.16, 148.97, 146.45, 144.33, 133.84, 129.46, 129.38, 125.20, 120.88, 119.37, 118.37, 116.84, 115.63, 115.42, 77.35, 77.03, 76.71, 65.16, 43.12, 14.70. IR (ATR) ν 3333.35, 2921.70, 2857.12, 2357.82, 1704.92, 1646.76, 1606.00, 1515.10, 1465.28, 1358.03, 1262.73, 1209.80, 1151.96, 1100.39, 1060.97, 1017.95, 963.48, 790.25, 734.38, 668.04 cm⁻¹. HRMS (ESI+) calculated for C₁₉H₁₆FNO₄ [M + H]⁺, 342.1142; found 342.1133. HPLC purity: 99.63 %, *t_R* - 6.943 min.

8-ethoxy-*N*-(4-methoxybenzyl)-2-oxo-2*H*-chromene-3-carboxamide (5hd)

Yield: 89%; off white solid; mp = 423-424 °C; ¹H NMR (400 MHz, CDCl₃) δ 9.17 (s, 1H), 8.93 (s, 1H), 7.32 (d, J = 2.3 Hz, 1H), 7.31 - 7.24 (m, 3H), 7.20 (dd, J = 7.6, 2.0 Hz, 1H), 6.90 (d, J = 8.6 Hz, 2H), 4.62 (d, J = 5.8 Hz, 2H), 4.23 (q, J = 7.0 Hz, 2H), 3.82 (s, 3H), 1.54 (t, J = 7.0 Hz, 3H). ¹³C NMR (100 MHz, CDCl₃) δ 161.54, 161.09, 158.99, 148.77, 146.42, 144.32, 130.13, 129.10, 125.13, 120.86, 119.41, 118.55, 116.76, 114.09, 65.15, 55.31, 43.33, 14.70. IR (ATR) ν 3596.88, 3339.22, 2922.74, 2858.87, 2357.71, 1705.40, 1647.29, 1605.89, 1516.84, 1461.67, 1359.45, 1238.66, 1168.39, 1100.00, 1029.36, 954.14, 826.76, 792.02, 736.13, 665.15 cm⁻¹. HRMS (ESI+) calculated for C₂₀H₁₉NO₅ [M + H]⁺, 354.1336; found 354.1327. HPLC purity: 99.06 %, *t_R* - 6.427 min.

8-ethoxy-2-oxo-*N*-(3,4,5-trimethoxybenzyl)-2*H*-chromene-3-carboxamide (5he)

Yield: 89%; off white solid; mp = 515-517 °C; ¹H NMR (400 MHz, CDCl₃) δ 9.23 (t, J = 6.1 Hz, 1H), 8.94 (s, 1H), 7.34 - 7.29 (m, 1H), 7.26 (d, J = 2.0 Hz, 1H), 7.21 (dd, J = 7.6, 1.9 Hz, 1H), 6.61 (s, 2H), 4.62 (d, J = 5.8 Hz, 2H), 4.23 (q, J = 7.0 Hz, 2H), 3.88 (s, 6H), 3.85 (s, 3H), 1.54 (t, J = 7.0 Hz, 3H). ¹³C NMR (100 MHz, CDCl₃) δ 161.62, 161.18, 153.45, 148.92, 146.45, 144.33, 137.32, 133.69, 125.20, 120.87, 119.39, 118.47, 116.81, 104.76, 104.73, 65.15, 60.85, 56.14, 44.08, 14.69. IR (ATR) ν 3357.50, 2930.91, 2843.45, 2357.88, 1695.68, 1659.68, 1601.53, 1525.04, 1458.36, 1358.93, 1325.74, 1238.65, 1118.95, 1007.57, 982.57, 879.91, 837.09, 788.69, 728.83, 684.88 cm⁻¹. HRMS (ESI+) calculated for C₂₂H₂₃NO₇ [M + H]⁺, 414.1547; found 414.1549. HPLC purity: 98.92 %, *t_R* - 5.140 min.

8-ethoxy-2-oxo-*N*-phenethyl-2*H*-chromene-3-carboxamide (5hf)

Yield: 92%; off white solid; mp = 389-390 °C; ¹H NMR (400 MHz, CDCl₃) δ 8.93 (t, J = 5.7 Hz, 1H), 8.89 (s, 1H), 7.38 - 7.29 (m, 4H), 7.28 - 7.15 (m, 4H), 4.22 (q, J = 7.0 Hz, 2H), 3.74 (q, J = 6.8 Hz, 2H), 2.96 (t, J = 7.2 Hz, 2H), 1.54 (t, J = 7.0 Hz, 3H). ¹³C NMR (100 MHz,

CDCl₃) δ 161.55, 161.08, 148.52, 146.42, 144.25, 138.84, 128.81, 128.63, 126.54, 125.10, 120.82, 119.39, 118.53, 116.62, 65.10, 41.37, 35.66, 14.72. IR (ATR) ν 3324.83, 2357.73, 1701.83, 1604.77, 1570.55, 1524.42, 1461.79, 1395.59, 1358.62, 1268.78, 1240.05, 1197.96, 1168.91, 1099.12, 1023.64, 1023.64, 973.31, 787.34, 734.20, 702.17, 636.11 cm⁻¹. HRMS (ESI+) calculated for C₂₀H₁₉NO₄ [M + H]⁺, 338.1387; found 338.1384. HPLC purity: 99.25 %, *t_R* - 7.833 min.

8-ethoxy-*N*-(4-methoxyphenethyl)-2-oxo-2*H*-chromene-3-carboxamide (5hg)

Yield: 90%; off white solid; mp = 435-437 °C; ¹H NMR (400 MHz, CDCl₃) δ 8.91 (t, J = 5.7 Hz, 1H), 8.88 (s, 1H), 7.31 - 7.23 (m, 2H), 7.21 - 7.15 (m, 3H), 6.92 - 6.83 (m, 2H), 4.22 (q, J = 7.0 Hz, 2H), 3.81 (s, 3H), 3.75 - 3.65 (m, 2H), 2.90 (t, J = 7.2 Hz, 2H), 1.53 (t, J = 7.0 Hz, 3H). ¹³C NMR (100 MHz, CDCl₃) δ 161.52, 161.08, 158.29, 148.48, 146.41, 144.25, 130.88, 129.75, 125.09, 120.82, 119.40, 118.56, 116.60, 114.05, 65.10, 55.24, 41.57, 34.75, 14.72. IR (ATR) ν 3342.66, 2986.29, 2930.75, 2358.24, 1706.12, 1657.34, 1609.60, 1575.37, 1609.60, 1575.37, 1513.28, 1465.68, 1362.06, 1277.94, 1238.32, 1093.91, 1021.91, 970.95, 879.84, 832.84, 789.54, 729.55 cm⁻¹. HRMS (ESI+) calculated for C₂₁H₂₁NO₅ [M + H]⁺, 368.1492; found 368.1492. HPLC purity: 100 %, *t_R* - 7.197 min.

***N*-(2-(1*H*-indol-3-yl)ethyl)-8-ethoxy-2-oxo-2*H*-chromene-3-carboxamide (5hh)**

Yield: 87%; off white solid; mp = 440-441 °C; ¹H NMR (400 MHz, DMSO-*d*₆) δ 10.87 (s, 1H), 8.84 (s, 1H), 8.82 (s, 1H), 7.63 (d, J = 7.8 Hz, 1H), 7.50 (d, J = 7.6 Hz, 1H), 7.43 - 7.29 (m, 3H), 7.22 (s, 1H), 7.08 (t, J = 7.5 Hz, 1H), 6.99 (t, J = 7.4 Hz, 1H), 4.18 (q, J = 7.0 Hz, 2H), 3.64 (q, J = 6.8 Hz, 2H), 2.98 (t, J = 7.3 Hz, 2H), 1.41 (t, J = 7.0 Hz, 3H). ¹³C NMR (100 MHz, DMSO-*d*₆) δ 161.43, 160.64, 148.18, 145.96, 143.71, 136.78, 127.61, 125.52, 123.33, 121.57, 121.45, 119.59, 119.40, 118.84, 118.73, 117.29, 111.92, 111.86, 64.99, 40.63, 25.45, 15.03. IR (ATR) ν 3332.67, 2905.19, 2357.89, 1709.71, 1648.14, 1606.39, 1569.10, 1525.03, 1465.62, 1350.79, 1273.78, 1240.89, 1200.09, 1154.15, 1094.33, 1005.42, 959.74, 788.10, 738.18, 676.41 cm⁻¹. HRMS (ESI+) calculated for C₂₂H₂₀N₂O₄ [M + H]⁺, 377.1496; found 377.1496. HPLC purity: 98.73 %, *t_R* - 6.260 min.

8-ethoxy-2-oxo-*N*-(3-phenylpropyl)-2*H*-chromene-3-carboxamide (5hi)

Yield: 94%; off white solid; mp = 400-402 °C; ¹H NMR (400 MHz, CDCl₃) δ 8.93 (s, 1H), 8.90 (s, 1H), 7.35 - 7.17 (m, 9H), 4.23 (q, J = 7.0 Hz, 2H), 3.51 (q, J = 6.7 Hz, 2H), 2.75 (t, J = 7.7 Hz, 2H), 2.00 (p, J = 7.4 Hz, 2H), 1.55 (t, J = 7.0 Hz, 3H). ¹³C NMR (100 MHz, CDCl₃) δ 161.59, 161.22, 148.51, 146.43, 144.30, 141.34, 128.44, 125.97, 125.11, 120.85, 119.45, 118.61, 116.70, 65.16, 39.34, 33.22, 30.96, 14.71. IR (ATR) ν 3845, 3742, 3617, 2314, 1698,

1526, 1225, 549, 457 cm^{-1} . HRMS (ESI+) calculated for $\text{C}_{21}\text{H}_{21}\text{NO}_4$ $[\text{M} + \text{NH}_4]^+$, 369.1809; found 369.1800. HPLC purity: 98.92 %, t_R - 7.813 min.

***N*-(2-(1*H*-indol-3-yl)ethyl)-7-((3-methylbut-2-en-1-yl)oxy)-2-oxo-2*H*-chromene-3-carboxamide (7a)**

Yield: 85%; light yellow solid; mp = 550-552 °C; ^1H NMR (400 MHz, CDCl_3) δ 8.89 (t, J = 5.7 Hz, 1H), 8.83 (s, 1H), 8.28 (s, 1H), 7.67 (d, J = 7.8 Hz, 1H), 7.54 (d, J = 8.7 Hz, 1H), 7.41 - 7.34 (m, 1H), 7.23 - 7.16 (m, 1H), 7.15 - 7.09 (m, 2H), 6.92 (dd, J = 8.7, 2.4 Hz, 1H), 6.83 (d, J = 2.5 Hz, 1H), 5.52 - 5.43 (m, 1H), 4.61 (d, J = 6.8 Hz, 2H), 3.85 - 3.75 (m, 2H), 3.15 - 3.07 (m, 2H), 1.83 (s, 3H), 1.78 (s, 3H). ^{13}C NMR (100 MHz, CDCl_3) δ 164.10, 162.07, 161.87, 156.54, 148.19, 139.75, 136.43, 130.86, 127.28, 122.25, 122.03, 119.33, 118.76, 118.25, 114.68, 114.52, 112.91, 112.30, 111.25, 100.95, 65.71, 40.20, 25.83, 25.30, 18.32. IR (ATR) ν 3173.50, 1698.66, 1644.14, 1614.01, 1589.62, 1451.89, 1430.37, 1374.42, 1335.68, 1256.78, 1170.69, 1120.48, 1008.58, 981.32, 813.46, 711.60, 609.74, 542.31 cm^{-1} . HRMS (ESI+) calculated for $\text{C}_{25}\text{H}_{24}\text{N}_2\text{O}_4$ $[\text{M} + \text{H}]^+$, 417.1809; found 417.1854. HPLC purity: 99.88 %, t_R - 3.517 min.

***(E)*-*N*-(2-(1*H*-indol-3-yl)ethyl)-7-((3,7-dimethylocta-2,6-dien-1-yl)oxy)-2-oxo-2*H*-chromene-3-carboxamide (7b)**

Yield: 84%; yellow solid; mp = 547-549 °C; ^1H NMR (400 MHz, CDCl_3) 8.90 (t, J = 5.6 Hz, 1H), 8.83 (s, 1H), 8.24 (s, 1H), 7.67 (d, J = 7.8 Hz, 1H), 7.55 (d, J = 8.7 Hz, 1H), 7.38 (d, J = 8.0 Hz, 1H), 7.20 (t, J = 7.5 Hz, 1H), 7.17 - 7.09 (m, 2H), 6.93 (dd, J = 8.7, 2.3 Hz, 1H), 6.83 (d, J = 2.4 Hz, 1H), 5.47 (t, J = 6.7 Hz, 1H), 5.09 (t, J = 6.5 Hz, 1H), 4.64 (d, J = 6.6 Hz, 2H), 3.80 (q, J = 6.7 Hz, 2H), 3.11 (t, J = 7.0 Hz, 2H), 2.18 - 2.06 (m, 4H), 1.77 (s, 3H), 1.67 (s, 3H), 1.61 (s, 3H). ^{13}C NMR (100 MHz, CDCl_3) δ 164.13, 162.08, 161.87, 156.55, 148.19, 142.82, 136.42, 132.02, 130.85, 127.29, 123.54, 122.23, 122.04, 119.34, 118.76, 118.04, 114.67, 114.53, 112.95, 112.30, 111.23, 100.99, 65.78, 40.20, 39.50, 26.21, 25.67, 25.30, 17.72, 16.80. IR (ATR) ν 3173.50, 1698.66, 1644.14, 1614.01, 1589.62, 1451.89, 1430.37, 1374.42, 1335.68, 1256.78, 1170.69, 1120.48, 1008.58, 981.32, 813.46, 711.60, 609.74, 542.31 cm^{-1} . HRMS (ESI+) calculated for $\text{C}_{30}\text{H}_{32}\text{N}_2\text{O}_4$ $[\text{M} + \text{H}]^+$, 485.2435; found 485.2481. HPLC purity: 98.02 %, t_R - 4.583 min.

7.3. Pancreatic lipase inhibition assay

The PL inhibitory activity of the coumarin analogues (**5e(a-i)**, **5f(a-i)**, **5g(a-i)**, **5h(a-i)** and **7(a-b)**) that were synthesized was evaluated utilizing the assay protocol that was standardized in our laboratory [5-7]. The enzyme Type II porcine PL has been used, with *p*-NPB as the substrate. Each inhibitor concentration was prepared utilizing DMSO as the solvent. Before

calculating IC_{50} values, the absorbance of the resultant mixture was measured at 405 nm using a microplate reader to determine the percentage of inhibition. It was determined that the IC_{50} values of all analogues were within the range of 1.25-46.93 μM (Table 7.1). A significant number of the analogues (**7b**, **7a**, **5fh**, **5eh**, **5fe**, **5fb**, **5ee**, **5fd**, **5eb**, **5hh**, **5fc**, **5ed** and **5fg**) exhibited good PL inhibitory activity (1.25-15.91 μM). Conversely, a set of the analogues (**5he**, **5eg**, **5ff**, **5ec**, **5gh**, **5hg**, **5hd**, **5ef**, **5ge**, **5gg**, **5gd**, **5hf**, **5fi**, **5hb**, **5gf**, **5ei**, **5hc** and **5gb**) showed moderate activity range (16.56-30.33 μM). A limited number of analogues (**5hi**, **5gc**, **5fa**, **5gi**, **5ha**, **5ga** and **5ea**) exhibited poor inhibitory activity, (ranging from 31.06-46.93 μM). **7b** and **7a** were identified as the most potent inhibitory analogues of PL among all the analogues ($IC_{50} = 1.25$ and 4.25 μM , respectively).

Table 7.1. *In vitro* PL inhibitory activity of the synthesized analogues (**5e(a-i)**, **5f(a-i)**, **5g(a-i)**, **5h(a-i)** and **7(a-b)**).

Code	IC_{50} (μM)	Code	IC_{50} (μM)
5ea	46.93 \pm 2.18	5ga	42.01 \pm 1.75
5eb	12.02 \pm 1.75	5gb	30.33 \pm 1.15
5ec	17.14 \pm 1.33	5gc	34.52 \pm 2.05
5ed	14.4 \pm 0.44	5gd	23.61 \pm 1.38
5ee	9.91 \pm 1.54	5ge	20.88 \pm 2.61
5ef	19.84 \pm 1.07	5gf	27.66 \pm 2.14
5eg	16.88 \pm 1.20	5gg	21.22 \pm 1.86
5eh	8.01 \pm 0.14	5gh	17.73 \pm 0.59
5ei	28.62 \pm 1.60	5gi	34.49 \pm 2.14
5fa	34.22 \pm 1.71	5ha	39.10 \pm 2.11
5fb	9.19 \pm 1.07	5hb	27.14 \pm 1.54
5fc	13.17 \pm 0.23	5hc	29.52 \pm 1.45
5fd	10.69 \pm 1.20	5hd	19.13 \pm 1.17
5fe	8.88 \pm 1.30	5he	16.56 \pm 0.08
5ff	17.06 \pm 1.04	5hf	25.69 \pm 1.94
5fg	15.91 \pm 1.06	5hg	18.01 \pm 1.77
5fh	6.21 \pm 0.34	5hh	12.12 \pm 2.06
5fi	25.92 \pm 1.33	5hi	31.06 \pm 1.02
7a	4.25 \pm 0.85	7b	1.25 \pm 0.55
Orlistat			0.97 \pm 0.31

*All experiments were performed in triplicate and the values are expressed in Mean \pm S.E.M.

7.4. Enzyme kinetics

To gain insight into the different types of inhibition (competitive, non-competitive, and uncompetitive), an analysis was conducted on the enzyme kinetics of the most potent analogues **7b** (Table 7.2). For the same, an inhibitor concentration range of three (0.0,

0.3125, and 2.5 μM) was utilized in conjunction with four different substrate concentrations (25, 50, 100, and 200 μM). K_m of **7b** and Orlistat increased proportionally to inhibitor concentration [6], whereas the Lineweaver-Burk plot converged at the y-intercept ($1/V_{max}$), as illustrated in **Fig 7.2**.

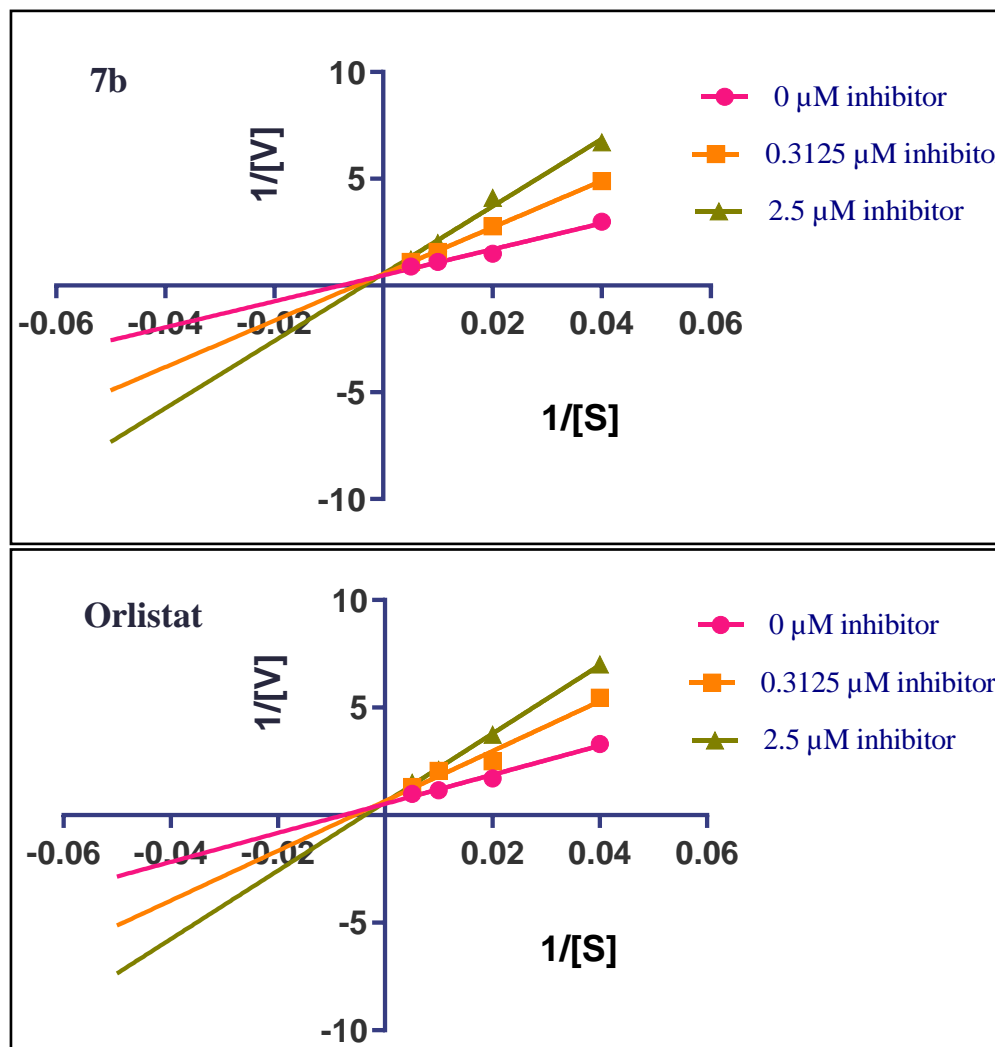


Figure 7.2. Double reciprocal Lineweaver-Burk plots of **7b** and Orlistat.

The competitive inhibition of PL by analogue **7b** indicated that the analogue binds to the active site of PL. As substrate concentration increased, so did the apparent K_m value; however, the V_{max} remained unaffected by substrate concentration, indicating the degree of reversible inhibition. The inhibition constant (K_i) was calculated utilizing the Cheng-Prusoff equation. The K_i values for analogues **7b** was 0.698 μM , respectively (**Table 7.2**). Orlistat, which served as the positive control, demonstrated competitive inhibition with a K_i value of 0.588 μM [7].

Table 7.2. K_m , V_{max} and K_i values of **7b** and Orlistat retrieved from the PL enzyme kinetics.

Code	K_m (apparent) at different concentration (μM)			V_{max} ($\mu\text{M}/\text{min}$)	K_i (μM)	Nature of inhibition
	0 μM	0.3125 μM	2.5 μM			
7b	47.321	61.541	88.021	1.066	0.698	Competitive
Orlistat	52.435	86.501	102.971	0.907	0.588	Competitive

7.5. Structure activity relationship (SAR)

The preliminary SAR was derived from the PL inhibitory activities of the synthesized coumarin analogues (**5e(a-i)**, **5f(a-i)**, **5g(a-i)**, **5h(a-i)** and **7(a-b)**). As shown in **Fig 7.3**, the SAR component was classified into the following three categories: 1) Impact of substituted coumarin ring (R, R₁, R₃ substitution); 2) Impact of substituted aromatic ring (R₂ substitution). 3) Impact of carbon linkage. The hydroxyl group-containing analogue **5ea**, placed solely at the 7th position of the coumarin ring, exhibited a minimal inhibitory effect on PL ($\text{IC}_{50} = 46.93 \pm 2.18 \mu\text{M}$). The research additionally examined the impact of electron-donating substituents (e.g., methoxy, ethoxy) on the coumarin ring at positions seven and eight. In comparison to analogues featuring substitutions at positions eight and seven, those containing substitution (R) at position seven demonstrated better inhibition of PL. On the R₂ position, the effect of several substituted aromatic amines was investigated. On the R₂ position, electron donating groups (EDG) were demonstrated to be more efficacious than electron withdrawing groups (EWG) in the context of aromatic substitution. Out of the trimethoxy and methoxy analogues, the one containing a 3,4,5-trimethoxy substitution exhibited better activity (**5fe**, **5ee**, **5ge**, **5he**; $\text{IC}_{50} = 8.88, 9.91, 20.88, 16.56 \mu\text{M}$, respectively). In contrast to analogue that contain electron-withdrawing groups (EWG), such as chloro, those in which the phenyl ring was substituted at the second position (**5fb**, **5eb**, **5hb**, **5gb**) demonstrated enhanced activity, as indicated by IC_{50} values of 9.19, 12.02, 27.14, and 30.33 μM , respectively. Analogues featuring fluoro substituents at the *para* position of the phenyl ring (**5fc**, **5ec**, **5hc**, and **5gc**; IC_{50} values of 13.17, 17.14, 29.52, and 34.52 μM) exhibited a decrease in activity in comparison to those featuring methoxy substituents at the same position (**5fd**, **5ed**, **5hd**, and **5gd**; respective IC_{50} values of 10.69, 14.4, 19.13, and 23.61 μM). The investigation also explored the influence of various carbon linkers on PL inhibition. Analogues featuring two carbon linker substitutions (**5ff**, **5ef**, **5hf**, and **5gf**) demonstrated comparably better PL inhibition profile, with IC_{50} values of 17.06, 19.84, 25.69, and 27.66 μM , respectively, in contrast to the analogues featuring three carbon chains (**5fi**, **5ei**, **5hi** and **5gi**; $\text{IC}_{50} = 25.92, 28.62, 31.06, \text{ and } 34.49 \mu\text{M}$, respectively). The analogues with prenyl (**7a**)

and geranyl (**7b**) substitution resulted in potent PL inhibition activity with IC_{50} values 4.25 ± 0.85 and $1.25 \pm 0.55 \mu\text{M}$, respectively. In summary, it is evident that the significance of substituents on the coumarin scaffold (R , R_1 , R_3), carbon linker and R_2 groups is critical in the chemical structure of a potentially effective PL inhibitor. **Fig 7.3** provides a succinct summary of the SAR analysis, illustrating how various substituents affect the inhibitory activity of PL.

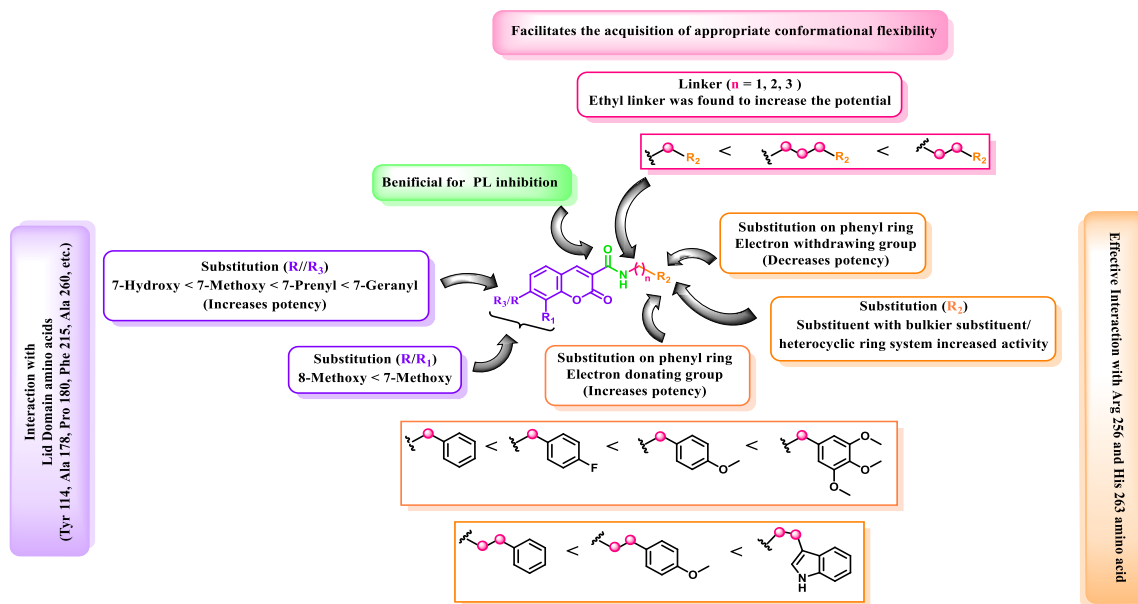


Figure 7.3. SAR study of coumarin analogues (**Series III**).

7.6. Fluorescence Quenching Measurements with PL

The effect of the **7b** analogue in the fluorescence quenching of PL was evaluated (See chapter 3) and the results are depicted in **Fig. 7.4** and **Table 7.3**. The **7b** analogue exerted a concentration-dependent quenching effect on the PL fluorescence.

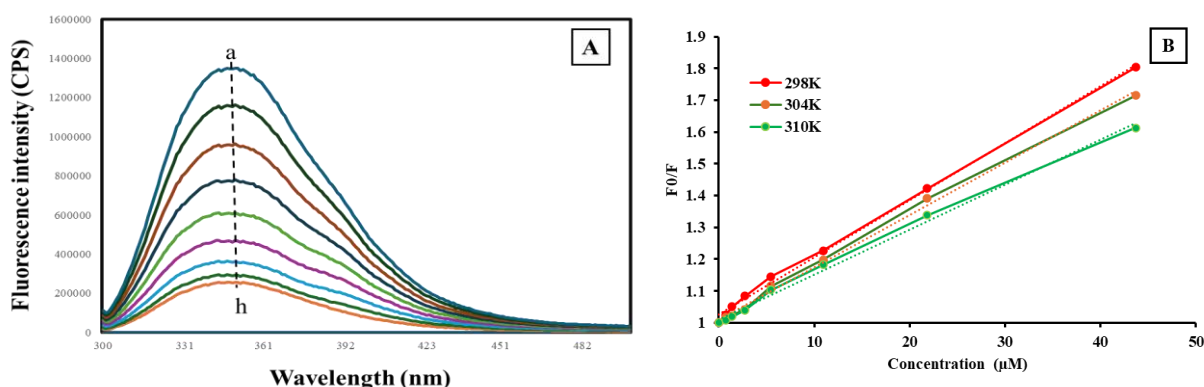


Figure 7.4. (A) The fluorescence spectra of PL in the presence of **7b** at various concentrations (pH 7.4, T = 298 K, a to h in increasing concentrations); (B) Stern-Volmer plot for the quenching of **7b** on the PL.

As illustrated in **Fig. 7.4.**, the PL fluorescence was quenched by the analogue (**7b**). Additionally, the fluorescence intensity decreased as the concentration of quencher (**7b**) increased, suggesting the formation of PL-quencher complexes. To identify the underlying mechanism of quenching, Stern-Volmer equation was utilized and the values were determined as per **Formula 3.3** (chapter 3).

Table 7.3. Bimolecular quenching constant (k_q), binding constant (K_b) and the number of binding sites (n) at different temperatures for **7b**.

#	T (K)	$K_{SV}/10^4$ (L/mol)	$k_q/10^{12}$ (L/mol sec)	R^2	$K_b/10^5$ (L/mol)	n	R^2
7b	298	1.28	8.11	0.9977	1.58	0.9316	0.9946
	304	0.86	5.37	0.9966	1.05	0.9155	0.9898
	310	0.59	3.76	0.9949	0.45	1.004	0.9967

As represented in **Table 7.3**, an inverse correlation between the K_{SV} and temperature suggested that the quenching effects on the PL may be mainly attributed due to static quenching rather than dynamic quenching.

The values of 'n' at the corresponding temperature were closer to 1, which indicated the presence of only one binding site in PL. This result further supported the competitive inhibition by **7b** in the enzyme kinetics study of PL. Additionally, the ' K_b ' values were in the range of 0.45 to 1.58×10^5 L/mol indicating the strong binding forces of **7b** analogue with PL.

7.7. Molecular docking analysis

Based on existing literature, it has been established that the PL enzyme's active region comprises two hydrophobic lid domains (Gly 76 - Lys 80, Tyr 114, and Leu 213 - Met 217) that encloses the Ser 152 - Asp 176 - His 263 amino acid catalytic triad. In order to determine whether the side chains of the lid domain play a role in the hydrophobic groove for substrate contact, the crystal structure of PL was analysed [13]. To gain access to the catalytic triad, a ligand must facilitate its opening by engaging in interactions with these hydrophobic lid domains, specifically through aromatic or alkyl contacts. By meticulously scrutinizing these facts, analogues were designed to facilitate the π - π interaction between the coumarin ring and the amino acids in the lid domain, thereby contributing to the opening of the lid domain. Furthermore, an amide warhead was incorporated to enhance the interaction with the amino acid residue located in the active site. The aromatic part of amines contains an electron-rich aryl/heteroaryl functionality in their aromatic regions, that can engage in a π -cation interaction with Arg 256, which is a crucial amino acid.

CHAPTER VII

The coumarin analogues (**5e(a-i)**, **5f(a-i)**, **5g(a-i)**, **5h(a-i)** and **7(a-b)**) were designed and the resulting docking data were analysed. All coumarin analogues exhibited MolDock scores ranging from -112.116 to -183.29 kcal/mol. The analogue **7b** had the highest MolDock score of -183.29 kcal/mol. Furthermore, analogue **7b** docking pose was analysed in order to identify potential docking interactions as illustrated in **Fig 7.5.** and **Table 7.4.**

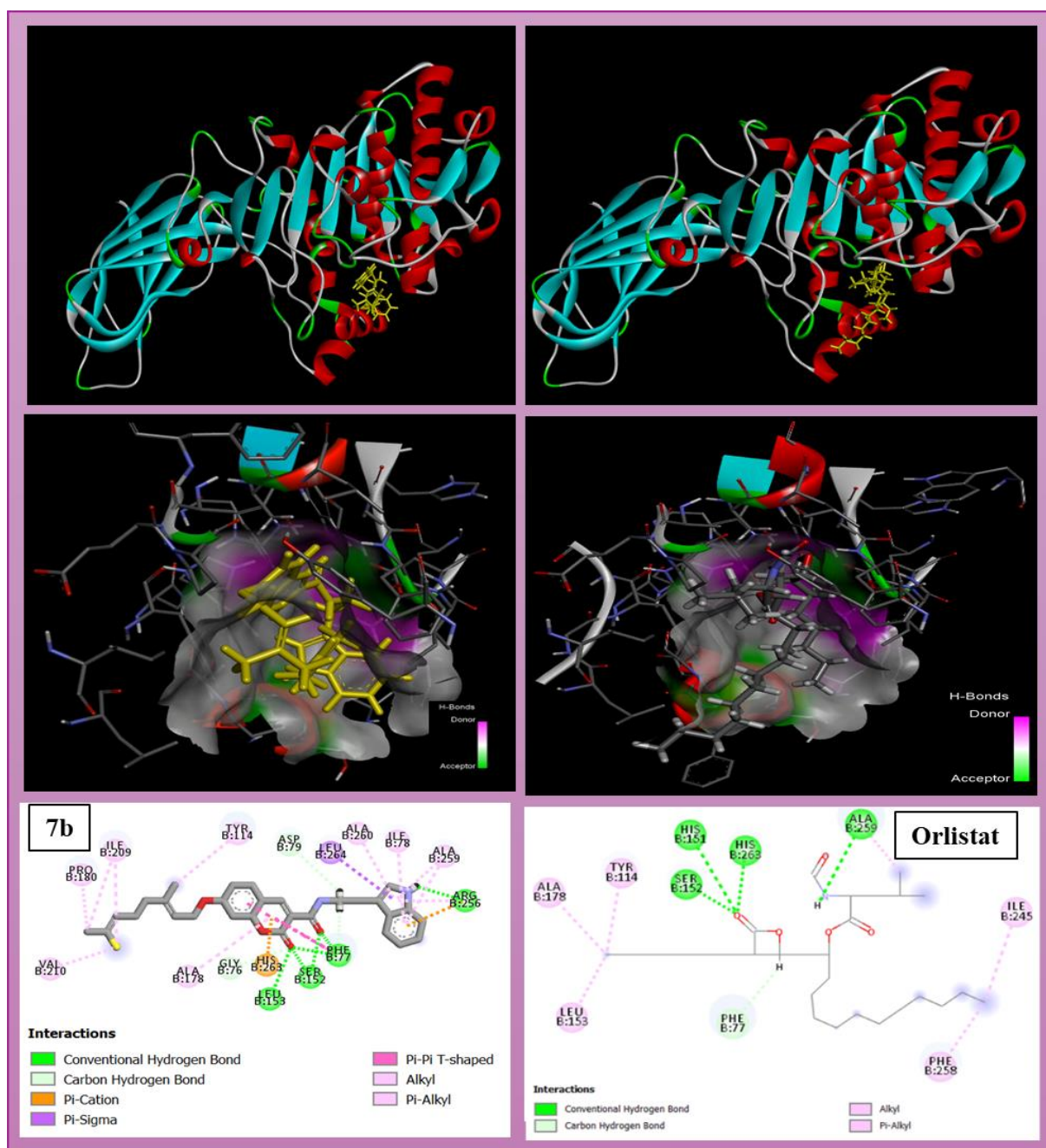


Figure 7.5. 2D and 3D interaction diagram of **7b** and Orlistat in the active site of PL (1LPB).

CHAPTER VII

The analogue **7b** demonstrated a number of crucial interactions with the amino acids that are located in the active region, as illustrated in **Fig 7.5**. H-bond, π -cation, and π -alkyl interactions were observed between the indole ring and Arg 256. π -alkyl interactions involving Ala 260, Ile 78, and Ala 259 with the indole ring were also discernible. The amide warhead exhibited hydrogen bonding interactions with Phe 77 and Ser 152. The coumarin ring demonstrated π -alkyl and π - π T-shaped interactions with Ala 178 and Phe 77, respectively. Coumarin's carbonyl oxygen facilitates the formation of hydrogen bonding connections with Leu 153, Phe 77, and Ser 152. Furthermore, the coumarin ring's alkyl chain, situated at the seventh position, participates in π -alkyl interactions with Tyr 114, Pro 180, Ile 209, and Val 210. Comparable interactions were also observed with Orlistat, as evidenced by its MolDock score of -139.41 kcal/mol.

Table 7.4. MolDock score (kcal/mol) and interaction summary of analogues (**5e(a-i)**, **5f(a-i)**, **5g(a-i)**, **5h(a-i)** and **7(a-b)**) at the active site of the PL.

Code	R	R ₁	R ₂	n	Mol Dock Score (kcal/mol)	H-bond	π - π interactions	π -cation	π -alkyl
5ea	OH	H	-H	1	-112.116	-	Phe 215	Arg 256, His 263	Leu 153, Ala 178, Ala 258
5eb			2-Cl	1	-117.351	Phe 77, Leu 153	Phe 215, Tyr 114	His 263	His 151, Ala 178, Pro 180
5ec			4-F	1	-119.847	-	Phe 215	His 263	Ile 78, Leu 153, Ala 178, Ala 259
5ed			4-OCH ₃	1	-124.636	-	Phe 215	Arg 256, His 263	Ile 78, Leu 153, Ala 178, Ala 259
5ee			3,4,5-tri-OCH ₃	1	-134.299	His 151, Ser 152	-	His 263	Ile 78, Leu 153, Ala 178
5ef			-H	2	-119.788	Phe 77	Phe 215	His 263	Leu 153, Ala 178, Arg 256, Ala 259, Ala 260, Leu 264
5eg			4-OCH ₃	2	-120.589	Phe 77, Leu 153, His 263	Phe 215, Tyr 114	Asp 79	Ile 78, Ala 178, Pro 180, Leu 264
5eh			1 <i>H</i> -indole	2	-135.245	Phe 215, Arg 256	Phe 77, Phe 215	His 263	Ala 178, Ala 259, Ala 260, Leu 264
5ei			H	3	-128.437	Phe 77, Leu 153, His 263	Tyr 114, Phe 215	-	Ala 178, Pro 180, Ala 260
5fa	OCH ₃	H	-H	1	-119.031	Tyr 114	Phe 77, Phe 215	Arg 256, His 263	Leu 153, Ala 178, Ala 259

CHAPTER VII

5fb			2-Cl	1	-123.789	Tyr 114	Phe 215	Arg 256, His 263	Ile 78, Leu 153, Ala 178, Ala 259
5fc			4-F	1	-127.307	Tyr 114	Phe 215	His 263	Ile 78, Leu 153, Ala 178, Ala 259
5fd			4-OCH ₃	1	-130.74	-	Phe 215	Arg 256, His 263	Ile 78, Leu 153, Ala 178
5fe			3,4,5-tri-OCH ₃	1	-137.879	His 151, Ser 152	Phe 215	His 263	Ile 78, Leu 153, Ala 178
5ff			-H	2	-121.273	Phe 77, Ser 152	Tyr 114, His 263	Arg 256	Ala 178, Ala 260, Leu 264
5fg			4-OCH ₃	2	-130.168	Phe 77, Ser 152	Tyr 114, Phe 215	Arg 256	Ala 178, Ala 259, Leu 264
5fh			1 <i>H</i> -indole	2	-145.735	Ser 152, Arg 256	Phe 215	His 263	Leu 153, Ala 178, Ala 259, Ala 260, Leu 264, Arg 256
5fi			H	3	-130.041	Phe 77, Leu 153	Tyr 114, Phe 215	-	Ala 178, Pro 180, Ala 260
5ga			H	OCH ₃	-H	1	-112.652	Phe 77, Ser 152	Phe 215, Tyr 114, His 263
5gb	2-Cl	1			-102.546	Phe 77, Ser 152, His 263	Phe 77, Tyr 114, Phe 215	Arg 256	Ile 78, Leu 264, Ala 260
5gc	4-F	1			-112.97	Ser 152, His 263	Tyr 114, Phe 215	Asp 79, Arg 256	Ile 78, Ala 178, Pro 180
5gd	4-OCH ₃	1			-124.51	Phe 77, Ser 152	Tyr 114, Phe 215, His 263	Arg 256	Ile 78, Ala 178, Pro 180
5ge	3,4,5-tri-OCH ₃	1			-130.954	Phe 77, Ser 152	Tyr 114	Arg 256	Ile 78, Ala 178, Pro 180

CHAPTER VII

5gf			-H	2	-117.089	Phe 77, Ser 152	Tyr 114, His 263	Asp 79, Arg 256	Ile 78, Ala 178, Pro 180
5gg			4-OCH ₃	2	-127.783	Phe 77, Ser 152	Tyr 114	Arg 256	Leu 264, Ala 178, Ala 259, Ala 260
5gh			1 <i>H</i> -indole	2	-134.23	Phe 77, Ser 152, His 263	Tyr 114, Phe 215	Arg 256	Ile 78, Ala 178, Pro 180, Ala 259, Ala 260, Leu 264
5gi			H	3	-123.898	Gly 76, Phe 77, His 151, Ser 152, Arg 256	-	His 263	Ala 260, Leu 264
5ha	H	OCH ₂ CH ₃	-H	1	-113.702	Phe 77, Ser 152	Phe 215, Tyr 114	Asp 79, Arg 256	Ile 78, Ile 209, Leu 264, Ala 178, Pro180
5hb			2-Cl	1	-117.678	Phe 77, Ser 152	Phe 77, Tyr 114	Arg 256	Ile 78, Ala 178, Pro 180, Leu 264, Ala 260
5hc			4-F	1	-121.586	Phe 77, Ser 152	Tyr 114, Phe 215	Asp 79, Arg 256	Ile 78, Ala 178, Pro 180, Leu 264
5hd			4-OCH ₃	1	-128.919	Phe 77, Ser 152, Arg 256	Tyr 114, Phe 215, His 263	Asp 79, Arg 256	Ile 78, Ala 178, Pro 180, Leu 264
5he			3,4,5-tri-OCH ₃	1	-130.578	Ser 152, His 263	Tyr 114, Phe 215	Arg 256	Ile 78, Ala 178, Pro 180
5hf			-H	2	-124.005	Phe 77, Ser 152	Tyr 114	-	Ala 178, Ala 260, Arg 256, Ala 259
5hg			4-OCH ₃	2	-128.171	Phe 77, Ser 152	Tyr 114, Phe 215	-	Ala 178, Ala 260, Leu 264, Arg 256, Ala 259

CHAPTER VII

5hh			1 <i>H</i> -indole	2	-142.74	Phe 77, Ser 152, Arg 256	Tyr 114	Arg 256	Ala 178, Pro 180, Ala 259, Ala 260
5hi			-H	3	-128.716	Phe 77, Ser 152	Tyr 114, His 263	Arg 256	Ile 78, Ala 178, Pro 180, Ala 259
Code	R₃	R₁	R₂	n	Mol Dock Score (kcal/mol)	H-bond	π-π interactions	π -cation	π -alkyl
7a	Prenyl	H	1 <i>H</i> -indole	2	-159.483	His 151, Ser 152, Arg 256	-	His 263	Ala 178, Pro 180, Ile 209, Ala 259, Ala 260, Leu 264
7b	Geranyl	H	1<i>H</i>-indole	2	-183.29	Phe 77, Ser 152, Leu 153, Arg 256	Phe 77	Arg 256, His 263	Ile 78, Tyr 114, Pro 180, Ala 178, Ile 209, Val 210, Ala 259, Ala 260, Arg 256
	Orlistat			-	-139.41	Phe 77, Ser 152, His 263, His 151, Ala 259	-	-	Tyr 114, Leu 153, Ala 178, Phe 258, Ile 245

7.8. Molecular dynamics simulations

Although molecular docking analysis offers a preliminary understanding of docking interactions, it lacks the capability to predict the extent of these interactions when they occur under dynamic conditions. In light of the constant variability demonstrated by all proteins in the human body, it is crucial to predict the actions of the ligand under these dynamic physiological circumstances [8]. Therefore, the ligand-protein complex of the analogue with the highest score, **7b**, was simulated for 100 ns using MD. After conducting MD simulations, the results were assessed using protein-ligand RMSD and protein-ligand contacts, in order to determine the time duration of effective amino acid interactions under dynamic conditions and to comprehend the stability of the complex. As illustrated in **Fig.7.6 (A)** the protein maintained its stability throughout the simulation. The ligand's RMSD remained below 7.2 Å till 100 ns. Further, the RMSF plot that offers valuable information regarding the flexibility and dynamic characteristics of residues within the protein was performed. RMSF values below 3.5 Å (**Fig 7.6 (B)**) were consistently recorded during the run, indicating that the binding site of the target 1LPB protein experienced minimal fluctuation.

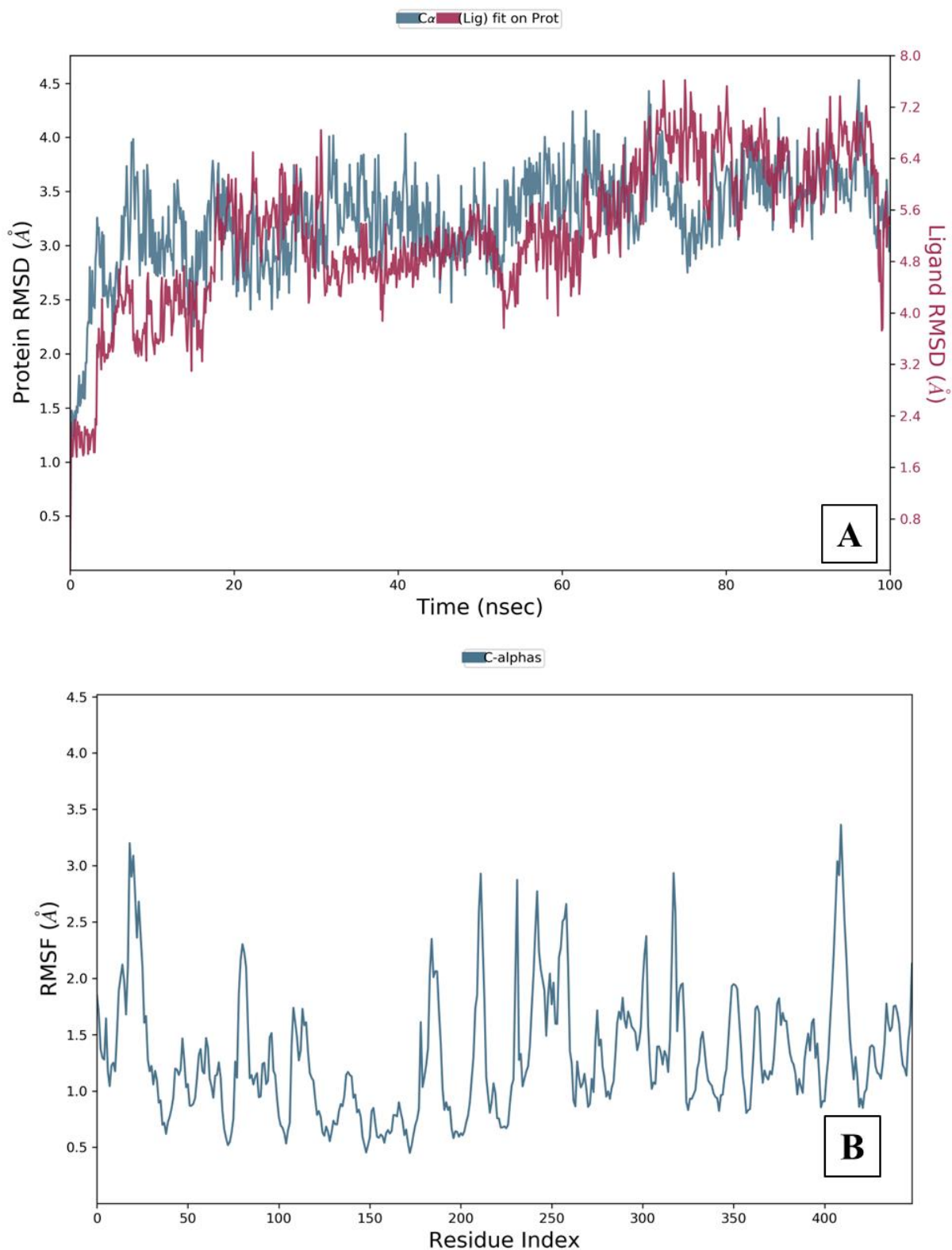


Figure 7.6. (A) RMSD plot of the protein-ligand (**7b**) complex (PDB ID: 1LPB); (B) Protein RMSF plot.

A multitude of interactions were identified within the protein-ligand complex (**7b**), encompassing hydrogen, hydrophobic, and water bridges. In order to inhibit PL, the

hydrophobic domain that encases the catalytic triad must be opened. Phe 77 participated in multiple interactions (including hydrophobic, hydrogen bonding, and water bridge) for a fraction of time greater than 0.2, as shown in the data in **Fig 7.7 (A)**. It was additionally noted that Ile 78 and Phe 215 engaged in hydrophobic interaction and water bridge formation for durations exceeding 0.7 fractions of time, respectively. Furthermore, **Fig 7.7 (A)** provides illustrations of extended interaction durations (>0.6) with the amino acids Ile 78, Tyr 114, Phe 215, Ala 259 and Ser 152. The effectiveness of the designed analogue (**7b**) is demonstrated by its interaction with the hydrophobic lid domain (Phe 77, Ile 78, Asp 79, Tyr 114 and Phe 215) and the catalytic triad (Ser 152- Asp 176 - His 263) [8]. A temporal representation of the interactions and contacts (ionic, hydrophobic, hydrophobic, and hydrophobic bridges) illustrated in **Fig 7.7 (A)**. The upper panel of **Fig 7.7 (B)** illustrates the cumulative count of specific contacts that occur between the protein and the ligand over the course of the trajectory. In the lower panel, the residues that engage in interactions with the ligand are illustrated for each trajectory frame. Specific residues form numerous distinct interactions with the ligand, as indicated by a darker orange coloration (as observed with Ser 152 between 30-60 sec) on the scale situated to the right of the plot.

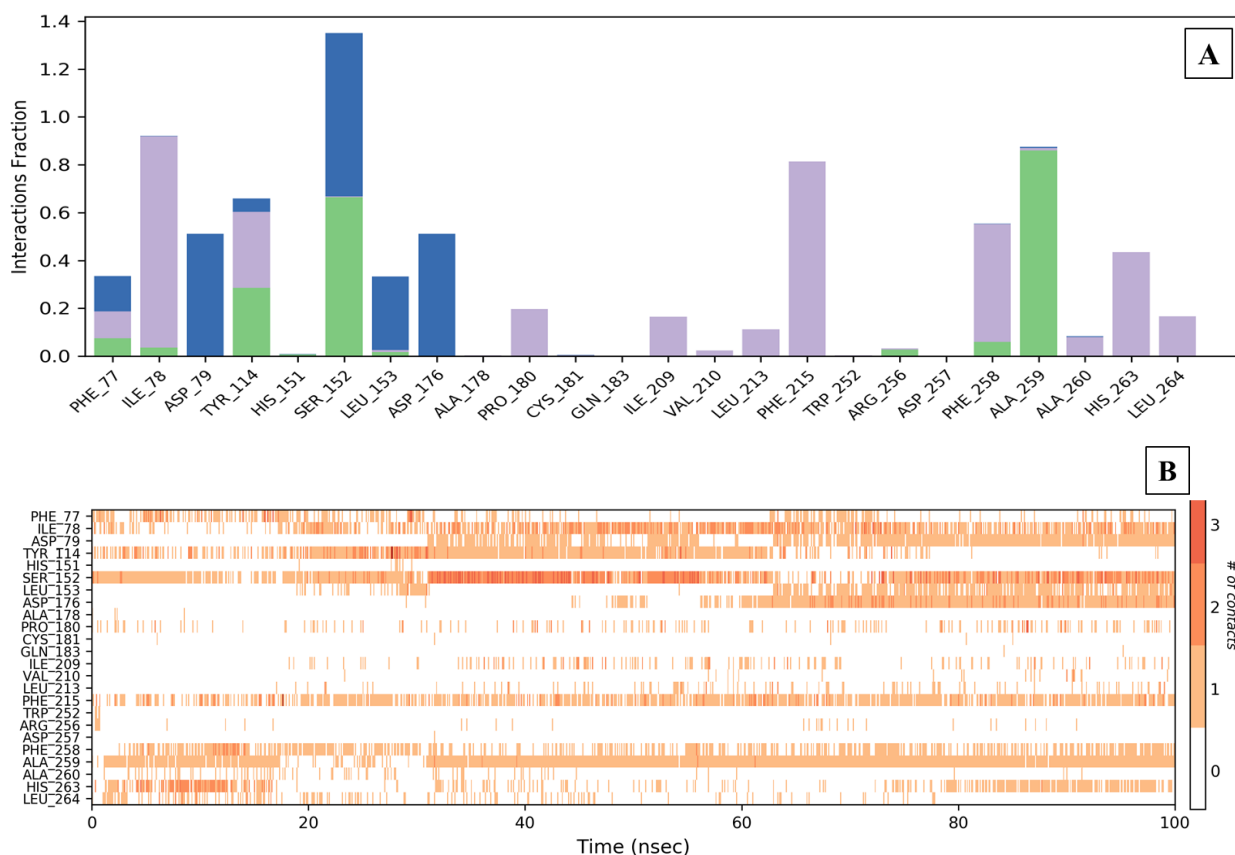


Figure 7.7. (A) Protein-ligand (**7b**) interaction bar charts stacked vertically (PDB ID: 1LPB); (B) Protein-ligand contact timeline (H-bonds, hydrophobic, ionic, water bridges)

CHAPTER VII

In conclusion, a series of thirty eight coumarin analogues were designed and synthesized followed by an evaluation of their PL inhibitory activity. Through suitable chemical reaction schemes, the designed analogues were synthesized and characterized *via* various spectroscopic methods. The PL inhibitory assay was performed to screen these analogues for PL inhibitory potential and a total of two analogues namely, **7b** and **7b** were found to be potent ($IC_{50} = 1.25$ and $4.25 \mu\text{M}$, respectively). The SAR was obtained by observing the IC_{50} values of various substituted analogues. The 7-*O*-alkyl substituent on coumarin was found to be effective in inhibiting the PL enzyme, while 8-*O*-alkyl substituted groups was found to show less PL inhibitory potential. The substitution of an indole ring *via* a two carbon linker was found to be effective in PL inhibition. Also, analogue **7b** was found to competitively inhibit the PL enzyme with K_i values of $0.698 \mu\text{M}$. Analogues **7b** was found to interact with the active site amino acid residues (Phe 77, Tyr 114, Ser 152, Phe 215, Arg 256, His 263, etc.) and was comparable to Orlistat. Furthermore, molecular dynamic simulation revealed that the protein-ligand complex of the most potent analogue **7b** remained stable at the PL active site under physiological conditions.

References

1. Yadav, N., & Paul, A. T. (2023). Synthesis of amide warhead containing coumarin derivatives as potential pancreatic lipase inhibitors: *In silico* and *in vitro* evaluation for obesity treatment. *Medicinal Chemistry Research*, 32(10), 2219-2233.
2. Sridhar, S. N. C., Ginson, G., Reddy, P. V., Tantak, M. P., Kumar, D., & Paul, A. T. (2017). Synthesis, evaluation and molecular modelling studies of 2-(carbazol-3-yl)-2-oxoacetamide analogues as a new class of potential pancreatic lipase inhibitors. *Bioorganic & Medicinal Chemistry*, 5(2), 609-620.
3. Brahmachari, G. (2015). Room temperature one-pot green synthesis of coumarin-3-carboxylic acids in water: A practical method for the large-scale synthesis. *ACS Sustainable Chemistry & Engineering*, 3(9), 2350-2358.
4. Chan, L. C., & Cox, B. G. (2007). Kinetics of amide formation through carbodiimide/N-hydroxybenzotriazole (HOBt) couplings. *The Journal of Organic Chemistry*, 72(23), 8863-8869.
5. George, G., Yadav, N., Auti, P. S., & Paul, A. T. (2023). Molecular modelling, synthesis and *in vitro* evaluation of quinazolinone hybrid analogues as potential pancreatic lipase inhibitors. *Journal of Biomolecular Structure and Dynamics*. 41(19), 9583-9601.
6. Lineweaver, H., & Burk, D. (1934). The determination of enzyme dissociation constants. *Journal of the American Chemical Society*, 56(3), 658-666.
7. Burlingham, B. T., & Widlanski, T. S. (2003). An intuitive look at the relationship of K_i and IC_{50} : A more general use for the Dixon plot. *Journal of Chemical Education*, 80(2), 214-218.
8. Pandey, V., Adhikrao, P. A., Motiram, G. M., Yadav, N., Jagtap, U., Kumar, G., & Paul, A. (2024). Biaryl carboxamide-based peptidomimetics analogs as potential pancreatic lipase inhibitors for treating obesity. *Archiv der Pharmazie*, 357(4), e2300503.

ADMET Prediction and *In-vivo* experiments

8. ADMET Prediction and *In-vivo* experiments

8.1. Rationale

The results from the previous **chapters 5-7** have indicated that analogues inspired by coumarins have the potential to inhibit PL. Nevertheless, the *in vivo* efficacy of a specific drug candidate is primarily influenced by its *in vitro* profile, as well as the pharmacokinetic parameters and toxicity properties that determine the drug's fate [1]. For example, more than 50% of drug failures throughout different phases of human trials have been linked to their unacceptable Absorption, Distribution, Metabolism, Excretion, and Toxicity (ADMET) properties [2]. A diverse array of *in vitro* assays, ranging from medium to high throughput, can be used to assess these properties. Nevertheless, these assays are both costly and time-consuming. Various data modeling methods have been employed to forecast the properties of *in silico* ADMET in recent years, utilizing high-quality experimental data as input [3]. In light of the aforementioned information, the current chapter is dedicated for comprehending the ADMET parameters of the most promising analogues from the preceding chapters. This, in turn, will determine the most suitable candidate for *in vivo* experiments.

8.2. Materials and methods

8.2.1. ADMET prediction

The ADMET prediction was carried out using a total of 7 analogues, which included the most promising analogues from the series I (**5k**, **5q**), series II (**5de**, **5dh**), and series III (**7a**, **7b**), as well as alloimperatorin (NP Lead) and orlistat (standard). The ADMET was determined using software available online such as SwissADME and ProTox-II [4,5].

8.2.2. *In vivo* experiments

All the experimental procedures on animals were in compliance with the Institutional Animal Ethics Committee of BITS Pilani (Ref No: IAEC/RES/32/14). Briefly, the protocol was divided into four experiments (**Fig. 8.1**).

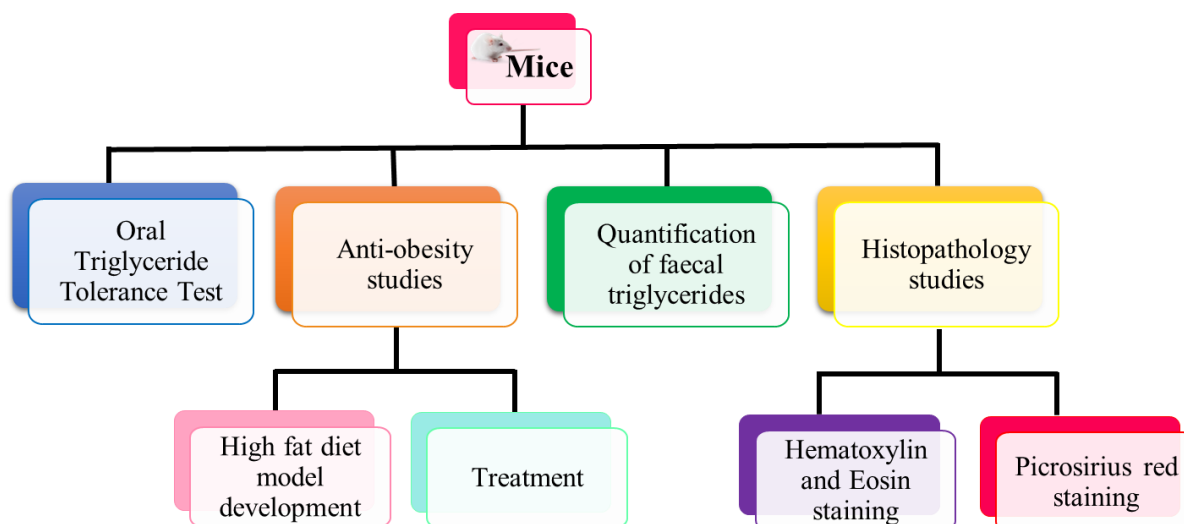


Figure 8.1. The *in-vivo* experiments performed on *Swiss albino* mice.

8.2.2.1. Animals and Diet

Male *Swiss albino* mice (weight: 22-25 g), aged four to five weeks, were procured from Rodent Research India Private Limited, located in Dhatrath, Haryana, India (Registration number: 87737). After one week of acclimatization, four mice were randomly assigned to each cage. The mice were provided with water and were subjected to various dietary regimens, as detailed in **Fig 8.2** and **Table 8.1**. All the ingredients for HFD were mixed together to create diet. The animals were maintained on a light-dark cycle of 12:12 hour and standard husbandry conditions (room temperature $22 \pm 1^\circ\text{C}$ and relative humidity of 60%). All animal procedures adhered to the guidelines set forth by the Committee for Control and Supervision of Experiments on Animals (CCSEA).

(I) Oral Triglyceride Tolerance Test (OTTT)

In order to assess the *in-vivo* impact on triglyceride intestinal absorption and to optimize the dose of **7b** for anti-obesity study, an OTTT was conducted in accordance with a protocol that had been previously documented [6,7]. Six groups ($n = 6$) of mice were deprived of sustenance for 18 h prior to the commencement of the experiment. Orlistat was administered at a dose of 10 mg/kg. Evaluations were conducted at low (5 mg/kg), medium (10 mg/kg), and high (20 mg/kg) doses of the test analogue (**7b**). The mice were orally administered with: (1) olive oil as a positive control, (2) filtered water as a negative control, (3) olive oil plus Orlistat (10 mg/kg) as reference control (4) olive oil plus **7b** (Low, medium and high dose). A consistent volume of 5 mL/kg of olive oil was administered to each animal. At 0, 1.5, 3, 4.5, and 6 h after olive oil administration, blood samples (serum) were collected and

commercially available assays kits (Spinreact S.A.U, Spain) were utilized to detect triglyceride levels.

(II) Anti-obesity studies

The most potent analogue **7b** at 10 mg/kg and 20 mg/kg doses was selected for further *in vivo* research. In total, five groups were considered, with eight animals in each group (**Fig 8.2**). Based on the outcomes of an *in vitro* PL inhibition assay and an *in vivo* OTTT, the dose of analogue **7b** was calculated [8,9]. Analogue **7b** activity was assessed at two distinct dose levels (low and high).

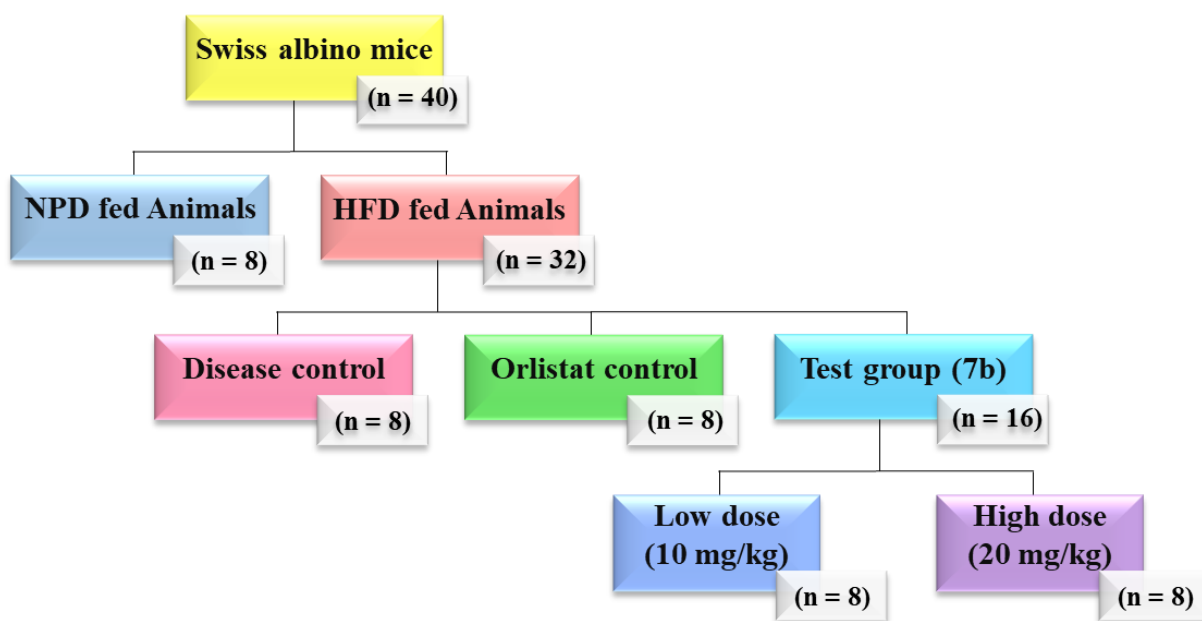


Figure 8.2. Summary of various groups and treatment given for the *in-vivo* experiments. Abbreviations: NPD - Normal pellet diet; HFD - High fat diet.

A three-month study was conducted in our laboratory to develop a high fat diet (HFD) mice model using the composition as given in **Table 8.1** [10-13].

Table 8.1. High Fat Diet Composition for the development of obese mice

No.	Ingredients	g/100g
1.	Casein	20
2.	Corn starch	10
3.	Cellulose	5
4.	Sucrose	10
5.	Lard	40
6.	Soybean oil	7
7.	DL- methionine	3
8.	Mineral and Vitamin mix	5
9.	Sodium chloride	3

The animals body weights were documented on a weekly basis. At the completion of each week, the animals underwent an overnight fast, after which blood samples were obtained *via* retro-orbital puncture. By centrifuging the blood samples (0.3 mL) at 5000 rpm for 10 mins, the serum was extracted. A range of biochemical parameters were measured in the serum, that included glucose, triglycerides, total cholesterol and high-density lipoproteins-cholesterol (HDL). These measurements were obtained using diagnostic assays kits that were commercially available (Spinreact S.A.U., Spain and Accurex Biomedical Pvt. Ltd., India). Using the formula documented in the literature, the low density lipoprotein cholesterol (LDL) was computed [13].

$$\text{LDL} = [(\text{TC} - \text{HDL}) * 0.9] - [\text{TG} * 0.1] \dots\dots\dots \boxed{\text{Formula 8.1}}$$

(III) Quantification of faecal triglycerides

The inhibition of PL is distinguished by the elimination of faeces that are abundant in triglycerides. Throughout the four-week treatment period, daily faeces samples were collected from the groups, and the triglyceride content was assessed at the completion of each week. The methodology employed to quantify faecal triglycerides was largely consistent with the literature report, with only minor modifications [15,16]. In summary, an amount of 1 g of faeces was transferred into a separatory funnel and vigorously shaken in 0.15 M NaCl. Chloroform/methanol (4:1 v/v) was introduced into the suspension while vigorously agitating the mixture to facilitate separation. Following this, the lower organic phase was filtered and desiccated in vacuum. The resulting triglycerides were subsequently dissolved in 1 mL of ethanol, and their concentration was determined using a commercially available kit (Spinreact S.A.U., Spain).

(IV) Histopathological studies

a. Hematoxylin and Eosin (H&E) staining

To conduct a histological investigation, the liver and adipose tissue were preserved in a solution of 10% buffered formalin and then enclosed in paraffin for embedding. Tissue sections of 5 µm in thickness were prepared and subsequently stained with hematoxylin and eosin (H&E). This staining technique was used to evaluate the presence of hepatocytes' ballooning and neutrophil infiltration in the liver. Additionally, the size of adipocytes and the formation of hypertrophy were measured in the same tissue section [16,17].

b. Picrosirius red staining (PSR)

Liver tissue sections of 5 µm in thickness were prepared and subsequently stained with Picrosirius red in order to quantify the extent of collagen deposition in the liver [17].

(V) Statistical analyses

To identify significant differences between the groups, the data were analysed using one-way analysis of variance (ANOVA) and post-hoc analysis of Tukey's multiple comparison test with all values expressed as means \pm SEM. The statistical calculations were executed utilizing GraphPad Prism, version 8.0. A significance level of **** $p \leq 0.0001$, *** $p \leq 0.001$; ** $p \leq 0.01$, * $p \leq 0.05$ was defined as statistically significant.

8.3. Results and Discussions

8.3.1. ADMET Predictions

A total of 7 analogues were selected for the *in-silico* ADMET predictions via SwissADME and ProTox-2. The obtained results are summarised in **Table 8.2**. Orlistat was found to possess a low GI absorption and did not possess blood-brain barrier (BBB) permeation properties. Nevertheless, analogues from all the series (I, II and III) exhibited a high GI absorption property. However, analogues in series II and III exhibited no BBB permeation. Since none of the designed analogues were identified as substrates of the Pgp transporter (**Table 8.2**), it is possible that they do not undergo efflux. All the screened analogues except **5de** were found to be devoid of the cardiotoxicity. Analogues **7a** and **7b** from the series III were found to be devoid of hepatotoxicity, cardiotoxicity, mutagenicity and cytotoxicity.

CHAPTER VIII

Table 8.2. Summary of ADMET parameters predicted for the potential analogues from each series along with alloimperatorin and Orlistat

Series	Molecules	Absorption	Distribution		Metabolism						Toxicity				
		GI absorption	BBB permeant	Pgp substrate	CYP 1A2	CYP 2C19	CYP 2C9	CYP 2D6	CYP 3A4	CYP 2E1	Hepato-toxicity	Cardio-toxicity	Muta-genicity	Cyto-toxicity	
NP Lead	Allo-imperatorin	High	Yes	No	No	No	Yes	Yes	No	No	No	No	No	Yes	No
I	5k	High	Yes	No	Yes	No	Yes	No	No	No	Yes	No	No	No	No
	5q	High	Yes	No	Yes	No	Yes	No	No	No	Yes	No	No	No	No
II	5de	High	No	No	No	No	Yes	No	Yes	No	No	Yes	Yes	No	No
	5dh	High	No	No	No	No	No	No	No	No	No	No	Yes	No	No
III	7a	High	No	No	No	No	Yes	No	Yes	No	No	No	No	No	No
	7b	High	No	No	No	No	Yes	No	Yes	No	No	No	No	No	No
Reference	Orlistat	Low	No	Yes	No	No	No	No	No	No	Yes	No	No	No	No

*Predicted value represented as mg/kg; Most potent analogue from each series and Orlistat highlighted in grey and bold

8.3.2. Oral Triglyceride Tolerance Test (OTTT)

The result of an OTTT study of the analogue **7b** effect on serum triglyceride levels following olive oil ingestion is summarized in **Fig 8.3**. A swift elevation in the concentration of serum triglycerides was detected in the olive oil control groups subsequent to the ingestion of the olive oil. Conversely, the administration of Orlistat inhibited the increase in triglyceride levels, suggesting that it may have an effect on triglyceride metabolism. However, it was observed that the **7b** at high and medium dose (20 and 10 mg/kg) produced results similar to those of Orlistat. On the other hand, the lowest dose (5 mg/kg) had no discernible impact on the absorption of triglyceride.

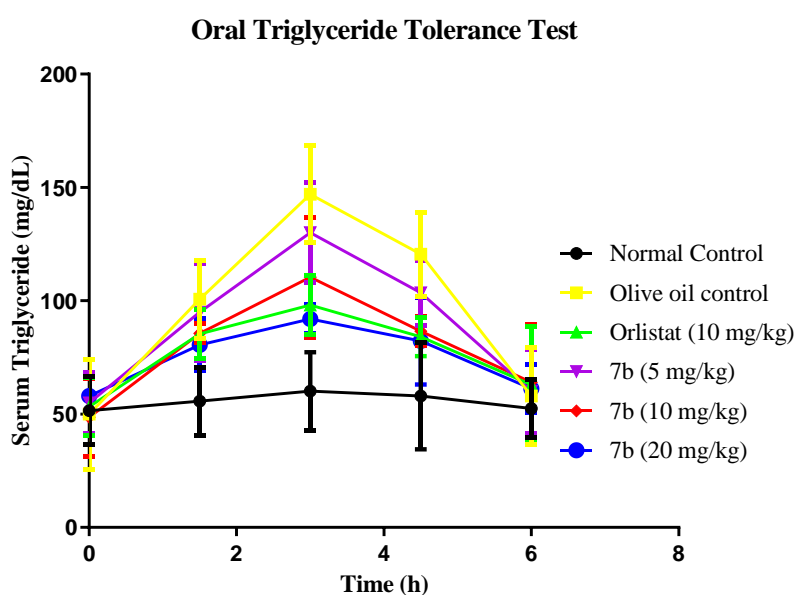


Figure 8.3. Results of the OTTT summarising the serum triglyceride levels at various time points.

On the basis of the aforementioned findings, high and medium doses of **7b** (10 mg/kg and 20 mg/kg, respectively) were chosen for the anti-obesity effect evaluation, which involved a 4-week treatment study.

8.3.3. Anti-obesity studies (4 weeks treatment)

8.3.3.1. Body weight

A four-week evaluation was conducted to assess the anti-obesity effect of **7b** in HFD-fed rodents. For the purpose of this study, two dose of **7b** (10 and 20 mg/kg) were chosen, with Orlistat (10 mg/kg) serving as the standard. The statistical data presented in **Fig 8.4** provides a summary of the body weights of the animals ascertained at the end of each week. The disease group exhibited a substantial increase in weight when compared to the normal control

group. In contrast, a substantial decrease in body weight was observed in the treatment groups (Orlistat and **7b**).

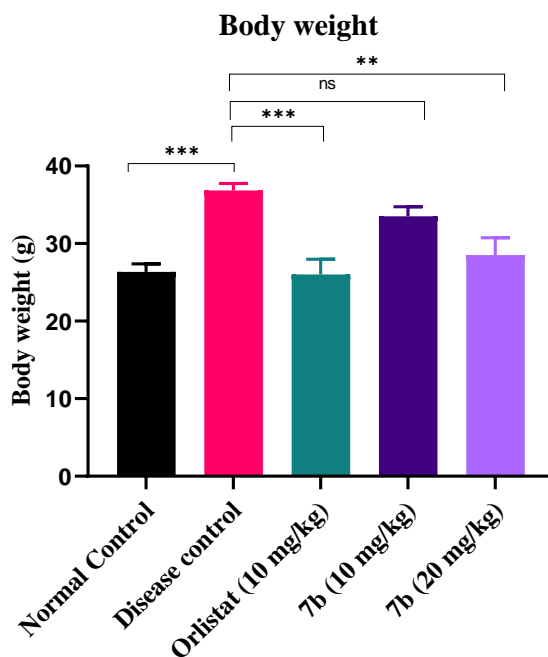


Figure 8.4. Body weights of animals after four week treatment. (The values are represented as mean \pm SEM; *** $p \leq 0.001$; ** $p \leq 0.01$).

8.3.3.2. Biochemical parameters

In addition, a range of biochemical parameters were assessed, including glucose, triglycerides (TG), total cholesterol (TC), high-density lipoprotein (HDL), and low-density lipoproteins (LDL). The outcomes of these measurements are illustrated in **Fig 8.5**. With the exception of glucose, all biochemical parameters of the disease control group changed significantly in comparison to the normal control. All serum biochemical parameters exhibited a decrease in the Orlistat treatment group in comparison to the disease control group. The dose of 20 mg/kg dose of **7b** led to a more significant reversal in all the profiles (except glucose) of the disease control mice. Overall, the anti-obesity potential of **7b** was validated by these studies during the four-week treatment period.

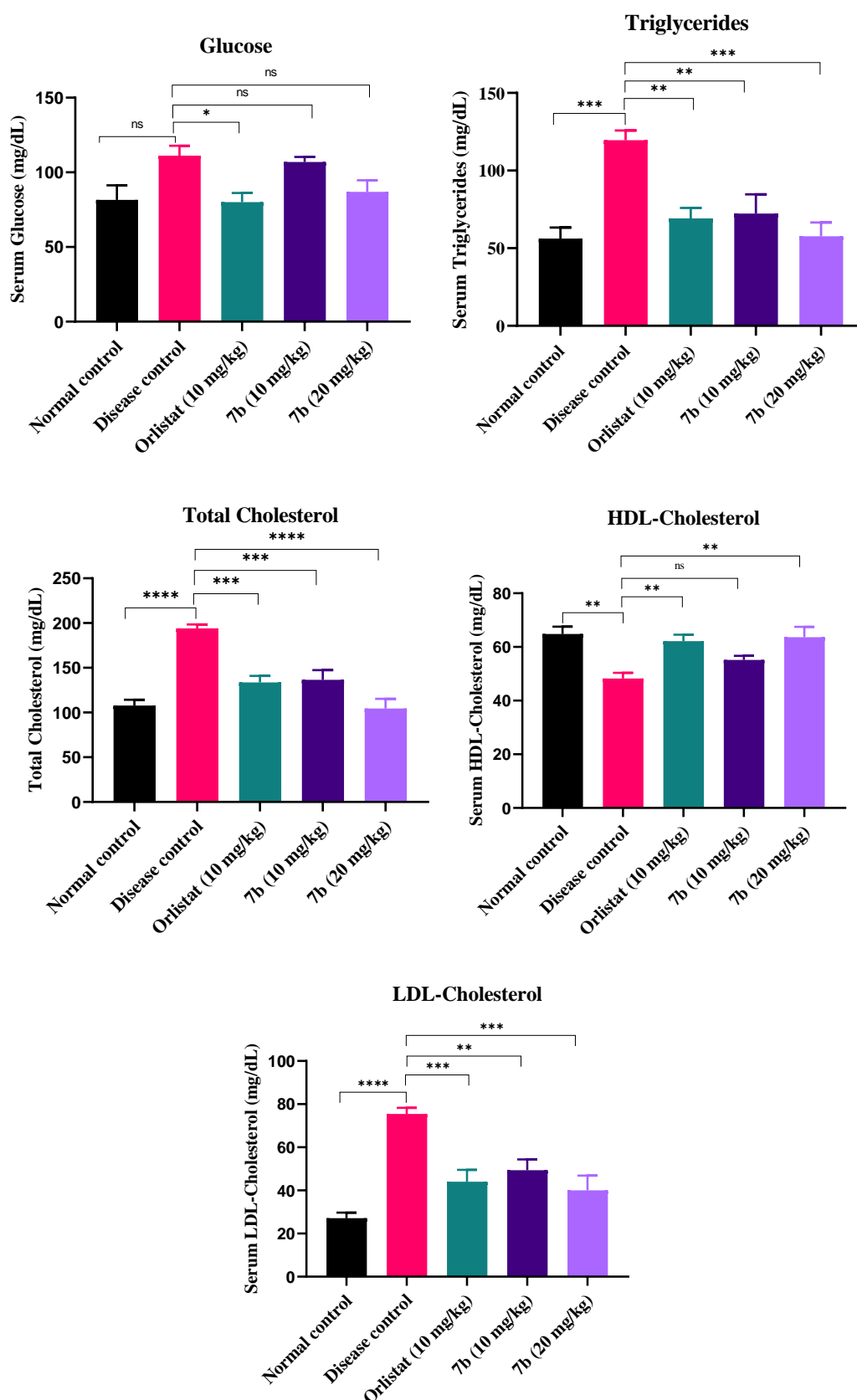


Figure 8.5. Effect of **7b** and orlistat on various biochemical parameters determined after the treatment period. (The values are represented as mean \pm SEM. **** $p \leq 0.0001$, *** $p \leq 0.001$; ** $p \leq 0.01$; * $p \leq 0.05$).

8.3.3.3. Quantification of faecal triglycerides

An excessive quantity of triglycerides detected in the faeces due to the fact that PL inhibition alters the digestion of triglycerides. To assess the magnitude of the anti-obesity impact induced by PL inhibition, the quantity of triglycerides detected in the faeces was measured. The findings are succinctly illustrated in **Fig 8.6**.

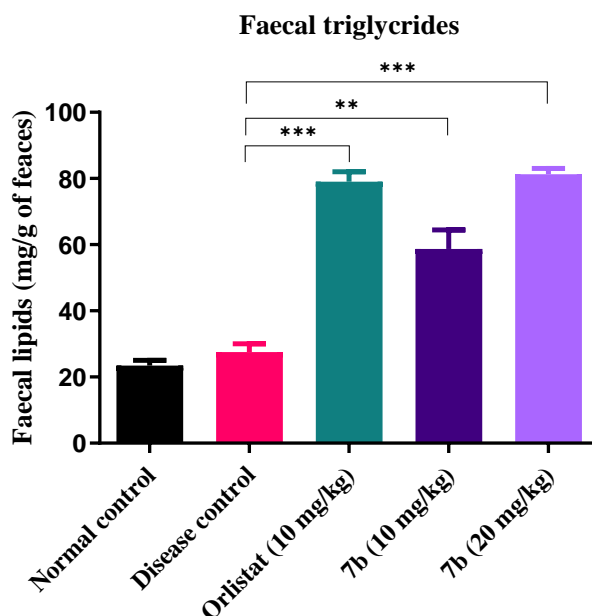


Figure 8.6. Faecal triglyceride levels determined from various groups. (The values are represented as mean \pm SEM. *** $p \leq 0.001$; ** $p \leq 0.01$).

In comparison to the disease/normal control group, the faecal triglyceride contents of the orlistat/treatment group varied considerably. The group that received orlistat and analogue **7b** (20 mg/kg) demonstrated the significant concentration of faecal triglycerides as compared to HFD group. As determined by the quantification of triglyceride contents, the screened analogue (**7b**) significantly altered fat absorption by inhibiting the PL.

8.3.3.4. Histopathological studies

Further, histopathological studies of liver and adipose tissues were performed. Microscopic examination of liver exhibited fatty changes or fat globule in disease control group as compared to normal control group due to continuous exposure to HFD. Also, extensive lipid deposition and hepatic ballooning was observed, indicating liver damage and metabolic stress in the hepatocytes. Low dose and high dose group of analogue **7b** was found to exhibit normal architecture of liver when compared to disease control (**Fig 8.7**) [15-19].

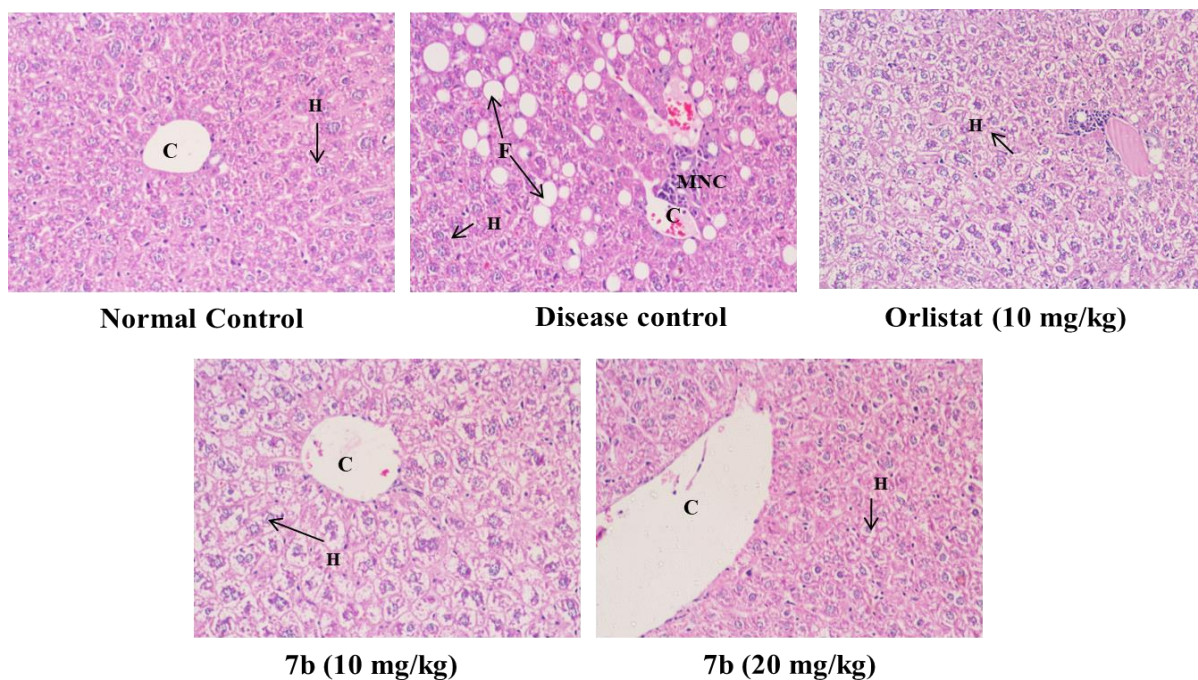


Figure 8.7. H&E Staining of liver (C - Central Vein, H - Hepatocyte, MNC - Mononuclear cells infiltration, F - Fatty change or steatosis that is fat globule).

PSR staining of the liver revealed collagen deposition and increase in fatty globules in the disease control group, in contrast to the normal control group. At low and high doses of analogue **7b** and Orlistat exhibited normal architecture of the liver in contrast to disease control (**Fig 8.8**) [16-18].

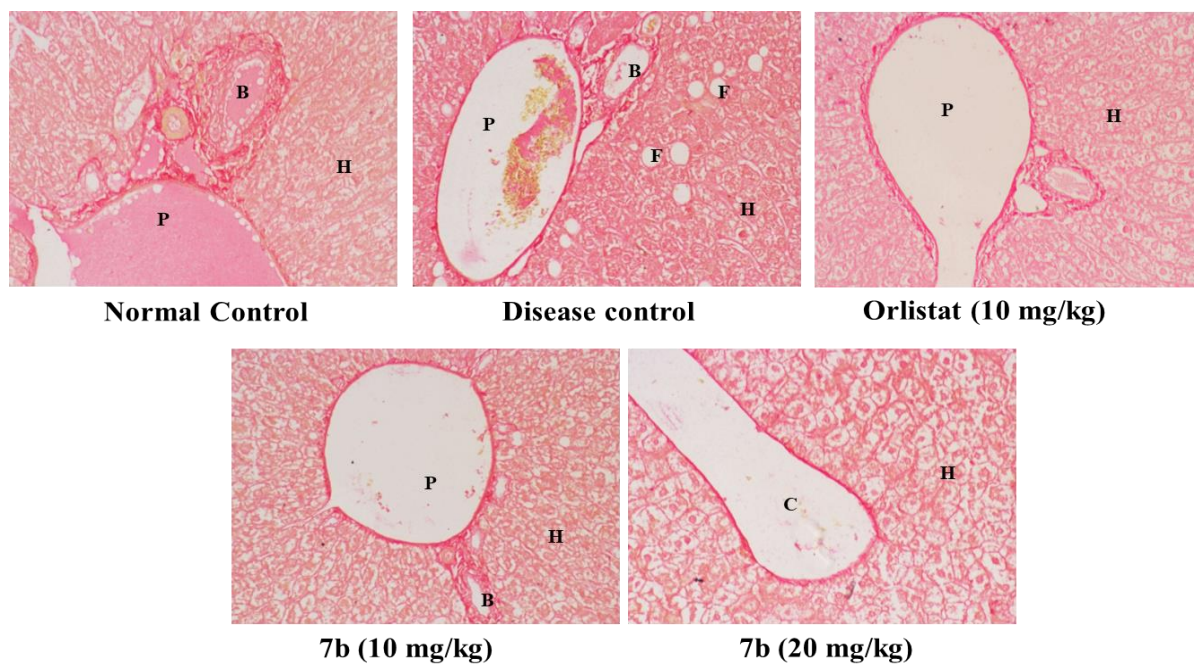


Figure 8.8. PSR Staining of liver (P - Portal vein, H - Hepatocyte, C - Central vein , F - Fatty change or steatosis that is fat globule, orange color indicate collagen fibre).

CHAPTER VIII

Adipose tissue undergoes hypertrophy and hyperplasia to enlarge. A tissue or organ that undergoes hypertrophy develops a greater volume as a result of the enlargement of its constituent cells. In hyperplasia, the number of cells increases while their size remains relatively constant. When isolated, white adipocytes are spherical, but they may appear polyhedral or oval when crowded together in adipose tissue. During standard histologic sections, the lipid was extracted using organic solvents like xylene, resulting in the formation of a delicate meshwork of polygonal profiles representing adipose tissue (**Fig 8.9**). In addition to representing the extracellular matrix, the thin strand of meshwork that divides the adjacent adipocytes also contained cytoplasm of both the cells [20].

The disease control group exhibited three characteristics (a) an enlarged cells as a result of lipid accumulation within the cells; (b) A flattened image of the nucleus, observed on one side of the lipid mass; (c) A narrow rim formed by the cytoplasm around the lipid.

In contrast to the disease control group, adipose tissue microscopic analysis revealed that Orlistat exhibited significant reduction in the size of the inflamed and hypertrophic adipocytes compared to the disease control group. In contrast to disease control group, **7b** (low and high dose) exhibited a normal architecture of adipose tissue (**Fig 8.9**) [20].

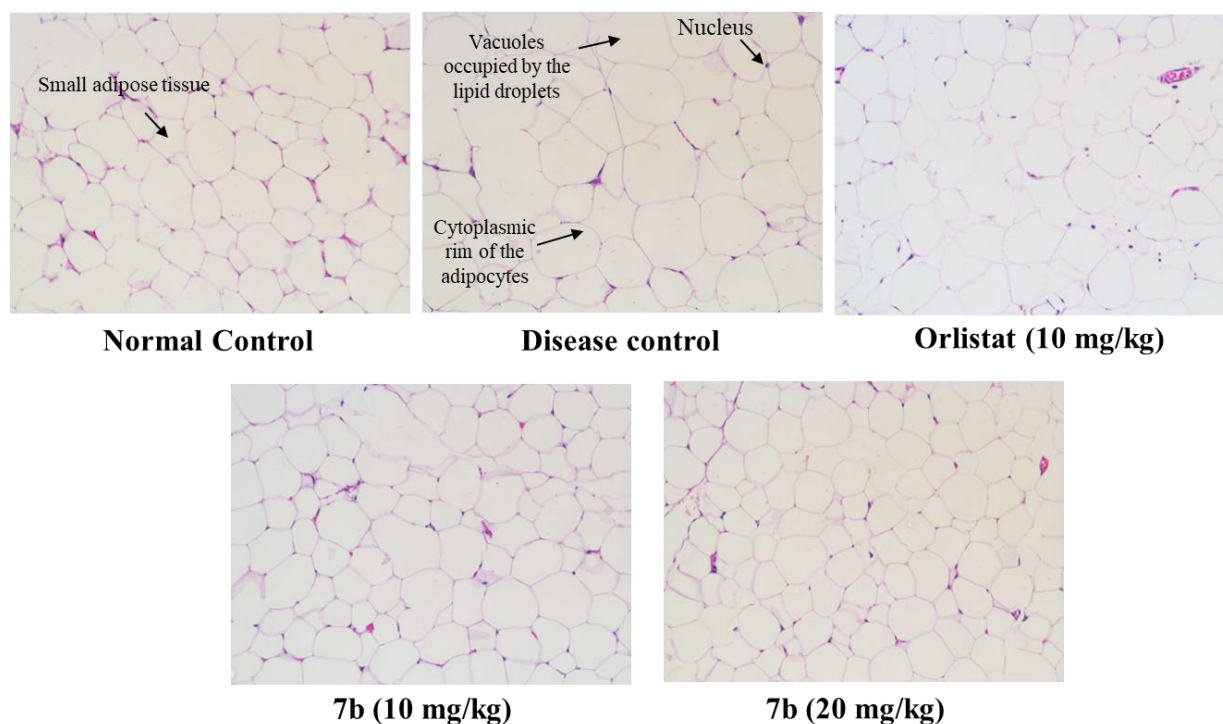


Figure 8.9. H&E Staining of Adipose tissue.

CHAPTER VIII

In brief, the current chapter provided an analysis of the pharmacological assessment of the most potent analogue (**7b**) across all the three series. In order to obtain a thorough understanding of the anti-obesity properties of the selected analogue (**7b**), four sets of experiments were performed. OTTT studies suggested that **7b** may play a role in the absorption of triglycerides, whereas four-week treatment studies in mice fed an HFD suggested that **7b** has anti-obesity properties. The investigation into faecal triglyceride profiles yielded insights into the PL inhibitory characteristics of **7b**, wherein it demonstrated an anti-obesity impact similar in nature to that of orlistat. Moreover, the estimation of faecal triglyceride levels unequivocally demonstrated that this anti-obesity effect was attributable to PL inhibition. Histopathology analyses of liver and adipose tissue following treatment with **7b** demonstrated that this analogue inhibited adipocyte hypertrophy. Additionally, it decreases collagen levels, neutrophil infiltration, and other hepatic damages caused by prolonged HFD exposure. Additionally, normal hepatic function was not disrupted with no evidence of toxicity.

References

1. Moroy, G., Martiny, V. Y., Vayer, P., Villoutreix, B. O., & Miteva, M. A. (2012). Toward *in silico* structure-based ADMET prediction in drug discovery. *Drug Discovery Today*, 17(1-2), 44-55.
2. Cheng, F., Li, W., Liu, G., & Tang, Y. (2013). *In silico* ADMET prediction: recent advances, current challenges and future trends. *Current Topics in Medicinal Chemistry*, 13(11), 1273-1289.
3. Kazmi, S. R., Jun, R., Yu, M. S., Jung, C., & Na, D. (2019). *In silico* approaches and tools for the prediction of drug metabolism and fate: A review. *Computers in Biology and Medicine*, 106, 54-64.
4. Daina, A., Michielin, O., & Zoete, V. (2017). SwissADME: A free web tool to evaluate pharmacokinetics, drug-likeness and medicinal chemistry friendliness of small molecules. *Scientific Reports*, 7(1), 42717.
5. Banerjee, P., Eckert, A. O., Schrey, A. K., & Preissner, R. (2018). ProTox-II: A webserver for the prediction of toxicity of chemicals. *Nucleic Acids Research*, 46(W1), W257-W263.
6. Chen, T. Y., Wang, M. M., Hsieh, S. K., Hsieh, M. H., Chen, W. Y., & Tzen, J. T. (2018). Pancreatic lipase inhibition of strictinin isolated from Pu'er tea (*Cammelia sinensis*) and its anti-obesity effects in C57BL6 mice. *Journal of Functional Foods*, 48, 1-8.
7. George, G., Auti, P. S., Sengupta, P., Yadav, N., & Paul, A. T. (2023). Synthesis, molecular modelling and pharmacological evaluation of novel indole-thiazolidinedione based hybrid analogues as potential pancreatic lipase inhibitors. *Journal of Biomolecular Structure and Dynamics*, 1-20.
8. Avcı, G., Küçük Kurt, I., Küpeli Akkol, E., & Yeşilada, E. (2010). Effects of escin mixture from the seeds of *Aesculus hippocastanum* on obesity in mice fed a high fat diet. *Pharmaceutical Biology*, 48(3), 247-252.
9. Han, L. K., Kimura, Y., Kawashima, M., Takaku, T., Taniyama, T., Hayashi, T., Zheng, Y.N., & Okuda, H. (2001). Anti-obesity effects in rodents of dietary teasaponin, a lipase inhibitor. *International Journal of Obesity*, 25(10), 1459-1464.
10. Rani, N., Vasudeva, N., & Sharma, S. K. (2012). Quality assessment and anti-obesity activity of *Stellaria media* (Linn.) Vill. *BMC Complementary and Alternative Medicine*, 12, 1-8.

11. Pesta, D. H., & Samuel, V. T. (2014). A high-protein diet for reducing body fat: mechanisms and possible caveats. *Nutrition & Metabolism*, *11*, 1-8.
12. Thibault, L. (2013). Animal models for the study of human disease: *Chapter 13. Animal models of dietary-induced obesity*. Elsevier Inc.
13. Chen, Y., Zhang, X., Pan, B., Jin, X., Yao, H., Chen, B., Zou, Y., Ge, J. & Chen, H. (2010). A modified formula for calculating low-density lipoprotein cholesterol values. *Lipids in Health and Disease*, *9*, 1-5.
14. Harach, T., Aprikian, O., Monnard, I., Moulin, J., Membrez, M., Béolor, J. C., Raab, T., Macé, K. & Darimont, C. (2010). Rosemary (*Rosmarinus officinalis* L.) leaf extract limits weight gain and liver steatosis in mice fed a high-fat diet. *Planta Medica*, *76*(06), 566-571.
15. Uchiyama, S., Taniguchi, Y., Saka, A., Yoshida, A., & Yajima, H. (2011). Prevention of diet-induced obesity by dietary black tea polyphenols extract *in vitro* and *in vivo*. *Nutrition*, *27*(3), 287-292.
16. Mujawdiya, P. K., Sharma, P., Sharad, S., & Kapur, S. (2020). Reversal of increase in intestinal permeability by *Mangifera indica* seed kernel extract in high-fat diet-induced obese mice. *Pharmaceuticals*, *13*(8), 190-210.
17. De Melo, T. S., Lima, P. R., Carvalho, K. M. M. B., Fontenele, T. M., Solon, F. R. N., Tomé, A. R., De Lemos, T.L.G., da Cruz Fonseca, S.G., Santos, F.A., Rao, V.S. & De Queiroz, M. G. R. (2017). Ferulic acid lowers body weight and visceral fat accumulation *via* modulation of enzymatic, hormonal and inflammatory changes in a mouse model of high-fat diet-induced obesity. *Brazilian Journal of Medical and Biological Research*, *50*, e5630.
18. Janoschek, R., Handwerk, M., Hucklenbruch-Rother, E., Schmitz, L., Bae-Gartz, I., Kasper, P., Lackmann, J.W., Kretschmer, T., Vohlen, C., Mesaros, A. & Purrio, M., (2023). Heterogeneous effects of individual high-fat diet compositions on phenotype, metabolic outcome, and hepatic proteome signature in BL/6 male mice. *Nutrition & Metabolism*, *20*(1), 8-23.
19. Yustisia, I., Tandiar, D., Cangara, M. H., Hamid, F., & Nu'man, A. S. (2022). A high-fat, high-fructose diet induced hepatic steatosis, renal lesions, dyslipidemia, and hyperuricemia in non-obese rats. *Heliyon*, *8*(10), e108096.
20. Bremer, A. A., & Jialal, I. (2013). Adipose tissue dysfunction in nascent metabolic syndrome. *Journal of Obesity*, *2013*, e393192.

Conclusion, Future Perspectives and Limitations

9. Conclusion, Future Perspectives and Limitations

9.1. Chapter Specific Summary and Conclusion

9.1.1. Chapter 1

- A recent study published in the Lancet revealed that the worldwide prevalence of obesity has exceeded one billion individuals in 2023. Since 1990, the global prevalence of obesity in adults has more than doubled, while it has climbed fourfold in children and adolescents aged 5-19. Furthermore, based on the above data, the prevalence of overweight adults in 2022 was 43%
- PL inhibition is regarded as a safe and efficacious approach for treating obesity owing to its peripheral location. Systemic absorption is not necessary for the inhibitor to function, and it effectively impedes fat absorption
- Orlistat, a highly effective PL inhibitor, is frequently prescribed for the long-term management of obesity. Nevertheless, in recent decades, there have been numerous reports of severe adverse effects associated with chronic Orlistat administration, such as acute pancreatitis and hepatotoxicity. These reports underscore the urgent need for the development of anti-obesity drugs that are both safe and effective

9.1.2. Chapter 2

- A detailed literature search on various natural and synthetic coumarin scaffolds reported for PL inhibition was performed to identify structural features required for potent PL inhibition
- A negligible expanse of research used the advantage of *in silico* techniques in understanding the molecular interactions with the active site
- Nevertheless, the naturally occurring coumarins exhibited weak PL inhibitory activity. On the contrary, structural modifications that include various substitutions on the coumarins resulted in a significant enhancement in their PL inhibitory activity
- The aim and the objectives were detailed considering the potential gaps in the existing research

9.1.3. Chapter 3

- The general procedures for **i)** plant material collection, processing and extraction; **ii)** PL inhibition assay and enzyme kinetics; **iii)** molecular docking and molecular dynamics **iv)** fluorescence spectroscopy were provided in detail

9.1.4. Chapter 4

- Screening of 60 plant extracts from 10 Indian medicinal plants/parts highlighted unripe fruits of *A. marmelos* as a source of potential leads
- Alloimperatorin was identified as a potential natural product lead for PL inhibition, with an IC_{50} of 27.75 μ M

9.1.5. Chapter 5

- A total of 17 coumarin analogues were synthesised and evaluated for PL inhibition assay
- **5q** and **5k** from this series exhibited potential PL inhibitory activity with IC_{50} of 19.41 and 21.30 μ M
- The structural requirements were identified in this chapter that can enhance the PL inhibitory potential of any ligand:
 - i) interaction with the lid domain amino acids (Ser 152, His 263)
 - ii) requirement of dense hydrophobic moieties to form a π -cation interaction with Arg 256
 - iii) Linker, A structural framework that facilitates the attainment of appropriate conformational flexibility is able to ensure a proper interaction with the active site amino acid and the lid domain

9.1.6. Chapter 6

- A total of 36 coumarin analogues were synthesised and evaluated for PL inhibition assay
- **5dh** and **5de** from this series exhibited potential activity with IC_{50} of 9.20 and 11.4 μ M
- A similar SAR as that of **series I** was observed with these analogues
- The importance of interaction with the Ser 152, and π -cation interaction with Arg 256 has been validated in this chapter

9.1.7. Chapter 7

- A total of 38 coumarin analogues were synthesised, evaluated for PL inhibition assay
- A potent PL inhibition with IC_{50} of 1.25 μ M was achieved with **7b** comparable to the standard drug, Orlistat ($IC_{50} = 0.97 \mu$ M)
- Presence of heteroaryl extension on the amide linked through two carbon chain resulted in enhanced activity

- The study highlighted that the C₇ positions of the coumarin analogues to be favourable for the substitution of alkyl chains, that resulted in potent PL inhibitory activity

9.1.8. Chapter 8

- ADMET prediction highlighted **7b** as a suitable candidate for *in vivo* experiments
- **7b** at 20 mg/kg dose exhibited comparable anti-obesity efficacy compared to Orlistat (10 mg/kg)
- The quantification of faecal triglycerides clearly indicated that **7b** acted through PL inhibition
- Histopathology of liver and adipose tissue after **7b** treatment showed that it inhibited adipocyte hypertrophy. Additionally, it reduced collagen levels, neutrophil infiltration, and liver damage from prolonged HFD exposure. There was no toxicity or disruption of normal liver function

9.2. Future Perspectives

Exploration of natural products, *in-silico* drug design, synthetic chemistry, *in-vitro* and *in-vivo* biological investigations were incorporated into an integrated strategy for the identification and generation of a library of structurally diverse novel chemical entities. Future developments pertaining to the endeavour are detailed below:

- The most potent synthetic analogue **7b** exhibited an IC₅₀ of 1.25 μM comparable to Orlistat. The potency of **7b** and its related hybrid analogues can be further augmented through diverse structural modifications, including substituting the indole functional and appending electron-donating substituents at various positions on the coumarin scaffold
- The addition of a three-carbon linker led to a decrease in the inhibitory potential of PL, a finding that warrants additional research
- The assessment of the interaction mechanism between the synthesized analogues and PL can be accomplished through the utilization of diverse techniques such as X-ray crystallography, cryo-electron microscopy, and isothermal titration calorimetry
- In addition, performing studies against different types of lipases (e.g., gastric, hepatic, lingual) could provide valuable insights into the impact of the hybrid analogues on the overall triglyceride digestion process
- The antiobesity potential of the PL inhibitor "**7b**" can be explored through *in vivo* investigations using different animal models of obesity
- Coumarin scaffold can be hybridized with a multitude of additional scaffolds/pharmacophores to facilitate the discovery of novel and potent PL inhibitors

- Additionally, the effect of **7b** on PL in combination with Orlistat can be determined through synergy experiments. This may lead to a substantial reduction in the dose of Orlistat while maintaining its efficacy

9.3. Limitations

Few limitations were identified in the present thesis, that are as follows.

- The scope of the current investigations was restricted to the *in-vitro* and *in vivo* (preclinical) assessment of the synthesized analogues; there was no execution of a clinical trial
- The metabolic stability of hybrid analogues under stimulated and physiological conditions was not assessed in the study
- Utilizing *in-silico* analysis, the interaction between the potent analogue and PL was investigated. The utilization of advanced techniques, including cryo-electron microscopy and X-ray crystallography, were not performed
- The current study entailed the synthesis of a small number of coumarin analogues. It is possible to synthesize a wider range of coumarin analogues in order to gain an in depth understanding of the way various substituents affect the inhibition of PL

Appendix

Patent & Publications

From Thesis

Patent

- Paul, A. T. **Yadav, N.**, B. B. Lavanya ‘Coumarin carboxamide Analogues as Potent Pancreatic Lipase Inhibitors’ filling at Indian Patent Office (Appl.no. 202411051970)

Publications

- **Yadav, N.**, & Paul, A. T. (2023). Pancreatic lipase and its related proteins: Where are we now? *Drug Discovery Today*, 103855. {**Impact factor - 7.4**}
- **Yadav, N.** and Paul, A.T. (2023). Synthesis of amide warhead containing coumarin derivatives as potential pancreatic lipase inhibitors: *in silico* and *in vitro* evaluation for obesity treatment. *Medicinal Chemistry Research*, 32(10), 2219-2233. {**Impact factor - 2.6**}
- Five decades of research on Golden apple (*Aegle marmelos*): A journey from sacred tree to commercial products (*Journal of Ethnopharmacology*, Communicated)
- Identification of coumarin analogues as promising anti-obesity agents: An *in silico* design, synthesis and *in vitro* pancreatic lipase inhibitory activity. (Communicated)
- Synthesis, molecular modelling, *in vitro* and pharmacological evaluation of coumarin amide warhead containing analogues as potential anti-obesity agents. (Communicated)

Allied work

- **N Yadav**, P Auti, G George and AT Paul (2020). Design, synthesis and biological evaluation of *O*-alkyl umbelliferone derivatives as pancreatic lipase inhibitors. *Journal of The Indian Chemistry Society*, 97(8), 1-6. {**Impact factor - 1.3**}
- George, G., **Yadav, N.**, Auti, P. S., & Paul, A. T. (2023). Molecular modelling, synthesis and *in vitro* evaluation of quinazolinone hybrid analogues as potential pancreatic lipase inhibitors. *Journal of Biomolecular Structure and Dynamics*. 41(19), 9583-9601. {**Impact factor - 5.4**}
- George, G., Auti, P.S., Sengupta, P., **Yadav, N.** and Paul, A.T. (2023). Synthesis, molecular modelling and pharmacological evaluation of novel indole-thiazolidinedione based hybrid analogues as potential pancreatic lipase inhibitors. *Journal of Biomolecular Structure and Dynamics*, 1-20. {**Impact factor - 5.4**}

- Dhiman, P., **Yadav, N.**, Auti, P. S., Jaswal, S., Singh, G., Mehan, S., Ghosh, B., Paul, A.T. & Monga, V. (2024). Discovery of thiazolidinedione-based pancreatic lipase inhibitors as anti-obesity agents: synthesis, *in silico* studies and pharmacological investigations. *Journal of Biomolecular Structure and Dynamics*, 1-23. {**Impact factor - 5.4**}
- Pandey, V., Adhikrao, P. A., Motiram, G. M., **Yadav, N.**, Jagtap, U., Kumar, G., & Paul, A. T. (2024). Biaryl carboxamide-based peptidomimetics analogs as potential pancreatic lipase inhibitors for treating obesity. *Archiv der Pharmazie*, 357(4), e2300503. {**Impact factor - 6.9**}

Book Chapter

- Paul, A. T., George, G., **Yadav, N.**, Jeswani, A., & Auti, P.S., (2021). “*Pharmaceutical Application of Bio-actives from Alstonia Genus: Current Findings and Future Directions*” in Book titled “*Bioactive Natural Products for Pharmaceutical Applications*”, Advanced Structured Materials 140, Editors: D. Pal and A. K. Nayak. Published by Springer Nature Switzerland AG 2021 (10.1007/978-3-030-54027-2_14)

Other Patent filed

- Paul, A. T., Sengupta, P., George, G., **Yadav, N.**, & Auti, P.S., (2020). ‘Compositions for Inhibiting Pancreatic Lipase’ filed at Indian Patent Office (Application No: 202011049373)

Conferences

- Oral presentation on “**Coumarin analogues from unripe fruits of *Aegle marmelos* as potential Pancreatic Lipase inhibitors: *In-silico* and *in-vitro* investigation**” in the “25th National Convention of Society of Pharmacognosy” & International Conference “New Horizons of Natural Products and AYUSH Remedies”, organized by Graduate School of Pharmacy, Gujarat Technological University (GTU) & Society of Pharmacognosy, November 27-28, 2021, at GTU Campus, Ahmedabad, Gujarat, India

- Poster presentation on “**Alkaloids and Coumarins from *Aegle marmelos* as potential Pancreatic lipase inhibitors: *In-silico* investigation**” at One Day Symposium on Integration of AYUSH Medicines and Ethnopharmacology: A Strategy towards evidence-based medicines, October 4th, 2022, NIPER, S.A.S. Nagar, Mohali, India
- Poster presentation on “**Design, synthesis and *in-vitro* evaluation of Coumarin scaffold inspired analogues for obesity treatment**” in the conference on “Recent Trends and Challenges in Drug Discovery (RTCDD),” March 3-4, 2023, BITS Pilani, Pilani Campus, India

List of Workshops/ Conferences attended

- Attended "Virtual Conference on Regulatory Aspects and Intellectual Property Rights in Pharmaceuticals " organized by the Department of Pharmacy, BITS Pilani, Pilani Campus on November 28, 2020
- Attended "Virtual Conference on Pharmacy: Always trusted for your health", organized by the Department of Pharmacy, BITS Pilani, Pilani Campus during September 25, 2021
- Participated in one day workshop on “Virtual Workshop on Introduction to Pharmacophore Modelling and Protein-Ligand Interactions: SeeSAR Software” organized by Department of Pharmacy, BITS Pilani, Pilani Campus on April 30, 2022
- Participated in one day workshop on “Applications of FTIR and 2D NMR in Pharmaceutical Research” organized by BITS Pilani, Pilani Campus, Sponsored by Labindia Analytical Instruments Pvt. Ltd., Bangalore on December 3, 2022
- Participated in two day workshop on “Cheminformatics and Machine Learning in Drug Discovery ” organized by BITS Pilani, Pilani Campus, Sponsored by Hapten Biotechnology, Varun Industries, S.N. Scientific Suppliers and Genaxy Scientific Pvt. Ltd. on March 18-19, 2024

Awards and Achievements

- DST-INSPIRE Fellowship
- Poster presentation (Third prize) at One Day Symposium on Integration of AYUSH Medicines and Ethnopharmacology: A Strategy towards evidence-based medicines, held at NIPER, S.A.S. Nagar, Mohali, India, October 4, 2022

BIBLIOGRAPHY OF THE SUPERVISOR

Prof. Paul Atish Tulshiram is Associate Professor & Faculty In charge HD & PhD Admissions at BITS-Pilani, Pilani Campus, India. He completed his bachelor's from University of Pune, Maharashtra. He pursued M.S and Ph.D in Natural Products from National institute of Pharmaceutical Education and Research (NIPER) S.A.S Nagar, Punjab. He completed his post-doctorate from the National Centre for Natural Products Research (University of Mississippi, USA) in the research group of Prof. Ikhlas Khan. His current research is design, synthesis, molecular modelling, and biological evaluation of pancreatic lipase inhibitors from natural products origin for obesity management. He has completed 7 research grants from DST-SERD, DST(SEED), DBT, ICMR and Industry. He has published more than 60 research articles in reputed international journals and contributed 24 official monographs on polyherbal formulations in the Ayurvedic Pharmacopeia of India. He has been granted 3 patents in the area of natural products and their derivatives and 7 patents are under evaluation. He has provided guidance to 6 doctoral students and is presently supervising 10 doctoral candidates. He is a reviewer of various journals of reputed publishers such as ACS, Elsevier, Wiley, Bentham, etc., and also for funding agencies such as DST-SERB and South African Medical Research Council.



BRIEF BIOGRAPHY OF THE CANDIDATE

Nisha Yadav was born in Kerala, Eranakulum, India. She pursued her Bachelor's (B. Pharmacy) and master's degree (M. Pharmacy in Pharmaceutical Chemistry) from Banasthali University during 2012-16 and 2016-18, respectively. She pursued her master's thesis under the guidance of Dr. Sumitra Nain (Associate Professor, Banasthali Vidyapeeth, Rajasthan) and Dr. Gautam Panda (Principal Scientist, CSIR-CDRI, Lucknow, Uttar Pradesh) on the topic "Synthesis of Antimicrobial Agents (Design and Synthesis of Corannulene derived unnatural amino acid based peptides as Antimicrobial agents)". In March 2019, she joined Department of Pharmacy, BITS Pilani (Pilani Campus) as a Ph.D. scholar under the supervision of Dr. Paul Atish Tulshiram in the area of anti-obesity. Ms. Nisha Yadav has authored 6 research publications, 1 review article and 1 book chapter in international peer reviewed journals. A part of her Ph.D. thesis is filed for patent. She has presented her work in several international and national conferences. She has received accolades, including the DST-INSPIRE Fellowship (2019-2024) and a 3rd prize in oral presentation.

